THÈSE

présentée par

Kristine NISS

pour obtenir le grade de DOCTEUR

DE L'UNIVERSITÉ DE PARIS XI

spécialité CHIMIE PHYSIQUE

Fast and slow dynamics of glass-forming liquids
–
What can we learn from high pressure experiments?

Soutenue le 19 Janvier 2007 devant le jury composé de:

Rapporteurs:	Dr.	Catherine Dreyfus
	Dr.	Helmut Schober
	Prof.	Giancarlo Ruocco
	Dr.	Jean-Philippe Bouchaud
	Prof.	Mehran Mostafavi
	Prof.	Jeppe Dyre
Directrice de thèse:	Dr.	Christiane Alba-Simionesco

Abstract

The focus in this study is on the fragility concept, that is the degree of departure from Arrhenius temperature dependence of the relaxation time in the viscous liquid. Fragility has in the course of the last decade been shown to (or suggested to) correlate with a large number of properties in the liquid and the corresponding glass. We develop a set of criteria for scrutinizing these types of correlations by introducing pressure as a control variable in addition to temperature. Particularly we show that correlations to isobaric fragility can be either signatures of a relation to the effect of density on the relaxation time, or on the relation to the temperature dependence of the relaxation time, or to a balanced combination of the two.

These criteria are used in the analysis of an extensive new set of data on the temperature and pressure dependence of a number of different dynamical variables in molecular and polymeric glass-forming systems. We particularly study the width of the alpha relaxation by dielectric spectroscopy, the relative intensity of the boson peak and the mean square displacement by neutron scattering and the nonergodicity factor by inelastic X-ray scattering.

In the study of the width of the alpha relaxation as well as the relative intensity of the boson peak we find that they do not relate to the effect of density on the relaxation time, and that a physically meaningful correlation in these cases should be a correlation to *isochoric* fragility rather than to the conventional isobaric fragility. The mean square displacement is found to relate to a balanced combination of temperature and density, while we suggest that the nonergodicity factor evaluated at T_g is correlated with the relative effect of density on the viscous slowing down.

Acknowledgement

First of all I would like to sincerely thank my supervisor Christiane Alba-Simionesco for letting me be her apprentice in the most genuine sense of the word; sharing, challenging and inspiring in science and in life. Secondly I owe a special thank to my companion and successor Cécile Dalle-Ferrier for her enormous moral and practical support.

I am grateful to Gilles Tarjus for always making things clearer and to Bernhard Frick for introducing me to the art and craft of neutron scattering. I am also thankful for fruitful discussions and collaborations with numerous other researches and I would particularly like to express my gratitude to : Alexei Sokolov, Vladimir Novikov, Jeppe Dyre, Niels Boye Olsen, Uli Buchenau and Tullio Scopigno. Moreover I would like to thank my jury and particularly the two rapportuers, Helmuth Schober and Cathrine Dreyfus, for the many useful comments and intriguing questions.

The work presented in this thesis has been carried out at the Laboratoire de Chimie Physique (LCP) in Orsay from January 2004 to December 2006, and I thank the former and present director, Alain Fuchs and Mehran Mostafavi for hosting me.

The INS experiments were performed at ILL and were only possible thanks to the staff on IN5, IN10 and the pressurelab : Jacques Ollivier, Luis Melesi, Tilo Seydel, Matthias Elender and Steve Jenkins.

The IXS measurements were made possible thanks to the staff on ID16 and ID28 : Michael Krisch, Roberto Verbeni and Alexandre Beraud. I am particularly grateful to Giulio Monaco for his help with the data treatment and for many inspiring discussions.

I would also like to thank Claudio Masciovecchio, Silvia Santucci and Allesandro Gessini for an enlightening week on the IUVS beam-line on ELETTRA.

The development and fabrication of the dielectric spectroscopy setup at LCP was made possible thanks to the expertise and efficiency technical staff at LCP, I would particularly like to acknowledge the work of Joél Jaffrë, Jean-Robert Bazouin an

Raymond Herren. The technical assistance and help of the staff at IMFUFA has also been indispensable for this work and I thank Ib Hst Petersen, Peter Jensen and Ebbe Hyldahl Larsen.

A special thank also goes to Jens Christian Niss for proofreading the whole manuscript in a very short time.

Albena Nielsen and coworkers are thanked for making available dielectric data prior to publication and I would at the same time like to thank every one in "Glass and Time" (Denmark) for moral support.

My three years in the TESMaC group have been a real pleasure, and I am greatly thankful to everyone for helping me out, supporting me and being overbearing with my French. I would especially like to thank Jean-Marie Teuler for solving at least million software problems, and Anne Boutin for strong support when it was most needed. I would also like to thank the former Ph.D.-student Aude Chauty-Cailliaux, from whom I overtook many results and experiences.

Finally I would like to thank ...

Maj and Bo for being present at all times no matter how far away (and for coming closer). Niels for being there at the best (or worst) time possible. Paola, Carmelo, Elisa, Javier and Kosima for making Grenoble feel like a second home. Christelle, Angela, Ricardo, Aurelie, Frederic, Silvian, Gilbert, Pernille, Jean Luc, Margrethe, Stephan, Lucie, Anders, Guara and all of ECAP for making Paris home. And all my other friends and my family - I am grateful that they are far too numerous to be listed here.

Kristine Niss April 2007

This work was supported by grant No. 645-03-0230
from Forskeruddannelsesrådet (Denmark).

Contents

Chapter 1

Introduction

A fundamental question in condensed matter science is to understand what governs the increase of relaxation time, and ultimately the glass formation, in liquids upon cooling. This transition from liquid to glass is intriguing because it is found in all types of systems, yet it happens in a qualitatively different way from one system to another: The increase of relaxation time and viscosity when the temperature is lowered and the formation of a non-equilibrium solid state are universal in the sense that it regards all types of materials ranging from metals to polymers. However, the relaxation time has qualitatively different temperature dependencies in different systems. This qualitative difference can be quantified via the notion of "fragility", which is a measure of departure from Arrhenius temperature dependence [Angell, 1991]. The fragility concept has become a darling in the community because it captures the notion of universal and specific at the same time. There is something universal we want to understand; namely, the viscous slowing down, particularly the super-Arrhenius temperature dependence of the relaxation time. Yet there is something specific to each system that we need to capture - this is embodied in the variations of fragility. The central question in the field - "what controls the viscous slowing down?" - can therefore be rephrased as "what governs the fragility of a system?"

The attempts to answer this question has spread in abundant jungle of empirical and theoretical results. Though the starting point of the studies is the same they branch out in each their direction. The aim of this work is to make contact between two of these branches: To test if the results found are consistent with each other, and to try to gain more understanding of one by imposing the consequences of the other.

Within the past decades a lot of experimental effort has been put into correlating

fragility with other properties of the liquid and the glass. These correlations all refer to the conventional fragility measured at constant atmospheric pressure, that is the *isobaric fragility at atmospheric pressure*. But glasses can also be formed along isobars at elevated pressure, at constant density by isochoric cooling, or by compression along isotherms. There has been an explosion in the amount of data on the viscous slowing down under pressure within the last couple of years. But what happens to the correlations with fragility when we study the liquid at high pressure? Do the properties we try to correlate with fragility share the pressure dependence of the isobaric fragility? How about *isochoric fragility*? Is it possible to extract a consistent picture? Can the pressure/density dependence of the dynamics help us understand the physical meaning of the correlations?

The primary aim of this thesis is to address the above questions. Our starting point is hence two types of empirical results

- Based on studies of relaxation in liquids under pressure it appears to be general that the relaxation time can be expressed as a function of $e(\rho)/T$. [Alba-Simionesco *et al.*, 2002; Tarjus *et al.*, 2004 a; Dreyfus *et al.*, 2004; Casalini and Roland, 2004]. It follows from this scaling law that the *isochoric* fragility is independent of density.

- Fragility has been shown (or suggested) to correlate large number of properties in the liquid and the corresponding glass. We shall focus on correlations between fragility and other dynamical properties. We consider the following four properties which have been suggested to correlate to larger fragility (i) a stronger deviation of the relaxation functions from an exponential dependence on time (a more important "stretching") [Böhmer *et al.*, 1993], (ii) a lower relative intensity of the boson peak [Sokolov *et al.*, 1993, 1997], (iii) a larger temperature dependence of the short time mean square displacement just above T_g [Buchenau and Zorn, 1992; Dyre, 2004; Ngai, 2000] (iv) a smaller ratio of elastic to inelastic signal in the X-ray Brillouin-spectra [Scopigno *et al.*, 2003].

The questions are addressed partly by a general analysis of the consequences one can draw by combining the two (types of) results and partly by extensive experimental studies of the pressure and temperature dependence of the properties i-iv.

Previous studies on boson peak, mean square displacement and X-ray Brillouin under pressure are very scarce. Our results therefore not only shed light on the proposed relations to fragility but also deals with understanding the respective role

of temperature and density for these dynamical properties themselves. It is especially the combination of the density dependence of different dynamical quantities presented here which is unique and interesting.

The report is structured as follows: Chapter 2 gives an introduction to the glass transition phenomenology as studies at atmospheric pressure, including a short introduction to the correlations that are considered in the later chapters. The phenomenology of the alpha relaxation when studied under pressure is reviewed in the first part of chapter 3, and the second part of chapter 3 deals with formulating how pressure can be used to test correlations between fragility and other properties. The principles of the experimental techniques, dielectric spectroscopy inelastic neutron and inelastic X-ray scattering are found in chapter 4 where we also present the background results used for treating the data. Chapters 5 to 8 present the experimental results on the temperature and pressure dependences of different dynamical properties. Each of these chapters has a section devoted to the proposed correlation between the property in question and the fragility. Chapter 5 presents a study of the relaxation time and spectral shape the alpha relaxation probed by dielectric spectroscopy. Chapter 6 contains a study of the high Q collective modes measured by inelastic X-ray scattering. The mean square displacement at the nanosecond time scale measured by neutron backscattering is presented in chapter 7. The effect of pressure on the boson peak is presented in chapter 8. The results of chapters 3 to 8 are finally combined, discussed and concluded on in chapter 9.

The samples we have used in the different experiments include a number of different organic molecular liquids as well as polyisobutylene of different molecular weights. The characteristic of the samples including their equation of state, data on fragility and related dynamical properties are given in appendix A.

Résumé du chapitre 2

De manière générale, les liquides cristallisent quand ils sont refroidis en dessous de leur température de fusion. Cependant, si on les refroidit suffisamment rapidement, il est souvent possible d'éviter la cristallisation et d'obtenir un liquide surfondu. Quand on abaisse encore la température leur viscosité augmente énormément jusqu'à ce que les molécules ne puissent plus bouger : tous les mouvements sont alors dits "gelés". A température plus basse, le liquide se comporte comme un solide et on dit que l'on a formé un verre. Cette transition entre le liquide et le verre s'appelle la transition vitreuse.

Dans ce chapitre, on introduit la transition vitreuse et les grandeurs dynamiques qui nous intéressent. Les premiers paragraphes sont consacrés à la dynamique lente : ils traitent de la transition vitreuse, de la fragilité et du caractère étiré de la relaxation. On présente ensuite une définition de la dynamique rapide et on discute la relation entre la dynamique rapide dans le liquide et la dynamique qui reste active dans le verre. Les corrélations proposées dans la littérature entre les caractéristiques dynamiques d'un liquide vitrifiable et sa fragilité sont présentées dans le dernier paragraphe de ce chapitre.

Chapter 2

Slow and fast dynamics

2.1 The glass transition

By cooling a liquid at sufficiently high rates it is possible to avoid crystallization and to form a supercooled liquid; a thermodynamical metastable equilibrium state with a higher free energy than the crystal. We will in general refer to the supercooled liquid as the *equilibrium liquid*, even if it is metastable, because the important point is that all properties are unique functions of the state point, for example defined by the temperature and the pressure.

The volume (and enthalpy) of a given liquid in general decreases with decreasing temperature, meaning that whenever the temperature is decreased by some amount, the volume will decrease by some amount given by the expansivity. However, the volume does not reach its new equilibrium value instantaneously, rather the liquid equilibrates in some way over time. This process is called *structural relaxation* and the associated characteristic time is the structural relaxation time or the alpha relaxation time. The alpha relaxation is what we refer to as the *slow dynamics* of the system. The alpha relaxation time is closely related to the viscosity of the liquid, and as the viscosity grows upon cooling so does the time required to reach equilibrium. The increase of relaxation time and viscosity, the *viscous slowing down*, is a dramatic phenomenon at low temperatures because changes of the temperature by a few percent leads to changes in the relaxation time by several orders of magnitude. The viscous slowing down has the consequence that there is a temperature, *the glass transition temperature* T_g, at which the volume can no longer reach its equilibrium value within the time scale of a given cooling experiment. At lower temperatures the liquid will no longer be an equilibrium liquid because the structural relaxation of the liquid is *frozen in*. The non-equilibrium solid formed in this way is called a

glass. The volume of the glass is also dependent on temperature, but its temperature dependence is weaker than that of the liquid. This is so because the molecules in the liquid rearrange upon cooling while the glass contracts only due to a decrease in the distance between the molecules. The difference between the liquid and the glass responses to temperature changes gives rise to an abrupt change in slope on a $T - V$ plot. A typical plot is shown in figure 2.1. The change in the temperature dependence of the volume gives rise to a discontinuity in the expansivity when passing T_g. The heat capacity and other thermodynamical derivatives have equivalent discontinuities at T_g. If the glass is kept below $T_g$the liquid approaches equilibrium, though it happens slowly, and the volume and other properties are therefore time dependent; the glass *ages*. This means that strictly speaking the thermodynamic derivatives are not strictly well defined in the glass. It also leads to hysteresis in the system. The hysteresis is seen in the re-heating curve which is also indicated in figure 2.1.

The relaxation time increases very rapidly in the vicinity of T_g; this means that the aging processes are very slow already a few degrees below T_g. When considered at times shorter than the relaxation time the glass behaves like a solid in all senses. It is therefore possible to measure and assign meaningful "apparent" values to the properties of the glass, including the thermodynamical derivatives (figure 2.1).

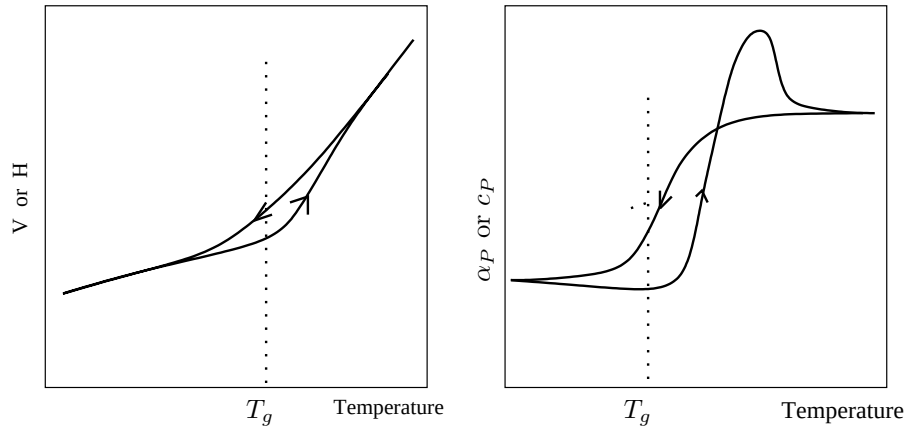

Figure 2.1: Illustration of the temperature dependence of volume, enthalpy and their temperature derivatives when passing the glass transition.

The freezing in of the liquid at T_g has the consequence that the structure of the glass is that of the liquid when it fell out of equilibrium at T_g. The glass is hence a disordered solid, and it cannot be distinguished from a liquid from a structural point of view.

A liquid has a T_g that depends on the cooling rate (lower cooling rates give lower T_g).

Cooling at very high rates is called quenching. The glasses formed by quenching have larger specific volume because their properties are frozen in at a higher temperature and a corresponding higher volume. The term T_g is traditionally used about the temperature at which the liquid falls out of equilibrium when cooled at standard experimental rates [Ediger *et al.*, 1996]. This in practice happens at the temperature where the viscosity is 10^{12} Pas $\sim 10^{13}$ Pas and the alpha relaxation time (τ_α) is of the order 100 s $\sim$ 1000 s. The criterion $\tau_\alpha = 100$ s is often used as a definition of the glass transition temperature.

The traditional route to glass-formation is to cool the liquid at constant atmospheric pressure. However, the characteristic alpha relaxation time also increases when pressure is increased along an isotherm. This leads to a freezing in of the structural relaxation at a given pressure P_g, where the relaxation time has reached 100 s $\sim$ 1000 s. The effects of pressure and temperature on the viscous slowing down can be considered jointly by describing the alpha relaxation time as a function of the two: $\tau_\alpha(P,T)$. Based on this function it is possible to determine lines of constant alpha relaxation time in the parameter space defined by pressure and temperature. We shall refer to lines of constant relaxation time as *isochrones* and consider the $T_g(P)$ line as a special case of an isochrone.

It has been suggested that the viscous slowing down observed at atmospheric pressure is due to the decrease of the specific volume which follows from cooling [Cohen and Turnbull, 1959]. However, measurements of the relaxation time as a function of temperature and pressure have clearly shown that volume alone does not control the relaxation time. One way to illustrate this is by showing that the isochrones are not parallel to the isochores in the $T - P$ diagram.

The other extreme would be a situation where the relaxation time is only temperature dependent. The simplest model of the temperature dependence would be an activated behavior, where the viscosity or relaxation time is controlled by some temperature independent activation energy (E_a, measured in units of temperature). This would lead to an Arrhenius temperature dependence:

$$\eta = \eta_p \exp\left(\frac{E_a}{T}\right) \quad \text{and} \quad \tau = \tau_0 \exp\left(\frac{E_a}{T}\right), \tag{2.1.1}$$

where η_p and τ_0 are the high temperature limits of the viscosity and the alpha relaxation time respectively. Arrhenius behavior is actually (almost) followed by some systems (see below), but this is not the general case. The dependence on temperature is usually super-Arrhenius, i.e. stronger than the Arrhenius form. It is possible to keep the notion of an activated behavior by allowing the activation

energy in equation 2.1.1 to be temperature dependent. In most cases, it also appears that this activation energy is density (or pressure) dependent. Such an activation energy can formally be defined from the equation:

$$\tau_\alpha(\rho, T) = \tau_0 \exp\left(\frac{E(\rho, T)}{T}\right), \tag{2.1.2}$$

or a similar expression for the viscosity.

Within the last ten years there has been a lot of progress in mapping out the temperature and pressure (or T and density) dependences of the alpha relaxation time particularly in terms of the temperature and density dependences of $E(\rho, T)$. This approach is central to the present work. However, before presenting the findings in this field we shall take a step back and introduce some of the other central concepts and findings in the field. These latter are originally based on studies performed at constant atmospheric pressure.

In chapter 3 we return to the temperature and density dependence of the dynamics and at this point we will commence the central aim of the present thesis, namely to revisit (discuss and test) results obtained at atmospheric pressure by combining them with our knowledge of the influence of pressure on the dynamics of glasses and glass-forming liquids.

2.2 Fragility

The glass transition is, as described above the passage from a thermodynamic (metastable) equilibrium state to a non-equilibrium state. This transition is a natural consequence of the fact that the relaxation time of the system surpasses the timescale on which we are able to perform observations. In our opinion the main question is therefore not to understand the glass transition itself, but rather to understand why the relaxation time increases so dramatically when the liquid is cooled.

While the viscous slowing down is universal, there are still large variations to be found when comparing the temperature dependences seen in different liquids. The classification and description of systems according to this difference play a major role in the attempt to understand the universal features of the slowing down.

The concept of "fragility" [Angell, 1991] has become a standard scheme for characterizing the temperature dependence of the relaxation time (or viscosity) of a liquid. Fragility is a measure of how much this temperature dependence deviates

from Arrhenius form; characterizing a large departure from Arrhenius behavior as *fragile* and Arrhenius behavior as *strong*. This concept of "fragility" is usually illustrated by a so-called Angell plot (figure 2.2) in which the logarithm of the relaxation time (or viscosity) is shown as a function of the inverse temperature normalized by the glass transition temperature. An Arrhenius temperature dependence, that is a strong behavior (equation 2.1.1), yields a straight line with slope $log(\tau_g/\tau_0)$ in this type of plot, while a fragile behavior corresponds to a concave curve.

Several different measures have been suggested in order to quantify the fragility. They are essentially equivalent, but they also express slightly different interpretations of the concept itself.

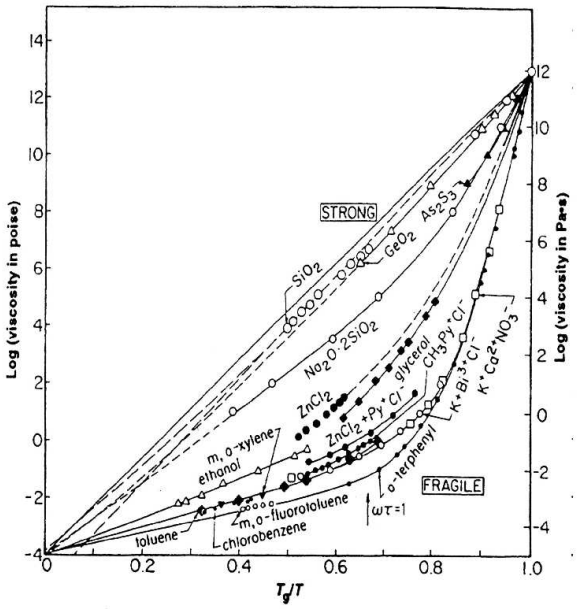

Figure 2.2: The logarithm of the viscosity as a function of the inverse temperature normalized by the glass transition temperature. Arrhenius temperature dependence, that is a strong behavior (equation 2.1.1) yields a straight line with slope $log(\tau_g/\tau_0)$ in this type of plot, while a fragile behavior corresponds a concave curve. This type of plot is often called an Angell plot. The figure is taken from Angell [1991].

The most common measure of fragility is the steepness index, which measures the low temperature limit of the slope of the curve in the Angell plot [Angell, 1991]. The steepness index is given by

$$m = \frac{\mathrm{d}\log_{10}(\tau)}{\mathrm{d}\,T_g/T}(T = T_g). \tag{2.2.1}$$

m equals 16 for strong liquids if it is assume that $\log_{10}\tau_0 = -14$ and increases with

increasing fragility, with $m \sim 80$ being a typical value for a fragile molecular liquid.

Another possible approach is to fragility is to use master curves, actually fitting formulae, for the temperature dependence of the relaxation time. The most common formula is the Vogel-Fulcher-Tammann (VTF) function [Vogel, 1921]

$$\log_{10}(\tau) = A_{VF} + \frac{B}{(T - T_0)} \tag{2.2.2}$$

where A_{VF}, B and T_0 are constants. The three constants give (as far as the fit is good) a characterization of the global temperature dependence and as a result of the fragility. More specifically, fragility is characterized by a unique dimensionless parameter $D = B/T_0$, a small D characterizing a fragile system and a large one a strong system (formally when $T \to 0$ one recovers an Arrhenius behavior and $D \to \infty$). A similar characterization has been proposed on the basis of the frustration limited domain theory, fragility being then measured by a unique dimensionless parameter related to the frustration strength [Kivelson and Tarjus, 1998]. The connection between these fragility parameters and the steepness index is found by differentiation of the expression for the relaxation time: ($m = BT_g(T_g - T_0)^{-2}$) in the case of equation 2.2.2. The VTF-function is useful for interpolating data over several decades in relaxation time, but it is rarely found to give a good fit over the total range from τ_0 to τ_g. The fragility so determined will therefore depend quite strongly on the range of data included when fitting (see also section 5.2).

On the other hand, one can consider the fragility as something that changes with temperature (or relaxation time). From figure 2.2 it is clear that even the liquids which become non-Arrhenian at low temperatures have an essentially Arrhenius temperature dependence at high temperatures. This change in temperature dependence can hence be considered as a transition from a strong to a fragile domain for a given liquid.

The steepness index is originally defined at T_g but it can in principle be evaluated at other times, leading to a more general definition, in which the steepness index becomes relaxation time dependent

$$m(\tau) = \frac{\mathrm{d}\log_{10}\tau}{\mathrm{d}T_\tau/T} \tag{2.2.3}$$

where $\tau(T_\tau) = \tau$ defines T_τ.

Inserting the Arrhenius temperature dependence (equation 2.1.1) we get the time

dependent steepness index of a strong liquid,

$$m_{strong}(\tau) = \log_{10}(\tau/\tau_0) \tag{2.2.4}$$

which takes the value $m_{strong}(\tau = 100s) = 16$ (assuming $\tau_0 = -14$) and decreases to $m_{strong}(\tau = \tau_0) = 0$ as relaxation time is decreased. The steepness index is thus relaxation time dependent even for a strong system and the steepness index is therefore an inconvenient measure of the relaxation time dependent departure from Arrhenius. A measure more adapted for studying the fragility at different times is the index introduced by Olsen [Dyre and Olsen, 2004].

$$I(\tau) = -\frac{\mathrm{d}\log E(T)}{\mathrm{d}\log T}(T = T_\tau) \tag{2.2.5}$$

where $E(T)$ is a temperature dependent activation energy defined by $E(T) = T(\ln\tau - ln\tau_0)$. The Olsen index will take the value 0 at all relaxation times in a system where the relaxation time has an Arrhenius temperature dependence. Systems with a typical fragile behavior have $I = 0$ at high temperatures (short relaxation times) where they follow an Arrhenius behavior and an increasing I as the temperature dependence starts departing from Arrhenius. Typical values of I at $T_g(\tau = 100s)$ are ranging from I=3 to I=8 corresponding to steepness indices of m=47 to m=127.

There is a one to one relation between the steepness index and the Olsen index [Dyre, 2006], and one finds that the Olsen index essentially is the relaxation time dependent steepness index normalized to its value in a strong liquid,

$$I(\tau) = \frac{m(\tau)}{\log_{10}\left(\frac{\tau}{\tau_0}\right)} - 1 = \frac{m(\tau)}{m_{strong}(\tau)} - 1, \tag{2.2.6}$$

where the last equality follows from inserting equation 2.2.4. This type of normalized fragility measure has also been suggested by Granato [2002].

In this work we mostly use the conventional shorthand of referring to the steepness index evaluated at T_g as the fragility of a given system. We also use the Olsen index, mainly conceptually, in some situations where it is particularly convenient.

2.3 Non-Debye relaxation

The understanding of the super-Arrhenius temperature dependence of the alpha relaxation discussed above is maybe the main question in the research field of glass-forming systems. Another key question is to understand the characteristics of the

(linear) relaxation itself.

Simple Debye (exponential) relaxation is very rarely found in viscous liquids, hence the relaxation is non-Debye. Instead the relaxation function is found to be broader than a Debye relaxation. This can either be described as a superposition of Debye processes or by one of the numerous phenomenological fitting functions which are used in the area (see section 5.3 for details).

The most general question, concerning non-Debye relaxation in macroscopic quantities, is whether it is due to an intrinsic non-Debye relaxation or whether the macroscopic departure from Debye relaxation is due to heterogeneous dynamics. In a homogeneous relaxation all the relaxation entities have relaxations identical to the average relaxation. In a heterogeneous scenario every entity behaves differently, and in this case it is possible that the individual relaxation is Debye. In this case the non-Debye average relaxation stems from the fact that it is an average. [Richert, 2002]

In the last decade there has been extensive studies, using different experimental techniques and simulations, of the heterogeneity of viscous liquids. The most common conclusion is that the liquid is structurally homogeneous but that the dynamics is heterogenous. This means that different parts of the liquid move in different ways at a given time. [Richert, 2002]

A stronger deviation of the relaxation functions from an exponential dependence on time (a more important "stretching") has been found to correlate with larger fragility Böhmer *et al.* [1993]. The reported correlation between the two is one of the bases of the common belief that both fragility and stretching are signatures of the cooperativity of the liquid dynamics. We discuss this correlation in chapter 5.

2.4 Energy landscape

The most detailed question we could ask regarding the dynamics of the liquid is of course the following: Where are all the molecules as a function of time? That is, we ask the time dependence of $3N$ coordinates (N being the number of particles). But these $3N$ values are of course not accessible (except in computer simulations) and moreover it is difficult, if not impossible, to interpret such an overwhelming amount of information. It is, however, very common in glass physics to think and argue in terms of the potential energy landscape. The energy landscape is a hypersurface which describes the potential energy of the system as a function of the $3N$ configurational coordinates. The dynamics of the liquid is viewed as an exploration

of this landscape. This view of the liquid dynamics was introduced by Goldstein [1969] and it has been used extensively in the last decade as a tool in computer simulations, theoretical work, as well as in the interpretation of experimental results.

In the temperature interval just above T_g, it is generally agreed on that the structural relaxation is dominated by hopping between energy minima, whereas short time dynamics can be viewed as vibrational modes around the minima. The structural relaxation and its timescale are thus governed by the typical barrier heights between the minima (directly related to the notion of the activation energy discussed in the preceding section), while the vibrations are governed by the shape of the minima. The characteristic time scales of the vibrations is $\sim 10^{-13}$ s while the alpha relaxation at temperatures close to T_g has a characteristic time of seconds, which means that there is a tremendous separation between the relevant time scales.

2.5 Fast dynamics and glassy dynamics

The vibrations mentioned above are also present in the glass, after the structural relaxation has been frozen in. This means that the dynamics of the liquid at short times is directly related to the dynamics in the glass. However, for the purpose of later discussions we would like to make a distinction between the fast (or high frequency) dynamics of the equilibrium liquid and the dynamics in glass.

2.5.1 Fast dynamics in equilibrium

At short times the liquid behaves like a solid in the sense that the particles appear to be just vibrating around equilibrium positions. At longer times the particles will start diffusing. The characteristic time defining the transition from solid-like behavior to liquid-like behavior is the structural (alpha-) relaxation time discussed in section 2.1. If the alpha relaxation time is very short, as it is the case at high temperatures in non-viscous liquids, then it is not possible to make this separation in different dynamic regimes.

Another way of picturing the separation of time scales in viscous liquids is to consider the response to an external perturbation. If the liquid is subjected to, say an instantaneous hydrostatic pressure, then it will be compressed by some finite quantity (quasi) instantaneously. This response is solid-like; it corresponds to the movements of all the particles against an effective spring constant at their current position. As time is increased the particles have time to rearrange, the liquid relaxes, and a new equilibrium is obtained.

The dynamics with characteristic time shorter than the alpha relaxation time is what we refer to as *fast dynamics* or equivalently *high frequency dynamics*.

Measurements at a fixed frequency or fixed time scale naturally do not probe the time dependence of the dynamics. What they see is the dynamics on the time scale they are sensitive to. This means that a measurement with a timescale considerably shorter than the alpha relaxation time (or a frequency larger than the inverse alpha relaxation time) only probes the fast dynamics of the viscous liquid.

The fast (linear) dynamics are, like any other property of the (viscous) liquid, dependent on the thermodynamic state determined by temperature and pressure. This means that properties characterizing fast dynamics, such as high frequency moduli, short time mean square displacement, etc. depend (sometimes strongly) on pressure and temperature. Fast dynamics are sometimes referred to as glassy dynamics because it is the dynamics at times faster than the structural relaxation, which governs the glass transition. However, fast dynamics measured in viscous liquids in their thermodynamic (metastable) equilibrium state are equilibrium properties. This means that they are not history nor path dependent, but uniquely determined by the thermodynamic state of the liquid.

2.5.2 Glassy dynamics

The glassy state is, as described in section 2.1, a non-equilibrium state obtained when the alpha relaxation becomes so long that it is not possible to wait for the liquid to reach its thermodynamic equilibrium. All dynamical processes happening on the alpha relaxation time scale are consequently frozen in. However the particles keep moving in a solid-like manner, hence the fast dynamics stay active, and these remaining dynamical processes are what we refer to as *glassy dynamics*. The important distinction between the fast dynamics in the equilibrium liquid and the glassy dynamics is that the former is a well defined equilibrium quantity while the latter is a property of the non-equilibrium glassy state. The properties characterizing glassy dynamics are therefore in principle path and time dependent, as is characteristic for properties in non-equilibrium systems.

It turns out that the path and time dependence of the glassy properties is only seen when the glass is subjected to quite extreme treatments such as very long waiting times, quenching or compression in the liquid and decompression in the glass. When the glass is cooled under “normal” isobaric conditions, not much happens under cooling. When the glass is formed the structure is frozen in, and this has the phenomenological consequence that most properties have very weak temperature

dependence in the glass. This is also true for the glassy dynamics, which as we shall see in many cases just correspond to the fast dynamics in the liquid measured at T_g. From the phenomenological point of view it is thus found that the major difference between glassy dynamics and fast dynamics in the liquid is that the former is virtually temperature independent while the latter can depend on temperature. Figure 2.3 illustrates how the glassy dynamics correspond to the fast dynamics.

2.5.3 Time scales - the actual phenomenology

In the above we have considered dynamics happening at two different timescales. The actual phenomenology of glass-forming liquids is somewhat more complicated and also system dependent. The structural relaxation often bifurcates in two separate relaxations when the structural relaxation time is lower than approximately 10^{-5} s. The process which appears in addition to the alpha process is faster and it has lower intensity as well as weaker temperature dependence. It is referred to as the slow beta-relaxation or the Johari Goldstein (JG) beta relaxation. The position of the bifurcation point differs by several decades from system to system (and from one experimental probe to another). Moreover, there are also numerous systems where this separation in two relaxations is not detectable. The JG-beta relaxation is faster than the alpha relaxation and it also stays active when the glass is formed. As such it is part of the fast as well as of the glassy dynamics. We shall deal a bit with the JG-process when discussing the interpretation of dielectric spectroscopy in chapter 5. However, the fast dynamics studied and discussed in this work occurs on a still faster time scale, namely in the pico-nanosecond range.

2.6 Fragility and other properties

The fragility introduced in section 2.2 is the central point in our description of slow dynamics, and the main problem addressed here is to understand which properties (if any) relate to the fragility. The ultimate goal is to look for causal relations and to use them to understand what governs the viscous slowing down.

We have already mentioned in section 2.3 that the fragility has been suggested to correlate to the departure from Debye relaxation. This correlation is just one among a large body of properties that have been suggested to correlate to the fragility.

The excess in entropy of the liquid as compared to that of the glass has been found to decrease faster as a function of decreasing temperature in fragile liquids than

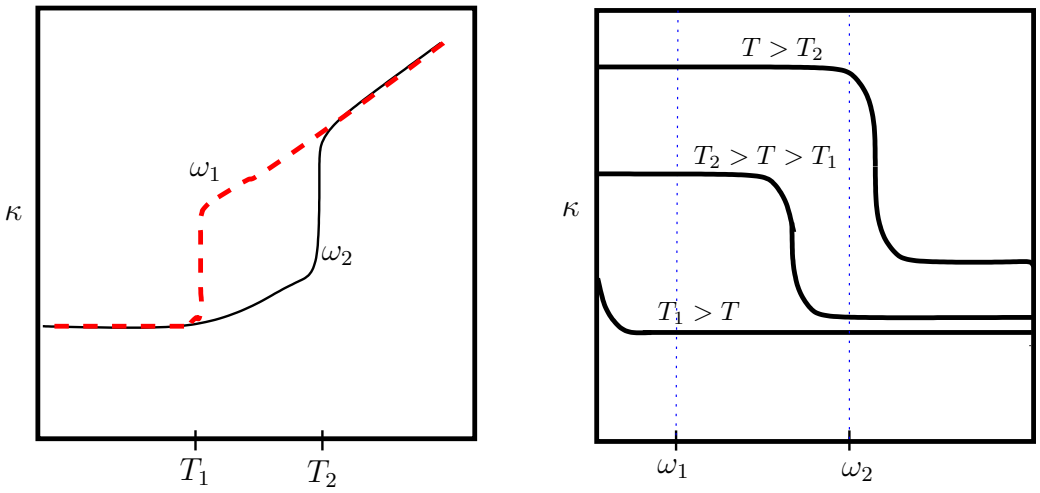

Figure 2.3: The left figure shows an idealized illustration of the temperature dependence of the compressibility measured at two different time scales, a high frequency ω_2 and a low frequency ω_1 (with the latter corresponding to the timescale of the cooling rate). The right figure shows the corresponding frequency dependent compressibility at different temperatures. The jump in level is the signature of the temperature dependent alpha relaxation. The probe frequencies are indicated with vertical lines. The figure illustrates three domains. At temperatures above T_2 the two probes measure the same low frequency compressibility - its value decreasing with decreasing temperature. At temperatures lower than T_2 but higher than T_1 the high frequency probe measures the high frequency value of the compressibility while the low frequency probe measures the low frequency value. Both high frequency and low frequency compressibility depend on temperature, but not *a priori* with the same temperature dependence. At temperatures lower than T_1 both probes see the high frequency compressibility. This is so because the alpha relaxation time has become longer than the time scale of both probes. The alpha relaxation is also longer than the characteristic time of cooling - meaning that liquid is frozen in its glassy state. This freezing in also has the consequence that the measured compressibility does not change significantly with decreasing temperature. The value of the compressibility in the glass corresponds to the high frequency compressibility at T_g when the liquid is frozen in.

in strong liquids. This correlation is originally rationalized in terms of the Adam-Gibbs model [Adam and Gibbs, 1965]. The Adam-Gibbs model is based on the notion of cooperative dynamics that demand larger and larger cooperative regions as the temperature is lowered. It is moreover assumed that the activation energy is proportional to the volume of the rearranging region. The fundamental assumptions of the model have been questioned several times, but the model continues to play an important role in the community and it has also re-derived from different starting points [Kirkpatrick *et al.*, 1989; Bouchaud and Biroli, 2004]. The related idea, that there is a dynamical length scale in the liquid which grows in the liquid as it is cooled, is widely believed to play an important role for understanding the viscous slowing down. The existence of dynamical length scales have been demonstrated by several techniques [Ediger, 2000; Berthier *et al.*, 2005], but it remains unclear if they are all interrelated and if the length scale or its evolution with temperature is related to fragility.

In this work we focus on results which suggest a relation between the viscous slowing down and other *dynamical* properties of the liquid or the glass. We particularly consider four situations, namely: the correlation between fragility and stretching of the alpha relaxation [Böhmer *et al.*, 1993] in chapter 5, the correlation between fragility and a smaller ratio of elastic to inelastic signal in the X-ray Brillouin-spectra [Scopigno *et al.*, 2003] in chapter 6, the correlation between fragility and the short time mean square displacement, its absolute value [Ngai, 2000] and its temperature dependence [Dyre and Olsen, 2004; Buchenau and Zorn, 1992] in chapter 7, and the correlation between fragility and a lower relative intensity of the boson peak [Sokolov *et al.*, 1993] in chapter 8. Other correlations which might be related but which we do not treat directly are the correlation between fragility and a larger Poisson ratio [Novikov and Sokolov, 2004] and the correlation between fragility and a stronger temperature dependence of the elastic shear modulus, G_∞, in the viscous liquid [Dyre, 2006].

The different correlations are in most cases not understood and their validity is often controversial [Yannopoulos and Papatheodorou, 2000; Yannopoulos *et al.*, 2006 a; Huang and McKenna, 2001].

The aim is to use these empirical correlations between m_P and glassy properties in testing and developing models and theories of the dynamics in viscous liquids. The correlations are mostly found empirically as correlations to the fragility measured under *isobaric* conditions. In the other hand, the interpretation of the correlations is always that the property which correlates to fragility is related to the *temperature* dependence of the relaxation times. In the same vein computer-simulation as well

as theoretical attempts to understand these correlations, and fragility in general, mainly consider *isochoric* conditions, hence taking only into account the effect of temperature (e.g. [Parisi *et al.*, 2004; Bordat *et al.*, 2004; Srivastava and Das, 2001; Ruocco *et al.*, 2004]).

2.7 Relation between fast and slow dynamics

The correlations regarding the stretching, which was introduced in section 2.3, relates different aspects of the alpha relaxation in the liquid to each other. The three other correlations, which we shall consider, fall in a category of results in which glassy or short time dynamics are related to the viscous slowing down. The hypothesis that there is a relation between fast and slow dynamics is based on striking empirical results reported in literature over the last decade [Novikov and Sokolov, 2004; Scopigno *et al.*, 2003; Ngai, 2004; Sokolov *et al.*, 1993, 1997; Dyre and Olsen, 2004; Buchenau and Wischnewski, 2004; Buchenau and Zorn, 1992]. A number of these results (and earlier related results) are reviewed and combined by Dyre [2004, 2006]. Also, Novikov and Sokolov [2004] and Novikov *et al.* [2005] discuss a variety of this type of results and suggest that they are intimately connected to each other.

In the following we shortly define the high frequency and glassy properties that have been suggested to relate to the viscous slowing down. More technical details as well as discussions of the interpretations are given in chapters 6 to 8 where we study these properties, and particularly how they depend on pressure.

2.7.1 Nonergodicity factor

Scopigno *et al.* [2003] define the nonergodicity factor from the ratio of the central line intensity over the total intensity of the frequency dependent dynamical structure factor measured by inelastic X-ray scattering (IXS). The authors look at the temperature dependence of this quantity in the low temperature limit of the glass phase and find that the stronger this temperature dependence the more fragile the liquid (see also section 4.3.7 and chapter 6). This result indicates that a property measured deep in the glass holds information about the viscous slowing down. The intensity of the side peaks (figure 2.4) is governed by the characteristics of the vibrational modes (see section 4.3.7) and as a result by the curvature of the visited minima of the energy landscape. The correlation therefore suggests that the shape of the minima is related to other properties of the energy landscape [Scopigno *et al.*, 2003]. However, it is also possible to take a different view on the correlation

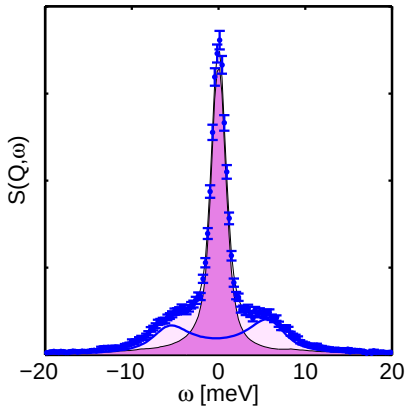

Figure 2.4: Dynamical structure factor measured by inelastic X-ray scattering (IXS). The nonergodicity factor is defined by the ratio of the central intensity over the total intensity.

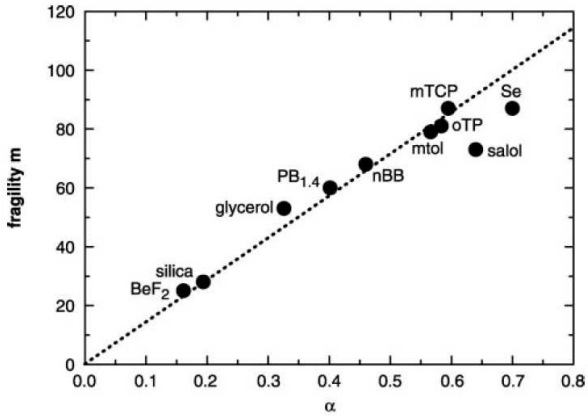

Figure 2.5: Correlation between fragility and the parameter α [Scopigno *et al.*, 2003]. α is a measure of the temperature dependence of the nonergodicity factor. See section 6.4.1.

and suggest that it is related to the intensity of the central peak [Buchenau and Wischnewski, 2004]. The central peak is a measure of the density fluctuation that are frozen in when the alpha relaxation is arrested at the glass transition. Hence, this view on the correlation points to a relation between the amplitude of the alpha relaxation at T_g and the temperature dependence of the alpha relaxation.

2.7.2 Mean squared displacement

The mean squared displacement is classically proportional to temperature in the harmonic approximation, where the shear and bulk moduli are constant. This linear behavior is often followed in the glass, but the temperature dependence of the short time mean squared displacement becomes stronger at temperatures above T_g (see figure 2.6). Moreover, the temperature dependence of the mean square displacement above T_g has been found to be stronger the more fragile the system is [Ngai, 2004]. In this situation it is therefore the high frequency (and not the glassy) dynamics of the equilibrium liquid that is related to fragility. Some of the interpretations of the finding are however very close to some of the notions suggested to understand the above result concerning the nonergodicity factor: namely, that the shape of the minima in the energy landscape are related to the energy barriers. In this view it is assumed that the vibrations stay essentially harmonic above T_g but that the curvature of the potential around the minima visited by the system changes as a function of temperature once the alpha relaxation becomes active. The change of curvature is expected to also change the barrier height and thereby the temperature dependence of the alpha relaxation time itself [Dyre and Olsen, 2004].

Another interpretation of the change in the temperature dependence of the mean square displacement is that it is related to the setting in of fast relaxational processes [Buchenau and Zorn, 1992; Ngai, 2000]. These processes are thought to serve as precursors of the alpha relaxation, with the alpha relaxation being faster the larger the amplitude of these relaxations.

There is in both views a subtle suggestion of a two way causality. A larger amplitude of the mean square displacement gives rise to a faster alpha relaxation, and the alpha relaxation itself changes the liquid structure and thereby changes the properties which govern the mean square displacement.

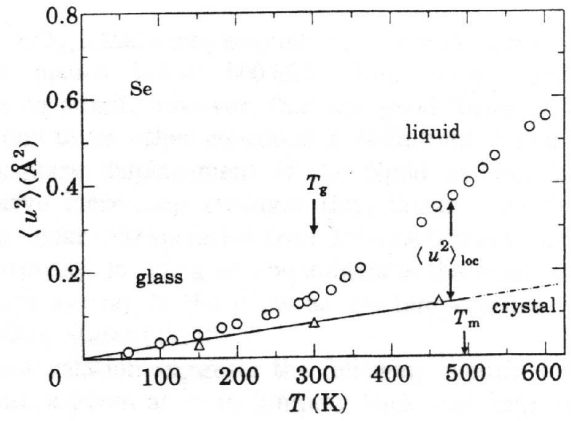

Figure 2.6: The mean square displacement of selenium as a function of temperature. It is clearly seen that there is a qualitative change in behavior at T_g. The authors find that the temperature dependence of $\langle u^2 \rangle_{loc}$ (indicated in the figure) is proportional to the temperature dependence of the logarithm of the alpha relaxation time, $\ln(\tau_\alpha)$. [Buchenau and Zorn, 1992]

2.7.3 Boson Peak

The low energy (<10 meV) vibrational modes in crystals are in general well described by the Debye model[1]. However, in glasses it is found that there is an excess in the vibrational density of states as compared to the Debye prediction. The origin of these extra modes is still controversial and has led to numerous experimental and theoretical studies (see also section 8.2). The boson peak is considered to be a characteristic feature of disordered solids. It is therefore common to the attempts made for explaining the boson peak to associate it with the "disorder strength" in the amorphous solid, even if the notion of disorder is different in different models.

The structure of a glass is, as earlier described, the frozen-in structure of the liquid. If the characteristics of the viscous slowing down occurs in terms of fragility, is either governed by structure or gives a signature in the structure, then it will lead to a different structure of liquids with different fragilities. This difference will be carried into the glass and leave a signature of the fragility in the structure of the glassy state. However, structure factor of amorphous solids describes the structure on a level where most features besides nearest-neighbor correlations are averaged out. Subtle aspects of the structure in glasses, such as possible heterogeneities, can therefore be detected only by indirect means.

[1]The Debye model is based on simple arguments in which the number of plane waves that "fit" in the Q-space are counted. It is described in introductory books on solid state physics and statistical physics, e.g. [Kittel, 1996; Bairlein, 1999].

The boson peak modes have an energy corresponding to the plane waves with nanometer wavelength. This leads to the expectation that it is the disorder on this length scale which will be determining for the boson peak. Similar length scales are often associated with the cooperative dynamics of the alpha relaxation close to the glass transition. [Leonforte *et al.*, 2006]

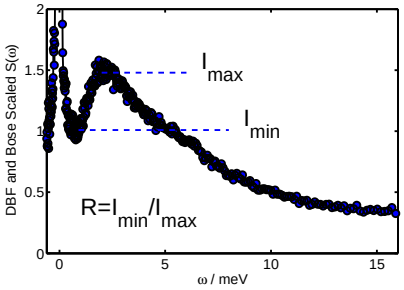

Figure 2.7: Incoherent dynamical structure factor measured by inelastic neutrons scattering (INS). It is illustrated of how to determine the ratio R which gives a measure of the relative boson peak intensity.

The most direct relation suggested between the boson peak in the glass and the slow dynamics in the liquid is the correlation between the relative boson peak intensity and fragility proposed by [Sokolov *et al.*, 1993, 1997] (see figures 2.7 and 2.8). It is speculated that this correlation means that strong systems have a larger degree of disorder than the fragile ones when the system is frozen in and the glass is formed [Novikov *et al.*, 2005].

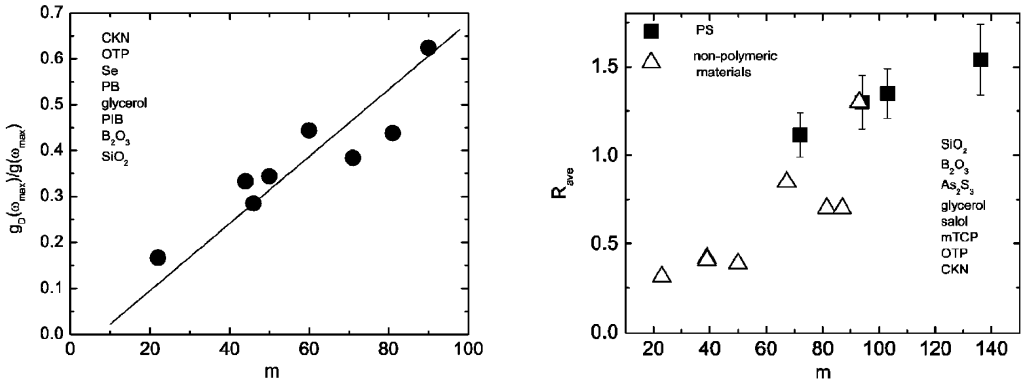

Figure 2.8: Correlation between m_P and relative boson peak intensity. The left figure shows the inverse boson peak intensity in terms of its amplitude over the Debye density of states $g(\omega)/g_D(\omega)$, the right figure shows the parameter R found as illustrated in figure 2.7. Both figures are from [Novikov *et al.*, 2005].

2.7.4 Other results

We shall shortly discuss two other results relating fast or glassy dynamics to the alpha relaxation. These results are not discussed nor tested in detail in this work, but are included here for completeness and because they have been suggested to relate to the results discussed above. Both these results concern the high frequency shear modulus of the liquid.

The shear modulus of a liquid goes to zero in the high temperature or low frequency limit while the bulk modulus is non-zero under all conditions. This means that longitudinal sound waves always are present in liquids, whereas shear modes exist only at low temperatures or short times, such that the probe frequency is faster than the alpha relaxation time $\tau_\alpha > 1/\omega_{probe}$. The non-zero shear modulus is thus a signature of being in a domain where the structural relaxation is frozen.

Shoving model

The shoving model [Dyre *et al.*, 1996] suggests that it is the high frequency shear modulus which controls the activation energy (equation 2.1.2). The rationale for suggesting that a high frequency property governs the alpha relaxation is that while the alpha relaxation is slow, the actual rearrangements (the hops in the energy landscape) happen on a short time scale. The choice of the shear modulus stems from a macroscopic elasticity theory calculation in which it is assumed that a local volume expansion is needed for the rearrangement to be possible. Such an expansion will in the simplest case of a spherical geometry be governed by the shear modulus. The shoving model is in one approximation[2] equivalent to a model where the activation energy is proportional to temperature over mean square displacement, $E(\rho, T) \propto T/\langle u^2 \rangle$. We follow Dyre [2006] and refer to the model in this form as the elastic model. We discus the elastic model in our study of the mean square displacement in chapter 7.

Poisson ratio

Novikov and Sokolov [2004] found from comparing about a dozen different glass formers that there is a correlation between fragility and the ratio of the bulk to the shear

[2]The equivalence follows from the fact that the shear modulus dominates over bulk modulus in determining the temperature dependence of the mean square displacement, see [Dyre and Olsen, 2004] for details.

modulus[3] K/G, meaning that a glass corresponding to a fragile liquid sustains bulk deformation better than shear deformation. The glassy moduli correspond to the high frequency moduli of the liquid at the glass transition (see section 2.5) and the correlation can therefore be expressed as a correlation to the ratio K_∞/G_∞ between the high frequency moduli in the liquid at T_g [Novikov *et al.*, 2005]. The authors moreover suggest that this correlation is directly related to the correlation suggested by Scopigno *et al.* [2003]. The argument is based on assuming that difference between high frequency and low frequency bulk moduli is much smaller than the high frequency shear modulus, $K_\infty - K_0 \ll G_\infty$. However, this assumption is not found to hold [Scopigno, 2007], rather the two are of similar size (e.g. [Barlow *et al.*, 1969; Christensen, 1994]). Lastly, it is worth mentioning that the correlation has been tested on a much larger set of glass-formers by Yannopoulos and Johari [2006] and Johari [2006], who demonstrated that different types of glass formers have different behaviors. The correlation does however seem to hold when comparing systems of the same class of glass-formers.

[3]The ratio K/G is larger the larger is the Poisson ratio $\sigma = \frac{3K/2G-1}{3K/2G+1}$, so this correlation implies a correlation between fragility and the Poisson ratio.

Résumeé du chapitre 3

Traditionnellement on forme un verre par refroidissement à pression atmosphérique, c'est à dire dans des conditions isobares. Le refroidissement isobare a deux effets simultanés sur le liquide : l'énergie thermique diminue et la densité augmente. La possibilité de former un verre soit par refroidissement isochore soit par compression isotherme montre bien que ces deux effets contribuent tous deux au ralentissement visqueux. Pour mieux comprendre le ralentissement visqueux et la transition vitreuse, il est donc important de pouvoir séparer l'effet de l'énergie thermique et l'effet de la densité. Ce type de séparation est uniquement possible si on a accès aux temps de relaxation (ou aux viscosités) et aux données PVT pour un même système. Durant les dix dernières années, de nombreuses études sur ce sujet ont permis d'aboutir à l'existence d'une loi d'échelle universelle.

Dans le premier paragraphe de ce chapitre, on introduit le formalisme nécessaire à la description de la dépendance en température et en densité du temps de relaxation. Le deuxième paragraphe résume l'émergence de cette loi d'échelle et ses conséquences.

Les corrélations proposées dans la littérature entre les caractéristiques dynamiques d'un liquide vitrifiable et sa fragilité ont toujours été proposées sur la base de données expérimentales mesurées à pression atmosphérique. Le but principal de cette thèse est de tester si les corrélations sont robustes en pression et d'utiliser la séparation entre effet de température et effet de densité pour mieux comprendre le sens physique de ces corrélations. Dans le dernier paragraphe de ce chapitre, on développe des arguments généraux dens ce sens, qui seront utiles dans les quatre chapitres suivants.

Chapter 3

What we learn from pressure experiments

In this chapter we first introduce earlier results on density and pressure dependence of the alpha relaxation (section 3.1 and 3.2) and next develope a framework in order to better understand different types of correlations with fragility (section 3.3 and 3.4).

The steepness index is mostly used as a measure of fragility, but the results and arguments, hold for other types of fragility criteria, e.g. the Olsen index just as well.

3.1 Isochoric and isobaric fragility

The measures of fragility which we introduce in section 2.2 are in their original form (implicitly) defined at constant atmospheric pressure because this is where most experiments are performed. For instance the steepness index is actually

$$m_P = \left.\frac{\partial \log_{10}(\tau)}{\partial T_\tau/T}\right|_P (T = T_\tau) \tag{3.1.1}$$

where the derivative is to be evaluated at T_τ. T_τ is defined as being the temperature at which the relaxation time reaches the value τ, e.g. $\tau = 100$ s. The conventional fragility is hence the *atmospheric pressure isobaric fragility*. However, the relaxation time can also be measured as a function of temperature along other isobars. This is illustrated in figure 3.1 where it can also be seen that the $T_\tau(P)$ increases when pressure increases. Isobaric fragility is well defined at any point on the isochronic

T_τ-line and isobaric fragility evaluated at a given relaxation time can be considered as a function of pressure. Empirically, it is most often found that isobaric fragility decreases with pressure, but it can also be increasing or virtually pressure independent [Roland *et al.*, 2005].

In addition to the isobaric fragility, it is also possible to define an isochoric fragility:

$$m_\rho = \left.\frac{\partial \log_{10}(\tau)}{\partial T_\tau/T}\right|_\rho (T = T_\tau). \tag{3.1.2}$$

The isochoric fragility is a measure of how much the temperature dependence of the relaxation time departs from Arrhenius when the liquid is subjected to isochoric cooling. Isochoric cooling is often performed in simulations which makes this distinction particularly important when comparing experimental and simulation results. Experimentally, it is difficult to perform isochoric cooling, but the isochoric derivative is nonetheless a well defined quantity.

The two fragilities are straightforwardly related by the chain rule of differentiation:

$$m_P = \left.\frac{\partial \log_{10}(\tau)}{\partial T_\tau/T}\right|_\rho (T = T_\tau) + \left.\frac{\partial \log_{10}(\tau)}{\partial \rho}\right|_T \left.\frac{\partial \rho}{\partial T_\tau/T}\right|_P (T = T_\tau) \tag{3.1.3}$$

$$= m_\rho + \left.\frac{\partial \log_{10}(\tau)}{\partial \rho}\right|_T \left.\frac{\partial \rho}{\partial T_\tau/T}\right|_P (T = T_\tau) \tag{3.1.4}$$

when both are evaluated at the same thermodynamic state point, e.g. at a given pressure P_1 defining $(T_\tau(P_1), \rho(P_1, T_\tau(P_1)))$. Expressed in this way the effects leading to the slowing down when cooling along an isobar is separated in two contributions: (i) the slowing down due to the decrease of temperature itself, and (ii) the contribution from the increase of density which follows as a consequence of decreasing temperature [Ferrer *et al.*, 1998].

Equation 3.1.3 can be rewritten to

$$m_P = m_\rho(1 - \alpha_P/\alpha_\tau) \tag{3.1.5}$$

where α_P is the isobaric expansivity $\alpha_P = \frac{-1}{\rho}\left.\frac{\partial \rho}{\partial T}\right|_P$ while $\alpha_\tau = \frac{-1}{\rho}\left.\frac{\partial \rho}{\partial T}\right|_\tau$ is the isochronic expansivity; that is a measure of volume changes as a function of temperature along an isochrone (a line where the alpha relaxation time is constant) [Ferrer *et al.*, 1998]. We want to stress that equation 3.1.5 is exact. It only builds on the definitions introduced and some standard differential algebra[1].

[1]The equivalence between equation 3.1.3 and 3.1.5 can be shown from the relation $\left.\frac{\partial \log_{10}(\tau)}{\partial T_\tau/T}\right|_\rho \left.\frac{\partial T_\tau/T}{\partial \rho}\right|_\tau \left.\frac{\partial \rho}{\partial log_\tau}\right|_T$=-1.

Equation 3.1.5 shows that the difference between m_P and m_ρ is determined by the ratio of two expansivities, α_τ and α_P. However, the difference is not determined by thermodynamics alone because α_τ contains dynamical information as well, since it is necessary to know the slope of the isochrone (e.g. the glass transition line) in order to evaluate it.

Turning now to the phenomenology, it is well known that α_P is positive[2]; α_τ on the other hand is negative because density increases as with increasing temperature when moving along an isochrone (see figure 3.1 a). By inserting these simple empirical facts in equation 3.1.5 can be seen that the isobaric fragility is larger than the isochoric fragility.

3.2 Empirical scaling law and some consequences

Within the last decade a substantial amount of relaxation time and viscosity data has been collected at different temperatures and pressures/densities, mainly by the use of dielectric spectroscopy. On the basis of the existing data it is relatively well established that the temperature and density dependence of the relaxation times can be expressed as first suggested by Alba-Simionesco *et al.* [2002], as

$$\tau(\rho, T) = F\left(\frac{e(\rho)}{T}\right). \tag{3.2.1}$$

The result is empirical and has been supported by the work of several groups for a variety of glass-forming liquids and polymers [Alba-Simionesco *et al.*, 2002; Tarjus *et al.*, 2004 a; Casalini and Roland, 2004; Roland *et al.*, 2005; Dreyfus *et al.*, 2004; Reiser *et al.*, 2005; Floudas *et al.*, 2006]. See also chapter 5 in this work.

3.2.1 The result and its history

The scaling can also be expressed in terms of the activation energy defined in equation 2.1.2. In fact is was first proposed in its general form from the idea of reducing the influence of density on the slowing down to a single density dependent activation energy scale [Alba-Simionesco *et al.*, 2002; Alba-Simionesco and Tarjus, 2006]:

$$\frac{E(\rho, T)}{E_\infty(\rho)} = \Phi\left(\frac{T}{E_\infty(\rho)}\right). \tag{3.2.2}$$

[2]Except for tetrahedral systems at certain temperatures, eg. water below 4°C.

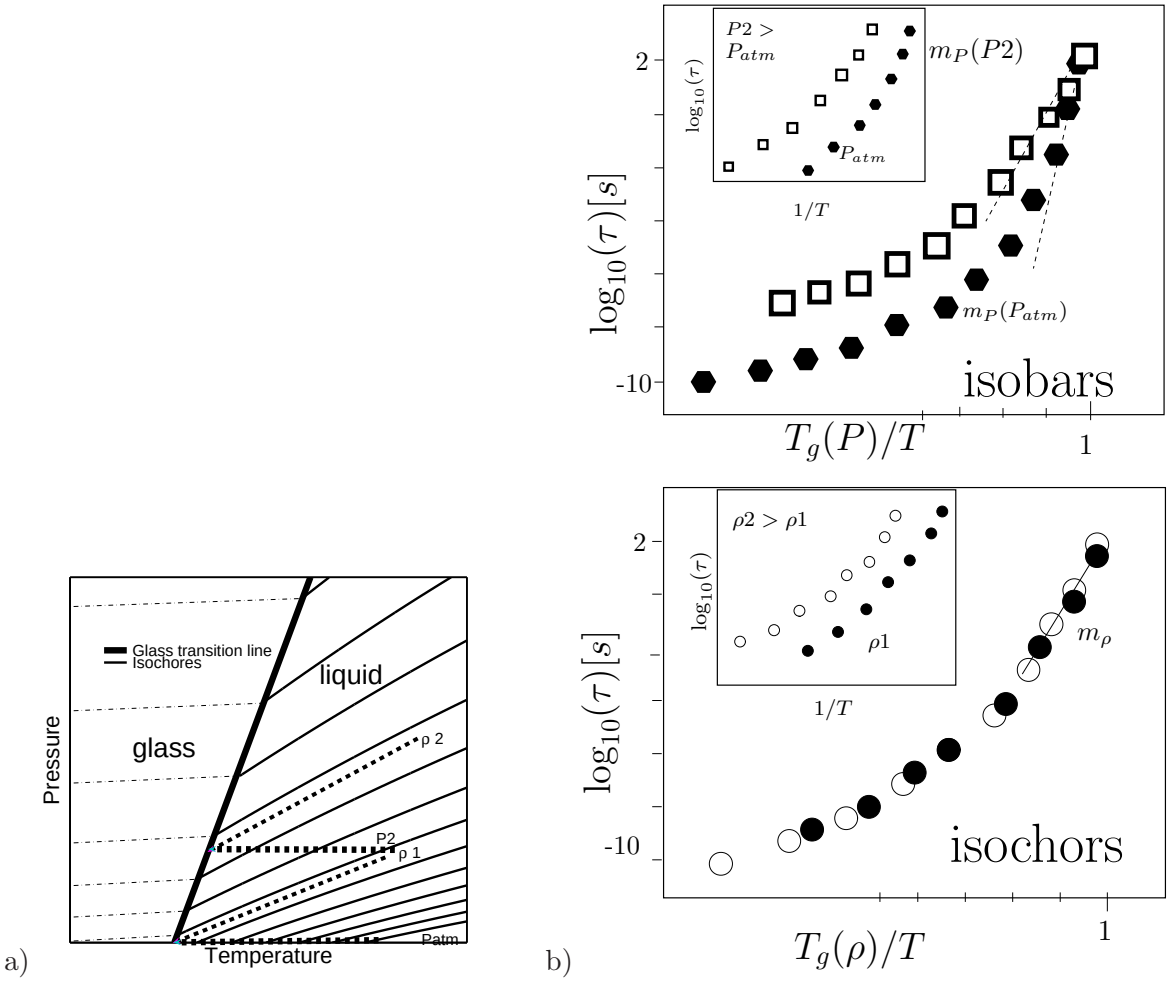

Figure 3.1: Typical PVT diagram for a glass-forming liquid. The glass transition line is the line where the structural relaxation time reaches $\tau = 100s$; the glass transition line is thus a specific example of an *isochrone*. The system is out of thermodynamical equilibrium on the left hand side of the glass transition line and the density is therefore path dependent. The thin dashed-dotted lines indicate typical glassy isochores corresponding to a density obtained by cooling isobarically after crossing the T_g line. The thin dashed lines illustrate two isochoric cooling paths in the liquid, while the bold dashed lines illustrate two isobaric cooling paths (P_{atm} and $P2 > P_{atm}$). b) top: typical temperature dependence of the relaxation time when followed at different isobars. It is illustrated that this temperature dependence persists after scaling with $T_g(P)$ leading to a pressure dependence in m_P. The open symbols correspond to the highest pressure (P2). b) bottom: typical temperature dependence of the relaxation time when followed along different isochores. The density dependence is canceled by scaling with $T_g(\rho)$ which means that m_ρ is density independent. The open symbols correspond to the highest density ($\rho 2 > \rho 1$).

The index ∞ refers to "$T \to \infty$" because Alba-Simionesco *et al.* [2002] associate $E_\infty(\rho)$ with the activation energy in the high-temperature liquid regime where the relaxation time has an Arrhenius temperature dependence.

Prior to this, partial results indicative, or compatible with, the above expression had been found. For instance, Tölle [2001] had shown that the relaxation time in liquid oTP at the nanosecond time scale measured at different pressures could be superimposed when comparing sets of temperature and pressure that correspond to the same value of $\Gamma = \rho T^{-1/4}$. This was motivated by the model of soft spheres in which the liquid is described by a single control parameter $\Gamma = \rho T^{-3/n}$, with n being the exponent of the repulsive pair potential r^{-n} [Hansen and McDonald, 1986]. Dreyfus *et al.* [2003] extended this finding for oTP in the viscous regime with relaxation times obtained from light scattering data.

The formulation by Tölle can be recast in the form proposed by Alba-Simionesco *et al.* [2002] if the density dependence of $E_\infty(\rho)$ is a power-law with exponent 4 as first demonstrated by Tarjus *et al.* [2004 a]. This can be seen from inserting equation 3.2.2 in equation 2.1.2 ($\tau(\rho,T) = \tau_0 \exp(E(\rho,T)/T)$):

$$\tau(\rho,T) = \tau_0 \exp\left(\frac{E_\infty(\rho)}{T}\Phi\left(\frac{T}{E_\infty(\rho)}\right)\right) \tag{3.2.3}$$

$$\tau(\rho,T) = F_1\left(\frac{E_\infty(\rho)}{T}\right), \tag{3.2.4}$$

which is equivalent to equation 3.2.1 and further inserting a power-law $E_\infty(\rho) = C\rho^x$

$$\tau(\rho,T) = F_1\left(C\frac{\rho^x}{T}\right) = F_2\left(\frac{\rho}{T^{1/x}}\right). \tag{3.2.5}$$

where F_1 is a system specific scaling function and $F_1(X) = F_2(X^{1/x})$.

[Chauty-Cailliaux, 2003] [Alba-Simionesco *et al.*, 2004] checked the above scaling on the dielectric data of several glass-forming polymers. In such system for which one does not have access to the high-temperature regime, hence to $E_\infty(\rho)$, they used different simple functional form for describing the density dependence of $E_\infty(\rho)$ or $e(\rho)$ (see equation 3.2.1), a linear and a power-law dependence, finding a similar quality of data collapse with the two functions. Casalini and Roland [2004] tested the power-law scaling on dielectric spectroscopy data in a number of different systems and found it to work provided the exponent 4 specific to oTP was allowed to become material dependent. They found it to vary from 0.13 for sorbitol up to more than 8. Dreyfus *et al.* [2004] did a similar compilation including also light scattering data. The scaling has since been tested on numerous systems (around 40) by several

different groups [Roland *et al.*, 2005; Reiser *et al.*, 2005; Floudas *et al.*, 2006]. The power law dependence is fulfilled to a good approximation for many systems, but the range in density is often too small to distinguish from other functional forms [Dreyfus *et al.*, 2004]. For DBP which we study in this work (chapter 5), we find significant deviations from the power-law form.

There are some differences in views regarding the physical interpretation of the scaling law, particularly regarding the meaning of the exponent x Tarjus *et al.* [2004 a,b]; Roland and Casalini [2004]. In this work we do not deal with the *explanation* of the scaling but rather consider its *consequences* when interpreting other results. It is therefore important to stress that, despite the controversies, there is agreement on the phenomenology, so far as to say that equation 3.2.1 gives a good description of the density and temperature dependences of the relaxation time.

If the density dependent energy $E_\infty(\rho)$ is determined from the high temperature Arrhenius behavior, then it is given in absolute units - and it is associated with a specific physical interpretation. However, most of the data leading to the scaling is obtained in the low temperature non-Arrhenius regime, and the energy is only obtained up to a multiplicative constant. We have therefore chosen the notation $e(\rho)$ rather than $E_\infty(\rho)$.

Most of the data supporting the scaling-law is from dielectric measurements in the 0.1 Hz-MHz range. Another limitation of the result is that all the data are on molecular liquids, Van der Waals bonded or hydrogen bonded or on polymers. Hence, strong glasses and inorganic glasses in general have not been studied so far. Nevertheless, the scaling law serves as a general description of the density and the temperature dependences of the alpha relaxation time in molecular liquids and polymers in the viscous regime where the super-Arrhenius behavior is seen. Note that if strong glasses have a strictly Arrhenius behavior, then equations 3.2.1 and 3.2.2 trivially apply with probably a weak or negligible dependence on density at least for moderate pressures.

3.2.2 The consequences on fragility

It can be seen directly from equation 3.2.1 that $X(\rho, T) = e(\rho)/T$, evaluated at $T_\tau(\rho)$ has the same value at all densities ($X_\tau = e(\rho)/T_\tau(\rho)$) if $T_\tau(\rho)$ is defined as the temperature where the relaxation time has a given value (e.g. $\tau = 100s$). Exploiting this fact, it is easy to show [Tarjus *et al.*, 2004 a; Alba-Simionesco and Tarjus, 2006] that the scaling law has the consequence that the isochoric fragility will be independent of density when evaluated at a T_τ corresponding to a given

relaxation time:

$$m_\rho = \left.\frac{\mathrm{d}\log_{10}(\tau)}{\mathrm{d}\,T_\tau/T}\right|_\rho (T=T_\tau) = F'(X_\tau)\frac{\mathrm{d}X}{\mathrm{d}T_\tau/T}(T=T_\tau) = X_\tau F'(X_\tau). \qquad (3.2.6)$$

The physical meaning is that temperature T_τ changes as a function of pressure, but the relaxation as a function of temperature will have the same degree of departure from Arrhenius along different isochores. We illustrate this situation in figure 3.1.

The fact that the relaxation time τ is constant when X is constant means that the isochronic expansion coefficient α_τ is equal to the expansion coefficient at constant X. Using this and the general result $\left(\frac{\partial\rho}{\partial T}\right)_X\left(\frac{\partial X}{\partial\rho}\right)_T\left(\frac{\partial T}{\partial X}\right)_\rho = -1$, it follows that

$$\frac{1}{\alpha_\tau} = -T\frac{\mathrm{d}\log e(\rho)}{\mathrm{d}\log\rho}, \qquad (3.2.7)$$

which inserted in equation 3.1.5 leads to

$$m_P = m_\rho\left(1+\alpha_P T_\tau\frac{\mathrm{d}\log e(\rho)}{\mathrm{d}\log\rho}\right), \qquad (3.2.8)$$

where m_P and m_ρ are again evaluated at a given relaxation time τ.

This expression illustrates that the relative effect of density on the slowing down upon isobaric cooling, i.e., the second term in the parentheses, can be decomposed into two parts: the temperature dependence of the density measured by $T_\tau\alpha_P = -\left.\frac{\partial\log\rho}{\partial\log T}\right|_P(T=T_\tau)$, and the density dependence of the activation energy, which is contained in $\frac{\mathrm{d}\log e(\rho)}{\mathrm{d}\log\rho}$.

Since m_ρ is constant along an isochrone, it follows from equations 3.1.5 and 3.2.8 that the change in m_P with increasing pressure is due to the change in $\alpha_P/\alpha_\tau = \alpha_P T_\tau\frac{\mathrm{d}\log e(\rho)}{\mathrm{d}\log\rho}$.

T_τ increases with pressure, $\alpha_P T_\tau(P)$ decreases, whereas $\frac{\mathrm{d}\log e(\rho)}{\mathrm{d}\log\rho} = x$ is often to a good approximation constant in the range of densities accessible[3]. The most common behavior seen from the data compiled by Roland *et al.* [2005] is that the isobaric fragility decreases or stays constant with pressure, with few exceptions. This indicates that the decrease of $\alpha_P T_g(P)$ usually dominates over the other factors.

[3]The DBP case at high density discussed in section 5.2.1 is one exception.

3.3 Correlations with fragility

As described in section 2.6 there is a flourishing variety of correlations between fragility and other properties of the liquids or its corresponding glass. These correlations hold a lot of empirical information which should be useful as guidelines and tests in the development of models and theories of the dynamics in viscous liquids. However in order for this to be possible, it is important to clarify if the correlations result from, and consequently unveil information on, the effect of density on the relaxation time, the intrinsic effect of temperature on the relaxation time, (or a balanced combination of the two). In the following we provide a framework for analyzing correlations between fragility and other properties of the liquid or glass by disentangling temperature and density effects [Niss and Alba-Simionesco, 2006; Niss *et al.*, 2007]. The arguments presented in this section are not relevant for correlations between fragility and the *temperature dependence* in the liquid of some other property. These types of correlations are specifically considered in section 3.4

3.3.1 Pressure and isobaric fragility

The correlations between fragility and other properties that have been suggested in literature all refer to the standard isobaric fragility. They are obtained empirically by plotting the property in question as a function of fragility (measured at T_g, $\tau \approx$ 100 s -1000 s). The plots obtained in this way are mostly very scattered, which is to be expected, because specific characteristics of the system can affect either the fragility or the property which is suggested to correlate with fragility.

Assuming that there is nothing special about atmospheric pressure (from the point of view of the liquid), then a strict correlation to m_P should follow this pressure dependence, where the property correlating to m_P is to be evaluated at the same pressure. Consequently, the simplest way in which pressure can be used to test this type of correlation is to view pressure as a smooth way to change the isobaric fragility without changing the chemistry of the system. The correlation between isobaric fragility and some chosen property can then be scrutinized by measuring both quantities as a function of pressure.

If the property in question has a pressure dependence which is consistent with the correlation then the situation would be the one illustrated in figure 3.2. This type of agreement would suggest that the property in question is sensitive to the same factors as the isobaric fragility, m_P.

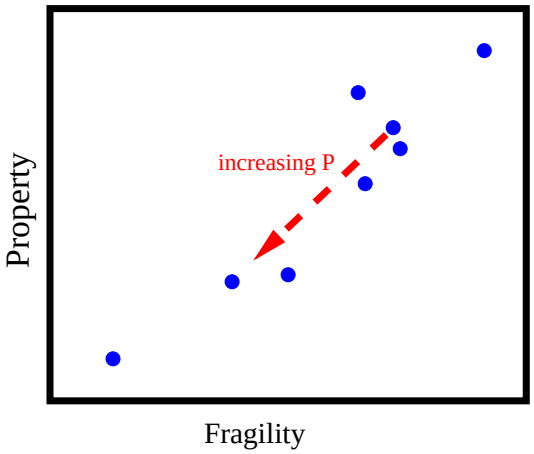

Figure 3.2: An illustration of how a correlation between a property and isobaric fragility could be most simply tested with pressure experiments (section 3.3.1).

3.3.2 Isochoric fragility

The existence of a correlation with fragility is always interpreted as indicating that the property in question is related to the effect of *temperature* on the structural relaxation. Moreover, computer simulations and theoretical attempts to understand these correlations, and viscous slowing down in general, mainly consider isochoric conditions, hence taking into account only the effect of temperature, see e.g. [Parisi *et al.*, 2004; Bordat *et al.*, 2004; Srivastava and Das, 2001; Ruocco *et al.*, 2004]. However, when a liquid is cooled isobarically the thermal energy decreases and the density increases at the same time and the isobaric fragility contains, as we have seen, information on both these effects.

According to the discussion in section 3.2.2, a property which is related to the pure effect of temperature should be correlated to the isochoric fragility. From equation 3.2.8 it can be seen that m_P contains m_ρ, and it has consistently been found by including a large amount of fragile and intermediate systems that m_ρ correlates to the ambient pressure m_P [Casalini and Roland, 2005 a]. It is therefore very possible that the correlations which have been proposed as correlations to the conventional isobaric fragility are in fact reminiscences of a more fundamental correlation to m_ρ.

The scaling described equation 3.2.1 must be taken as an empirical result and despite the variety of systems for which it has been shown to hold, there is no guarantee that it is universal. However, the scaling gives a rationalized picture of the pressure and temperature dependence of the relaxation time in the data obtained so far on polymers and molecular liquids. The emerging picture is that m_ρ is intrinsic to the system in the sense that it is density independent. A quantity correlating to the

pure temperature dependence of the relaxation time as it is measured by m_ρ should then possess the same intrinsic characteristic and be independent of pressure along the T_g-line. This means that the pressure dependence of a property can help clarify if it is fundamentally correlated to the intrinsic effect of temperature as measured by m_ρ or rather to the pressure dependent combined effect of density and temperature as measured by m_P.

3.3.3 The relative effect of density

In section 3.3.1 we have considered the pressure dependence of a correlation between a given property and the isobaric fragility without taking the consequences of the scaling law into account. If we now incorporate the scaling it follows that m_ρ is density independent and that the pressure dependence of $m_P(P)$ is due to a pressure dependence of α_P/α_τ (equation 3.1.3). This term is a measure of the relative effect of density on the viscous slowing down. This underlines that if a correlation follows the pressure dependence of m_P then it is because the property in question is not just related to the effect of temperature but also to the relative effect of density on the viscous slowing down.

A last situation which should also be considered is that the correlations suggested between m_P and other properties could in fact be a reflection of the effect of density on the relaxation time. That is they could fundamentally be correlations to α_P/α_τ. In general it is found, as mentioned above, that m_ρ is the dominating term governing m_P, which makes such a proposition appear unlikely. However, some of the most archetypal glass formers, glycerol, salol and oTP who cover a range of $m_P \approx 50$ to $m_P \approx 80$, have a very similar isochoric fragility ranging only from $m_\rho \approx 38$ to $m_\rho \approx 45$ (see appendix B). Hence, the difference in isobaric fragility found at atmospheric pressure when comparing these three liquids is not related to an intrinsically different response to temperature but rather to a different effect of the change in density upon isobaric cooling (just as it is the case for the change of $m_P(P)$ when changing pressure). If a property is related to the relative effect of density on the viscous slowing down, then it is expected to correlate with the ratio α_P/α_τ. This implies that the property in question should also follow the pressure dependence of α_P/α_τ, and as a consequence usually decrease with increasing pressure.

3.3.4 How to evaluate pressure dependence in the glass ?

The properties that are correlated to fragility are often considered at T_g. This is for example true for the stretching parameter β_{KWW} and for the boson peak intensity

measured in terms of the parameter R (see figure 2.7). The liquid is at (metastable) equilibrium at T_g and the quantity measured is thus a unique function of the state point. The fragilities m_P and m_ρ as well as the ratio α_P/α_τ are likewise uniquely defined at these state points. The comparison of the pressure dependence of a property and the fragilities is therefore naturally done by monitoring the relevant quantities along the glass transition line $T_g(P)$.

The situation is slightly more difficult when the considering a correlation between fragility and a property in the glass, because the glassy properties under pressure are path dependent [Chauty-Cailliaux, 2003]. We propose that the relevant path is the one followed by compressing in the equilibrium liquid and subsequently forming the glass by cooling. The glass formed in this way has a history equivalent to the glass formed at atmospheric pressure and the structure in which it is frozen is that corresponding to the equilibrium liquid at the same pressure. Secondly, one could in principle distinguish isobaric and isochoric cooling in the glass itself. However, the expansion coefficient in the glassy state is very small so that this difference can probably be ignored at least insofar as the dynamics appear to be harmonic.

3.3.5 Temperature dependence of a correlation

In the above we have focused on the pressure dependence of fragility and we have suggested that a correlation to fragility should be expected also to hold under pressure. A related question is the relation between dependence on the relaxation time (or equivalently on temperature) of the chosen property and of the fragility. Should a property correlated to fragility at T_g also be expected to have the same evolution as the fragility when temperature is raised? And what is the relevant high temperature-limit in the regime where the liquid follows the Arrhenius behavior? These questions are hardly meaningful if the property correlated to fragility is a glassy property. On the other hand they are relevant questions for a property in the liquid which correlates to fragility. In deed T_g is an arbitrary point and if a correlation is reported at T_g it should also be valid at other temperatures, at least when the liquid stays viscous and equilibrated. Extrapolation of the correlation to high temperatures and microscopic times may however be meaningless.

3.4 Temperature dependences

The fragility is sometimes suggested to correlate to the temperature dependence of another property in the liquid. In other words this means that the temperature

dependence of the alpha relaxation is suggested to relate to the temperature dependence of some other property. These types of correlations are typically based on simple models, e.g. the Adam Gibbs entropy model and the shoving model, but there are also purely empirical results of this type. Correlations between temperature dependence of a given property and fragility are somewhat different from the correlations discussed above. This is because the temperature dependence of a given property can also be considered both along isochoric paths and along isobaric paths. The natural expectation is then that the isobaric temperature dependence should relate to the isobaric fragility whereas the isochoric temperature dependence should relate to the isochoric fragility. For this scenario to be consistent one hence expects that the isochoric temperature dependence of the property in question should be the same along different isochores, corresponding to the fact that isochoric fragility is density independent.

We now specifically consider the case where the correlation is based on a model in which the alpha relaxation is considered to be activated with a temperature and density dependent activation energy which is governed by the property in question, namely

$$E(\rho,T) \propto G(\rho,T) \quad \text{with} \quad \tau = \tau_0 \exp\left(\frac{E(\rho,T)}{T}\right). \tag{3.4.1}$$

where $G(\rho,T)$ is the property suggested to govern the activation energy, for instance the high frequency shear modulus or the inverse configurational entropy.

The first observation is that such models predict that

$$\frac{G(\rho,T)}{T} = \text{constant} \quad \text{along an isochrone,} \tag{3.4.2}$$

with the isochrone being $T_g(P)$ or any other line of constant alpha relaxation time. Secondly, it follows that there is a direct relation between the temperature dependence of G and the fragility. In terms of the Olsen index, this can be expressed as

$$\left.\frac{\mathrm{d}\log G}{\mathrm{d}\log T}\right|_P (T=T_\tau) = I_P(\tau) \;\text{ and }\; \left.\frac{\mathrm{d}\log G}{\mathrm{d}\log T}\right|_\rho (T=T_\tau) = I_\rho(\tau). \tag{3.4.3}$$

The prediction holds at any given relaxation time and for isobaric and isochoric conditions alike.

The predictions presented so far (equation 3.4.2 and 3.4.3) are direct consequences of equation 3.4.1 without any further assumptions. If we now make the additional

assumption that the empirical scaling law (equation 3.2.1) holds, it moreover follows that the temperature and density dependence of G should be described in terms of an equivalent scaling law. This is most easily seen by inserting equation 3.4.1 in equation 3.2.2 (where Φ' below is proportional to Φ) :

$$G(\rho, T) = e(\rho)\Phi'\left(\frac{T}{e(\rho)}\right) \tag{3.4.4}$$

where $e(\rho)$ is the same as in (equation 3.2.1). See also [Alba-Simionesco and Tarjus, 2006] for similar ideas.

3.5 Summary

Fragility involves a variation with temperature that *a priori* depends on the thermodynamic path chosen, namely constant pressure (isobaric) versus constant density (isochoric) conditions. On the other hand, many quantities that have been correlated to fragility only depend on the thermodynamic state at which they are considered. It has been found empirically that the isochoric fragility is intrinsic in the sense that it is independent of pressure when evaluated along an isochrone. Based on these observation we conclude that a property which is related to the "pure" effect of temperature on the relaxation time, should correlate to the isochoric fragility (when comparing systems), and that it should possess the same type of intrinsic character; that is, they should be constant along an isochrone for a given system. Properties related to a combined effect of temperature and density are on the other hand expected to correlate with isobaric fragility and to have a pressure dependence that corresponds to its pressure dependence - that is most often decrease with increasing pressure. The ideas put forward in this chapter are a central part of the work and serve as a reference point for a large part of the analysis in the proceeding chapters.

Résumé du chapitre 4

Au cours de ce travail, on a étudié la dynamique des liquides vitrifiables et des verres par trois méthodes expérimentales : la spectroscopie diélectrique, la diffusion inélastique de neutrons et la diffusion inélastique de rayons X. Les principes de base de ces trois techniques sont présentés dans ce chapitre.

La spectroscopie diélectrique repose sur la mesure de la polarisation d'un échantillon lorsqu'il est soumis à un champ électrique. On mesure la fonction de réponse, qui est le rapport entre le champ électrique et la polarisation de l'échantillon. Les expériences effectuées au cours de cette thèse ont été réalisées en fréquence. Le champ électrique appliqué est alors sinusoïdal et la réponse est mesurée en fonction de la fréquence.

La diffusion inélastique repose sur l'interaction entre un faisceau incident, d'énergie et de vecteur d'onde bien définis, et l'échantillon. On mesure ensuite les modifications de l'énergie et du vecteur d'onde, qui dépendent des caractéristiques de l'échantillon. Si on travaille en diffusion neutronique incohérente, on a principalement accès au facteur de structure incohérent, donc à la fonction d'auto-corrélation. Lors des expériences de diffusion inélastique de rayons X, on mesure en revanche, le facteur de structure cohérent, et on sonde donc la dynamique collective de l'échantillon.

Chapter 4

Experimental techniques and observables

We have so far discussed dynamics in rather loose terms as the relaxations and vibrations taking place in the liquid. This notion will be precised in this chapter, where we introduce the dynamical variables we have studied, namely the dielectric response function and the dynamical structure factor. In this chapter we also present the basic principles for measuring these quantities while the experimental details related to the specific methods are given in the beginning of the respective chapters.

4.1 Linear response and two-time correlation functions

The dielectric response we study is the linear response and the dynamical structure factor is a two-time correlation function. Linear response and two time correlation function are related via the fluctuation dissipation theorem (FD-theorem), and they therefore probe the same type of information. We shall not consider other types of dynamical properties, even if non-linear response and four (or more) time correlation functions are also considered important for understanding the dynamics in viscous liquids.

4.1.1 Linear response

When a change of conditions is imposed on a system its equilibrium is changed and other properties will therefore adjust to this new equilibrium. Such a change in condition is called an *input* and the time dependent readjustment of other properties

is the *output response*. The input could for example be a change in pressure and the response considered could be the change in volume, as discussed when describing the glass transition in section 2.1.

If the input is small then the output will depend linearly on the input, and the response is then in the linear response regime. It can be described by

$$B(t) = \int_{-\infty}^{t} \mu(t-t')h(t')dt' = \int_{0}^{\infty} \mu(t')h(t-t')dt'. \tag{4.1.1}$$

with $B(t)$ being the time dependent output and $h(t)$ the applied input. $\mu(t)$ is called the memory function, as it describes how the system remembers its past.

The time (domain) response function, $R(t)$ is defined as the output of a Heaviside step input[1], $H(t)$,:

$$B(t) = \int_{-\infty}^{t} \mu(t-t')\, H(t')\, dt' = \int_{0}^{t} \mu(t')dt' = R(t), \tag{4.1.2}$$

from which it is seen that the memory function μ is the time derivative of the time response function. It is also seen that $R(t) = 0$ for $t < 0$.

Alternatively, the linear response can be considered in the frequency domain. The input will in this case be a harmonic oscillating function, $h(t) = h_0 \mathrm{e}^{i\omega t}$. Its linear output oscillates with the same frequency and can be described by the relative amplitude and phase with respect to the input. The ratio between the input and the output is called the frequency dependent response function $R(\omega)$:

$$B_0 \mathrm{e}^{i\omega t+\Phi} = R(\omega) h_0 \mathrm{e}^{i\omega t}. \tag{4.1.3}$$

Combining this definition with equations 4.1.1 and 4.1.2 it follows directly that the relation between the time domain response function and the frequency response function is given by

$$R(\omega) = \int_{0}^{\infty} \left.\frac{\mathrm{d}R(t)}{\mathrm{d}t}\right|_{t=t'} \mathrm{e}^{-i\omega t'} dt' \tag{4.1.4}$$

[1]The Heaviside input is defined by

$$H(t) = \begin{cases} 0 & t \leq 0 \\ 1 & t > 0 \end{cases}$$

.

4.1.2 Two time correlation and FD-theorem

The special interest in linear response stems from the fact that it is directly related to the thermally driven fluctuations which are present when the system is at thermodynamic equilibrium. The fluctuations can be described by two time correlation functions, the simplest case being a self correlation function,

$$C_{BB}(t) = \langle B(t)B(0)\rangle, \tag{4.1.5}$$

where the brackets denote ensemble average.

The FD-theorem gives the relation between linear response and time correlation functions

$$\frac{\mathrm{d}R(t)}{\mathrm{d}t} = -\frac{1}{k_B T}\frac{\mathrm{d}}{\mathrm{d}t}\langle B(t)B(0)\rangle\,. \tag{4.1.6}$$

The correlation functions are also considered in the frequency domain, namely in terms of their Fourier transforms

$$C_{BB}(\omega) = \frac{1}{2\pi}\int_{-\infty}^{\infty} C_{BB}(t)\exp(-i\omega t)dt. \tag{4.1.7}$$

Note that this definition is slightly different from the definition of the frequency dependent response function (equation 4.1.4). This difference in convention has the consequence that the frequency dependent response function and the frequency domain correlation function look differently even if they contain the same information. A relaxation process with a characteristic time τ will for example give a peak in the imaginary part of $R(\omega)$ at $\omega_{max} \sim 1/\tau$, while the signature in $C_{BB}(\omega)$ is a peak centered at $\omega = 0$ with a width given by $\Delta\omega \sim 1/\tau$.

4.2 Dielectric spectroscopy

Dielectric spectroscopy is one of the most employed techniques in the study of liquids close to the glass transition. The advantage of the technique is that it routinely covers 9 decades of frequency (or time) and can be extended to cover up to 18 decades [Lunkenheimer and Loidl, 2002]. The principle of the dielectric measurement is simple, which makes it relatively easy to employ control external parameters, such as temperature, cooling rates, or pressure. These factors have made dielectric spectroscopy indispensable in the study of both the temperature dependence of the relaxation time and the frequency (or time) dependence of the relaxation function in

viscous liquids. Particularly the studies of relaxation time as a function of pressure, which have lead to the scaling law presented in section 3.2 are to a very high degree obtained by dielectric spectroscopy. The drawback of dielectric spectroscopy, is that the exact relation between the macroscopic measured quantity and the microscopic dynamics is not totally understood. Also the relation between dielectric relaxation and other more fundamental macroscopic properties, such as the frequency dependent shear response remains unresolved.

In this section we present the basic principle of the dielectric spectroscopy as well as give a brief discussion of the physical interpretation. The details of our experimental setup are given in section 5.1.1.

4.2.1 Basic principle

The basic principle of dielectric spectroscopy is the measurement of a frequency dependent capacitance of a capacitor filled by the sample. The measuring capacitance is usually made up of two equally sized parallel plates. This gives the following capacitance of the empty capacitor,

$$C_0 = \frac{\epsilon_0 A}{d}, \tag{4.2.1}$$

where ϵ_0 is the vacuum permittivity, A is the area of the electrodes and d is the distance between the plates. The capacitance of the capacitor filled sample with sample is given by

$$C(\omega) = \epsilon(\omega)\frac{\epsilon A}{d} = \epsilon(\omega)C_0 \tag{4.2.2}$$

where $\epsilon(\omega)$ is the frequency dependent dielectric constant of the sample. Hence, $\epsilon(\omega)$ is determined by dividing the frequency dependent capacitance of the filled capacitor by the capacitance of the empty capacitor.

The dielectric constant, ϵ, of a sample is defined from the ratio between the applied electric field, $\boldsymbol{E}$, and the displacement field, $\boldsymbol{D}$,

$$\boldsymbol{P} = \epsilon_0 \chi \boldsymbol{E}_m, \quad \boldsymbol{D} = \boldsymbol{P} + \epsilon_0 \boldsymbol{E}_m = \epsilon_0(\chi + 1)\boldsymbol{E}_m = \epsilon_0 \epsilon \boldsymbol{E}_m, \tag{4.2.3}$$

where $\boldsymbol{P}$ is the polarization per unit volume. Thus, $\epsilon(\omega)$ is the response function (see section 4.1.1), when the applied macroscopic field is the input and the displacement field is the output.

The experiments reported and discussed in this study are all performed with low

fields strengths and the response is therefore linear. However, non-linear dielectric spectroscopy also has applications in the study of the viscous slowing down [Schiener *et al.*, 1997; Bouchaud and Biroli, 2005].

The polarization stems from two physical processes: polarization of the molecules due to a change in the electron distribution and reorientation of the permanent dipoles[2]. The adjustment of the electron cloude of the electrons happens essentially instantaneously and does not contribute to the frequency dependence of the signal. It is the reorientation of the molecules that gives rise to the frequency dependence and the measurement therefore give information of the fluctuations of molecular orientation of the equilibrium liquid (see also section 4.1).

4.2.2 Typical frequency dependence

At low frequencies the dielectric constant will approach its equilibrium value, ϵ_{eq}, asymptotically. At higher frequencies the molecules will no longer be able to adjust their orientation to the field and the real part of the dielectric constant approaches a new lower plateau value ϵ_h. The difference between high frequency and low frequency plateau value of the dielectric constant is called the dielectric relaxation strength of the sample. It is essentially governed by the dipole moment of the molecules.

Between the equilibrium value and the high frequency plateau the dielectric constant exhibits a loss peak because the motion of the dipolar molecules is out of phase with the applied field. The position of the peak corresponds to a characteristic time $\tau = 1/\omega_{max}$ which is associated with the alpha relaxation time of the liquid. The peak height is roughly proportional to the dielectric strength and thereby the dipole moment of the sample. This means that the larger the dipole moment of the molecule is, the more precise is dielectric spectroscopy. This frequency dependence is a signature of the alpha relaxation process as we have described it earlier.

4.2.3 Macroscopic versus microscopic

Dielectric spectroscopy is not sensitive to molecular motions which turn around the axis of the dipole. Moreover, in molecules with internal degrees of freedom it is very possible to imagine a situation, where the dipole is only related to some modes of motion, while others are totally decoupled from the dipole. This type of situation can lead to a big difference between dielectric relaxation and other macroscopic response functions [Olsen, 2006].

[2] If the molecule in question is not totally non-polar.

A more general problem with dielectric spectroscopy is the so-called local field problem, which we shall shortly discuss in the following. The problem has minor importance for the present work, we therefore refer to textbooks for more details (e.g. [Böttcher, 1973]). The specific implications of the local field problem on the interpretation of dielectric relaxation in viscous liquids is moreover discussed in [Niss and Jakobsen, 2003; Fatuzzo and Mason, 1967; Daz-Calleja *et al.*, 1993].

The microscopic response corresponding to the dielectric susceptibility is the polarizability, α, given by[3]

$$\boldsymbol{p} = \alpha \boldsymbol{E}_l, \tag{4.2.4}$$

where $\boldsymbol{p}$ is polarization of a molecule and $\boldsymbol{E}_l$ is the field strength applied over the dipole. The macroscopic polarization is given by the sum of the microscopic polarizations, $\sum \boldsymbol{p} = \boldsymbol{P}$. However, the relation between the macroscopic field in the sample and the field "seen" by a molecule is more complicated. This is because the field of the molecule itself is part of the macroscopic field while it is not part of the local field. The most common description of the local field is the Lorentz field, which leads to the Clausius-Mossotti approximation. The Lorentz field is the field in a spherical *imaginary* vacancy in the liquid. By imaginary is meant that the polarization of the rest of the liquid is calculated as if the dipole was there. This description includes the polarization of the surroundings due to the dipole, and the fact that this polarization gives rise to a field acting back on the dipole. Only the field from the dipole itself is excluded from the calculation of the local field.

The Lorentz field is given by

$$\boldsymbol{E}_l = \left(1 + \frac{\chi}{3}\right) \boldsymbol{E}_m = \frac{\epsilon + 2}{3} \boldsymbol{E}_m. \tag{4.2.5}$$

and inserting this in equation 4.2.4, combined with $\sum \boldsymbol{p} = \boldsymbol{P}$ and equation 4.2.3 gives the Clausius-Mossotti relation

$$\frac{\chi}{\chi + 3} = \frac{\epsilon - 1}{\epsilon + 2} = \frac{N\alpha}{3\epsilon_0}. \tag{4.2.6}$$

In deriving the Lorentz field it is assumed that the macroscopic field and the polarization of each molecule are always parallel. A general field, without this assumption is given by Onsager [1936]. However the Onsager field is not adequate when the response is frequency dependent, because the derivation assumes that the field and

[3]The polarizability should in general be a tensor quantity as field and polarization are not necessarily parallel. However, the average polarization $\langle \boldsymbol{p} \rangle$ will in isotropic material be parallel to the average local field $\langle E_l \rangle$, and this leads to a meaningful definition of α as a scalar.

the polarization are in phase. Fatuzzo and Mason [1967] propose a solution to this situation.

The most important problem with the conversion from microscopic polarizability to macroscopic susceptibility can already be anticipated from equation 4.2.6, namely that the two are not proportional. This has the consequence that the frequency dependence of characteristic time of $\alpha(\omega)$ will not be the same as the characteristic time of $\chi(\omega)$. Moreover, this difference will systematically depend on the strength of the dielectric relaxation, meaning that it will have a different consequence depending on the size of the molecular dipole moment. However, the differences are still smaller than the type of differences which are always found depending on which experimental probe one uses to study the liquid [Daz-Calleja *et al.*, 1993; Niss and Jakobsen, 2003]. In this work we shall not attempt to extract microscopic information from the dielectric relaxation, rather we follow the convention of taking the macroscopic dielectric relaxation time as a signature of the structural alpha relaxation.

4.3 Inelastic Scattering Experiments

Neutron and X-ray scattering have several common features and we therefore introduce them at the same time. We start from neutron scattering and generalize to X-ray scattering by comments at relevant places.[4]

We start by describing the principle of an inelastic scattering experiment and continue by discussing some practical limitations, regarding the energy and Q-domain that can be accessed by different probes. We subsequently give some general results which we shall later use in the analysis of our data. More technical information on the experimental methods is given in the relevant chapters.

4.3.1 The basic principle

The basic principle inelastic scattering experiment is to let an incoming beam of probe with a well defined energy and wave vector hit a sample and to measure the wave vector and energy of the scattered beam. The difference in momentum and energy between the incoming and the out coming beam has been lost to (or gained from) the sample. This exchange of energy and momentum will in the limit where the interaction between the probe and the sample is weak only depend on the properties of the sample (linear response). The property which is measured is called the cross

[4]Standard references for neutron scattering are [Lovesey, 1984; Squires, 1978], while inelastic X-ray scattering, is relatively new technique which is not yet treated in text books.

section, $\frac{\partial^2\sigma}{\partial\Omega\partial E}$. It is given by the number of out coming neutrons (or photons) per energy interval per solid angle per flux of the incoming probe. The cross section is a function of the transferred energy and angle at which the probe is scattered. The basic idea is illustrated in figure 4.1. Scattering where there is no transfer of energy is called *elastic* scattering. Scattering where there is an exchange of energy between the sample and the probe is called *inelastic* scattering. Contributions to the inelastic scattering which have their maximum at zero energy transfer are called *quasi-elastic* scattering.

The transfer in momentum is given by

$$\boldsymbol{Q} = \boldsymbol{Q}_{out} - \boldsymbol{Q}_{in} \tag{4.3.1}$$

and the transfer in energy is given by[5]

$$\hbar\omega = E_{out} - E_{in} \tag{4.3.2}$$

The relation between the scattering angle, 2θ, and the transfer of momentum is for elastic scattering given by $Q = 2Q_{in}sin(\theta)$, while the general relation is

$$Q = (Q_{in}^2 + Q_{out}^2 - 2Q_{in}Q_{out}cos(2\theta)) \tag{4.3.3}$$

Neutrons do not interact with the electrons but only with the nucleus of the atoms[6].

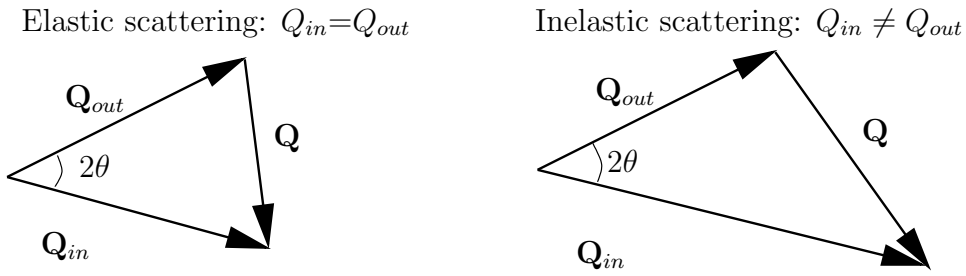

Figure 4.1: Illustration of the principle of a scattering experiment. The scattering is called elastic if there is no transfer of energy between the probe and the sample.

The interaction is extremely short ranged as compared to the distances we are interested in. The corresponding potential is therefore described by a Dirac delta function, the Fermi pseudo-potential $V(\boldsymbol{r}) = b\delta(\boldsymbol{R} - \boldsymbol{r})$ where $\boldsymbol{R}$ is the position of

[5]In this chapter we refer to ω as a quantity of dimension inverse time. However, the difference between angular velocity and energy is just a $\hbar$. The actual measurement is a measure of the transferred energy, and we measure ω units of energy (meV) in chapters 6 to 8.

[6]Ignoring the magnetic interaction between the neutron and the electron, because it plays no role in the type of systems we consider.

the neutron and $\boldsymbol{r}$ is the position of the nucleus. b is the scattering length of the nucleus, this quantity depends on the spin state of the nucleus and can hence differ for different atoms of the same species.

The calculation of the scattering cross section is based on the following assumptions. (i) That the neutron can always both before and after scattering, be described by a plane wave. (ii) That the neutron is only scattered once by the sample (iii) The probability of a transition where the neutron goes from state $\boldsymbol{Q}$ to $\boldsymbol{Q}'$ and the sample goes from λ to λ' is given by first order perturbation theory "Fermis Golden rule", meaning that it is proportional to the matrix element $|\langle \boldsymbol{Q}'\lambda'|V|\boldsymbol{Q}\lambda\rangle|^2$.

The result is the basic expression for the partial differential cross-section

$$\frac{\partial^2\sigma}{\partial\Omega\partial E} = \frac{Q_{out}}{Q_{in}}\frac{1}{2\pi\hbar}\sum_{i,j} b_i b_j \int_{-\infty}^{\infty} \langle \exp(-i\boldsymbol{Q}\cdot\boldsymbol{r}_i(0))\exp(i\boldsymbol{Q}\cdot\boldsymbol{r}_j(t))\rangle \exp(-i\omega t)\,\mathrm{d}t. \tag{4.3.4}$$

where the sums over i and j are to be taken over all the atoms in the system.

In the case of photons it is the interaction with the electrons that strongly dominates over the interaction with the nucleus. The dominating term is due to Thomson scattering which describes the coupling between the electronic current and the electric photon field[7]. When using photons in the study of the structure and dynamics on an intermolecular scale it is assumed that the electrons have a fixed position with respect to the nucleus (the adiabatic approximation). By doing so it becomes possible to factor out the relative positions of the electrons in a form factor. (The expression for the cross section is given the next section). The form factor then plays a role similar to that of the scattering length in neutron scattering. The two major differences between the scattering length and the form factor is (i) the form factor is Q-dependent and this leads to an intrinsic decrease of intensity as Q increases. (ii) the magnitude of the form factor is proportional to the number of electrons meaning that larger atoms give larger contribution to the scattering.

4.3.2 Coherent and Incoherent Scattering

The scattering length b depends on the spin state of the nucleus interacting with the neutron beam. Since we consider scattering from a large system $b_i b_j$ is replaced by its average value $\overline{b_i b_j}$. Assuming that b_i and b_j are statistically independent it

[7]Considering only Thomson scattering means that we again ignore magnetic interactions.

follows that

$$\overline{b_i b_j} = \overline{b}^2 \text{ for } j \neq i \text{ and } \overline{b_i b_j} = \overline{b^2} \text{ for } j = i. \tag{4.3.5}$$

consequently

$$\sum_{i,j} \overline{b_i b_j} = \sum_{i \neq j} \overline{b}^2 + \sum_j \overline{b^2} \tag{4.3.6}$$

$$= \sum_{i,j} \overline{b}^2 + \sum_j \left(\overline{b^2} - \sum_j \overline{b}^2 \right) \tag{4.3.7}$$

where the second equality follows from adding and subtraction the term $\sum_j \overline{b}^2$. Based on this, one defines the coherent and the incoherent scattering cross sections as

$$\sigma_{coh} = 4\pi \overline{b}^2 \text{ and } \sigma_{inc} = 4\pi \left(\overline{b^2} - \overline{b}^2 \right). \tag{4.3.8}$$

Using these expressions it is possible to separate the sum in equation 4.3.4 in two terms.

$$\frac{\partial^2 \sigma}{\partial \Omega \partial E} = \left(\frac{\partial^2 \sigma}{\partial \Omega \partial E} \right)_{coh} + \left(\frac{\partial^2 \sigma}{\partial \Omega \partial E} \right)_{inc} \tag{4.3.9}$$

where

$$\left(\frac{\partial^2 \sigma}{\partial \Omega \partial E} \right)_{coh} = \frac{\sigma_{coh}}{4\pi} \frac{Q_{out}}{Q_{in}} \frac{1}{2\pi\hbar} \sum_{i,j} \int_{-\infty}^{\infty} \langle \exp(-i\boldsymbol{Q} \cdot \boldsymbol{r}_i(0)) \exp(i\boldsymbol{Q} \cdot \boldsymbol{r}_j(t)) \rangle \exp(-i\omega t)\, \mathrm{d}t. \tag{4.3.10}$$

and

$$\left(\frac{\partial^2 \sigma}{\partial \Omega \partial E} \right)_{inc} = \frac{\sigma_{inc}}{4\pi} \frac{Q_{out}}{Q_{in}} \frac{1}{2\pi\hbar} \sum_{j} \int_{-\infty}^{\infty} \langle \exp(-i\boldsymbol{Q} \cdot \boldsymbol{r}_j(0)) \exp(i\boldsymbol{Q} \cdot \boldsymbol{r}_j(t)) \rangle \exp(-i\omega t)\, \mathrm{d}t, \tag{4.3.11}$$

In the case of X-ray scattering we replace the scattering length by the form factor, $|f(Q)|$, which is the same for all the molecules of a given species. A sample consisting of only one species therefore only gives rise to coherent X-ray scattering. The

expression for the cross section reads

$$\left(\frac{\partial^2\sigma}{\partial\Omega\partial E}\right)_{Xray} = \left(\frac{e^2}{4\pi\epsilon_0 m_e c^2}\right)^2 (\boldsymbol{e}_{in}\cdot\boldsymbol{e}_{out})^2 |f(Q)|^2 \frac{Q_{out}}{Q_{in}} \frac{1}{2\pi\hbar} \sum_{i,j}\int_{-\infty}^{\infty} \langle \exp(-i\boldsymbol{Q}\cdot\boldsymbol{r}_i(0))\exp(i\boldsymbol{Q}\cdot\boldsymbol{r}_j(t))\rangle \exp(-i\omega t)\,\mathrm{d}t. \tag{4.3.12}$$

where e and m_e is the charge and mass of the electron, c is the speed of light, ϵ_0 and $\boldsymbol{e}_{in}$ and $\boldsymbol{e}_{out}$ are the polarizations of the incoming and outgoing beams respectively.

4.3.3 X-ray and Neutrons in Practice

Scattering cross sections

In the above we have already touched upon one difference between neutron and X-ray scattering. Namely that the intensity of X-ray scattering is given by the form factor, which yields purely coherent scattering (in mono component systems) and which gives rise to stronger scattering the larger the atom is. The neutron scattering length on the other hand, is dependent on the spin state of the nucleus the variation of which differs from atom to atom. The systems we study are organic systems which have a large amount of hydrogens. Hydrogen has an incoherent cross section which is an order of magnitude larger than the total cross section of the other atoms in our systems. We therefore neglect the coherent contribution to the scattering and consider our neutron scattering data to be incoherent.

Transmission and multiple scattering

One of the assumptions in deriving the expression for the scattering cross section is that the probe is not scattered more than once before it leaves the sample. However, the scattering probability for neutrons in hydrogenated samples is high. It is therefore necessary to use samples of submillimeter thickness in order to have less than 10% of the neutrons be scattered.

4.3.4 The dynamical range

The maximal Q-value which can be studied by elastic scattering from a given probe is given by $2Q_{in}$. The smallest value is given by $Q_{min} = Q_{in}sin(2\theta_{min})$, where θ_{min} is the smallest angle at which the outgoing neutrons are detected. This means that the Q-range studied will be of same order of magnitude as the Q-value of the

probe used. Thermal neutrons and X-ray in the keV range both have Q-vectors of the order of magnitude 1 Å^{-1} such that $1/Q$ is comparable to the characteristic distances between nearest neighbors in condensed matter. Both probes are therefore well suited for studying structure in matter unlike for example visible light, which probes Q values that are 3 orders of magnitude smaller.

The energy loss of the probe is of course limited by the energy of the probe itself, the neutron can not loose more energy than it has. There is moreover for a given Q-value an additional limitation because the transfer of energy and momentum are interdependent. This is the so called kinematic limitation. It is anticipated from inserting the relation between energy and momentum in equation 4.3.3. This relation is not the same for neutrons and photons. For neutrons we have

$$E_{neutron} = \frac{\hbar^2 Q_{neutron}^2}{2m_{neutron}} \tag{4.3.13}$$

while the relation for photons is

$$E_{photon} = \hbar\, c\, Q_{photon}, \tag{4.3.14}$$

where c is the speed of light. The difference between the expressions above lead to different kinematic limitations, even if there are kinematic limitations in both cases. However, kinematic limitation does not have any practical importance for inelastic X-ray scattering because the energy transfers of interest when studying dynamics on an intermolecular scale is of the order of magnitude meV while the energy of the X-ray is in the keV range. Inelastic X-ray scattering has therefore given access to a domain in energy-Q-space which where not accessible by neutrons.

The transfer of energy in a real experiment is always given by a certain resolution. The resolution function is the actual measured signal in a situation where an ideal experiment would have given a delta function. The measured signal is therefore in general given by a convolution of the ideal signal and the resolution function. The shape and width of the resolution is in most cases determined empirically. It depends on the scattering geometry, the characteristics of the beam (monochromation and collimation) and on how precisely the change in energy can be measured. The total energy of thermal neutrons is of the same order of magnitude as the transfer of energy and this is why neutron scattering is the classical technique for this type of study. The relative resolution needed in X-ray scattering is on the other hand of the order of magnitude 10^{-7}. The achievement of such a high resolution is amazing, however the resolution in absolute values is still far from matching that obtained by high resolution neutron scattering.

4.3.5 Correlation functions

The intermediate scattering function is defined as[8]

$$I_{coh}(\boldsymbol{Q},t) = \frac{1}{N}\sum_{i,j}\langle \exp(-i\boldsymbol{Q}\cdot\boldsymbol{r}_i(0))\exp(i\boldsymbol{Q}\cdot\boldsymbol{r}_j(t))\rangle \tag{4.3.15}$$

and its time Fourier transform is called the dynamical structure factor

$$S_{coh}(\boldsymbol{Q},\omega) = \frac{1}{2\pi\hbar}\int_{-\infty}^{\infty} I_{coh}(\boldsymbol{Q},t)\exp(-i\omega t)\,\mathrm{d}t. \tag{4.3.16}$$

Equivalent definitions are used for the incoherent scattering yielding the following expression for the total scattering cross section.

$$\frac{\partial^2\sigma}{\partial\Omega\partial E} = N\frac{Q_{out}}{Q_{in}}\frac{\sigma_{coh}}{4\pi}S_{coh}(\boldsymbol{Q},\omega) + N\frac{Q_{out}}{Q_{in}}\frac{\sigma_{inc}}{4\pi}S_{inc}(\boldsymbol{Q},\omega). \tag{4.3.17}$$

For X-ray scattering it follows from equation 4.3.12 that the cross section is given by

$$\left(\frac{\partial^2\sigma}{\partial\Omega\partial E}\right)_{Xray} = N\quad\left(\frac{e^2}{4\pi\epsilon_0 m_e c^2}\right)^2(\boldsymbol{e}_i\cdot\boldsymbol{e}_f)^2|f(Q)|^2\frac{Q_{out}}{Q_{in}}S_{coh}(\boldsymbol{Q},\omega) \tag{4.3.18}$$

4.3.6 General Results - limiting behavior

In this work we study the temperature dependence of the elastic and the integrated scattered intensity both in the coherent and the incoherent case. In the following section we therefore spend some time on the details of the information that can be extracted from these quantities. Particularly the differences between the coherent and the incoherent cases are considered. Results that hold for both the coherent and the incoherent case are given without the subscript *coh* or *inc*.

Short time limit

The static structure factor, $S(\boldsymbol{Q})$, is defined as the integral over energy of the dynamic structure factor. Combining this definition with equation 4.3.16, it is seen that the static structure factor is equal to the intermediate scattering function at time zero, $S(\boldsymbol{Q}) = I(\boldsymbol{Q}, t = 0)$:

[8]The correlation functions which we introduce in this section are also described in [Lovesey, 1984] and [Squires, 1978]. Solids are not so treated in this frame in introductory textbooks, because the spatial crystalline solids leads to a simpler description. Relevant references on the liquid state include [Egelstaff, 1994; Hansen and McDonald, 1986; Boon and Yip, 1980].

$$\begin{aligned} S(\boldsymbol{Q}) &= \int_{-\infty}^{\infty} S(\boldsymbol{Q},\omega)\,\mathrm{d}\hbar\omega \\ &= \int_{-\infty}^{\infty} \frac{1}{2\pi\hbar}\int_{-\infty}^{\infty} I(\boldsymbol{Q},t)\exp(-i\omega t)\,\mathrm{d}t\,\mathrm{d}\omega \\ &= \int_{-\infty}^{\infty} I(\boldsymbol{Q},t)\frac{1}{2\pi\hbar}\int_{-\infty}^{\infty} \exp(-i\omega t)\,\mathrm{d}\hbar\omega\,\mathrm{d}t \\ &= \int_{-\infty}^{\infty} I(\boldsymbol{Q},t)\delta(t)\,\mathrm{d}t = I(\boldsymbol{Q},t=0). \end{aligned} \tag{4.3.19}$$

The coherent static structure factor holds information of the structure of the system, it is in fact the space Fourier transform of the pair correlation function. The incoherent structure factor on the other hand, does not hold any information as it is always equal to one:

$$S_{inc}(\boldsymbol{Q}) = I_{inc}(\boldsymbol{Q},t=0) = \langle \exp(-i\boldsymbol{Q}\cdot\boldsymbol{r}_j(0))\exp(i\boldsymbol{Q}\cdot\boldsymbol{r}_j(0))\rangle = 1. \tag{4.3.20}$$

Long time limit

Consider now the case where $I(\boldsymbol{Q},t)$ has a finite value in its long time limit. It can then be expressed as a sum of a time independent and a time dependent term

$$I(\boldsymbol{Q},t) = I_\infty(\boldsymbol{Q}) + I_t(\boldsymbol{Q},t) \;\text{ where }\; I_t(\boldsymbol{Q},t)\to 0 \text{ for } t\to\infty. \tag{4.3.21}$$

Fourier transforming this to get the dynamical structure factor yields

$$\begin{aligned} S(\boldsymbol{Q},\omega) &= \frac{1}{2\pi\hbar}\int_{-\infty}^{\infty} I_\infty(\boldsymbol{Q})\exp(-i\omega t)\,\mathrm{d}t + \frac{1}{2\pi\hbar}\int_{-\infty}^{\infty} I_t(\boldsymbol{Q},t)\exp(-i\omega t)\,\mathrm{d}t \\ &= I_\infty(\boldsymbol{Q})\delta(\hbar\omega) + \frac{1}{2\pi\hbar}\int_{-\infty}^{\infty} I_t(\boldsymbol{Q},t)\exp(-i\omega t)\,\mathrm{d}t. \end{aligned} \tag{4.3.22}$$

From this, it is seen that the dynamical structure factor will have a peak at $\omega = 0$ and that the intensity of this peak is given by the long time value of the intermediate scattering function, $I_\infty(\boldsymbol{Q})$. Note that the second term does not have strictly zero intensity at $\omega = 0$.

4.3.7 Simple model - solid

Consider a solid, disordered or crystalline. There is no diffusion in the system, which means that the particles are essentially vibrating (harmonic or not) around a fixed position in space. In the case of a crystal, this position is the equilibrium position

in the lattice. In the case of the disordered solid this position is less well defined. However, it is in both cases possible to describe the time dependent position of the particle by a sum of a time dependent and a time independent term:

$$\boldsymbol{r}_i(t) = \boldsymbol{r}_{i,eq} + \boldsymbol{u}_i(t) \tag{4.3.23}$$

where $u_i(t)$ has a finite maximum value corresponding to the furthest distance of the particle from its "equilibrium" position, $\boldsymbol{r}_i$. For the incoherent intermediate scattering this gives

$$\begin{aligned} I_{inc}(\boldsymbol{Q},t) &= \langle \exp(-i\boldsymbol{Q}\cdot\{\boldsymbol{r}_{i,eq}+\boldsymbol{u}_i(0)\})\exp(i\boldsymbol{Q}\cdot\{\boldsymbol{r}_{i,eq}+\boldsymbol{u}_i(t)\})\rangle \\ &= \langle \exp(-i\boldsymbol{Q}\cdot\boldsymbol{u}_i(0))\exp(i\boldsymbol{Q}\cdot\boldsymbol{u}_i(t))\rangle \exp(-i\boldsymbol{Q}\cdot\{\boldsymbol{r}_{i,eq}-\boldsymbol{r}_{i,eq}\}) \\ &= \langle \exp(-i\boldsymbol{Q}\cdot\boldsymbol{u}_i(0))\exp(i\boldsymbol{Q}\cdot\boldsymbol{u}_i(t))\rangle. \end{aligned} \tag{4.3.24}$$

Here we again see that the incoherent signal holds no information of the structure of the system, as it depends only on the dynamic part, $\boldsymbol{u}_i(t)$, of the particle position $\boldsymbol{r}_i(t)$.

The coherent intermediate scattering function following from equation 4.3.23 is given by

$$\begin{aligned} I_{coh}(\boldsymbol{Q},t) &= \frac{1}{N}\sum_{i,j}\langle \exp(-i\boldsymbol{Q}\cdot\{\boldsymbol{r}_{i,eq}+\boldsymbol{u}_i(0)\})\exp(i\boldsymbol{Q}\cdot\{\boldsymbol{r}_{j,eq}+\boldsymbol{u}_j(t)\})\rangle \\ &= \frac{1}{N}\sum_{i,j}\langle \exp(-i\boldsymbol{Q}\cdot\{\boldsymbol{r}_{i,eq}-\boldsymbol{r}_{j,eq}\})\exp(-i\boldsymbol{Q}\cdot\boldsymbol{u}_i(0))\exp(i\boldsymbol{Q}\cdot\boldsymbol{u}_j(t))\rangle. \end{aligned}$$

One can now define a structure factor corresponding to the structure of given by the "equilibrium" position of the particles. We call this structure factor the *inherent structure* structure factor $S_{is,coh}(Q)$

$$S_{is,coh}(\boldsymbol{Q}) = \frac{1}{N}\sum_{i,j}\langle \exp(-i\boldsymbol{Q}\cdot\{\boldsymbol{r}_{i,eq}-\boldsymbol{r}_{j,eq}\})\rangle = \sum_i \langle \exp(-i\boldsymbol{Q}\cdot\boldsymbol{r}'_{i,eq})\rangle \tag{4.3.25}$$

where $\boldsymbol{r}'_{i,eq} = \boldsymbol{r}_{i,eq} - \boldsymbol{r}_{j,eq}$ and the $\langle\ \rangle$ denote ensemble average. Note that *inherent structure* structure factor differs from the actual structure factor of the system, $S_{is,coh}(\boldsymbol{Q}) \neq I(\boldsymbol{Q}, t=0) = S(\boldsymbol{Q})$ because

$$\boldsymbol{u}_i(0) \neq \boldsymbol{u}_j(0) \ \text{ and therefore } \ \exp(-i\boldsymbol{Q}\cdot\boldsymbol{u}_i(0))\exp(i\boldsymbol{Q}\cdot\boldsymbol{u}_j(0)) \neq 1. \tag{4.3.26}$$

There is a difference between the static structure factor $S_{coh}(\boldsymbol{Q})$ which describes the particles in a snapshot where they will be displaced from their equilibrium position

and the inherent structure factor $S_{is,coh}(\boldsymbol{Q})$ which describes the structure when the particles are at their equilibrium position. In the incoherent case on the other hand, we compare the position of one particle to its own position and $S_{inc}(\boldsymbol{Q}) = 1$ because a particle is in the same position as itself at time $t = 0$, while $S_{is,inc}(\boldsymbol{Q}) = 1$ because a particle has the same equilibrium position as itself.

Long time limit - Gaussian solid

The displacement $\boldsymbol{u}_i(0)$ and $\boldsymbol{u}_i(t)$ of the same particle at different times, which appear in the expression for the incoherent scattering function (Eq. 4.3.24), will obviously be correlated at short times. The same is true for the displacements of different particles $\boldsymbol{u}_i(0)$ and $\boldsymbol{u}_j(t)$. In this latter case the correlations will moreover depend on the displacement between the two particles $(\boldsymbol{r}_i - \boldsymbol{r}_j)$ which is the reason why the inherent structure factor cannot be taken outside as a factor in equation 4.3.25. In the long time limit we may assume that all these correlations are lost. Moreover, we may assume that the average long time dynamics of all particles are the same (eliminating the difference between $\boldsymbol{u}_i$ and $\boldsymbol{u}_j$) and that the system is time homogeneous such that the ensemble average $\langle \boldsymbol{u}(t) \rangle$ is independent of time. Combining these assumptions we get for the incoherent case:

$$\lim_{t\to\infty} I_{inc}(\boldsymbol{Q}, t) = \langle \exp(2\boldsymbol{Q} \cdot \boldsymbol{u}) \rangle, \tag{4.3.27}$$

The factor $\langle \exp(2\boldsymbol{Q} \cdot \boldsymbol{u}) \rangle$ is called the Debye Waller factor. Since the total intensity $S_{inc}(\boldsymbol{Q}) = 1$ at all $\boldsymbol{Q}$-values (and under all conditions) it follows that the ratio of the elastic to the total intensity is also equal to $\exp(-2W)$. The coherent analogue to equation 4.3.27 reads:

$$\lim_{t\to\infty} I_{coh}(\boldsymbol{Q}, t) = S_{is,coh}(\boldsymbol{Q}) \langle \exp(2\boldsymbol{Q} \cdot \boldsymbol{u}) \rangle \tag{4.3.28}$$

It is seen that the elastic intensity is given by $\exp(-2W) S_{is,coh}(\boldsymbol{Q}) \delta(\omega)$. This result is exploited when determining the structure of materials, particularly crystals in which case the $\boldsymbol{Q}$-dependence of $S_{is,coh}(\boldsymbol{Q})$ is a sum of delta functions - Bragg peaks.

By making additionally two assumptions we may give a more explicit expression for the Debye Waller factor. In disordered systems and cubic Bravais crystals we moreover have that the average of $\boldsymbol{Q} \cdot \boldsymbol{u}$ is independent of the direction of $\boldsymbol{Q}$. We assume that this is true and include also the assumption that the probability function of the displacement $\boldsymbol{u}$ is Gaussian. This last assumption holds for harmonic vibrations

(see also section 4.3.8). Combining all this we get

$$\lim_{t\to\infty} I_{inc}(\boldsymbol{Q},t) = \exp\left(-\frac{Q^2\langle u^2\rangle}{3}\right). \tag{4.3.29}$$

We use the above expression in order to calculate the mean square displacement from measured elastic intensities in chapter 7. The analogous result in the coherent case reads

$$\lim_{t\to\infty} I_{coh}(\boldsymbol{Q},t) = S_{is}(\boldsymbol{Q})\exp\left(-\frac{Q^2\langle u^2\rangle}{3}\right). \tag{4.3.30}$$

The incoherent intermediate scattering function goes from $I_{inc}(\boldsymbol{Q},t=0)=1$ to $I_{inc}(\boldsymbol{Q},t=\infty)=\exp(-2W)$. The coherent intermediate scattering function goes from $I_{coh}(\boldsymbol{Q},t=0)=S_{coh}(\boldsymbol{Q})$ to $I_{coh}(\boldsymbol{Q},t=\infty)=\exp(-2W)S_{is,coh}(\boldsymbol{Q})$ (see figure 4.2). The inherent structure factor, $S_{is,coh}$, contains only structural information, the Debye Waller factor, $\exp(-2W)$, contains only dynamical information, while the structure factor, $S_{coh}(\boldsymbol{Q})$ depends on both on the structure and the dynamics of the system.

The long time limit of the normalized coherent intermediate scattering function is called the nonergodicity factor, f_Q, (figure 4.2), because it measures the relative intensity of the correlations which survives in the long time limit. It has a non-trivial Q-dependence. It also has a non-trivial dependence of the structure because it contains both dynamical and structural information. If the structure is somehow changed, then the nonergodicity factor also changes even if the amplitude of the vibrations is kept constant.

One phonon scattering

In the approximation where only the harmonic part of the forces in a solid are taken into account then the displacements of each particle can be described by the sum of displacements due to the normal modes of the system. Each normal mode is associated with an eigen-vector and a frequency. The harmonic modes give rise to harmonic oscillations in the time dependence of $I_{coh}(\boldsymbol{Q},t)$ and hence to delta peaks in its Fourier transform $S_{coh}(Q,\omega)$. The contribution to the coherent dynamical structure factor is for plane waves in the one-phonon approximation given by

$$\begin{aligned} S_{coh,inel}(\boldsymbol{Q},\omega) &= \frac{\exp(-2W)}{4\pi MN}\sum_{i,s}\exp(-i\boldsymbol{Q}\cdot\boldsymbol{r}_i)\frac{(\boldsymbol{Q}\cdot\boldsymbol{e}_s)^2}{\omega_s}\int_{-\infty}^{\infty}[exp(-i(\boldsymbol{Q}\cdot\boldsymbol{r}_i-\omega_s t))\langle n_s+1\rangle \\ &\quad + exp(i(\boldsymbol{Q}\cdot\boldsymbol{r}_i-\omega_s t))\langle n_s\rangle]\,exp(-i\omega t)dt \end{aligned} \tag{4.3.31}$$

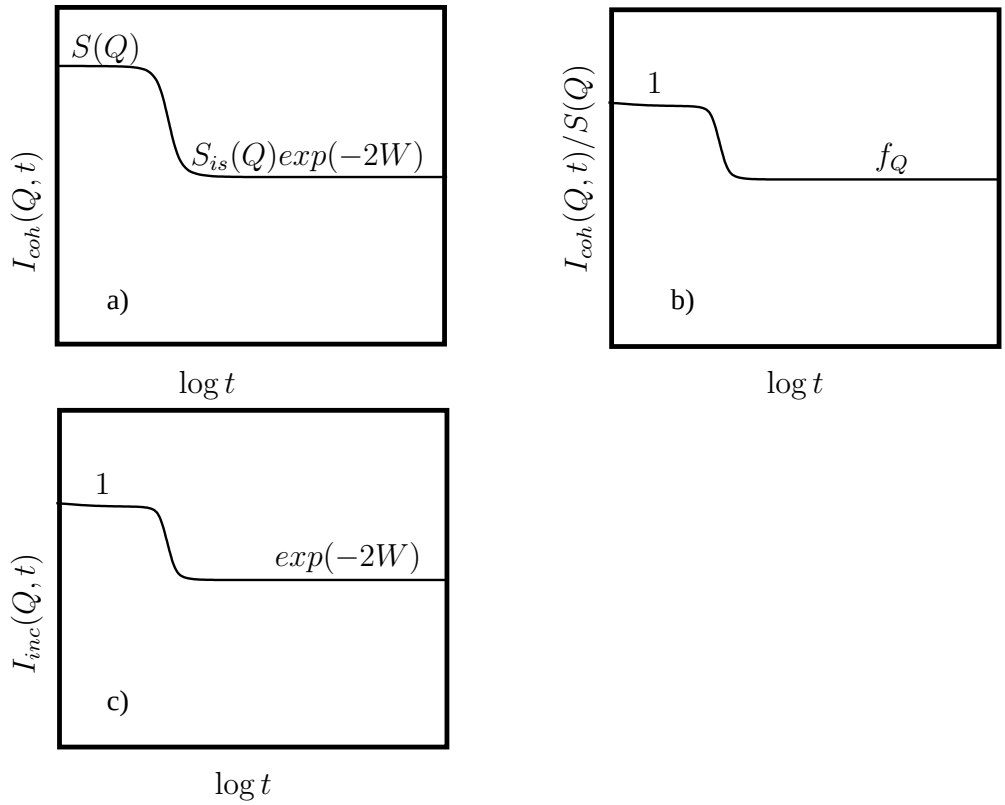

Figure 4.2: Illustration of the time evolution of the intermediate scattering functions in a solid. a) The *coherent* intermediate scattering function, b) The *normalized coherent* intermediate scattering function, c) The *incoherent* intermediate scattering function, which is intrinsically normalized.

Where ω_s is the frequency of the modes s with wave vector $\boldsymbol{Q}$ and $\boldsymbol{e}_s$ is the corresponding polarization vector. The summation over i gives a delta function in the wave vector dependence $\delta(\boldsymbol{Q})$, meaning that only the modes with wave vector $\boldsymbol{Q}$ will contribute. For a disordered state one will measure the ensemble average over the different inherent structures. The terms $\langle n_s \rangle$ is the bose factor, which gives the occupation number of the mode. The bose factor is given by

$$\langle n_s \rangle = \left(\exp\left(\frac{\hbar\omega}{k_B T} \right) - 1 \right)^{-1} \quad , \quad \langle n_s + 1 \rangle = \left(\exp\left(\frac{\hbar\omega}{k_B T} \right) - 1 \right)^{-1} + 1 \tag{4.3.32}$$

which in the classical limit $\hbar \to 0$ gives

$$\langle n_s \rangle = \langle n_s + 1 \rangle = \frac{k_B T}{\hbar\omega}, \tag{4.3.33}$$

from which it is seen that the intensity of the one-phonon contribution (after normalization with the Debye Waller factor) is proportional to the temperature T.

Combining this observation with equation 4.3.28 it follows that the temperature dependence of the non-ergodicity factor is given by

$$f(\boldsymbol{Q},t) = \frac{\exp(-2W)S_{is}(\boldsymbol{Q})}{\exp(-2W)S_{is}(\boldsymbol{Q}) + \exp(-2W)aT} = \frac{1}{1+a'T} \tag{4.3.34}$$

where the factor a encompasses all the $\boldsymbol{Q}$-dependent prefactors in equation 4.3.31 and $a' = a/S_{is}(\boldsymbol{Q})$. This temperature dependence is the starting point for the definition of the parameter α which is studied in section 6.4.

The one-phonon contribution to the incoherent structure factor is not dependent on the wave vector of the modes but only on their frequency. The dynamical structure factor is given by an expression similar to equation 4.3.31

$$S_{inc,inel}(\boldsymbol{Q},\omega) = \frac{\exp(-2W)}{2MN}\sum_s \frac{(\boldsymbol{Q}\cdot\boldsymbol{e}_s)^2}{\omega_s}\left[\langle n_s+1\rangle\delta(\omega-\omega_s) + \langle n_s\rangle\delta(\omega+\omega_s)\right]$$

where the sum over s is to be taken over all modes independent of their wave vector. It is conventional (and convenient) to introduce the vibrational density of states, $g(\omega)$, and to replace the sum over the modes by an integral:

$$S_{inel,inc}(Q,\omega) = \frac{1}{2M}\exp(-2W)Q^2\frac{n(\omega)}{\omega}g(\omega). \tag{4.3.35}$$

Here $(\boldsymbol{Q}\cdot\boldsymbol{e}_s)^2$ is replaced by its averaged over all modes with frequency ω_s, which in a cubic Bravais crystal or an isotropic system is given by $Q^2/3$. This expression is used for analyzing the data presented in chapter 8.

4.3.8 Simple models for liquids

In this work we do not study "normal" non-viscous liquids, but a notion of the dynamics in this high temperature limiting case is useful in the interpretation of the dynamics in highly viscous systems. Liquids are traditionally modeled as classical systems. The comparison between the result of models and experimental data is made by adjusting the result of the model to obey the principle of detailed balance [Squires, 1978];

$$S(\omega) = \exp\left(\frac{\hbar\omega}{2k_BT}\right)S_{classic}(\omega). \tag{4.3.36}$$

Liquids are disordered and therefore isotropic on average. This means that the structure factor and the intermediate scattering function depend only on the magnitude of the Q-vector, not on its direction.

Coherent - linearized hydrodynamics

At small wave vectors and long times the liquid can be described as a continuum, this limit is called the hydrodynamic limit. When dealing with fluctuations it is sufficient to consider the linearized form of the equations.

The collective dynamics splits up in two uncorrelated parts, one is due to entropy fluctuations, which are modes with no particular frequency giving rise to a central peak in $S_{coh}(Q,\omega)$. The other part corresponds to the sound waves in the liquid and is due to pressure fluctuations. Each sound wave has a well defined frequency and wave vector, and they therefore give rise to *Brillouin* peaks at non-zero ω-values in $S_{coh}(Q,\omega)$. The sound modes are damped due to the viscosity of the liquid and this leads to a broadening of the corresponding Brillouin peaks.

Coherent - compressibility

The static structure factor $S(Q)$ is a measure of the amount of density fluctuation seen on the wavelength $2\pi/Q$. In the limit of $Q \to 0$ this becomes the macroscopic density fluctuations, $(\langle\rho^2\rangle - \langle\rho\rangle^2)/\rho$. The macroscopic density fluctuations are related to the macroscopic isothermal compressibility, κ_T, via the fluctuation dissipation theorem. This yields

$$\lim_{Q\to 0} S(Q) = \rho\kappa_T k_B T. \tag{4.3.37}$$

The ratio between the integral of the Brillouin peaks and the total integral $S(Q)$ is in the zero Q limit given by the so called Landau Placzek ratio:

$$\lim_{Q\to 0} \frac{I_{brill(Q)}}{S(Q)} = \frac{\kappa_s}{\kappa_T} = \frac{v_T^2}{v_s^2}, \tag{4.3.38}$$

where κ_s is the adiabatic compressibility and v_T and v_s are respectively the isotherm and adiabatic sound speeds.

Combining equation 4.3.38 with equation 4.3.37 it follows that the intensity in the Brillouin peaks is proportional to the adiabatic compressibility, κ_s, while the intensity in the central peak is proportional to the difference between adiabatic and isothermal compressibility; $\kappa_T - \kappa_s$. This difference is small in solids while it is large in liquids particularly close to critical points.

Incoherent - diffusion

The intermediate scattering function is for a classical system given by

$$I_{inc}(Q,t) = \langle \exp(-i\boldsymbol{Q}\cdot\boldsymbol{r}_i(0))\exp(i\boldsymbol{Q}\cdot\boldsymbol{r}_i(t))\rangle = \langle \exp(i\boldsymbol{Q}\cdot\boldsymbol{r}(t))\rangle \tag{4.3.39}$$

where the definition of the displacement $\boldsymbol{r}(t)$ is $\boldsymbol{r}(t) = \boldsymbol{r}_i(t) - \boldsymbol{r}_i(0)$. If the probability function of $\boldsymbol{r}(t)$ is a Gaussian and if the system is isotropic (average displacement is the same in all directions) then it follows that

$$I_{inc}(Q,t) = \exp\left(\frac{-Q^2\langle r^2\rangle(t)}{6}\right). \tag{4.3.40}$$

To arrive at this equation it was assumed that the system was classical, Gaussian and isotropic, but no particular assumptions about the time dependence of $\langle r^2\rangle(t)$ were included. This means that the equation also could describe the incoherent intermediate scattering function in a solid. The mean squared displacement, $\langle r^2\rangle(t)$, in a solid has a finite value in its long time limit. This leads to a plateau in $I_{inc}(Q,t)$ and the above result is equivalent to equation 4.3.29. The physical explanation difference of the factor 6 vs 3 in the denominator arises from the difference of the definition of $\langle r^2\rangle(t)$ which is the mean squared displacement from a position at $t = 0$ while $\langle u^2\rangle$ is the mean distance from an equilibrium position in the solid.

If the time evolution is given by diffusion then one has $\langle r^2(t)\rangle = 2Dt$ which leads to an exponential decay of the intermediate scattering function:

$$I_{inc}(Q,t) = \exp\left(\frac{-Q^2Dt}{3}\right), \tag{4.3.41}$$

and correspondingly a Lorentzian line shape of the dynamical structure factor.

4.3.9 Glasses and viscous liquids

One of the most characteristic features of the dynamics on highly viscous liquids is the separation of time scales which was also discussed in section 2.5. This means that the correlation functions on short time scales are similar to those of solids while they on long times decay to zero as in liquids. When describing and interpreting the dynamics in viscous liquids and glasses it is therefore useful to "lend" and generalize both the description used for solids and hydrodynamics.

Incoherent case

Relaxations in systems close to the glass transition are never found to follow the exponential behavior seen in liquids (equation 4.3.41) but are stretched (see section 2.3). This means that the relaxation does not give rise to a Lorentzian central peak. However the qualitative relation between the relaxation and the dynamical structure factor is still the same. Meaning that the shorter time scale the relaxation has, the wider and lower is the peak associated to it. In addition to the alpha relaxation which decays the correlations to zero in the long time limit, there can also be fast relaxations. These have a limited amplitude meaning that the intermediate scattering function has a finite long time limit (if the alpha relaxation does not set in at longer times) and hence that the dynamic structure factor has an elastic contribution in addition to the quasi-elastic contribution associated with the relaxation.

The dynamics will be dominated by vibrations, at shorter times than the relaxations. The vibrational contribution to the dynamical incoherent structure factor is described by 4.3.35. In the simplest approximation the relaxation and the vibrations can be considered to give additive contributions to the dynamic structure factor [Frick and Richter, 1993].

Coherent

The coherent modes we study in this work are at high frequency and large wave vectors where hydrodynamics fail to work even in simple liquids, because the properties governing the dynamics become wave vector dependent in this regime. It is convenient to describe the inelastic part of the signal by the Damped Harmonic Oscillator (DHO), which in its normalized form is given by

$$S_{coh,inel}(Q,\omega) = \frac{1}{\pi}\frac{\Omega^2\Gamma(Q)}{(\omega^2-\Omega^2(Q))^2+\omega^2\Gamma^2(Q)}. \tag{4.3.42}$$

This function has two peaks at positions $\pm\Omega(1-(\Gamma^2/2\Omega^2))$ with the width given by Γ. The model can describe the hydrodynamic Brillouin peaks if the right Q dependence of the parameters are inserted, and it can describe the delta-shaped Brillouin peaks seen in crystalline solids in the limit where $\Gamma \to 0$. We use the DHO model to fit the IXS spectra presented in chapter 6.

The actual measured Brillouin peaks in the Q-regime we study ($>2\text{nm}^{-1}$) are relatively broad[9] in the glass and in the liquid. The physical reason for the broadening

[9] By relatively broad we mean that Γ and Ω are of similar order of magnitude.

is highly controversial and we shall not enter in this discussion. Suggestions are that it is due to disorder, fast relaxation or that it is a signature of the fact that the normal modes of the systems are not plane waves. [Ruocco *et al.*, 2000; Ruffle *et al.*, 2003; Matic *et al.*, 2004]

One of our main interest in the current study of the coherent dynamical structure factor is the nonergodicity factor. The nonergodicity factor is in principle the long time limit of the intermediate scattering function but it is operationally defined as the ratio of the central peak over the total coherent intensity. The intensity of the central peak is associated with the correlations that decay slower than the Brillouin frequency considered. It follows from equation 4.3.38 that this ratio in the hydrodynamic limit will be given by

$$f_q = 1 - \frac{v_T^2}{v_s^2}. \tag{4.3.43}$$

The difference between the adiabatic and isothermal sound speeds is small in viscous liquids close to the glass transition. However, the relevant adiabatic sound speed is the sound speed at the Brillouin frequency, while the isothermal sound speed is the low frequency equilibrium sound speed. The generalization of this result in the viscoelastic liquid (still in the low Q limit) is therefore

$$f_q = 1 - \frac{v_0^2}{v_\infty^2}. \tag{4.3.44}$$

We apply this interpretation of the measured f_Q in section 6.3.3.

4.3.10 Long time limit and the resolution function

The measured intensity in a scattering experiment includes a convolution with the experimental resolution function, $R(\omega)$. The delta function in equation 4.3.22 therefore becomes a broadened central peak in the experimental result

$$\begin{aligned} S_{exp}(\boldsymbol{Q},\omega) &= R(\omega) \otimes I_\infty(\boldsymbol{Q})\delta(\omega) + R(\omega) \otimes \frac{1}{2\pi\hbar}\int_{-\infty}^{\infty} I_t(\boldsymbol{Q},t)\exp(-i\omega t)\,\mathrm{d}t \\ S_{exp}(\boldsymbol{Q},\omega) &= R(\omega) I_\infty(\boldsymbol{Q}) + R(\omega) \otimes \frac{1}{2\pi\hbar}\int_{-\infty}^{\infty} I_t(\boldsymbol{Q},t)\exp(-i\omega t)\,\mathrm{d}t. \end{aligned} \tag{4.3.45}$$

$R(\omega)$ is normalized and the long time limit of the intermediate scattering function, $I_\infty(\boldsymbol{Q})$, can therefore be found from the integral over the central peak

$$I_\infty(\boldsymbol{Q}) = \int_{-\Delta\omega}^{\Delta\omega} S_{exp}(\boldsymbol{Q},\omega)\,\mathrm{d}\omega. \tag{4.3.46}$$

In the above we ignore the non-zero contribution of the second term in equation 4.3.22. Another approach which we shall actually use in chapter 6 is to separate the elastic and the inelastic part of the intensity by fitting the total result to a sum of two functions. This latter approach requires some assumption regarding the dynamics of the system in order to choose a proper function for the inelastic part of the signal.

The experimental intermediate scattering function, $I_{exp}(Q,t)$ found from the inverse Fourier transform of the experimental dynamic structure factor, decays to zero at $t \approx \Delta\omega$, where $\Delta\omega$ is the width of the resolution function. This effect can in principle be corrected by deconvolution with the resolution function

$$I(\boldsymbol{Q},t) = \frac{I(\boldsymbol{Q},t)}{R(t)} \quad \text{where } R(t) = \int_{-\infty}^{\infty} R(\omega)\exp(i\omega t)\,\mathrm{d}t \tag{4.3.47}$$

but we can never get any reliable information about dynamics slower than $1/(\Delta\omega)$. The resolution function therefore determines the timescale of the experiment. Figure 4.3.10 illustrates how two different dynamical structure factors which cannot be distinguished with a given experiment, because the difference is on a timescale which is not accessed with the given resolution.

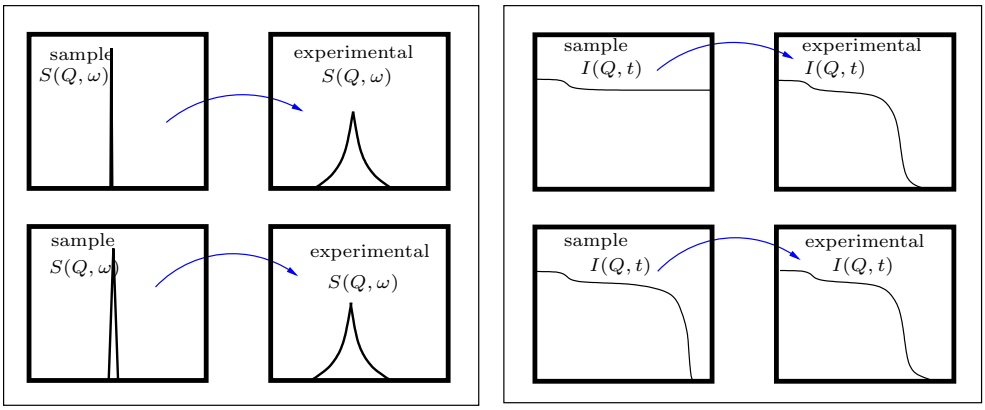

Figure 4.3: The figure illustrates two different dynamical structure factors which cannot be distinguished with a given experiment, because the difference is on a timescale which is not accessed with the given resolution. The left figure shows the dynamical structure factor at fixed Q as a function of temperature. The right figures show the intermediate scattering function at fixed Q as a function of logarithm of the time. Upper figures: The dynamical structure factor of the sample has a a delta function at zero energy transfer and the actual intermediate scattering function of the sample never decays to zero. Lower figures: There is a slight broadening of the central peak seen in dynamical structure factor and the intermediate scattering function decays to zero at long times.

Résumé du chapitre 5

La relaxation structurale dans la m-toluidine et le DBP à été mesurée par spectroscopie diélectrique en fonction de la température et de la pression. Les expériences et les résultats sont présentés dans ce chapitre.

Une cellule de haute pression permettant des expériences jusqu'à 400 MPa a été conçue et fabriqueé au laboratoire pendant cette thèse. Cette cellule permet de faire des mesures à la fois quand on augmente et quand on diminue la pression, on peut ainsi vérifier la réversibilité des mesures.

La relaxation du DBP a été etudiée sur 4 isothermes et 2 isobares et celle de la m-toluidine a été etudiée sur une isotherme. Les résultats obtenus ont été combinés avec des données de temps de relaxation et des données PVT de la littérature. Ils sont cohérents avec la loi d'échelle, ce qui implique une fragilité isochore constante. On constate que la forme de la relaxation structurale (facteur d'étirement) reste inchangée pour des temps de relaxation identiques.

Sur la base du schéma developpé dans le chapitre trois, on discute l'effet respectif de la température et de la densité sur une corrélation possible entre l'étirement de la fonction de relaxation et la fragilité du liquide. On suggère que la fragilité à considérer dans le cadre d'une corrélation avec l'étirement est la fragilité isochore.

Chapter 5

Alpha Relaxation

The two most distinctive features of the slow dynamics of liquids approaching the glass transition is the non-Arrhenius temperature dependence of the alpha relaxation time characterized by the fragility (section 2.2) and the non-Debye character of the alpha relaxation time (section 2.3) [Angell *et al.*, 2000]. It could even be claimed that "understanding the glass transition" essentially means understanding these two phenomena [Dyre, 2006]. The hypothesis that they might be correlated, is therefore appealing. Böhmer *et al.* [1993] correlates larger (isobaric) fragility with larger deviation from Debye relaxation, with the latter measured in terms of stretching and the paper has been cited 703 times, which is one illustration of the impact of this idea.

In this chapter we present a study of the pressure and temperature dependence of the dielectric alpha relaxation time and peak shape in two molecular liquids. We rationalize the temperature and density dependence in terms of the scaling law presented in section 3.2 and determine isobaric and isochoric fragility.

We combine our data with data from the literature to revisit the proposed correlation between stretching and fragility. We do this in terms of the ideas developed in section 3.3.

5.1 Dielectric spectroscopy

5.1.1 Experimentals

The dielectric measurements were performed at the laboratory, LCP, in Orsay on a homebuilt setup. The pressure environment was developed prior to this work, while

the dielectric cell and the details of the electric connections were developed during the course of this work. The specifications of the setup are not reported elsewhere, and we will therefore present it in some detail below.

The cell and sample environment

The setup is depicted in figure 5.1. The pressure environment is based on liquid compression using a commercial piston-and-cylinder device connected to the home-built autoclave in which the dielectric cell is placed. The autoclave is cylindrical with a diameter of 4 cm and a length of 15 cm. It has a wall thickness of 4 cm and is made of metal . The dielectric sample cell is entered into the autoclave from the end opposite the entrance of the compression fluid. Sealing of the autoclave is accomplished with a metallic threaded conical piece and a system of metallic and rubber o-rings. One of the major difficulties is to lead the electrical connections of the dielectric cell out of the autoclave. This is done by leading two thin wires through the metal closing piece. The wires are isolated from the metal by thin cones of rezine. The pressure setup can resist pressures up to slightly above 400 MPa. The pressure is measured using a strain gauge connected to the compression liquid system.

Cooling is performed by flow of thermostated cooling liquid running inside the metallic walls of the autoclave. The temperature and the temperature stability are monitored by two Pt100 sensors. One is placed in the wall of the autoclave; the other is emerged in the compression liquid and is at a distance of maximum 0.3 cm from the sample. The connections to the second temperature control are led through the walls of the autoclave with rezine isolation of the same kind as that used for the electric connections of the dielectric cell. The temperature is held stable within ± 0.1 K for a given isotherm. The temperature during the time it takes to record a spectrum is stable within ± 0.01 K. The accessible temperature range is 210 K to 340 K.

The capacitor used for the dielectric measurements is totally immersed in the sample liquid, which is isolated from the compression liquid by a flexible Teflon cell. The Teflon cell is cylindrical and closed with a threaded lead and a rubber o-ring. The electric contacts to the electrodes are forced through the Teflon cell will which is approximately 1 cm at this point. In this system no mixing occurs between the sample liquid and the compression liquid. The Teflon cell has the additional advantage that the electrodes are electrically isolated from the metallic walls of the autoclave. The Teflon cell is surrounded by the compression liquid from all sides and it has one end

with a thickness of 0.5 mm in order to ensure that the pressure is well transmitted from the compression liquid to the sample liquid.

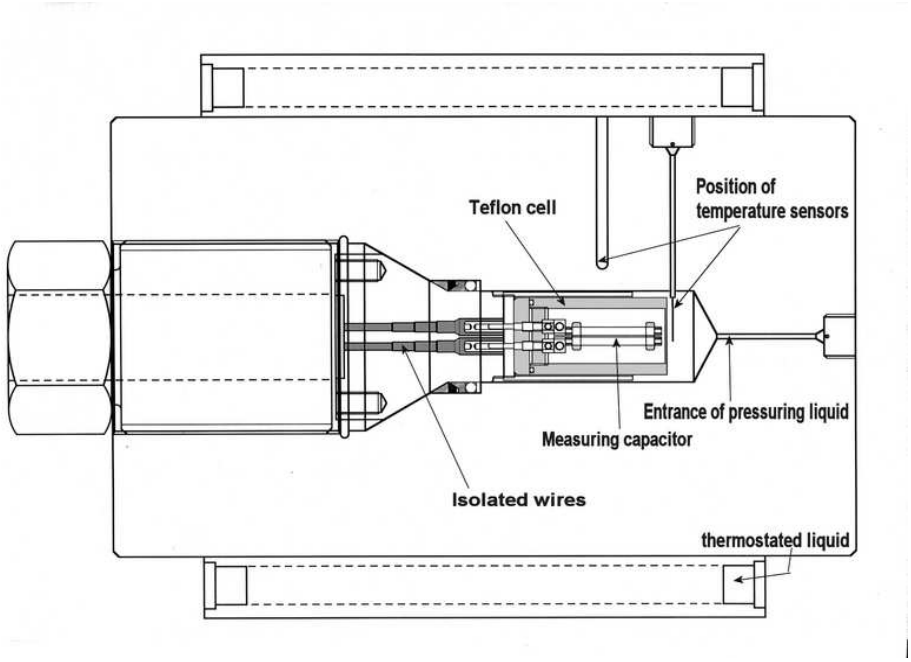

Figure 5.1: The experimental setup for dielectric spectroscopy under pressure at Orsay. The Teflon parts shown in grey to distinguish from the metal. The length of the autoclave is $\sim$ 30 cm, the Teflon cell is 5 cm long. The parts are shown separately in appendix C.

The advantage of this setup, compared to other setups for dielectric spectroscopy under pressure, is that it ensures a hydrostatic pressure because the sample is compressed from all sides. It is moreover possible to take spectra both under compression and decompression, and it can hence be verified that there is no hysteresis in the system.

The capacitor used for the measurement is composed by two gold coated electrodes separated by small Teflon spacers. The distance between the capacitor plates is adjustable and the area is 5.44 cm^2. We report data measured with a plate distance of 0.3 mm giving an empty capacitance of 16 pF. The strength of the measured signal is proportional to the area and inversely proportional to the distance between the plates. It is therefore an advantage, especially for measurements on systems with small dipole moments, to maximize the area and minimize the plate distance. Although the area is limited by the dimensions of the pressure cell, the distance could in principle be smaller; however it is crucial that the plates do not touch, even when the pressure is applied, as this would lead to an electrical short cut.

Measuring the capacitance.

The capacitance is measured using a HP 4284A LCR-meter which covers the frequency range from 100Hz to 1MHz. The LCR-meter gives the complex capacitance directly as output. The measurement is based on a four point method. This means that the signal of the wires leading to the sample is eliminated. In order to exploit this advantage to its maximum it is important that the connection point of the wires is as close as possible to the dielectric cell, and it is therefore placed right outside the conical closing piece.

The low frequency range from 100Hz to 1Hz is covered using a SR830 lockin. The lockin measures the amplitude and phase of output voltage with respect to an input voltage at a specified frequency. The sample capacitor is connected with a grounded known resistance. The frequency dependent capacitance of the sample is calculated based on the known characteristics of this network.

The experiments

Liquid m-toluidine was measured on one isotherm at 216.4 K. DBP was measured along 4 different isotherms: 205.5 K, 219.3 K, 236.3 K and 253.9 K, at pressures up to 4 kbar. DBP was moreover measured at different temperatures along two isobars: atmospheric pressure and 230 MPa. [Niss *et al.*, 2007] (See appendix A for details on the samples).

The pressure was continuously adjusted during the experiment along the 230 MPa isobar in order to compensate for the decrease of pressure which follows from the contraction of the sample due to decreasing temperature. It is of course always possible to reconstruct isobars based on experiments performed under isotherm conditions. However, such a procedure mostly involves interpolation of the data, which is avoided by performing a strictly isobaric measurement. For DBP we have obtained relaxation-time data at times shorter than $10^{-6.5}$ s by using the high-frequency part of the spectrum and assuming time-temperature and time-pressure superposition (TTPS). Although TTPS is not followed to a high precision (see section 5.3.2), the discrepancies lead to no significant error on the determination of the relaxation time. This is verified by comparison to atmospheric-pressure data from the literature (see figure 5.2). Data were in all cases taken both by compression and decompression. By doing so we have verified that there was no hysteresis in the pressure dependence of the dynamics. This serves to confirm that the liquid has been kept at thermodynamical equilibrium at all stages.

Data treatment

The relaxation time is determined from a polynomial fit of the logarithm of the loss as function of the logarithm of the frequency. The fit is performed over less than a decade around the top. The further treatment, e.g. evaluation of the fragility and analysis of the spectra shape, is discussed in detail in the course of the chapter.

5.2 Relaxation time

5.2.1 Dibutyl phtalate

The relaxation time of DBP at atmospheric pressure is shown in figure 5.2 along with literature results. $T_g(P_{atm}) = 177$ K, when defined as the temperature where $\tau_\alpha = 100$ s. We also present the data taken at $P = 230$ MPa in this figure. It is clearly seen that T_g increases with pressure. An extrapolation of the data to $\tau_\alpha = 100$ s gives $T_g = 200$ K for $P = 230$ MPa, corresponding to $dT_g/dP = 0.1$ K.MPa^{-1}. This corresponds well to the pressure dependence of T_g (at $\tau_\alpha = 1$ s) reported by Sekula *et al.* [2004], based on measurements taken at pressures higher than 600 MPa. It is however a stronger pressure dependence than $dT_g/dP = 0.06$ K.MPa^{-1} reported by Fujimori *et al.* [1997] based on isothermal calorimetry. This indicates that the calorimetric and the dielectric relaxation may have somewhat different dependence of density.

In figure 5.3 we illustrate the determination of T_g and of the fragility m_P for the atmospheric-pressure data, using the part of the atmospheric-pressure data of figure 5.2 where the relaxation time is longer than a millisecond. Along with the data we show the VTF fit (equation 2.2.2) from Sekula *et al.* [2004] extrapolated to low temperatures, which gives $T_g = 177.4$ K and $m_P = 84$. We have also performed a new VTF fit restricted to the data in the 10^{-6} s-10^2 s region. The result of this fit yields $T_g = 176.6$ K and $m_P = 82$. Finally, we have made a simple linear estimate of $\log_{10}\tau_\alpha$ as a function of $1/T$ in the temperature range shown in the figure. This linear slope fits the data close to T_g better than any of the VTF fits. The corresponding glass transition temperature and fragility are $T_g = 176$ K and $m_P = 70$. This illustrates that the determination of T_g is rather robust while this is less so for the fragility. This latter depends on how it is obtained, and the use of extrapolated VTF fits can lead to an overestimation. (Of course, a VTF fit made over a very narrow range, e.g. $10^{-2}s - 10^2$ s, will agree with the linear fit, because the VTF becomes essentially linear over the relevant range.) The fragility of DBP

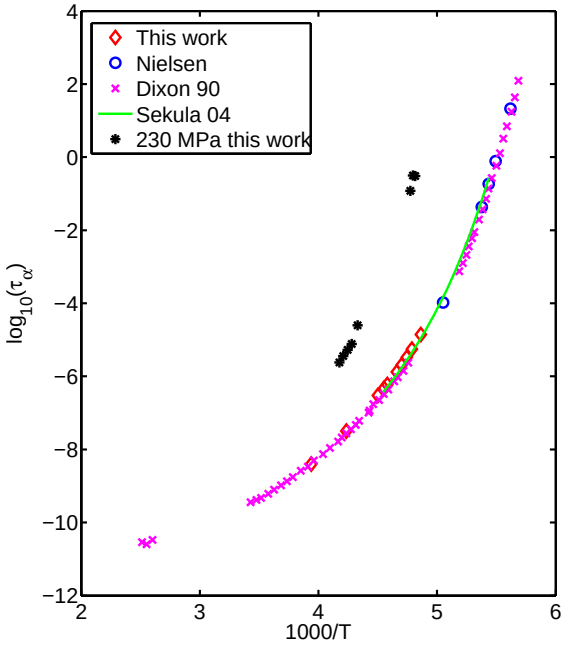

Figure 5.2: Temperature dependence of the alpha-relaxation time (from dielectric measurements, $\tau_\alpha = 1/\omega_{peak}$) of liquid DBP at atmospheric pressure and at 230 MPa (Arrhenius plot). Data from other groups are also included: unpublished data from Nielsen *et al.* [2006], the VTF fit of Sekula *et al.* [2004] shown in the range where it can be considered as an interpolation of the original data, and data taken from figure 2(a) [Dixon *et al.*, 1990].

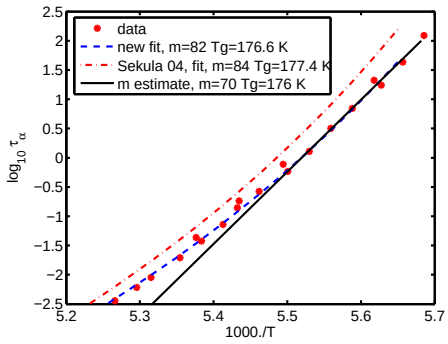

Figure 5.3: Atmospheric-pressure data of figure 5.2 with relaxation times longer than a millisecond. Also shown are the VTF fit of Sekula *et al.* [2004] extrapolated to low temperatures (dashed-dotted line), a new VTF fit made by using data in the 10^{-6} s -10^2 region (dashed line), and estimated slope of the data in the long-time region (full line). The Tg's estimated from these three methods are very similar, whereas the fragility varies significantly from $m = 65$ to $m = 85$.

has earlier been reported to be $m_P = 69$ by Böhmer *et al.* [1993] based on the data of Dixon *et al.* [1990]. We take $m_P = 75$ as a representative value.

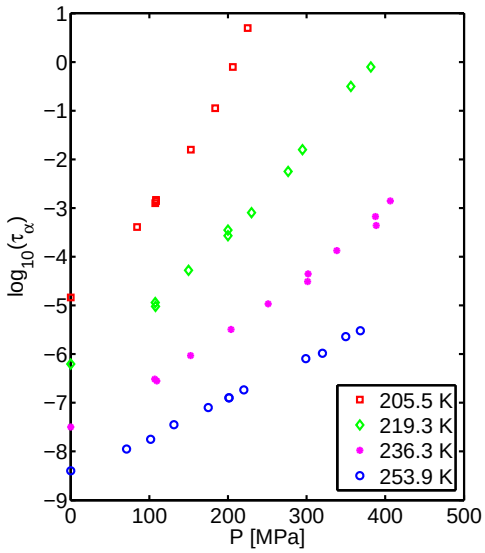

Figure 5.4: Alpha-relaxation time of DBP (from dielectric measurements, $\tau_\alpha = 1/\omega_{peak}$) as a function of pressure along 4 different isotherms, (log-linear plot).

The relaxation-time data along four different isotherms are displayed as a function of pressure in figure 5.4. Figure 5.5 shows the density dependence of the relaxation times along the same four different isotherms, along with data from the atmospheric pressure isobar and the 230 MPa isobar (see appendix A regarding the determination of density.). We have also included the room-temperature dielectric data of Paluch *et al.* [2003 a]. The viscosity data and the dielectric relaxation time do not decouple under pressure for DBP [Sekula *et al.*, 2004], and we have therefore also included the room-temperature viscosity data of Cook *et al.* [1993].

In figure 5.6 we show the data of figure 5.5 plotted as a function of the scaling variable ρ^x/T, choosing for x the value that gives the best collapse for the data of this work. This corresponds to testing the scaling in equation 3.2.1 assuming that $e(\rho)$ is a power law. The data taken at low density collapse quite well using $x = 2.5$, while this is not true for the data of Paluch *et al.* [2003 a] taken at densities higher than approximately 1.2 g/cm^3. The absence of collapse in figure 5.6 cannot be explained by errors in estimating the PVT data: this is discussed in more detail in appendix A.

To test the more general version of the scaling we construct the function $e(\rho)$ from the following procedure. The 100 s isochrone is described using an adapted form of the fit

for the 1 s isochrone in [Paluch *et al.*, 2003 a]. Along this 100 s isochrone we calculate α_τ and determine $\frac{\mathrm{d}\log e(\rho)}{\mathrm{d}\log\rho}$ from $\frac{\mathrm{d}\log e(\rho)}{\mathrm{d}\log\rho} = 1/(T_g|\alpha_\tau|)$. From this we determine $\ln(e(\rho))$ (up to an additive constant) by integrating $\frac{d\ln(e(\rho))}{\ln\rho} d(\ln(\rho))$, and $\ln(e(\rho))$ is finally converted by $e(\rho) = \exp(\ln(e(\rho)))$. This gives $e(\rho)$ with an arbitrary multiplicative constant. The quality of the data collapse is independent of this constant, as it only depends on the density dependence of $e(\rho)$ not on its absolute value. In figure 5.7 we show the data as a function of $e(\rho)/T$, using the $e(\rho)$ found from this construction. The constructed $e(\rho)$ has an apparent "power-law" exponent $x(\rho) = dloge(\rho)/dlog\rho$ that increases from 1.5 to 3.5 with density in the range considered. It is seen that this makes the higher density data fall reasonably well on the master curve and that gives an even better collapse in the low density region than with the scaling with a simple power law.

As a last note regarding the $e(\rho)/T$-scaling in figure 5.7, we want to stress that we cannot test the scaling (Eq. 3.2.1) in the density range above 1.25 g/cm^3 where there is only one set of data. Indeed, with a unique set of data in a given range of density it is always possible to construct $e(\rho)$ in this range to make the data overlap with data taken in other density ranges.

We have determined the ratio between the isochoric fragility and the isobaric fragility at atmospheric pressure by calculating α_τ along the isochrone of 100 s and inserting it in equation 3.1.5. This leads to $m_P/m_\rho \approx 1.2$, when m_P is the atmospheric-pressure fragility. In figure 5.8 we show the isobaric data taken at atmospheric pressure and at 230 MPa scaled by their respective $T_g(P)$. No significant pressure dependence of the isobaric fragility is observed when going from atmospheric pressure to 230 MPa, which is consistent with the result of Sekula *et al.* [2004]. The pressure independence of m_P is connected to the relatively low value of $m_P/m_\rho = 1.2$, (typical values are 1.2-2 [Alba-Simionesco *et al.*, 2002]); m_ρ is pressure independent and the ratio m_P/m_ρ cannot be lower than one (see Eq. 3.1.5), so that m_P can at most decrease by 20% from its atmospheric-pressure value. Moreover, the increase in $\frac{d\ln(e(\rho))}{\ln\rho}$ with density will tend to cancel the decrease in $\alpha_P T_g$, which is usually responsible for the decrease in fragility with increasing pressure.

5.2.2 m-Toluidine

The glass transition temperature at atmospheric pressure is $T_g = 187$ K and the isobaric fragility based on dielectric spectra is reported to be $m_P = 82\pm3$ [Mandanici *et al.*, 2005; Alba-Simionesco *et al.*, 1999]. (There has been some controversy on the dielectric relaxation in m-toluidine at atmospheric pressure, see [Carpentier *et al.*,

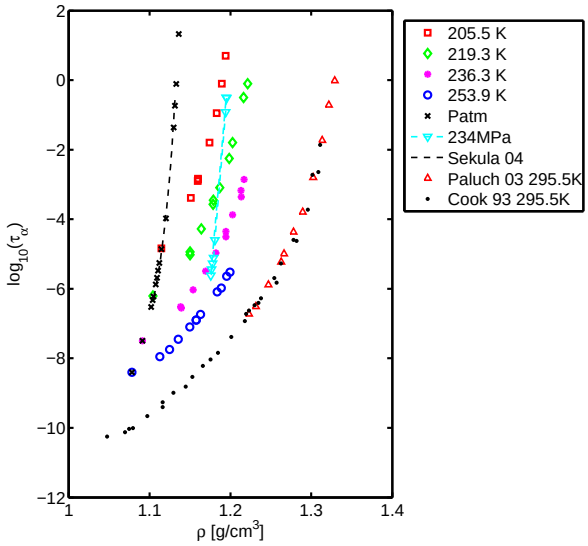

Figure 5.5: Logarithm of the alpha-relaxation time of DBP versus density (see the text regarding the calculation of density). Included are data from this work along with dielectric data from figure 3 in [Paluch *et al.*, 2003 a], and viscosity data from Cook *et al.* [1993]. The viscosity data are shifted arbitrarily on the logarithmic scale in order to make the absolute values correspond to the dielectric data of Paluch *et al.* [2003 a], which are taken at the same temperature.

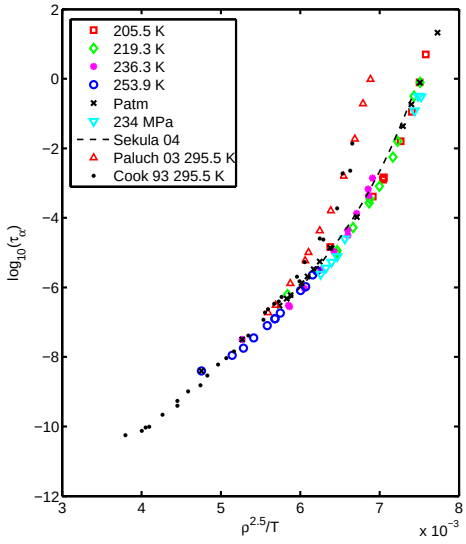

Figure 5.6: The alpha-relaxation times shown in figure 5.5 plotted as a function of $\rho^{2.5}/T$.

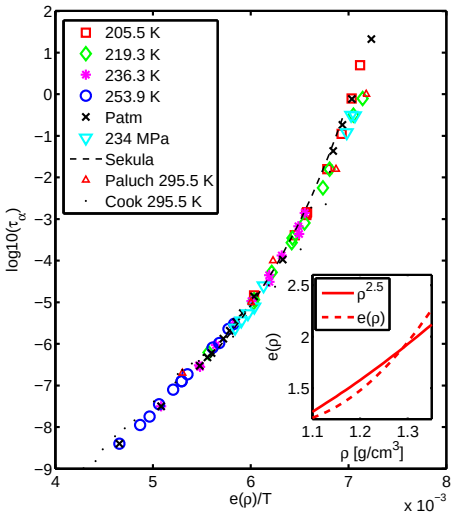

Figure 5.7: The alpha-relaxation times shown in figure 5.5 plotted as a function of $X = e(\rho)/T$, with increasing $\mathrm{d}log e(\rho)/\,\mathrm{d}log\rho$ as ρ increases. The inset shows the density-dependent activation energy $e(\rho)$ (dashed line) used in the scaling variable $X = e(\rho)/T$ for collapsing data in (a) (the associated $x(\rho) = \frac{\mathrm{d}\log e(\rho)}{\mathrm{d}\log \rho}$ increases from 1.5 to 3.5 in the density range under study). We also display the power law giving the best scaling, $\rho^{2.5}$, at low density (full line).

2004; Mandanici *et al.*, 2005] and references therein.)

In the inset of figure 5.9 we show the pressure-dependent relaxation time at 216.4 K. Extrapolating the data to $\tau_\alpha = 100$ s leads to $P_g = 340 \pm 10$ MPa, corresponding to $dT_g/dP = 0.085$ K.MPa^{-1}. This value is, as we also saw it in the case of DBP, about a factor 2 higher than the $dT_g/dP = 0.045$ K.MPa^{-1} reported for the calorimetric glass transition by Alba-Simionesco *et al.* [1997]. This could suggest that this type of decoupling is common, however there are also examples where no such decoupling is found [Chauty-Cailliaux, 2003].

In figure 5.9 we show the alpha-relaxation time as a function of density along the atmospheric pressure isobar (data from Mandanici *et al.* [2005]) and the 216.4 K isotherm (see appendix A regarding the determination of density). The data taken at atmospheric pressure and the data taken along the 216.4 K isotherm cover two different ranges in density. It is therefore not possible from this data to *verify* the validity of the scaling in $X = e(\rho)/T$. Moreover, it is seen in figure 5.9 that there is not complete agreement at ambient pressure between the two experiments. Our data actually correspond better to the results of Carpentier *et al.* [2004] than those of Mandanici *et al.* [2005]; it would be ideal to measure the high pressure and the

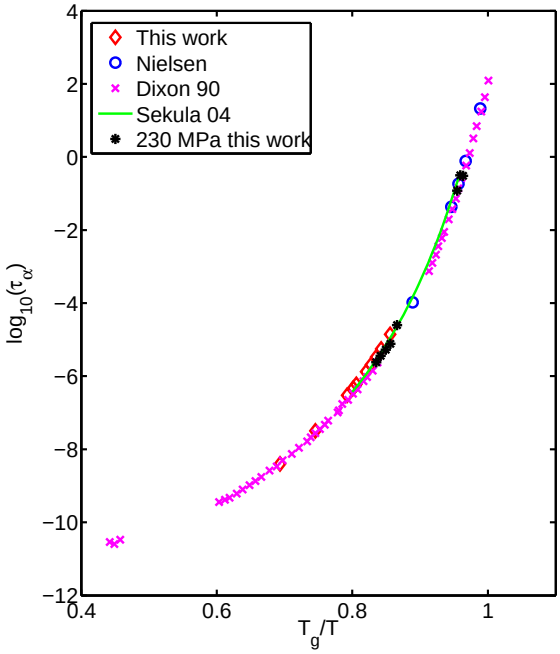

Figure 5.8: Arrhenius plot of the alpha-relaxation time of DBP at atmospheric pressure and at 230 MPa, when the temperature is scaled with the pressure dependent T_g, $T_g(Patm) = 176$ K and T_g(230 MPa)=200 K. As in figure 5.2, data from other groups are also included: unpublished data from Nielsen *et al.* [2006], the VTF fit of Sekula *et al.* [2004] shown in the range where it can be considered as an interpolation of the original data and data taken from figure 2 a) in [Dixon *et al.*, 1990].

atmospheric pressure data in the course of the same experiment, in order to eliminate the extra uncertainty from differences in absolute temperature scale and possible in the purity of the sample.

We *assume* that the scaling is possible. Moreover, we describe $e(\rho)$ by a simple power law, $e(\rho) = \rho^x$. We find the exponent x by exploiting the fact that the scaling variable $X = e(\rho)/T$ is uniquely fixed by the value of the relaxation time; applying this at T_g, namely setting $X_g(Patm) = X_g(216\text{K})$, leads to $x = 2.3$ and gives a ratio of $m_P/m_\rho = 1.2$.

5.3 Spectral shape

Our main aim in the study of the spectral shape is to analyze the possible correlation between the degree of departure from Debye relaxation and the fragility (see also section 2.3). In the end of this chapter we discuss this correlation in the frame

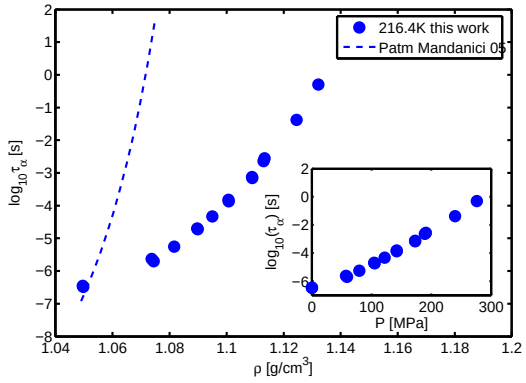

Figure 5.9: Logarithm of the alpha-relaxation time of m-toluidine as a function of density along the isotherm $T = 216.4K$ (symbols). The VTF fit of the atmospheric pressure data of Mandanici *et al.* [2005] is also shown in the range where the fit can be considered as an interpolation of the data (dashed line). The inset shows the alpha-relaxation time of m-toluidine as a function of pressure along the isotherm T=216.4 K.

of analysis proposed in chapter 3, based on the data presented here as well as on literature data. However, there is no consensus on how to best characterize the shape of the relaxation spectrum of viscous liquids, and this of course complicates the situation. In the first part of this section, we therefore review these procedures and test different descriptions on one of our spectra. We more specifically look at schemes for converting one type of description to another.

5.3.1 On the characterization of the spectral shape

The (normalized) Kohlrausch-William-Watts function or stretched exponential is defined in the time domain by $\varphi_{KWW}(t) = exp\left[-\left(\frac{t}{\tau}\right)^{\beta_{KWW}}\right]$. Its equivalent in the frequency domain is found by inserting in 4.1.4. We consider only the imaginary part:

$$\varphi''_{KWW}(\omega) = \int_0^\infty -\frac{\mathrm{d}\varphi_{KWW}(t)}{\mathrm{d}t}.\sin(\omega t)\,\mathrm{d}t \tag{5.3.1}$$

The low-frequency behavior of this function is always a power law with exponent 1. The high frequency behavior is a power law with exponent $-\beta_{KWW}$ [Lindsey and Patterson, 1980]. β_{KWW} is the only parameter describing the shape of the relaxation function. Hence it controls both the exponent of the high frequency power law and the width of the relaxation function.

The Havriliak-Negami (HN) function,

$$\varphi_{HN}(\omega) = \frac{1}{[1 + (i\omega\tau_{HN})^{\alpha}]^{\gamma}}, \tag{5.3.2}$$

gives a power law with exponent $(-\alpha\gamma)$ in the high-frequency limit and a power law of exponent α in the low frequency-limit of its imaginary part.

The HN function reduces to Cole-Davidson (CD) one when $\alpha = 1$. (In the case of a CD function we follow the convention and refer to the γ above as β_{CD}.) The CD spectrum has the same general characteristics as the KWW one: a high-frequency power law with exponent given by β_{CD} and a low-frequency power law with exponent one. However, the shape of the two functions is not the same. The CD function is narrower for a given high frequency exponent (given β) than the KWW function (see figure 5.10 a)). The best overall correspondence between the CD-function and the KWW-function has been determined by Lindsey and Patterson [1980]. (see figure 5.10 b)).

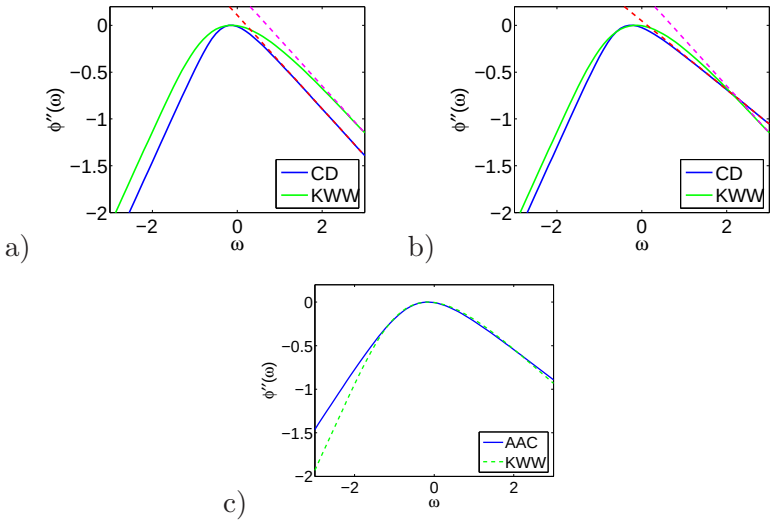

Figure 5.10: Log-log plots of the different showing the loss of different fitting functions a) KWW-function with $\beta_{KWW} = 0.5$ CD-function with β_{CD}. Dashed lines illustrate the high frequency power-law. b) KWW-function with with $\beta_{KWW} = 0.5$ and the corresponding CD-function according to Lindsey and Patterson [1980] giving $\beta_{CD} = 0.367$. Dashed lines illustrate the high frequency power law. c) KWW-function with $\beta_{KWW} = 0.5$ and the corresponding AAC-function.

No good correspondence exists in general between the HN and the KWW functions. First of all because the former involves two adjustable shape parameters and the latter only one (plus in both cases a parameter for the intensity and one for the time scale). The KWW function always has a slope of one at low frequencies while the HN

function has a generally nontrivial α. Nonetheless, Alvarez *et al.* [1991] numerically found that the two functions can be put in correspondence by fixing the relation between the two HN parameters $\gamma = 1 - 0.812(1-\alpha)^{0.387}$ and choosing $\beta_{KWW} = (\alpha\gamma)^{(1/1.23)}$. This restricted version of the HN-function is sometimes referred to as the AAC-function [Gomez and Alegria, 2001]. The shape is described by one parameter. However, it is clear that this function cannot correspond to the KWW function in the frequency range where the loss can be described by power laws, as it was also noted by Gomez and Alegria [2001]. The AAC function inherits the behavior of the HN function; as a result it has a nontrivial exponent α at low frequencies and an exponent $-\alpha\gamma$ at high frequencies, while the associated KWW function has exponents one and $-\beta_{KWW} = -(\alpha\gamma)^{(1/1.23)}$ at low and high frequencies, respectively (see figure 5.10 c).

Another approach is to describe the dielectric spectrum by a distribution of Debye relaxations

$$(\epsilon(\omega) - \epsilon_\infty)/\Delta\epsilon = \int_{-\infty}^{\infty} D(ln\tau)\frac{1}{1+i\omega\tau}dln\tau, \tag{5.3.3}$$

and to fit the shape of the distribution $D(ln\tau)$ rather than the spectral shape directly. The following form has been suggested for the distribution function [Blochowicz *et al.*, 2003],

$$D(ln\tau) = N\exp\left(-\beta/\alpha(\tau/\tau_0)^\alpha\right)(\tau/\tau_0)^\beta\left(1+\left(\frac{\tau\sigma}{\tau_0}\right)^{\gamma-\beta}\right), \tag{5.3.4}$$

where N is a normalization factor. The function above is known as the extended generalized gamma distribution, GGE. The last term (and the parameters γ and σ) describes a high frequency wing, corresponding to a change from one power-law behavior (-β) to another (-γ). This term can therefore be omitted if no wing is observed in the spectrum. This results in a simpler distribution; the generalized gamma distribution (GG) whose shape is described by two parameters: α determines the width and β gives the exponent of the high frequency power-law. The low frequency is always a power law with exponent one.

Finally, it is possible to describe the spectra phenomenologically in terms of the full width at half maximum, usually normalized to the full width at half maximum of a Debye peak [Dixon *et al.*, 1990] (W/W_D, $W_D = 1.14$ decade), and by the exponent of the power-law describing the high frequency side. The power law exponent is not always well defined, as there can be a high frequency wing or a secondary process appearing at high frequencies. Olsen *et al.* [2001] therefore suggest to characterize the alpha peak by the minimal slope found in a double logarithmic plot of the

dielectric loss as a function of frequency. Note that this phenomenological description requires two parameters to describe the shape of the relaxation spectrum, while the commonly used CD and the KWW functions use only one shape-parameter.

In figure 5.11 we show one of the dielectric spectra of m-toluidine along with fits to the functions described above. The minimal slope is -0.44 and $W/W_D = 1.56$. The best fits to the different functions are displayed in figure 5.11. The CD-fit gives $\beta_{CD} = 0.42$, which with the Patterson scheme corresponds to $\beta_{KWW} \approx 0.55$. The direct fit with the Fourier transform of the KWW gives $\beta_{KWW} = 0.57$. The best AAC fit gives $\alpha = 0.85$ leading to $\gamma = 0.61$ and $\beta_{KWW} \approx (\gamma\alpha)^{1/1.23} = 0.59$. This shows that both the Patterson and the AAC approximations reasonably well reproduce the β_{KWW} value found from using KWW directly. Another point worth noticing is that the β_{KWW} value does not correspond to the actual high frequency slope. This is because the overall agreement between the fit and the data is much more governed by the width of the relaxation function than by its high frequency slope, as it is also clearly seen for the KWW fit in figure 5.11. Note that the AAC approximation for the relation between the HN parameters and β_{KWW} only holds when the HN parameters are fixed according to $\gamma = 1 - 0.812(1 - \alpha)^{0.387}$. The original HN function has two adjustable parameters to describe the shape. The best HN fit gives $\alpha = 0.95$, and $\gamma = 0.46$. The Gamma distribution which also has two free parameters gives $\alpha = 40$ and $\beta = 0.49$. Finally we have fitted with the GGE using the constraint $\beta = 3\gamma$ (see [Blochowicz *et al.*, 2006]), meaning that the function has 3 free parameters to describe the shape, the values being $\alpha = 40$, $\beta = 0.7$ $\sigma = 53$ and $\gamma = \beta/3 = 0.23$. It is not surprising that the GGE with 3 free parameters gives by far the best fit. However it is also striking that the CD with only one parameter describing the shape gives a good fit over the whole peak, for the temperature and sample considered, whereas this is not true for the KWW nor for the AAC.

From the above we conclude the CD-function gives a good description of the shape of the relaxation using only one parameter to describe the shape. We therefore use this function to fit our data. The KWW exponent, β_{KWW}, does not give a proper measure of the high frequency slope, but it does give a reasonable one-parameter measure of the overall shape of the dispersion. The KWW function is moreover the function most commonly used in literature, which is the main reason for using it when comparing broadening of the alpha relaxation to the temperature dependence of the alpha relaxation (section 5.3.4).

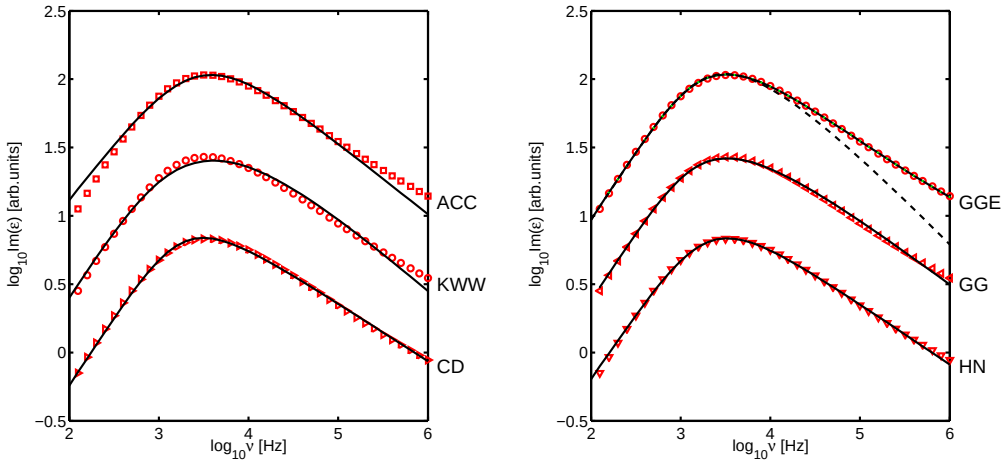

Figure 5.11: Log-log plot of the dielectric loss of m-toluidine at T=216.4K and 122MPa along with best fits to several common functional forms. Figure a) show the fitting functions from below and up; CD, KWW, AAC. Figure b) shows from below and up; HN, Gamma distribution, Generalized gamma distribution. CD, KWW and AAC have 1 parameter characterizing the shape, HN and Gamma have 2, and Generalized gamma has been fitted using 3 adjustable parameters. The dashed line shows the Gamma distribution corresponding to the generalized gamma distribution. The curves are displaced along the y-axis by regular amounts.

5.3.2 Spectral shape DBP

The frequency-dependent dielectric loss for a selected set of different pressures and temperatures is shown in figure 5.12. The first observation is that cooling and compressing have a similar effect as both slow down the alpha relaxation and separate the alpha relaxation from higher-frequency beta processes. The data depicted are chosen so that different combinations of temperature and pressure give almost the same relaxation time. However, the correspondence is not perfect. In figure 5.13 we have thus slightly shifted the data, by at most 0.2 decade, in order to make the peak positions overlap precisely. This allows us to compare the spectral shapes directly. It can be seen from the figure that the shape of the alpha peak itself is independent of pressure and temperature for a given value of the alpha-relaxation time (*i.e.*, of the frequency of the peak maximum), while this is not true for the high-frequency part of the spectrum, which is strongly influenced by the beta-relaxation peak (or high-frequency wing). When comparing datasets that have the same alpha-relaxation time one finds that the high-frequency intensity is higher for the pressure-temperature combination corresponding to high pressure and high temperature.

In figure 5.14 we show all the datasets of figure 5.12 superimposed and we zoom on

the region of the peak maximum. The overall shape of the alpha relaxation is very similar at all pressures and temperatures. However, looking at the data in more detail, one finds a significantly larger degree of collapse between spectra which have the same relaxation time, and a small broadening of the alpha peak is visible as the relaxation time is increased: see figure 5.14. At long relaxation times there is a perfect overlap of the shape of the alpha-relaxation peaks which have the same relaxation time. At shorter relaxation time, $log_{10}(\omega_{max}) \approx 5$, the collapse is not as good: the peak gets slightly broader when pressure and temperature are increased along the isochrone. In all cases, the alpha peak is well described by a Cole-Davidson shape. The β_{CD} goes from 0.49 to 0.45 on the isochrone with shortest relaxation time and decreases to about 0.44 close to T_g at all pressures. A KWW fit close to T_g gives $\beta_{KWW} = 0.65$.

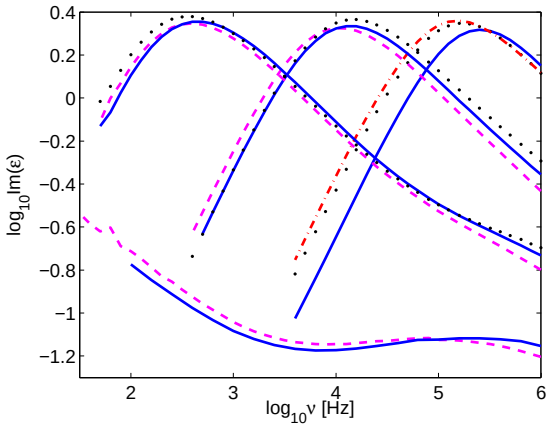

Figure 5.12: Log-log plot of the frequency-dependent dielectric loss of DBP. Red dashed-dotted curve: T=253.9 K P=320 MPa; black dots: T= 236.3 K and, from right to left, P=153 MPa, P=251 MPa, P=389 MPa; full blue line: T=219.3 K and, from right to left, P=0 MPa, P=108 MPa, P=200 MPa, P=392 MPa; magenta dashed curve: T=206 K and, from right to left, P=0 MPa, P=85 MPa, P=206 MPa.

5.3.3 Spectral shape m-toluidine

The frequency dependent dielectric loss of m-toluidine for several pressures along the T=216.4 K isotherm is shown in figure 5.15. The data are then superimposed by scaling the intensity and the frequency by the intensity and the frequency of the peak maximum respectively: this is displayed in figure 5.16. When zooming in (figure 5.16 b) we still see almost no variation of the peak shape. For the present set of data pressure-time-superposition is thus obeyed to a much higher degree than in DBP, and the changes are too small to give any pressure dependence in the parameters when

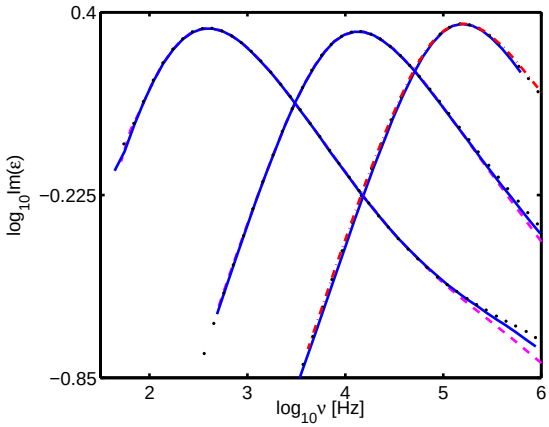

Figure 5.13: Same dielectric loss data as in figure 5.12 of DBP with a slight shift of the peak frequencies (less than 0.1 decade) to make the data taken under quasi isochronic conditions coincide precisely. The symbols are the same as in figure 5.12, but the data at T=206 K and P=206 MPa and 219.3 K and P=392 MPa are not shown.

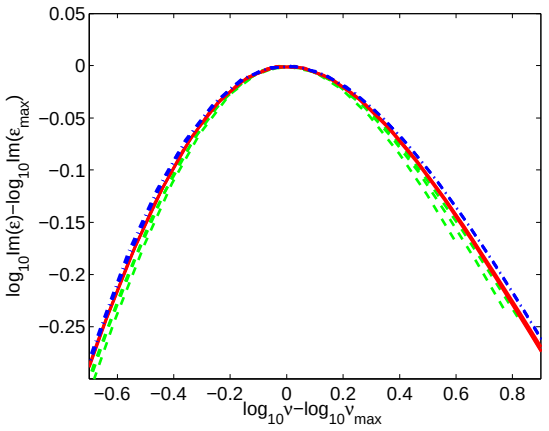

Figure 5.14: Same dielectric-loss data as in figures 5.12 and 5.13, with the frequency and intensity now scaled by the values at the maximum. We show only a 1.5 decade in frequency in order to magnify the details. Notice a small broadening as the characteristic relaxation time increases: Blue dashed-dotted line are three different data sets with $log_{10}\nu_{max} \approx 2.6$ (P=320 MPa,T=253.9 K and P=153 MPa,T=236.3 K and P=0 Mpa,T=219.3 K). Red full lines are three data sets with $log_{10}\nu_{max} \approx 4.1$ (P=251 MPa,T=236.3 K and P=108 MPa,T=219.3 K and P=0 Mpa,T=205.6 K). Green dashed lines are three data sets with $log_{10}\nu_{max} \approx 5.2$ (P=339 MPa,T=236.3 K and P=200 MPa,T=219.3 K and P=85 Mpa,T=205.6 K).

fitting the m-toluidine data. The Cole-Davidson fit to the m-toluidine gives $\beta_{CD} = 0.42$ (see also section 5.3.1). Mandanici *et al.* [2005] have reported a temperature independent value of $\beta_{CD} = 0.45$ for data taken at atmospheric pressure in the temperature range 190 K-215 K, a value that is compatible with ours.

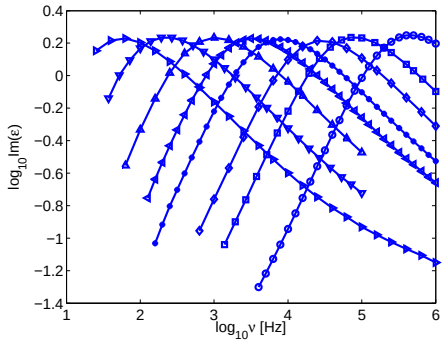

Figure 5.15: Log-log plot of the frequency-dependent dielectric-loss of m-toluidine at T=216.4K and pressures 0 MPa, 59 MPa, 79 MPa, 105 MPa, 122 MPa, 142 MPa, 173 MPa and 191 MPa. The peak shifts left as pressure is applied. Lines are guides to the eye.

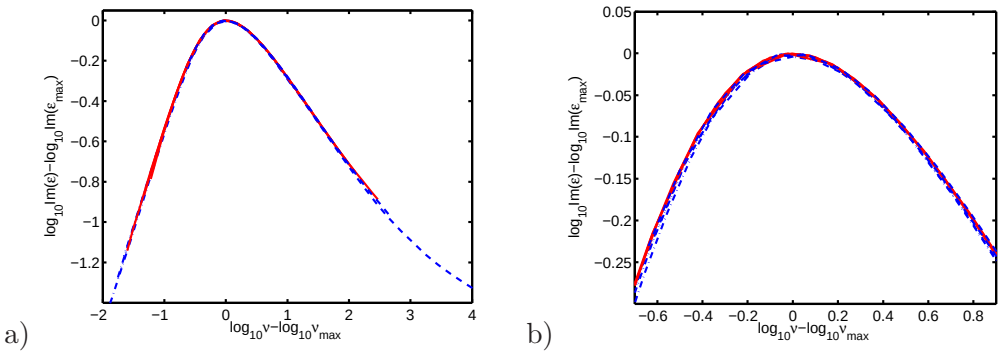

Figure 5.16: Same dielectric-loss data as in figure 5.15, now with the intensity and frequency scaled by the values of the peak maximum. Figure b) shows a zooming in of the data in a) to focus on the alpha relaxation region near the peak maximum.

5.3.4 Stretching and fragility

When Böhmer *et al.* [1993] suggested a correlation between fragility and the non Debye character of the relaxation function, expressed in terms of the stretching parameter β_{KWW}, it was the isobaric fragility which was considered.

The data we report here confirm the earlier finding [Ngai *et al.*, 2005] that the spectral shape of the alpha relaxation does not vary when pressure is increased while

keeping the relaxation time constant. If this finding is indeed general then it suggests that the spectral shape of the alpha relaxation has the same intrinsic character as the isochoric fragility, namely that it stays constant along an isochrone (chapter 3). The isobaric fragility on the other hand will in general change when pressure changes. Hence, the pressure dependence of the isobaric fragility and spectral shape is in disagreement with the behavior expected from the correlation between the two. This leads us to suggest that the stretching might/or better correlate to the isochoric fragility than to the isobaric fragility.

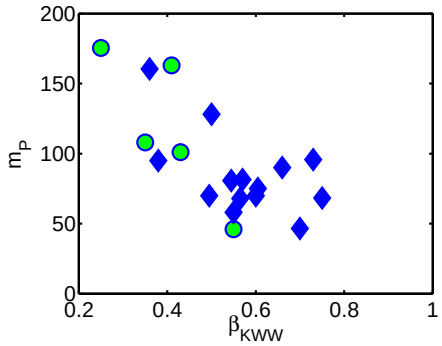

Figure 5.17: Isobaric fragility as a function of the stretching parameter. Circles represent polymers, diamonds represent molecular liquids. See the table in appendix B for numerical values and references.

To test this hypothesis we have collected data from literature reporting isobaric fragility and stretching of the relaxation at T_g. We consider here the description of the shape of the relaxation function in terms of the KWW stretching parameter β_{KWW}. This choice is made because it is convenient to use a description with only one parameter for the shape and because β_{KWW} is the most reported of the liquids where m_ρ is also available (see section 5.3.1).

The compilation of this data is shown in figures 5.17 and 5.18 where both the isochoric (figure 5.18) and isobaric fragility at atmospheric pressure (figure 5.17) are plotted against the stretching parameter. There is a great deal of scatter in both figures. There is however an observable trend, the fragilities decrease with the stretching. The relative effect on the slowing down of the relaxation is characterized by the term $\alpha_P T_g \frac{\mathrm{d}\log e(\rho)}{\mathrm{d}\log\rho} = m_P/m_\rho - 1$. In figure 5.19 we show the ratio m_P/m_ρ as a function of β_{KWW}. It is clear that no correlation is found between this ratio and the stretching. This indicates that there is no relation between the effect of density on the correlation time and the spectral shape (see chapter 3).

Based on the pressure dependence and the clear lack of correlation between stretching and the relative effect of density (seen in figure 5.19) we suggest that a possible

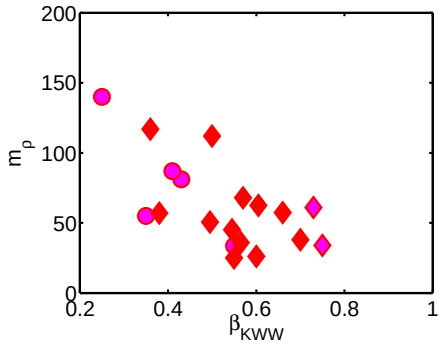

Figure 5.18: Isochoric fragility m_ρ the stretching parameter β_{KWW}. Circles represent polymers, diamonds represent molecular liquids. See the table in appendix A for numerical values and references.

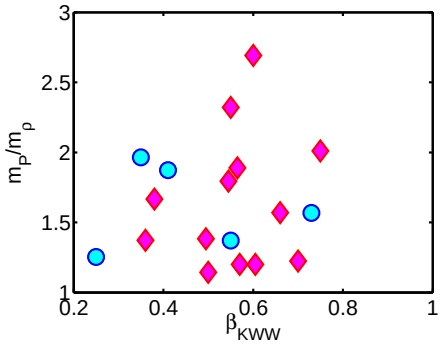

Figure 5.19: The ratio between isochoric and isobaric fragility as a function of the stretching parameter β_{KWW}. Circles represent polymers, diamonds represent molecular liquids. See the table in appendix A for numerical values and references.

correlation between stretching and fragility should be interpreted as a correlation between stretching and the isochoric fragility, while a correlation to isobaric fragility is an indirect consequence hereof. This means that the stretching is related to the "pure" effect of temperature on the relaxation time. This is consistent with the fact that the fragility and the stretching both stay constant on an isochrone.

So far we have considered only fragility and stretching at the conventional glass transition temperature, that is around $\tau_\alpha = 100$ s. However, the stretching depends on the relaxation time and also the departure from Arrhenius temperature dependence and hence the fragility depend on relaxation time (see sections 2.2 and 3.3.5). The general qualitative behavior is that the fragility decreases approaching the strong limit when the relaxation time is decreased and the "normal" liquid regime is approached. The decrease in relaxation time is also accompanied by a decrease in stretching (increase in β_{KWW}) and a Debye behavior is approached as the liquid regime is reached. This gives support to the idea that the intrinsic (isochoric) fragility of a liquid is correlated to the intrinsic stretching of the relaxation function.

5.4 Summary

We report dielectric relaxation data under pressure for two molecular liquids, m-toluidine and DBP. We combine the relaxation time data with the available thermodynamic data and analyze the respective effect of density and temperature on the dynamics. This result is consistent with a general picture in which the isochoric fragility is constant on an isochrone. The shape of the relaxation function (eg. expressed by the stretching parameter β_{KWW}) is also found to be constant on an isochrone. We use the framework in chapter 3 in order to discuss effect of density on the possible correlation between the fragility and the stretching of the relaxation function. We suggest that if the stretching correlates to fragility then it should be correlated to isochoric rather than isobaric fragility.

Résumé du chapitre 6

Le facteur de structure cohérent a été mesuré dans le polyisobutylène pour différentes masses molaires et dans le cumène en fonction de la température à pression atmosphérique et à 300 MPa. Les expériences et les résultats sont présentés dans ce chapitre.

L'effet principal de la pression est une augmentation du vitesse de son, tandis que son amortissement reste plus ou moins le même.

Le facteur de non-ergodicité (rapport entre l'intensité élastique et l'intensité totale) mesuré dans les verres (en dessous de T_g) ne varie pas avec la pression. Cela implique une augmentation du paramètre α défini par Scopigno *et al.* [2003] du fait de la dépendance en pression de la température de transition vitreuse. Le paramètre α augmente aussi avec la masse molaire. L'évolution de α avec la pression comme celle avec masse molaire ne suivent pas l'évolution attendue du fait de la correlation entre α et la fragilité isobare.

Sur la base du schéma developpé dans le chapitre trois, on discute l'effet respectif de la température et de la densité sur une corrélation possible entre α et la fragilité du liquide. On suggère que la grandeur à considérer dans le cadre d'une corrélation avec α n'est pas une fragilité mais la derivée $\frac{\mathrm{d}\log e(\rho)}{\mathrm{d}\log\rho}$. C'est-à-dire que α est relié à l'effet de la densité sur le temps de relaxation plutôt qu'à l'effet de la température.

Chapter 6

High Q collective modes

In this chapter we present a study of temperature, pressure and molecular weight dependence of the coherent dynamical structure factor measured by IXS in cumene and PIB. The study of the molecular weight dependences allows to change macroscopic characteristics of the sample while the relaxing entity is kept the same. It is in this sense analogous to pressure studies. The IXS spectra give information on the collective modes in the Q-range 1-10 nm $^{-1}$ which gives $1/Q \sim$ 0.1-1 nm. This means that we are studying "sound" at wavelengths so small that they are comparable to the distance between the molecules (or the monomers of a polymer). The modes in this Q region have frequencies of the same order of magnitude as the boson peak frequency, and the information on their behavior is therefore relevant in order to understand the meaning of the boson peak. Some of the results of this chapter therefore play a central role in chapter 8 where we analyze the pressure dependence of the boson peak in polyisobutylene.

The main focus of the analysis and discussion in this current chapter is the pressure and temperature dependence of the nonergodicity factor as measured by IXS and particularly to scrutinize the proposed correlation to fragility [Scopigno *et al.*, 2003]. The correlation was briefly introduced in section 2.7.1 and more details will be given in section 6.4.1.

6.1 Inelastic X-ray scattering

6.1.1 The experimental technique

The IXS experiment on cumene was performed on the IXS beamline ID16 at the ESRF, while the experiment on PIB was performed on its sister beamline ID28. In

this section we briefly describe the technique and give details regarding the specific experiments in the following section.

The study of phonons by inelastic X-ray scattering (IXS) requires resolution of the energy transfer in the meV range while the incoming photon has an energy in the 10 keV range. This means that the relative resolution has to be in the 10^{-7} range. This is obtained by using higher order reflections of silicon crystals in a backscattering geometry. The scan in energy is done by changing the temperature of the crystal steps of $\sim$ 5 mK and hereby varying the lattice spacing .

The temperature changes are made at the monochromator, while the analyzers are kept at a constant temperature, meaning that the scan in energy is done by changing the incoming energy and keeping the outgoing energy constant. The (11 11 11) reflection of the Si monochromator and analyzer crystals was used for the reported experiments yielding an energy resolution of FMHW=1.6 meV.

There are 5 analyzers on a moving arm, with a fixed position with respect to each other. This allows spectra to be recorded at 5 Q values simultaneously with a difference of 3 nm^{-1} between them.

6.1.2 The experiment

The dynamical structure factor of cumene was recorded at different temperatures in the glass and in the liquid at atmospheric pressure and at 300 MPa. See appendix A for details on the sample. The analyzers were set to give the Q values 2 nm^{-1}, 1 nm^{-1}, 4 nm^{-1} 7 nm $^{-1}$ and 10 nm^{-1}. The integration time per point was minimum 60 s per point and was increased by a factor 2 or 3 at lower temperatures where the inelastic intensity is lower.

We measured the dynamical structure factor as a function of temperature at atmospheric pressure for four PIB samples, with different molecular weight: PIB680, PIB1100, PIB3580 and PIB500k. See appendix A for details on the samples. The PIB680 and PIB3580 samples were moreover studied at 300 MPa. The Q setting 2 nm^{-1}, 5 nm^{-1}, 8 nm^{-1} 11 nm $^{-1}$ and 14 nm^{-1} was used for all the samples under all P-T conditions. Several additional Q settings were used at some conditions. The integration time per point was 70 s.

The samples were in both experiments placed in a 10mm (or 20mm) long cylindric pressure cell, which was sealed at both ends by 1 mm thick diamond windows. The pressure was applied using a piston-and-cylinder device. The pressure was always imposed above the (pressure dependent) glass transition temperature, and cooling was done isobarically by adjusting the imposed pressure upon cooling.

The experiment on PIB was performed using ethanol as the pressurizing medium. Ethanol does not dissolve PIB (at ambient pressure). Moreover, we isolated the sample from the ethanol by placing it in a 9.9 mm long Teflon cylinder closed in both ends with a Teflon film. The Teflon cell was subsequently mounted in the pressure cell.

The experiment on cumene was performed using the cumene itself as pressurizing medium. Thus, more sample was added in the cell, and therefore in the beam, when the pressure was increased.

6.1.3 Data treatment

Since the incoming photon looses less than a ppm of its initial momentum we can neglect this change and take $Q_{in} = Q_{out}$. This means that the conversion from angle to Q is given simply by $Q_{out} = 2Q_{in}sin(\theta)$ and the Q_{in}/Q_{out} factor in equation 4.3.10 is equal to one. Hence $S(Q, \omega)$ at a given Q is given directly by the measured intensity as a function of energy at a given angle. Apart from the sample we also

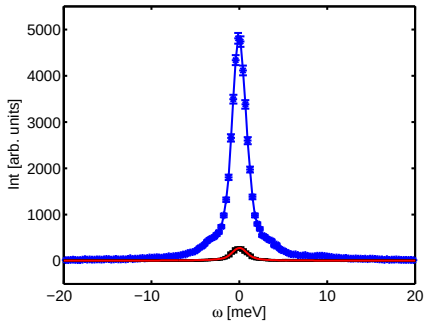

Figure 6.1: The figure illustrates a typical spectrum at $Q = 2$ nm^{-1} from raw data along with the signal of the empty cell. The intensity of the empty cell is in the order of magnitude 10% of the total signal. The red curve shows the resolution function scaled in intensity to the empty cell signal. The resolution function collapses with the cell signal and the cell signal can therefore be considered as purely elastic.

have the diamond window of the cell and the capton window in the beam. In the PIB experiments we moreover had a thin teflon film and possibly ethanol (between the teflon and the diamond window). The background gives rise to an elastic signal of order of magnitude 10% of the total intensity of the sample (figure 6.1). This background signal is subtracted from the measured elastic intensity. The subtraction of the background does not affect the determination of the position of the side peaks nor of their widths because the background intensity is purely elastic. However, it

does influence the nonergodicity factor. This leads to a relatively larger systematic error in the nonergodicity factor as compared to measurements at ambient pressure.

Fitting

The data are fitted by use of a damped harmonic oscillator for the inelastic signal and a delta function for the elastic line

$$S(Q,\omega) = S(Q)\left(f(Q)\delta(\omega) + [1-f(Q)]\frac{1}{\pi}\frac{\Omega^2\Gamma(Q)}{(\omega^2-\Omega^2(Q))^2+\omega^2\Gamma^2(Q)}\right). \quad (6.1.1)$$

The normalization of the functions ensures that the integral $\int S(Q,\omega)d\omega = S(Q)$ and $\int_{-\Delta\omega}^{\Delta\omega} S(Q,\omega)d\omega/S(Q) = f(Q)$. The wavelength studied is $2\pi/Q$, Ω gives the frequency of the mode in question, and Γ denotes the damping/attenuation of the sound mode.

The above function is symmetric in ω. Detailed balance is obtained by multiplying with the factor $\hbar\omega/(k_BT)/(1-exp(-\hbar\omega/(k_BT)))$. Note that the sample gain of energy is taken as positive energy in this case. This is done to follow the convention in the IXS community, however it is the opposite of the convention in neutron scattering. The neutron convention is used in section 4.3 and in chapter 8. The last point of the analysis is the convolution with the resolution function. The resolution is obtained experimentally at the beamline by a measurement on a plexiglass sample. The complete function used in the fitting procedure is hence

$$\begin{aligned} I(Q,\omega) &= A\int R(\omega-\omega')\left(f(Q)\delta(\omega')+\right. \quad (6.1.2)\\ &\left.\frac{\hbar\omega'\beta}{1-exp(-\hbar\omega'\beta)}[1-f(Q)]\frac{1}{\pi}\frac{\Omega^2\Gamma(Q)}{(\omega'^2-\Omega^2(Q))^2+\omega'^2\Gamma^2(Q)}\right)d\omega'. \end{aligned}$$

Where A is a factor that contains $S(Q)$ as well as the total number of scatterers, scattering length etc., see section 4.3.2. The quality of the fits is generally very convincing, this is illustrated in figure 6.2.

6.2 Sound speed and attenuation

6.2.1 PIB

Figure 6.3 shows the dispersion of the longitudinal sound modes in the Q-range 2 nm^{-1} to 20 nm^{-1} measured at ambient pressure and at 300 MPa, for the PIB680 at

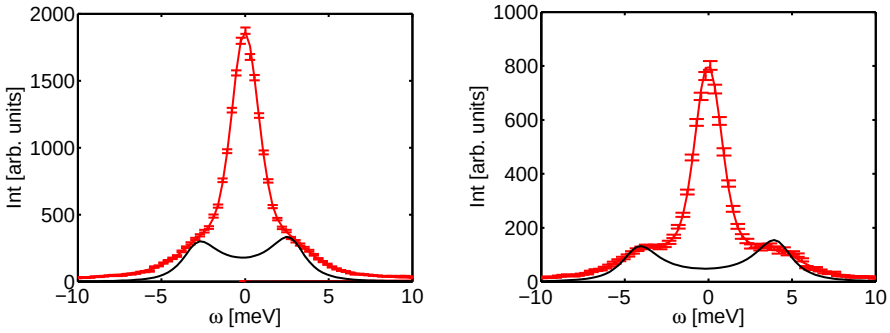

Figure 6.2: $S_{coh}(Q,\omega)$ of PIB3580 at Q =2 nm^{-1} at room temperature and ambient pressure (left) and 300 MPa (right). The full red line illustrates the fit to equation 6.1.2. The black curve shows the inelastic signal before convolution with the resolution function (second term of equation 6.1.1) .

room temperature. The qualitative behavior is the same at other temperatures and with samples of other molecular weights. The dispersion is linear up to Q=2 nm^{-1} where it starts bending slowly off becoming flat around Q =5 nm^{-1}. The result corresponds to the dispersion generally seen for disordered materials [Ruocco and Sette, 2001]: showing a maximum at about $Q_m/2$, with Q_m being the position of the first structure factor maximum. $Q_m \approx 10\,\mathrm{nm}^{-1}$ for PIB [Farago *et al.*, 2002] (see also figure 6.4). The effect of pressure is a shift of the Brillouin lines to higher frequency (figure 6.2), corresponding to an increase in sound speed. The shift corresponds to a change in sound speed from 2070 m/s to 2860 m/s for the PIB680 at room temperature (the dispersion shown in figure 6.3).

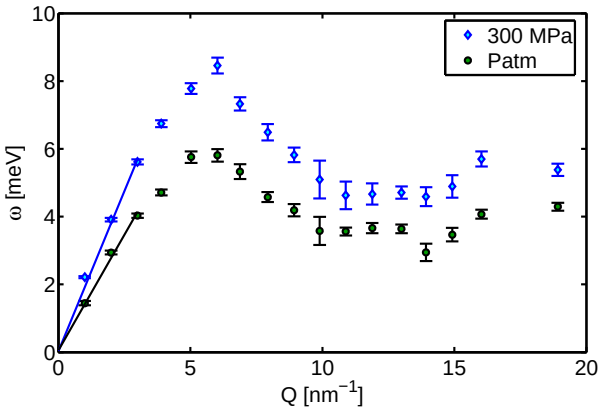

Figure 6.3: The dispersion of longitudinal sound modes of PIB680 measured by IXS at room temperature at atmospheric pressure and 300 MPa.

The sound speed in the glass is temperature independent within error-bars, while the

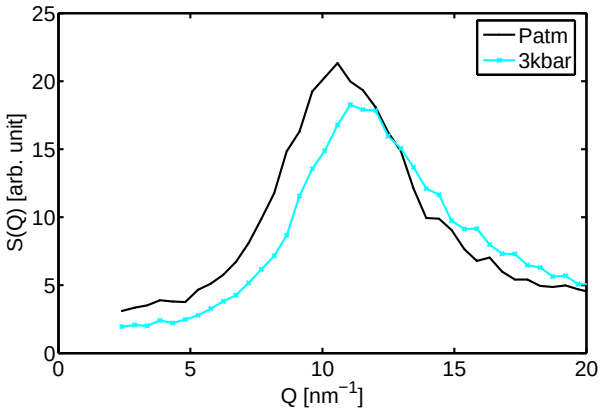

Figure 6.4: The static structure factor of PIB680 at room temperature at atmospheric pressure and 300 MPa.s, measured on ID28.

sound speed decreases when temperature is increased above T_g. This is illustrated by the data of PIB680 in figure 6.5. This change in temperature dependence of the high frequency sound speed is a signature of the transition from glassy to high frequency equilibrium dynamics according to the definitions given in section 2.5.

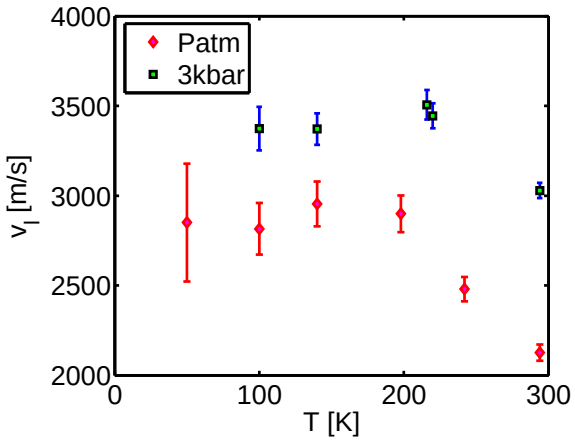

Figure 6.5: The sound speed of PIB680 at room pressure and at 300 MPa as a function of temperature (calculated from the excitation at Q=2nm^{-1}). The sound speed in the glass is temperature independent within error-bars, while the sound speed decreases when temperature is increased above T_g. An equivalent behavior is found for PIB3850 (not shown).

The sound speed increases with increasing molecular weight at ambient pressure and room temperature, with a molecular weight dependence that levels off around Mw=10000 g/mol. However, when comparing the (temperature independent) sound speeds in the glass we see no molecular weight dependence (figure 6.6).

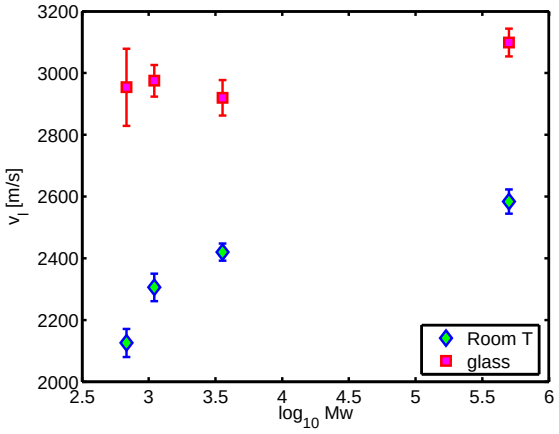

Figure 6.6: The sound speed as a function of molecular weight at ambient pressure. At room temperature and in the glass. The values are calculated from the excitation at Q=2nm^{-1}.

The relatively low sound speed of the PIB samples have the consequence that the Brillouin peaks are very close to the central line and in some cases almost inside the resolution function. There is consequently a large error on the determination of the sound attenuation factor using the IXS technique. This is particularly a problem for PIB680 in which case we had to fix the gamma value in order to get reasonable fits of the data.

Figure 6.7 shows the temperature dependence of the sound attenuation at atmospheric pressure and at 300 MPa for PIB3580 at Q=2 nm^{-1}. It is seen that sound attenuation is independent of pressure and of temperature and has the value Γ = 2.5 meV$\pm$ 0.5 meV at Q =2 nm^{-1}.

The sound attenuation is best determined at high temperature, high molecular weight and high pressure, because these condition gives a combination of high intensity and high sound speeds, yielding the most prominent and well separated Brillouin peaks in the raw data. This also means that we can get a reasonable fit at 1 nm^{-1} under this condition. Figure 6.8 shows the Q-dependence of Γ in this condition. The functionality of Q-dependence cannot be separately extracted but is consistent with a $\Gamma \propto Q^2$ behavior in the low Q range .

6.2.2 Cumene

The qualitative behavior is similar to that of PIB, and of other systems, with a linear dispersion at low Q and a bend at around $Q_m/2$. The dispersion appears to stay linear in a longer range than in the case of PIB, being close to linear all the

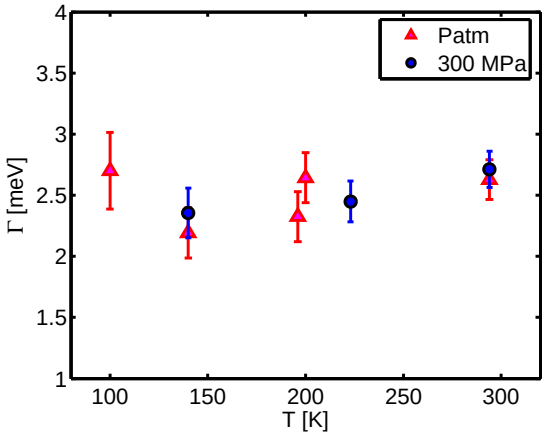

Figure 6.7: The sound attenuation at two different pressures as a function of temperature. PIB3580, Q=2 nm^{-1}.

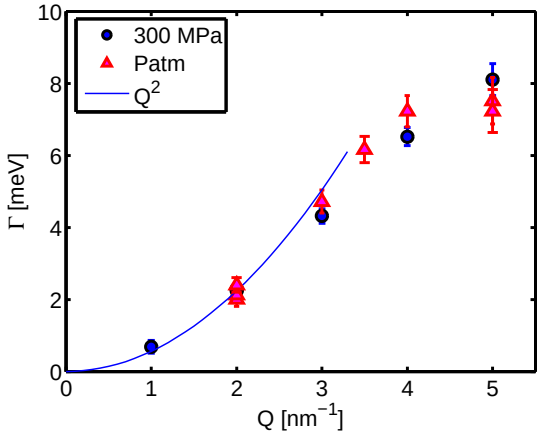

Figure 6.8: The sound attenuation of PIB500k room temperature at two different pressures as a function of Q.

way up to 4 nm^{-1}, and bends after this (figure 6.2.2). Though this is difficult to determine precisely with the relatively scarce number of Q-values.

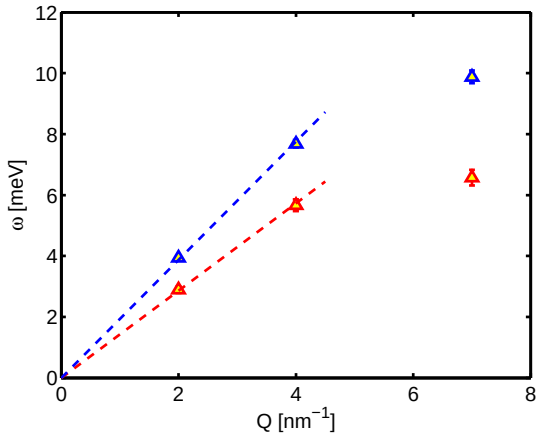

Figure 6.9: The dispersion of cumene at T=160 K at ambient pressure and at 300 MPa. The dashed lines are guides to the eye. A few of the spectra are shown in figure 6.10.

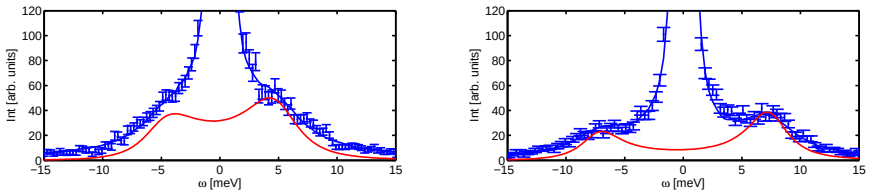

Figure 6.10: $S_{coh}(Q,\omega)$ of cumene at Q =4 nm^{-1} at T=160 K and ambient pressure (left) and 300 MPa (right). The full blue line illustrates the fit to equation 6.1.2. The red curve shows the inelastic signal before convolution with the resolution function (second term of equation 6.1.1) .

In figure 6.11 we show the sound speed, calculated as ω/Q at Q=2 nm^{-1} and Q=4 nm^{-1} respectively, as a function of temperature and at ambient pressure as well as at 300 MPa. The figure confirms that the dispersion is close to linear almost up to Q=4 nm^{-1}. The speed seen at Q=4 nm^{-1} is systematically slightly lower, the beginning of the deviation from linear dispersion, but the sound speed determined from the two Q-values is the same within error-bars[1].

The sound speed decreases with increasing temperature in the melt at atmospheric pressure, while the sound speed at 300 MPa essentially is temperature independent over the entire temperature range (figure 6.11). It is moreover striking that the

[1]The fit for cumene at 2 nm^{-1} T =142 K and atmospheric pressure appears to be unreliable. It is an outlier and the result is not robust to a change of fitting program.

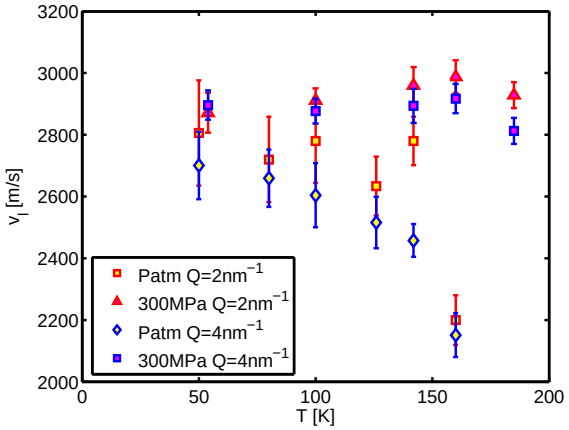

Figure 6.11: Sound speed of cumene calculated at Q=2 nm^{-1} and Q=4 nm^{-1} respectively, as a function of temperature at ambient pressure and at 300 MPa.

pressure dependence of the sound speed in the glass is very weak if present at all.

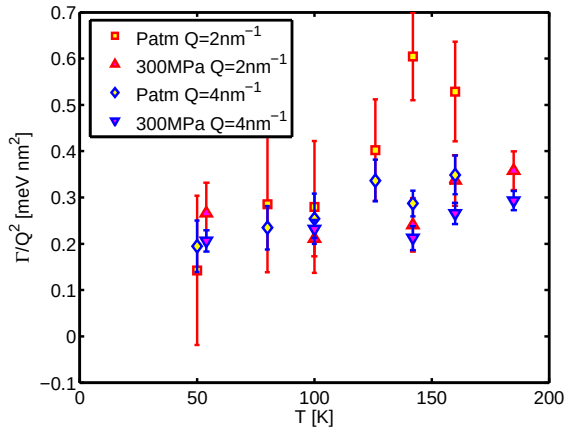

Figure 6.12: Sound attenuation of cumene as a function of temperature. The results are shown in terms of Γ/Q^2, to illustrate that the data are consistent with a $\Gamma \propto Q^2$ behavior.

The sound attenuation is shown in figure 6.12. We do not determine the Q-dependence of the sound attenuation directly since we, as in the case of PIB, have few Q values. In figure 6.16 we plot Γ/Q^2 at Q=2 nm^{-1} and Q=4 nm^{-1} respectively, as a function of temperature and at ambient pressure as well as at 300 MPa. It is seen that Γ/Q^2 is Q-independent, except in the melt at ambient pressure, meaning that the Q dependence generally is consistent with the $\Gamma \propto Q^2$ behavior which is often found in glasses [Ruocco and Sette, 2001]. It is moreover seen that the pressure dependence of Γ is very weak, with only a slight shift to lower values at high temperatures,

whereas there is no pressure dependence in the glass. Lastly a slight increase in Γ is observed as temperature increases. The effect of temperature is most pronounced at ambient pressure at Q=2 nm^{-1}.

6.3 Nonergodicity factor

6.3.1 PIB

Before looking at the nonergodicity factor (the ratio of inelastic to total intensity) we take a look at the total intensity itself (figure 6.13). The total intensity at low Q, is weakly linearly increasing with temperature at 300 MPa while it is strongly temperature dependent above T_g at ambient pressure (figure 6.13). Note that the absolute values of the different molecular weights cannot be compared directly as these will depend on the number of scattering centers in the beam. This depends both on how the cell was filled and on how it was placed in the beam. However, the experiments at different pressures where performed on the same samples without moving the cell. It is significant that the total intensity decreases as pressure is increased, particularly at high temperatures.

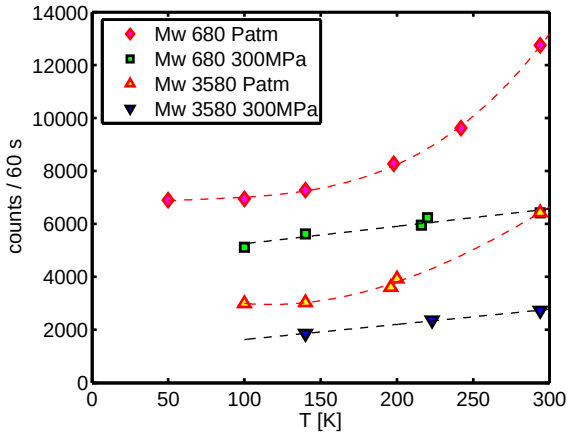

Figure 6.13: The integrated intensity as a function of temperature at Q=2 nm^{-1}. Two molecular weights and two pressures. The lines are guides to the eye.

The nonergodicity factor evaluated at Q=2 nm^{-1} decreases with temperature, but there is no pressure dependence within error-bars. This is seen in figure 6.14. On the other hand, it is seen in the figure that there is a strong dependence on the molecular weight, with the nonergodicity factor increasing with increasing molecular weight at all pressures.

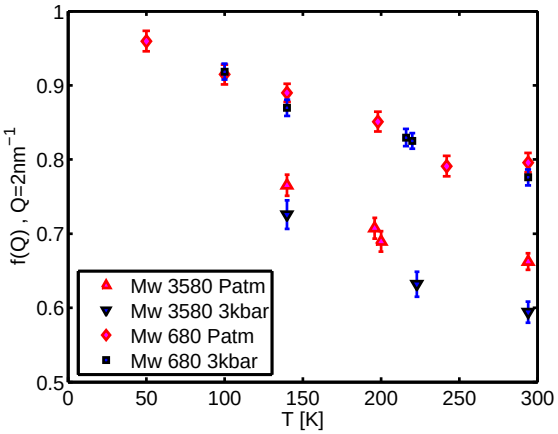

Figure 6.14: The nonergodicity factor as a function of temperature. Two molecular weights and two pressures.

The wave-vector dependence of the nonergodicity factor follows the expected oscillation with the $S(Q)$. That is, it is Q-independent in the low Q-region and increases when approaching the structure factor maximum (figure 6.15).

6.3.2 Cumene

Unlike the case of PIB, there is a pressure dependence of the non ergodicity factor of cumene. It is moreover non-trivial in the sense that it is different in the glass as compared to the melt. The nonergodicity factor at Q=2 nm^{-1} increases with increasing pressure in the melt while the effect is opposite in the glass (figure 6.16). The latter effect is weak and maybe not significant compared to the error-bars. The pressure dependence of the nonergodicity factor at Q=4 nm^{-1} is qualitatively the same at all temperatures with an increase in f_Q with increasing pressure. The effect is most pronounced at high temperatures, while the difference between the two temperatures essentially disappears in the glass.

6.3.3 Interpretation in terms of compressibility

In this section we rationalize the pressure dependence of the inelastic and the total intensities of PIB3580 in terms of compressibilities. The nonergodicity factor is determined from the ratio between the elastic intensity (total intensity minus inelastic intensity) over the total intensity. The considerations presented here are therefore directly relevant for understanding the nonergodicity factor, particularly its pressure dependence is of interest.

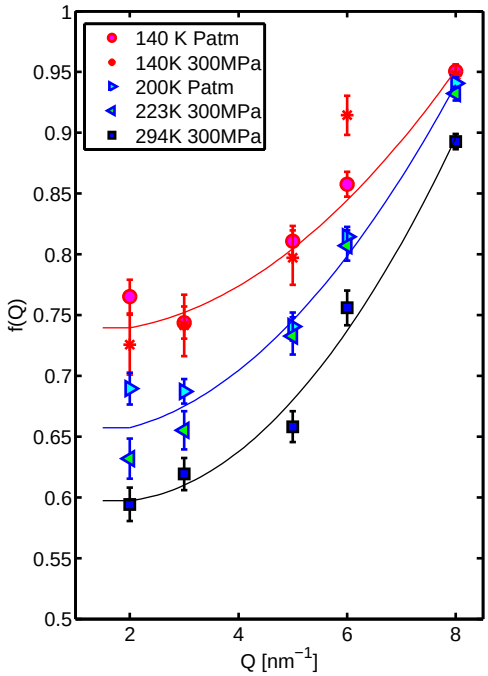

Figure 6.15: The nonergodicity factor, f_Q, as a function of Q. PIB3580 at different temperatures and pressures. It is seen that the Q dependence is leveling off at low Q. Lines are guides to the eye.

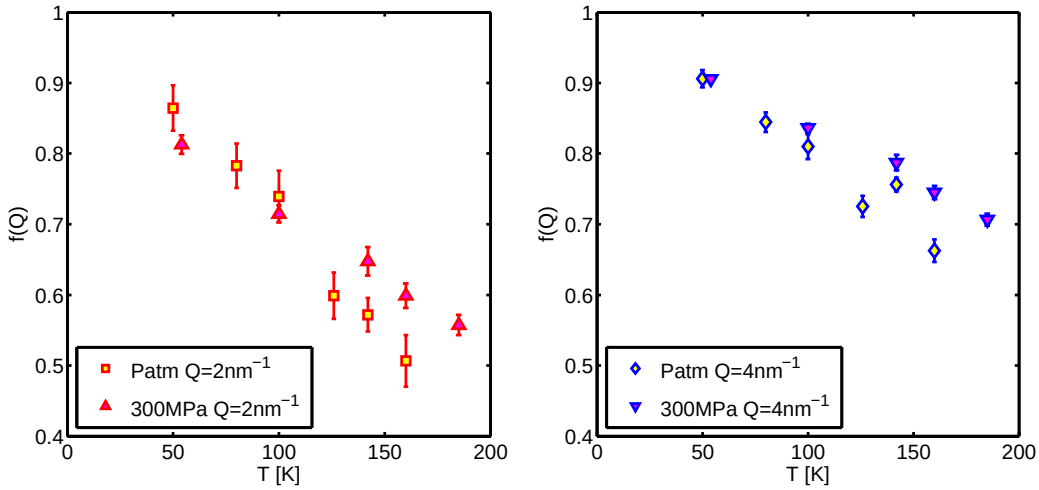

Figure 6.16: Nonergodicity factor of cumene as a function of temperature at atmospheric pressure and 300 MPa. The left figure shows the result at Q=2 nm^{-1} and the right figure shows data from Q=4 nm^{-1}

The low Q limit of $S(Q)$ is given by $k_B T \rho \kappa_T$ (equation 6.3.1). This result is based on the fluctuation dissipation theorem which relates the global density fluctuations to the response function the $\rho\kappa_T$. The energy dependent $S(Q,\omega)$ splits the compressibility in two parts. One is the central line which contains the density fluctuations that fluctuate slower than the time characteristic to the resolution, that is the relaxational part of the compressibility. The other part is the fluctuations which vary at frequencies corresponding to the sound modes at the studied Q-value, these are seen in the Brillouin lines. The fast density fluctuations are the phonons and the compressibility related to these also governs the sound speed. This leads to the following relations

$$\lim_{Q\to 0} S(Q) = k_B T \rho \kappa_T \tag{6.3.1}$$

$$AI_{tot} = T\rho\kappa_T \tag{6.3.2}$$

$$AI_{inel}(T,P) = T\rho(T,P)\kappa_{inf}(T,P) = \frac{T}{v_l^2(T,P)} \tag{6.3.3}$$

Where A is a factor that contains the total number of scatterers, the form factor etc., see section 4.3.2.

The result above holds in the low Q limit (equation 6.3.1), while the measurements are performed at a rather high Q-value, meaning that it is not *a priori* expected to find agreement with the IXS data. Q=2 nm^{-1} is on the other hand in the region where $S(Q)$ as well as f_Q are approaching their low Q plateaus and the dispersion is still linear in this range. This observation suggests that an agreement with the long wavelength behavior can be anticipated even in this region. Figure 6.17 shows that the consistency is in fact rather convincing. We show the total and the inelastic intensities as a function of temperature at atmospheric pressure as well as at 300 MPa. We moreover show $T\rho\kappa_T$ calculated from the equation of state (see appendix A) and $\frac{T}{v_l^2(T,P)}$ calculated from the sound speed determined by the position of the peaks in the IXS spectra[2]. The intensities are scaled by a factor, A, to make numerical values comparable to the $T\rho\kappa_T$. The *same* factor is used at all pressures and temperatures and for total and inelastic intensities alike. It is seen that the differences in intensity are very well interpreted in terms of the compressibilities: (i) The compressibility increases with temperature above T_g, and this effect is much more pronounced at ambient pressure than at 300 MPa. (ii) The compressibility is larger at ambient pressure than at elevated pressure. (iii) The

[2]This sound speed agrees with the sound speed at lower Q-values, see section 8.2.2.

high frequency compressibility is roughly one third of the total compressibility. The most marked discrepancy is the temperature dependence above T_g; here we find that the temperature dependence of the measure $I(Q)$ is weaker than the temperature dependence of $T\rho\kappa_T$.

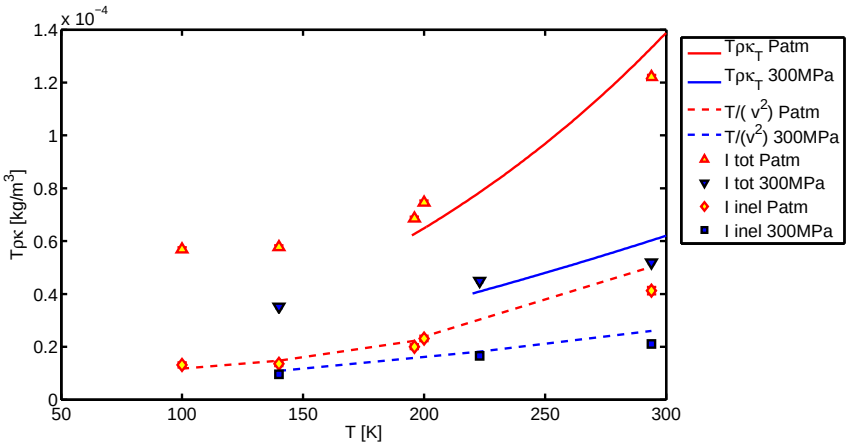

Figure 6.17: Intensities and compressibilities as a function of pressure.

The interpretation above is restricted to temperatures above T_g because density fluctuations are frozen in in the glass and there is no longer a correspondence between the density fluctuations measured by scattering and the compressibility one would measure in a macroscopic experiment where the system is compressed. The compressibility measured by volume changes as a function of applied pressure, will as other thermodynamic derivatives be discontinuous at T_g. It is more over ill-defined in the glass because the system is out of equilibrium and the values obtained will depend on the thermodynamic path. $S(Q)$ on the other hand does not change abruptly when T_g is passed. $S(Q)$ stays more or less constant in the glass. The intensity decreases weakly due to the decreasing intensity of the inelastic signal, while the elastic intensity is temperature independent.

The change of the nonergodicity factor with temperature in the glass is essentially governed by the temperature population factor of the phonons. Neither the sound speed nor the frozen in fluctuations seen in the elastic intensity change significantly with temperature. This means that f_Q inevitably decreases as temperature increases in the glass. The pressure dependence is however more complicated. Pressure will decrease the frozen in fluctuations and at the same time increase the glassy-modulus. These two effects will have opposite effects on the nonergodicity factor. There is no *a priori* reason why one of them should be the dominant effect.

6.4 Nonergodicity factor and fragility

It has been found that the temperature dependence of the nonergodicity factor, f_Q, in the glass correlates to the fragility of the liquid [Scopigno *et al.*, 2003]. In this chapter we will discuss this correlation based on our pressure and molecular weight dependent data. We will moreover include literature data and give a more general discussion of how the correlation reflects the effect of temperature versus the effect of density on the alpha relaxation time.

6.4.1 The proposed correlation

The nonergodicity factor is Q independent in the low Q-region (see the previous section), and the result regards the nonergodicity factor in this low Q domain. Scopigno *et al.* [2003] use Q=2 nm^{-1} as a reference Q-value when comparing systems, and we follow this convention.

The temperature dependence of the nonergodicity factor can in the harmonic approximation be described by $f_Q(T) = 1/(1 + aT)$, where a is given by the eigenvectors and eigenvalues of the vibrational normal modes and the inherent structure structure-factor (see section 4.3.7). In order to define a dimensionless parameter[3], α, to characterize the temperature dependence of the nonergodicity factor Scopigno *et al.* [2003] introduce a scaling with T_g

$$f_Q(T) = \frac{1}{1 + \alpha \frac{T}{T_g}}. \tag{6.4.1}$$

The temperature dependence predicted from the harmonic approximation is always found at low temperatures in the glass, and most often all the way up to T_g. The parameter α can therefore easily be extracted as the low temperature slope of $1/f_Q$ as a function of T/T_g (see e.g. figure 6.18). By comparing 10 different glass-forming systems Scopigno *et al.* [2003] find that α is proportional to the isobaric fragility m_P with $m_P = 135\alpha$.

If the linear dependence of $1/f_Q$ holds up to T_g then there is a one to one correspondence between $f_Q(T_g)$ and α [Buchenau and Wischnewski, 2004]:

$$f_Q(T_g) = \frac{1}{1 + \alpha}. \tag{6.4.2}$$

[3]The parameter α is a measure of the temperature dependence of the nonergodicity factor in the glass, it should not be confused with a thermal expansivity. We always give a subscript for the latter, i.e. α_P.

This means that the correlation between fragility and α hints that there could be an anti-correlation between $f_Q(T_g)$ and fragility, and this has also been verified for a number of glass formers [Buchenau and Wischnewski, 2004; Novikov *et al.*, 2005]. However, the harmonic behavior is not always followed all the way up to T_g. Using α determined from low temperatures rather than from equation 6.4.2 is therefore not in general equivalent, and the difference appears to be larger the larger is the fragility [Scopigno, 2007].

The liquid is in thermodynamic equilibrium at T_g and the low Q limit of $f_Q(T_g)$ is therefore determined by the high frequency adiabatic longitudinal compressibility, $1/(\rho v_{l,\infty}^2)$ and the equilibrium isothermal compressibility [Buchenau and Wischnewski, 2004] (see also section 4.3.9);

$$f_Q = 1 - \frac{1}{\rho \kappa_T v_{l,\infty}^2}. \tag{6.4.3}$$

In the previous section we showed that this interpretation in terms of compressibilities appears to be relevant even at the relative high Q-value of 2 nm^{-1}. In this frame the correlation can be expressed in the following way: the larger the high frequency compressibility is, compared to the isothermal compressibility, the larger is the fragility.

6.4.2 Pressure and Mw dependence

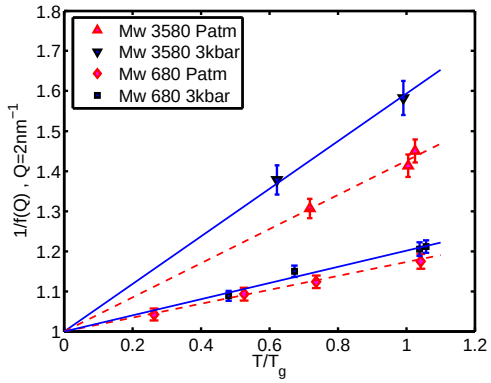

Figure 6.18: The inverse nonergodicity factor as a function of temperature normalized to glass transition temperature. PIB3580 and PIB680 at ambient pressure and 300 MPa. Lines are fits to equation 6.4.1, the slope of the lines is equal to α.

Figure 6.18 shows the inverse nonergodicity factor as a function of temperature normalized to glass transition temperature for PIB3580 and PIB680 at ambient

pressure and 300MPa. Note first of all that the $f_Q(T) = 1/(1 + aT)$ behavior is followed all the way up to T_g in this case, meaning that equation 6.4.2 is valid.

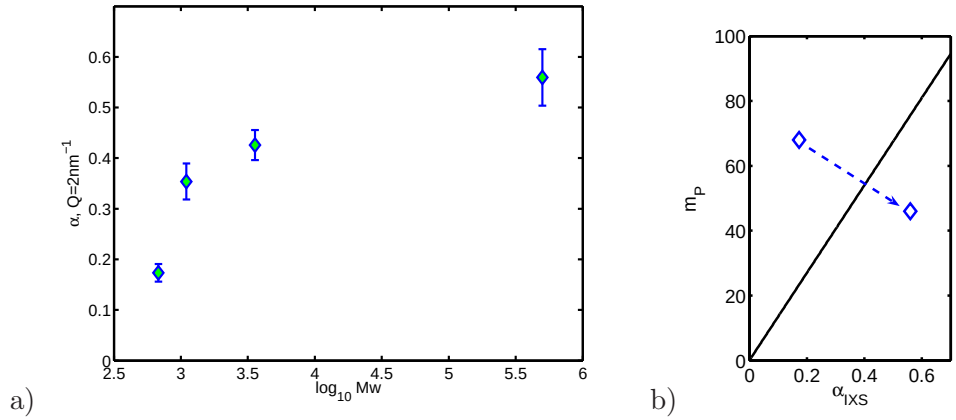

Figure 6.19: The parameter α (see text) as a function of molecular weight. $Q = 2$ nm^{-1}, ambient pressure.

It is clearly seen the slopes on figure 6.18 that α is larger for the larger molecular weight. We have also determined α for the PIB1100 and the PIB500k samples (figure 6.19 a) and find a monotonous molecular weight dependence which levels off around Mw=10.000 g/mol much like the sound speed in the liquid (figure 6.6) and other dynamical properties. We do not have the fragility of the samples at intermediate molecular weight, but the low molecular weight sample has considerably higher fragility than the high molecular PIB (see appendix A). The molecular weight dependence of α is thus opposite to what one expected from the correlation between α and fragility. This is illustrated in figure 6.19 b).

From figure 6.18 we can also anticipate the pressure dependence of α; for the PIB3580 sample it is seen that α increases significantly when the pressure is increased from atmospheric pressure to 300 MPa. The tendency is the same for the PIB680 sample although the effect is much weaker (almost within the error-bars). We will return to this result after considering the situation for cumene.

The temperature dependence of the inverse nonergodicity factor of cumene at atmospheric pressure and 300MPa is shown in figure 6.20. The data is shown both on an absolute temperature scale and as a function of T/T_g. The value of α increases when pressure is increased from atmospheric pressure to 300MPa. The isobaric fragility on the other hand decreases (see appendix A). The pressure dependence is hence not consistent with a correlation between α and m_P.

It is striking in figure 6.20 that there are deviations from the harmonic $f_Q(T) = 1/(1 + aT)$-behavior below T_g at atmospheric pressure. The harmonic behavior

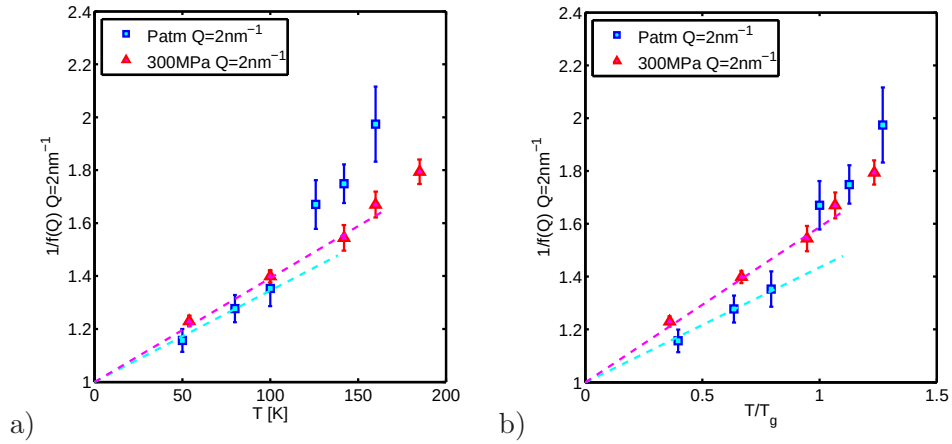

Figure 6.20: The inverse nonergodicity factor of cumene as a function of temperature. Figure a) shows an absolute temperature scale while figure b) shows temperature normalized to the pressure dependent glass transition temperature. Lines are fits to equation 6.4.1 , the slope of the lines in figure b) is equal to α.

implies that the moduli are constant, but when looking back at figure 6.11 we see that also the sound speed of cumene increases below T_g. From this we conclude that there is a high frequency relaxation in the glassy cumene which brings down the longitudinal modulus and the nonergodicity factor. There are no similar changes at 300 MPa, and it is why there is a crossover in the pressure dependence of f_Q, seen in figures 6.16 and 6.20 a).

The crossover in the pressure dependence has the consequence that while α determined from low temperatures is pressure dependent then $f_Q(T_g)$ is almost pressure independent. Moreover the weak change in $f_Q(T_g)$ is consistent with an anti correlation between $f_Q(T_g)$ and m_P.

For the mean square displacement which relates to the single particle dynamics seen from the incoherent scattering we find that the pressure dependence can be scaled out by scaling temperature with T_g (section 7.3). For α it appears that the situation is quite different. The pressure dependence seen in the $1/f(Q)$ versus T/T_g is largely (PIB3580) or solely (PIB680 and cumene) due to the scaling of the temperature axis by T_g as the isothermal pressure dependence of the nonergodicity factor is weak (PIB3580) or non existing (PIB680 and cumene). IXS data taken under pressure have earlier been performed on DBP by Mermet *et al.* [2002]. From this experiment it is also reported that the nonergodicity factor does not change as a function of pressure at constant temperature. The change in T_g with pressure therefore makes α of DBP increase with increasing pressure. DBP is an example of a liquid with no significant pressure dependence of the isobaric fragility while the

isobaric fragility of cumene decreases as a function of temperature. Yet it seems that the increase of α with increasing pressure is quite general.

6.4.3 Comparing different systems

In this section we consider the proposed correlation(s) between nonergodicity factor and isobaric fragility in terms of isochoric fragility and in terms of the effect of density on the relaxation time (see section 3.3). We shall in all cases consider α and $f_Q(T_g)$ in parallel.

In figure 6.22 we show the isobaric fragility α and $f_Q(T_g)$ respectively. We show only data points which correspond to samples for which the isochoric fragility is also known, the original correlation is indicated with a line. The first observation is that the originally proposed correlation to m_P fails when considering this limited set of data. It has been suggested that the correlation might fail if Johari Goldstein beta relaxations or other fast relaxations contribute to the intensity of the central peak [Scopigno, 2007]. This could explain the outliers lying above the line in figure 6.22 while it could not explain the outlier below the line[4].

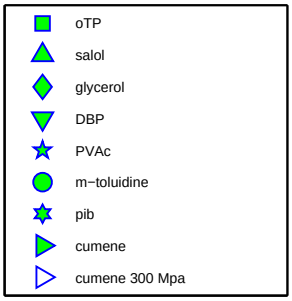

Figure 6.21: The legends for the symbols used in figures 6.22 to 6.25. The value of alpha is not known for PVAc, and we have therefore calculated it from $f_Q(T_g)$ assuming equation 6.4.2. The value of $f_Q(T_g)$ is not published for salol and was therefore calculated from α also assuming equation 6.4.2. These two values are shown with small symbols in all the figures in order not to emphasize them.

[4]DBP, which is an outlier in figure 6.22, is an example of a systems where the JG-relaxation is rather prominent. However, it is worth noticing that it still has an intensity which is orders of magnitudes lower than the alpha relaxation, meaning that its contribution to the nonergodicity factor probably can be neglected. This is illustrated in the plots below with dielectric data of Nielsen *et al.* [2006].

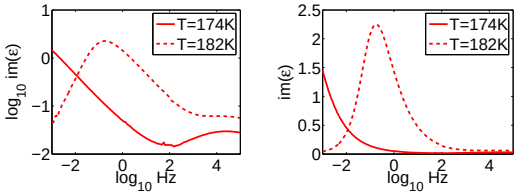

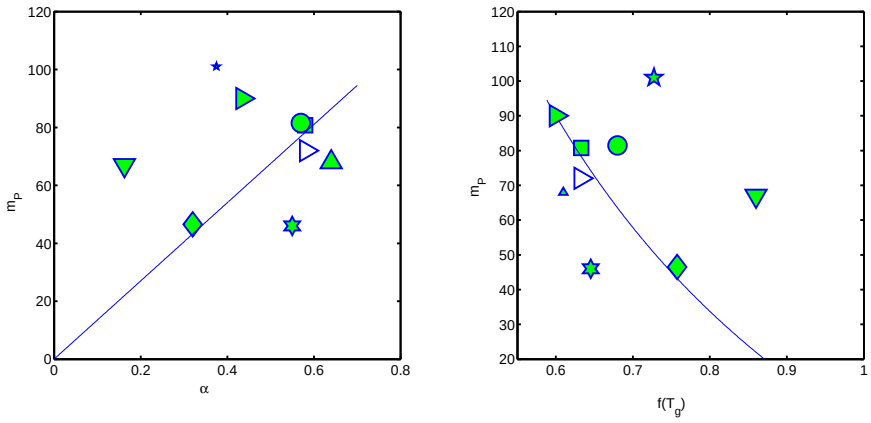

Figure 6.22: Isobaric fragility as a function of $f_Q(T_g)$ and α. The legend is found in figure 6.21.

The next observation is that the correlation to m_ρ is even poorer (figure 6.23). This indicates that the correlation proposed between $f(T_g)$ and m_P is not related to the effect of temperature on the alpha relaxation time. However, there does seem to be a correlation to the ratio m_P/m_ρ (figure 6.24) implying a correlation between $f(T_g)$ and the effect of density on the relaxation time.

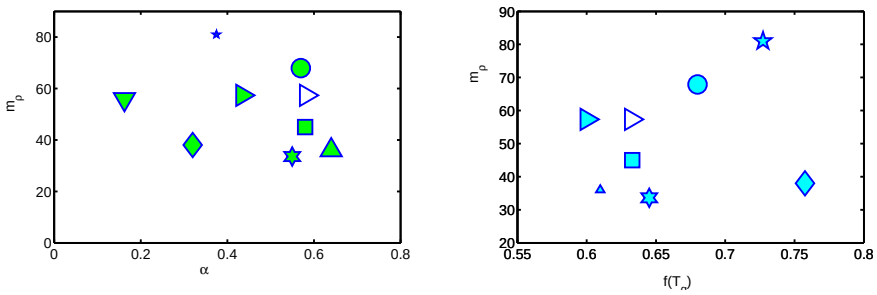

Figure 6.23: Isochoric fragility as a function of $f_Q(T_g)$ and α. The legend is found in figure 6.21.

To examine the significance of this further we start by noting that the scaling law (equation 3.2.1) leads to the following relation

$$m_P/m_\rho = \left(1 - \left.\frac{\mathrm{d}\log\rho}{\mathrm{d}\log T}\right|_P \frac{\mathrm{d}\log e(\rho)}{\mathrm{d}\log\rho}\right). \tag{6.4.4}$$

This expression clearly illustrates that the effect of density on the slowing down upon isobaric cooling as measured by m_P can itself be decomposed in two parts: the temperature dependence of the density measured by $\left.\frac{\mathrm{d}\log\rho}{\mathrm{d}\log T}\right|_P (T = T_g) = -T_g\alpha_P$

[Alba-Simionesco *et al.*, 2004; Casalini and Roland, 2004], *and* the density dependence of the relaxation time, which is contained in $\frac{\mathrm{d}\log e(\rho)}{\mathrm{d}\log\rho}$.

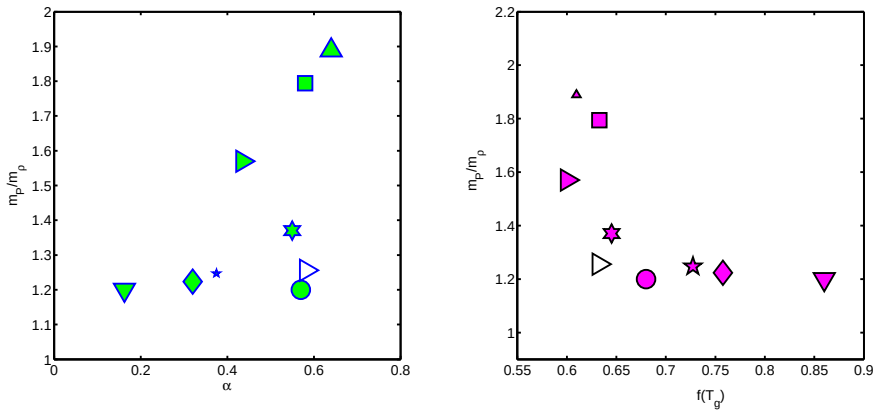

Figure 6.24: The ratio between isochoric and isobaric fragility as a function of $f_Q(T_g)$ and α. The legend is found in figure 6.21.

In figure 6.25 we show the $f_Q(T_g)$ value versus $\frac{\mathrm{d}\log e(\rho)}{\mathrm{d}\log\rho}$. The amount of data is limited and the uncertainty on this type of data is large, but it is striking that we obtain a new correlation. The smaller $f_Q(T_g)$ is the larger is $\frac{\mathrm{d}\log e(\rho)}{\mathrm{d}\log\rho}$. It is striking most of all because $\frac{\mathrm{d}\log e(\rho)}{\mathrm{d}\log\rho}$ can be determined from the dynamics of the non-viscous liquid at high temperatures [Alba-Simionesco *et al.*, 2002]. We contemplate that the correlation proposed between $f_Q(T_g)$ and m_P is a reminiscent signature of a correlation between $f_Q(T_g)$ and $\frac{\mathrm{d}\log e(\rho)}{\mathrm{d}\log\rho}$. An excellent test case for this hypothesis would be to measure $f_Q(T_g)$ on sorbitol which has a very high m_P-value combined with an exceptionally low value of $\frac{\mathrm{d}\log e(\rho)}{\mathrm{d}\log\rho}$ [Roland *et al.*, 2005].

It appears that the anti-correlation between $\frac{\mathrm{d}\log e(\rho)}{\mathrm{d}\log\rho}$ and $f_Q(T_g)$ is better than the correlation between $\frac{\mathrm{d}\log e(\rho)}{\mathrm{d}\log\rho}$ and α. This is particularly true when considering the pressure dependence of the quantities in the case of cumene; $\frac{\mathrm{d}\log e(\rho)}{\mathrm{d}\log\rho}$ does not depend on pressure and the pressure dependence of $f_Q(T_g)$ is weak whereas α has a significant pressure dependence. It is difficult to know if the pressure independence of $f_Q(T_g)$ of cumene is a coincidence or if this could be general for systems with constant $\frac{\mathrm{d}\log e(\rho)}{\mathrm{d}\log\rho}$. $f_Q(T_g)$ decreases with pressure both in the case of PIB and DBP, the correlation suggested from figure 6.25 therefore implies that $\frac{\mathrm{d}\log e(\rho)}{\mathrm{d}\log\rho}$ should increase with pressure. In section 5.2.1 we show that DBP is in fact a system where $\frac{\mathrm{d}\log e(\rho)}{\mathrm{d}\log\rho}$ increases with pressure, and PIB could be a similar system (see appendix A).

A physical significance of the correlation is that the larger the vibrational compressibility is relative to the total compressibility the more sensitive to density is the

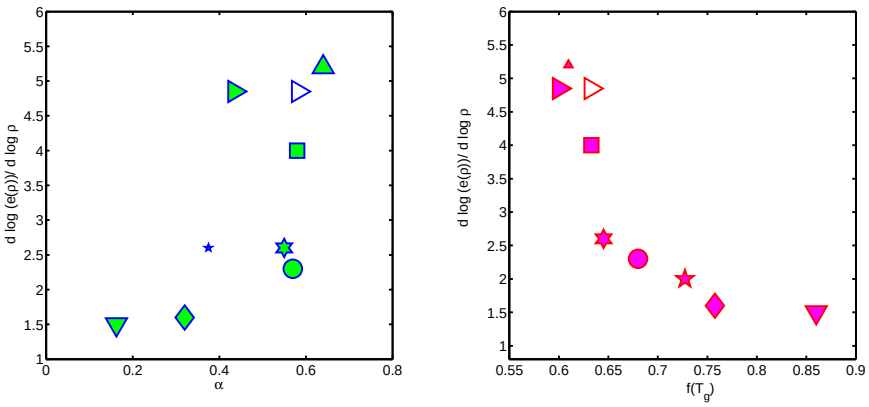

Figure 6.25: The value of $\frac{\mathrm{d}\log e(\rho)}{\mathrm{d}\log \rho}$ as a function of $f_Q(T_g)$ and α.

characteristic energy scale of the system.

6.5 Summary

The high Q sound modes have been measured in PIB of different molecular weights and in cumene, as a function of temperature at atmospheric pressure and at 300 MPa.

The most pronounced effect of pressure is an increase in the measured sound speed. This effect is much more pronounced in the liquid than in the glass. The sound attenuation is pressure and temperature independent over the whole range measured within the (relatively large) error-bars.

The pressure dependence of the nonergodicity factor appears to be non-universal. It differs from system to system and can differ when passing from the glassy to the liquid state of the same system. The pressure dependence of the nonergodicity factor in the glass is always weak. The pressure dependence of the parameter α which describes the evolution of the nonergodicity factor as a function of temperature normalized to the glass transition temperature, T_g is therefore mainly due to the pressure dependence of T_g.

The observed pressure dependence as well as the molecular weight dependence of α are opposite to the evolution expected from the correlation between α and isobaric fragility.

We have compared literature data of the α and $f_Q(T_g)$ to fragility in systems where both isochoric and isobaric fragility is known. For this limited set of data we do not

find any correlation to neither of the fragilities. However, it appears that there is a correlation between nonergodicity factor and the effect of density on the relaxation time, the most promising being a correlation between $\frac{\mathrm{d}\log e(\rho)}{\mathrm{d}\log\rho}$ and $f_Q(T_g)$. This hypothesis is based on limited data and more systems are needed to verify the trend.

We find that $f_Q(T_g)$ at $Q = 2$ nm^{-1} is well interpreted in terms of compressibilities. A physical interpretation of the correlation is that therefore the larger the vibrational compressibility is relative to the total compressibility the more sensitive to density is the characteristic energy scale of the system.

Résumé du chapitre 7

Dans ce chapitre on présente des mesures du déplacement carré moyen en fonction de la température à l'échelle de la nanoseconde, obtenues en rétro-diffusion des neutrons pour cinq liquides moléculaires. Les mesures ont été effectuées à pression atmosphérique, on a par ailleurs realisé des mesures à pression élevée sur trois de ces systèmes.

On observe que la dépendance en température du déplacement carré moyen au dessus de T_g est plus forte dans les liquides fragiles, ce qui est cohérent avec la variation attendue par le modèle élastique. Par ailleurs, l'importance de la dépendance en température est du même ordre de grandeur que celle prédite par le modèle. Le modèle élastique implique un critère de Lindemann, c'est-à-dire que le déplacement carré moyen relatif à la distance entre les molécules au carré, soit universel à T_g. Les résultats obtenus pour la série de systèmes étudiés ne sont pas cohérent avec un critère de Lindemann. Par contre, il s'avère que la dépendance du déplacement carré moyen normalisé par $\rho^{(-2/3)}$, en (T/T_g) ne change pas avec la pression. Cela indique que les amplitudes des mouvements des molécules sont fortement corrélés avec le temps de relaxation structurale.

Chapter 7

Mean squared displacement

In this chapter we report mean squared displacements at the nanosecond timescale measured by neutron scattering. We study the mean squared displacement as a function of temperature in 5 different molecular liquids at atmospheric pressure, 3 of these systems are also studied at elevated pressure. The liquids are chosen such that they span a range from ~ 45 to ~ 150 in isobaric fragility. The mean square displacement at this time scale has been shown to change its temperature dependence in the vicinity of the calorimetric glass transition temperature. This is one of the earliest observations of a relation between fast and slow dynamics [Buchenau and Zorn, 1992], and several different scenarios have been suggested to explain it [Angell, 1995; Ngai, 2000; Starr *et al.*, 2002; Dyre and Olsen, 2004]. We discuss these scenarios, the predictions one can draw from them and the agreement with data in sections 7.3 to 7.5. A common feature of these scenarios is that they predict a correlation between the *temperature dependence* of the mean square displacement and the fragility. We therefore use the arguments developed in section 3.4 in order to consider the effect of temperature and density.

7.1 Backscattering

7.1.1 Experimentals

The experiments were carried out on the back scattering instrument IN10 at the ILL. The experiments performed where so called elastic scans, in which the elastic scattering was measured as a function of temperature. This is done by using the instrument in a mode where the incoming neutron has a fixed wavelength of 6.27 Å and one measures the outgoing flux at the same energy. The outgoing neutrons were

collected at 7 detectors, which for the experiments reported here were positioned such that they spanned a range in angle (2θ) from 14° to 156° corresponding to a Q range of 0.2 Å^{-1} to 2 Å^{-1}.

The monochromation of the incoming beam as well as the scattered beam is done by use of crystals in backscattering geometry. The use of backscattering geometry optimizes the energy resolution. The (1 1 1) reflection of Si was used in our experiment yielding an energy resolution of FWHM=1 μeV. This energy resolution corresponds to a timescale in the order of a few nanoseconds. Hence, intensity corresponding to processes that are slower than this, will contribute to the measured elastic intensity (see section 4.3.10).

Cumene, m-toluidine, and DBP were studied at atmospheric as well as at elevated pressure, while DHIQ was studied at atmospheric pressure only. See appendix A for details on the samples.

The elastic scattering was measured as a function of temperature in a temperature range of of 2 K to $\sim 1.5T_g \approx 300$ K. This was done in cooling in order to avoid crystallization of the sample. The cooling rate was approximately 0.5 K/min.

The experiments at atmospheric pressure were performed using a standard cylindrical aluminum cell for liquid samples. This cell has about the size of the beam, namely about 4 cm^2. The sample thickness was 0.05 mm. This yields a transmission of roughly 95% for organic liquids, depending on density and the exact composition of the sample.

The experiments at elevated pressure were performed using clamp cells (of slightly different dimensions depending on pressure range). The cells had outer diameters of 1 cm and a wall thickness of about 2 mm. The compression was in the case of cumene performed in the pressure lab and the cell was subsequently sealed. However, we found that this method yields a large uncertainty on the pressure[1]. The measurements on DBP were performed while applying *in situ* compression and readings of the pressure. This allowed us to adjust the pressure during the cooling and to have a more precise reading of the pressure.

The cell (and the sample) only cover a small part of the beam. We therefore placed a cadmium mask in front of the sample in order to absorb the excess part of the beam and thereby reduce the background signal.

We place a small cylindrical aluminum inset in the center of the cell in order to avoid too thick a sample, since this leads to multiple scattering. The sample thickness was

[1]The actual pressure in the cell can be estimated from the point of fusion which is easily seen in the raw data when heating.

0.2 mm giving a transmission of about 80%. This value is lower than one would prefer for this type of experiment. However, the signal was weak already under these conditions (see below), and it was impossible to get a reasonable signal with a reduced sample thickness.

Along with the data from IN10 we include non-published data on glycerol obtained prior to this work on IN16 [Frick and Alba-Simionesco, 2003]. IN16 is also a backscattering instrument with almost the same energy resolution as IN10. However, IN16 has a larger flux and finer grid in Q because of a larger number of detectors. Another advantage of this experiment is that it was performed using a niobium pressure cell. This cell only goes up to ≈ 3 kbar, but has a much lower background signal.

7.1.2 Corrections

The raw data are total measured elastic intensities at 7 different Q values. The preliminary treatment of the data was performed using the standard ILL software sqwel. sqwel takes care of correcting for the different detector efficiency by normalizing to the signal of a vanadium sample. sqwel moreover performs corrections for sample self absorption and can subtract a measured background signal.

The aluminum cell gives a very small signal, and the subtraction of the empty cell therefore has almost no effect on the final result. The situation for the pressure cell, however, is quite different. The pressure cell gives as much elastic intensity as the sample itself, and the cell subtraction procedure can lead to large errors in the final result. We therefore subtracted the cell in an explicit procedure after using sqwel. This allowed us to verify that the subtracted cell signal corresponded to the total measured intensity at high temperatures where the sample liquid has no elastic scattering. The high pressure data carries a low signal to noise ratio, due to the relatively high intensity of the subtracted cell. The measured intensity of the sample in the high pressure cell is moreover lower, because the sample exploits a smaller part of the beam. Figure 7.1 illustrates the raw data (treated in sqwel, but with no cell subtraction) from an atmospheric pressure and a high pressure experiment respectively.

7.2 Elastic intensity and mean square displacement

The measured quantity, the elastic intensity, corresponds to the intermediate scattering function at a given timescale as explained in section 4.3.10. The characteristic timescale of the experiment is $1/\delta\omega \sim 1$ ns. The scattering is dominated by the

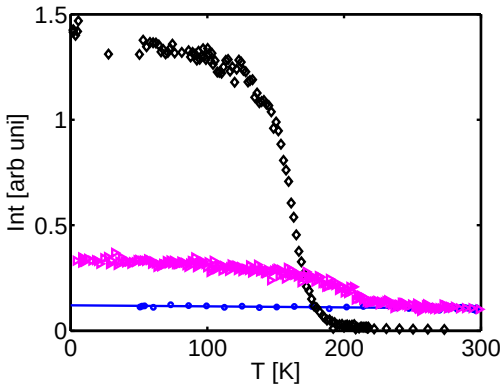

Figure 7.1: The raw data of cumene at ambient pressure in aluminum cell (diamonds) and at 100 MPa in the high pressure clamb cell (triangles). The signal of the clamb cell is also shown (circles). The signal of the aluminum cell is not shown, as it would be almost invisible on this scale.

incoherent signal and it is consequently the incoherent intermediate scattering function at $\sim$ 1 ns which is probed. The measured intensity at a fixed Q gives direct information on the pressure and temperature dependence of the dynamics on the nanosecond timescale.

Figure 7.2 shows the temperature dependence of the measured intensity of DBP at atmospheric pressure and at 500 MPa at $Q = 1.96$ Å. The curves are in both cases normalized, to start in Int=1 at $T = 0$ K, which corresponds to assume that the molecules have no zero-point movement.

At both pressures we see the measured intensity decreasing to essentially zero in the high temperature limit. This corresponds to a situation where the intermediate scattering function is totally decayed, $I_{inc}(Q,t) = 0$, at the nanosecond timescale. The curve hence shows the transition from relaxed to non-relaxed dynamics on the nanosecond timescale. It is clearly seen that this happens at a higher temperature at elevated pressure, and also that $I_{inc}(Q,t)$ increases with increasing pressure at all temperatures.

7.2.1 Calculating $\langle u^2 \rangle$

The mean square displacement is calculated from the measured intensities by assuming the Gaussian approximation, such that equation 4.3.29 holds. This gives

$$\ln(I) = A + \frac{-Q^2\langle u^2 \rangle}{3} \tag{7.2.1}$$

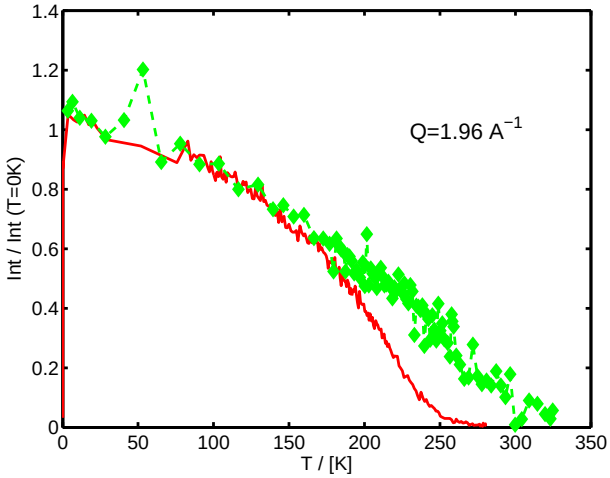

Figure 7.2: The incoherent intermediate scattering function of DBP as a function of temperature at atmospheric pressure (full line) and at 500 MPa (diamonds).

and $\langle u^2 \rangle$ can hence be found from the slope in a plot with $\ln(I)$ versus Q^2. Figure 7.3 illustrates the Q and the temperature dependence of the measured elastic signal. It is seen that there is a small systematic deviation from the Q^2 behavior, with a peak-like feature around $Q = 1$ Å^{-1}. This could be due to the coherent contribution of the scattering. In order to cancel this contribution, we assume that the mean square displacement is zero when the temperature is zero, and normalize the Q-dependent intensities at all temperatures to the low temperature limit of the Q-dependence. Apart from this small systematic deviation it is seen that the Q^2 dependence is followed even at temperatures in the range 1.2 T_g. However, this is not true at even higher temperatures, which means that the Gaussian approximation becomes inadequate.

7.2.2 The mean square displacements

Figure 7.4 shows the mean square displacement of DBP at atmospheric pressure and at 500 MPa. The mean square displacement increases linearly with temperature at low temperatures. The slope gradually increases at higher temperatures. The departure from linear is smooth and starts well below $T_g(P)$ both at atmospheric pressure and at elevated pressure.

The mean square displacement of cumene at atmospheric pressure and 500 MPa is displayed in figure 7.5. A linear increase with temperature is seen almost up to T_g and an increase in slope in the vicinity of T_g.

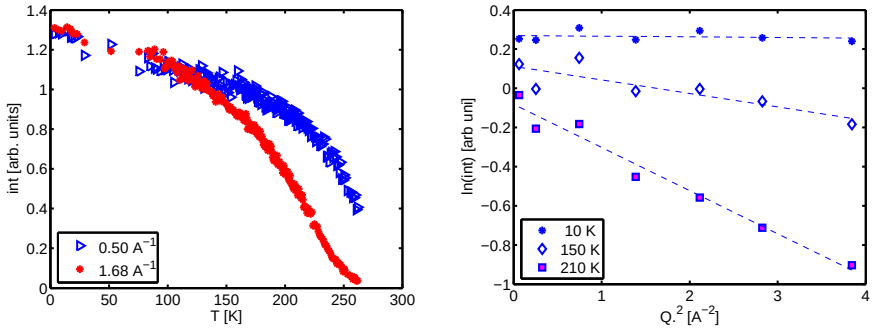

Figure 7.3: Illustration of the temperature and Q dependence of the measured elastic intensity (DBP at atmospheric pressure). Left: the temperature dependence of the intensity at two different Q-values. Right: The logarithm of the measured intensity as a function of Q^2 at three different temperatures. The lines are fits to the Gaussian approximation.

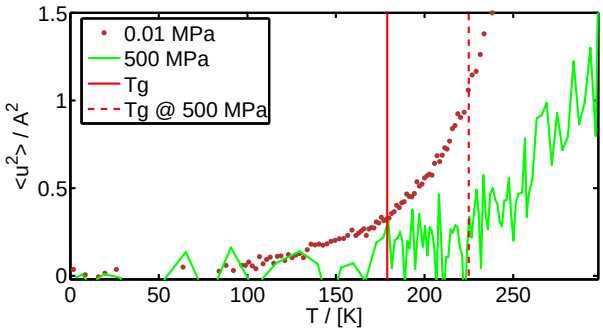

Figure 7.4: The mean square displacement of DBP as a function of temperature at atmospheric pressure (dots) and at 500 MPa (full line). The vertical lines illustrate the positions of T_g at these two pressures.

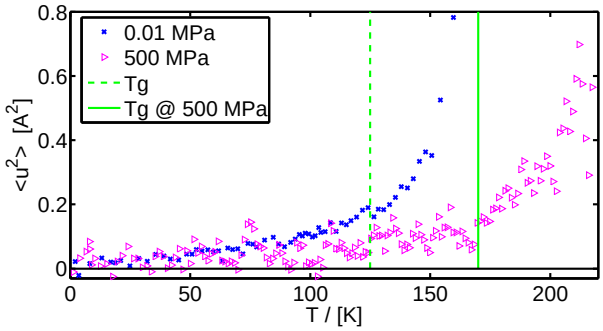

Figure 7.5: The mean square displacement of cumene at atmospheric pressure (squares) and 500 MPa (triangles). The vertical lines illustrate the positions of T_g at these two pressures.

Glycerol is known to be a case where the temperature dependence of the mean square displacement passes smoothly through T_g at atmospheric pressure. This is seen in figure 7.6, where we also display the mean square displacement at 300 MPa. The slope changes rapidly at about $1.25T_g$ in both cases (figure 7.7).

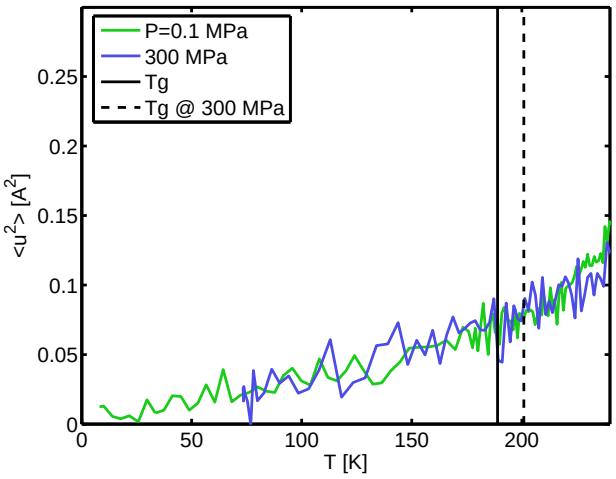

Figure 7.6: The $\langle u^2 \rangle$ of glycerol at ambient pressure and at 300 MPa.

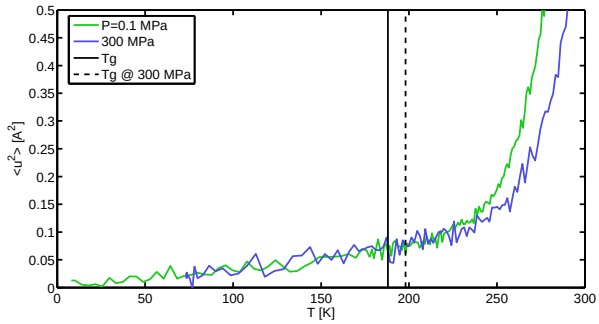

Figure 7.7: The $\langle u^2 \rangle$ of glycerol at ambient pressure and at 300 MPa.

7.3 Relation to alpha relaxation

From the data shown in the previous section it is seen that the mean square displacement at the nanosecond timescale often has a change in its temperature dependence in the vicinity of T_g, which is governed by the dynamics on the time scale of hundreds of seconds. This is a general observation and it is probably the most clear example of a coupling between fast and slow dynamics [Buchenau and Zorn, 1992; Angell, 1995; Casalini and Ngai, 2001; Ngai, 2000]. The origin of this coupling is considered

a central question for understanding the glass transition phenomenon [Angell *et al.*, 2000].

Several more specific relations between the temperature dependence of the alpha relaxation time and the mean square displacement have been proposed. It is common to these relations that they associate a larger mean square displacement to a shorter alpha relaxation time, and hence expect the change of the mean square displacement just above T_g to be more dramatic the more fragile the liquid is. The physical pictures and starting points vary, but the conclusions can essentially be condensed to two different hypothesis.

One view is, that the activation energy related to the alpha relaxation time, should be proportional to T and inversely proportional to the total temperature dependent mean square displacement, $E(\rho, T) \propto \frac{T}{a^2\langle u^2\rangle(T)}$, where a is a characteristic distance between the relaxing entity. This yields:

$$\tau(T) = \tau_0 exp\left(\frac{Ca^2}{\langle u^2\rangle(T)}\right) \tag{7.3.1}$$

where C is a constant. This view point has mainly been based on so called elastic models [Dyre and Olsen, 2004], (for a review see [Dyre, 2006]), but it has also been proposed by Starr et al [Starr *et al.*, 2002] based on a Voronoi volume analysis and computer simulations.

The other view is that it is a non-harmonic part of $\langle u^2\rangle$ that should be considered instead of the total $\langle u^2\rangle$. That is $E \propto \frac{T}{\langle u^2\rangle_{loc}(T)}$, where $\langle u^2\rangle_{loc}(T) = \langle u^2\rangle(T) - \langle u^2\rangle_{harm}(T)$. It is a little over-simplifying to call this *one* view, as the definitions proposed for $\langle u^2\rangle_{loc}(T)$ are not completely equivalent - however this has minor importance in the present context. This second view point leads to

$$\tau(T) = \tau_0 exp\left(\frac{K}{\langle u^2\rangle_{loc}(T)}\right), \tag{7.3.2}$$

where K is a constant.

We refer to this viewpoint as *the relaxational hypothesis*. The relaxational hypothesis was originally proposed from a phenomenological relation found between viscosity and $\langle u^2\rangle$ in selenium [Buchenau and Zorn, 1992]. It has later been supported by Ngai and coworkers, based on qualitative analysis of data-compilations and an extension of the coupling model [Ngai, 2000, 2004].

7.4 Lindemann criterion

If the constant C in equation 7.3.1 is assumed to be universal, then it follows that $a^2/\langle u^2\rangle$ will be the same for different liquids at the same value of the relaxation time, eg. at T_g. It has the consequence that the mean square displacement at T_g is a universal fraction of a^2 independent of the fragility or other properties of the liquid. The elastic model thus predicts a Lindemann criterion at T_g. The Lindemann criterion is the rule that $\langle u^2\rangle/a^2 \sim 1\%$ when the crystal melts. A Lindemann criterion for the glass transition has also been proposed several times independently of the elastic model. This is done by combining the two phenomenological "facts", the 2/3 rule and the Lindemann criterion for melting [Buchenau and Wischnewski, 2004; Dyre, 2006].

In order to test the Lindemann criterion, the data needs to be normalized to the squared characteristic distance between the molecules, a^2. Figure 7.8 shows the mean square displacement for the five studied liquids in one plot. The temperature is scaled to T_g, (but all liquids except cumene have very similar T_g's). The $\langle u^2\rangle$ values are normalized to a^2 where a is taken to be $v^{1/3}$ and v is the specific volume of the molecules at ambient conditions. The figure does not appear to support a Lindemann criterion as the $\langle u^2\rangle(T_g)/a^2$ varies with a factor of 3 going from glycerol to m-toluidine.

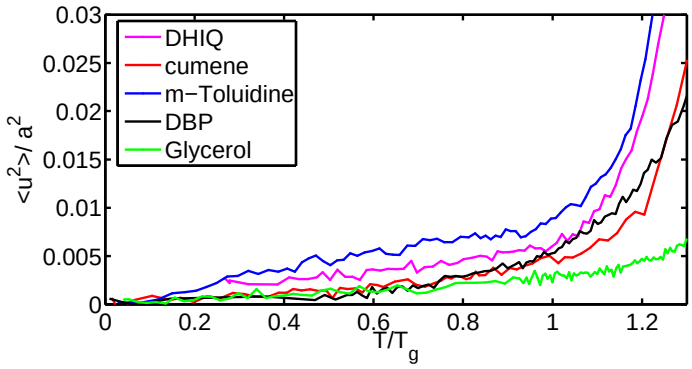

Figure 7.8: The temperature dependence of $\langle u^2\rangle$ scaled to $a^2 = v^{2/3}$ (see text for details) for 5 different liquids. The temperature is scaled to T_g.

A proposition quite opposite to that of the Lindemann criterion is suggested based on the coupling model by Ngai [2000, 2004]. Namely, that $\langle u^2\rangle$ at T_g should be larger the more fragile the liquid is. This hypothesis is substantiated by a compilation of data, mainly on polymer samples [Ngai, 2004]. Such correlation is not found in figure 7.8. The data on extremely fragile DHIQ fall in the middle of the curves again and

cumene fall closer to the much less fragile glycerol than it does to m-toluidine, which has fragility similar to that of cumene.

As an alternative figure 7.9 shows the absolute values of mean square displacement for the five liquids in one plot. The temperature is again scaled to T_g, but the $\langle u^2 \rangle$'s are given in absolute units of Å^2. This plot is the same type of plot as the ones presented in figure 4 and figure 5 of [Ngai, 2004]. It is this type of plot which is used to argue that the absolute values of $\langle u^2 \rangle$ at T_g are larger for liquids with larger n (smaller β_{KWW} larger fragility in the frame of Ngai's coupling model). In figure 7.9 we see that least fragile liquid, glycerol does indeed have the lowest absolute value. However, the extremely fragile DHIQ falls just between the liquids with much lower fragility, at odds with the results reported by Ngai [2004].

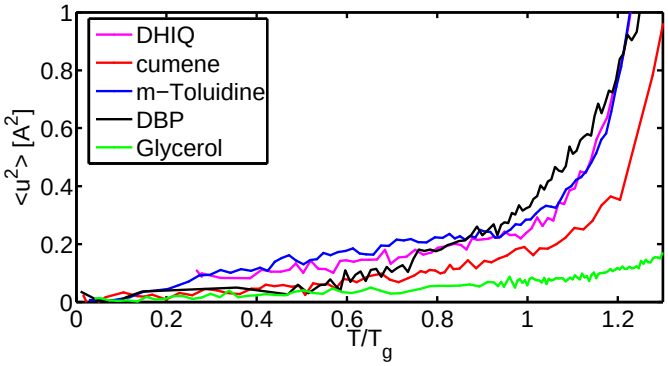

Figure 7.9: $\langle u^2 \rangle$ as a function of temperature for 5 different liquids. The temperature is scaled to T_g.

7.4.1 Pressure dependence

The value of $\langle u^2 \rangle / a^2$ at T_g does not appear to be universal, when considering the 5 liquids studied here. This breakdown of the Lindemann criterion can be *ad hoc* explained by allowing C in equation 7.3.1 to be material dependent. The Lindemann prediction becomes weaker, but can still be scrutinized by looking at the pressure dependent T_g of a given system. The "pressure dependent" Lindemann criterion following from equation 7.3.1 says that $\langle u^2 \rangle / a^2$ should be constant on an isochrone, particularly $T_g(P)$ (This is a special case of equation 3.4.2). The change in density will lead to a change in $\langle u^2 \rangle$ but also to a change in a^2. The simplest assumption for the density dependence is to assume that it follows the change in density; $a \propto \rho^{-1/3}$ [Dyre, 2006].

Figure 7.10 shows the temperature dependence of the mean square displacement in

DBP at atmospheric pressure and 500 MPa. The temperature scale in this figure is scaled by the pressure dependent T_g and the y-axis is scaled with $a^2 \propto \rho^{-2/3}$ evaluated at $(T_g(P), P)$. This scaling makes the entire temperature dependence collapse on one curve (see figure 7.4 for the raw data). The scaling of the temperature axis is by far the most important for this data collapse. The estimated increase in density is less than 10% (see appendix A for equation of state). This gives a decrease of a^2 by approximately 5%. This difference is almost indistinguishable in figure 7.10 due to the scatter of the data. The same type of data collapse is found for

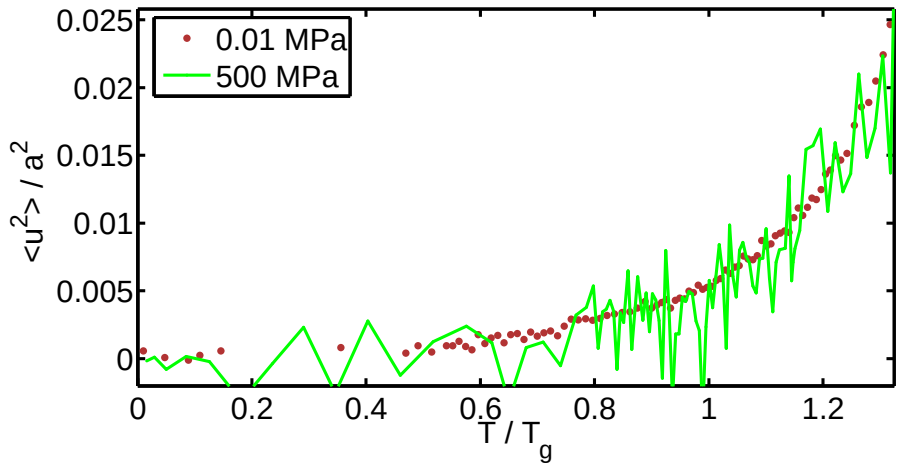

Figure 7.10: The temperature dependence of the mean square displacement in DBP at atmospheric pressure and 500 MPa. The temperature is scaled by the pressure dependent T_g and the y-axis is scaled with $a^2 \propto \rho^{-2/3}$ evaluated at $(T_g(P), P)$.

cumene (figure 7.11) within the rather large error-bars of the data on the measured pressure (see section 7.1.1). A similar result has bean found earlier by Frick and Alba-Simionesco [1999] on polybutadiene.

This scaling strongly supports the notion of a Lindemann criterion for the glass transition. It is moreover striking to see that the whole temperature dependence of the mean square displacement in the glass *and* in the liquid state collapses after applying this scaling. This is particularly clearly seen in the case of glycerol, in which case the deviation from linear temperature dependence sets in much above T_g (figure 7.12).

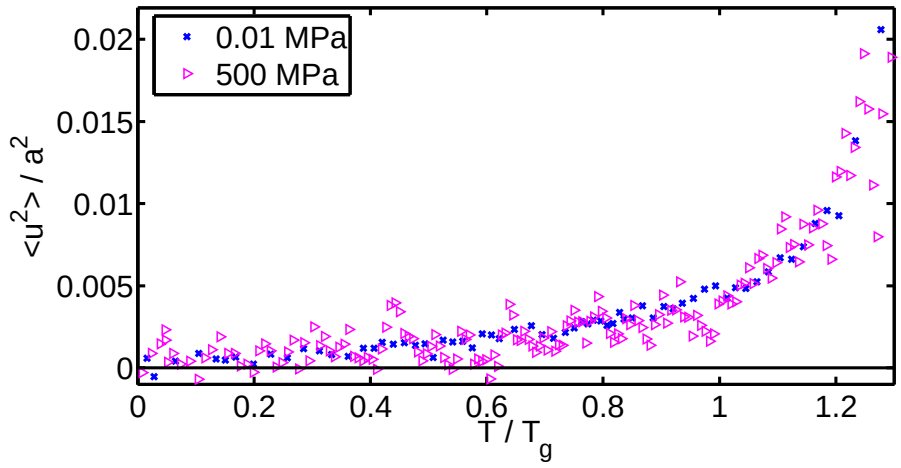

Figure 7.11: The temperature dependence of the mean square displacement of cumene at ambient pressure and at 500 MPa. The temperature is scaled by the pressure dependent T_g and the y-axis is scaled with $a^2 \propto \rho^{-2/3}$ evaluated at $(T_g(P), P)$.

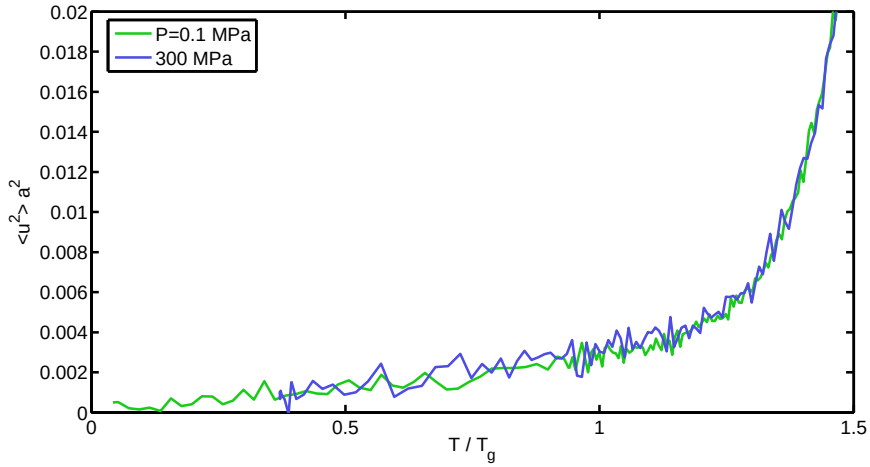

Figure 7.12: The temperature dependence of the mean square displacement of glycerol at ambient pressure and at 300 MPa. The temperature is scaled by the pressure dependent T_g and the y-axis is scaled with $a^2 \propto \rho^{-2/3}$ evaluated at $(T_g(P), P)$.

7.5 Temperature dependence

The figure 7.13 shows the $\langle u^2\rangle_T/\langle u^2\rangle_{T_g}$ as a function of T/T_g. Hence the figure illustrates the relative change in the total $\langle u^2\rangle$ as a function of the relative change in T. The $\langle u^2\rangle$ value of the very fragile DHIQ rises most dramatically, the $\langle u^2\rangle$ of glycerol the least, while the three remaining liquids, which all have similar intermediate fragilities fall in between. The five systems studied hence follow the general trend that more fragile liquids have more temperature dependent mean square displacement above T_g [Ngai, 2004].

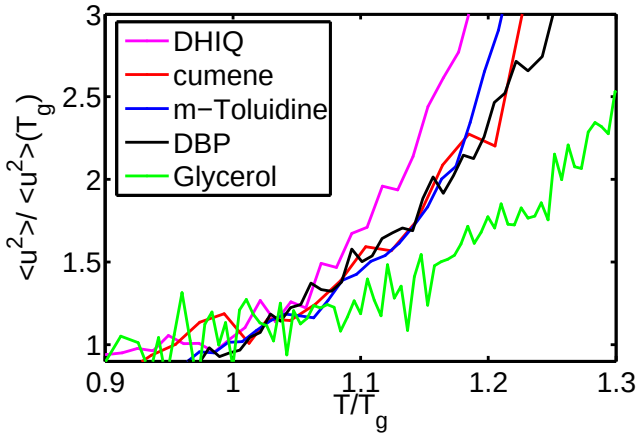

Figure 7.13: $\langle u^2\rangle$ scaled to $\langle u^2\rangle_{T_g}$ for 5 different liquids. The temperature is scaled to T_g.

The elastic model moreover makes a quantitative prediction regarding the relation between the temperature dependence of $\langle u^2\rangle$ and that of the alpha relaxation time. The elastic model leading to equation 7.3.1 is based on

$$\frac{E(\rho,T)}{k_BT} = \frac{C\rho^{-(2/3)}}{\langle u^2\rangle(\rho,T)} \tag{7.5.1}$$

(assuming that $a^2 \propto \rho^{-2/3}$). Recalling the definition of the Olsen fragility index (equation 2.2.5) it follows that the model predicts (a special case of equation 3.4.3)

$$I_P = -\left.\frac{\mathrm{d}\log E(\rho,T)}{\mathrm{d}\log T}\right|_P \tag{7.5.2}$$

$$= -\frac{\mathrm{d}\log T}{\mathrm{d}\log T} + \left.\frac{\partial\log\langle u^2\rangle}{\partial\log T}\right|_P + \frac{2}{3}\left.\frac{\partial\log\rho}{\partial\log T}\right|_P \tag{7.5.3}$$

$$= -1 + \left.\frac{\partial\log\langle u^2\rangle}{\partial\log T}\right|_P - \frac{2}{3}T\alpha_P. \tag{7.5.4}$$

I_P is of the order of magnitude 4 for fragile liquids at $T_g(\tau = 100s)$ while $T_g\alpha_P \sim 0.1$, meaning that the last term can be neglected. Using the general relation between the conventional steepness index and the Olsen index (equation 2.2.6) it subsequently follows that the model predicts a proportionality between fragility and the relative change of $\langle u^2 \rangle$ with relative change in temperature:

$$m_P = \log_{10}\left(\frac{\tau_g}{\tau_0}\right)(1 + I_P) = \log_{10}\left(\frac{\tau_g}{\tau_0}\right)\left.\frac{\partial \log\langle u^2\rangle}{\partial \log T}\right|_P \tag{7.5.5}$$

$$= 16\left.\frac{\partial \log\langle u^2\rangle}{\partial \log T}\right|_P. \tag{7.5.6}$$

The last equality follows if all values are evaluated at T_g defined by $\tau_g = 100$ s and if it is assumed that $\tau_0 = 10^{-14}$ s. Hence the elastic model predicts a correspondence between the slope seen in figure 7.13 and the fragility found from the temperature dependence of the alpha relaxation time.

Figure 7.14 tests this relation, using fragilities and T_g's taken from literature (see appendix for values and references). We also include some $\left.\frac{\partial \log\langle u^2\rangle}{\partial \log T}\right|_P (T = T_g)$ calculated on the basis of mean square displacements reported in literature. The value of $\left.\frac{\partial \log\langle u^2\rangle}{\partial \log T}\right|_P (T = T_g)$ is in all cases calculated in a narrow range temperature range from T_g to $\sim 1.1T_g$, because this corresponds to the range where fragility is determined. It has to be stressed when considering this figure that the elastic model not only predicts a proportionality between m_P and $\left.\frac{\partial \log\langle u^2\rangle}{\partial \log T}\right|_P$, the elastic model predicts the proportionality constant as well, hence the line is not a fit nor a guide to the eye. The line appearing in the figure is a parameter free prediction of the elastic model. It is therefore quite striking and not at all trivial, that the order of magnitude is correct. Secondly it also appears that the variations in m_P follow the variations in $\left.\frac{\partial \log\langle u^2\rangle}{\partial \log T}\right|_P$ except for the very fragile liquids.

A further test of the predicted correlation, could in principle be to consider the pressure dependence of fragility and $\left.\frac{\partial \log\langle u^2\rangle}{\partial \log T}\right|_P$. This correlation is of the type discussed in section 3.4, that is a correlation between fragility and the *temperature* dependence of another quantity. This means that both quantities are path dependent, and the isobaric $\left.\frac{\partial \log\langle u^2\rangle}{\partial \log T}\right|_P (T = T_g)$ is hence expected to follow the pressure dependence of the isobaric fragility. The isobaric fragility of DBP is not pressure dependent in the relevant range. It is therefore consistent that we find that the whole $\langle u^2 \rangle$ temperature dependence collapses after scaling with $\rho_g^{(-2/3)}$ and $T_g(P)$ (figure 7.10). The isobaric fragility of cumene increases with pressure. This means that the correlation implies that the slope of $\langle u^2 \rangle$ should be lower above T_g. Figure 7.11 does not support this prediction, it could even be argued that it contradicts it. However, the

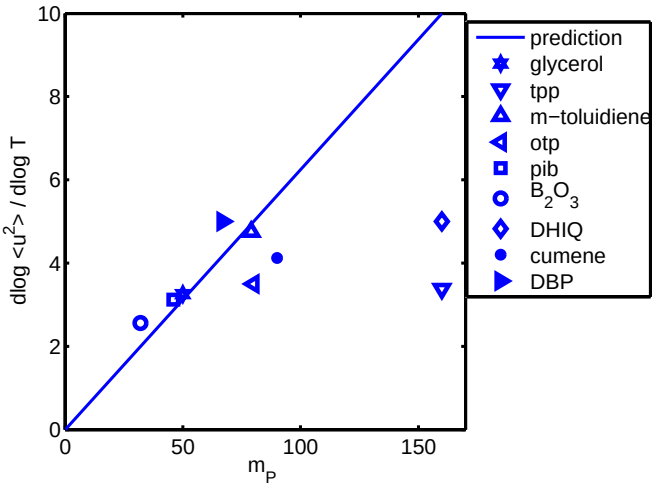

Figure 7.14: $\left.\frac{\partial \log\langle u^2\rangle}{\partial \log T}\right|_P$ as a function of isobaric fragility. The line shows the prediction of the elastic model (equation 7.5.6). .

scatter in the data points is too large for us to draw any conclusions on this basis. In glycerol it has been observed that the fragility increases with pressure [Cook *et al.*, 1994; Paluch *et al.*, 2002]. This should mean a larger temperature dependence of $\langle u^2\rangle$ above T_g. This is not seen in figure 7.12. But the expected change is again very small compared to the precision of the data.

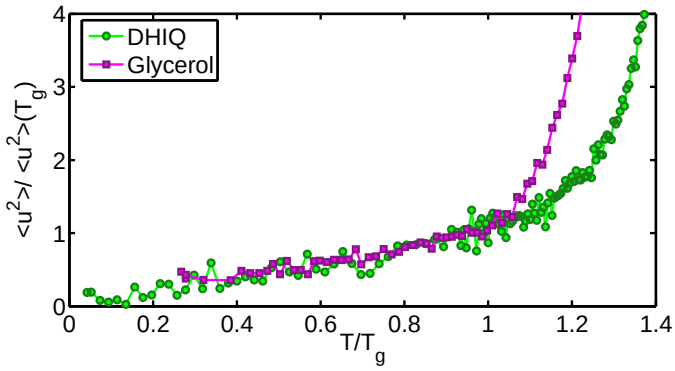

Figure 7.15: $\langle u^2\rangle$ scaled to $\langle u^2\rangle_{T_g}$ for the most fragile sample, DHIQ, and the least fragile sample, glycerol. The temperature is scaled to T_g.

7.6 Relaxational contributions

The elastic model is based on the idea that the barrier height is related to curvature of the harmonic potential, and the decreasing barrier height above T_g is rationalized

as being due to the softening of the harmonic potential. The break in $\langle u^2 \rangle$ around T_g is in this frame understood as being due the change in temperature dependence of the high frequency elastic constants (sound speeds) at T_g (see sections 2.5 and 6.2). The arguments behind the elastic model ignore/disregard any possible contributions to $\langle u^2 \rangle$ from non-harmonic and relaxational movements.

In order to test the elastic model it is necessary to assume that there is no extra relaxational motion contributing to $\langle u^2 \rangle$ around T_g. However, it is not likely that this assumption is fulfilled. We know from the time of flight spectra that DHIQ has strong quasi-elastic scattering already at T_g (section 8.3.3). The time of flight has a broader resolution function, so this quasi-elastic scattering correspond to relaxation at even shorter times than the $\langle u^2 \rangle$ we probe with backscattering. If the relaxational contribution is larger for more fragile liquids, then it might explain that the prediction of the elastic model appears to hold better for stronger systems. The alpha relaxation itself also enters the experimental window at some time, maybe already when $\tau_\alpha \approx 1\mu$s. This happens intrinsically faster for fragile liquids than for strong liquids.

The fragility dependent difference in the temperature dependence of $\langle u^2 \rangle$ seen in figure 7.13 is difficult to anticipate very close to T_g but becomes significant only above $1.1T_g$. This explains why differences that are apparent to the naked eye in figure 7.13 correspond to relatively small differences in figure 7.14. The liquids are already quite far from the glass transition at $1.1T_g$ and the actual alpha relaxation time depends intrinsically and strongly on the fragility of the liquid. In figure 7.15 we show the mean square displacement of the least fragile of the systems we study, glycerol, and of the most fragile liquid, DHIQ. The mean square displacement is scaled with its values at T_g as a function of temperature scaled with T_g (hence, it is the same type of plot as the one depicted in figure 7.13, just with a different scale). Glycerol has $\tau_\alpha \approx 0.01$ s while the very fragile DHIQ has an alpha relaxation time of only $\tau_\alpha \sim 1\mu$s, meaning that their alpha relaxation time differ by four orders of magnitude when compared at $T = 1.1T_g$. The alpha relaxation time of glycerol only becomes as fast as $\tau_\alpha \sim 1\mu$ s at a much higher temperature, namely around $T = 1.3T_g$, where the mean square displacement of glycerol also increases rapidly.

7.7 Summary

The mean square displacement at the nanosecond timescale has been studied as a function of temperature in a set of molecular liquids which covers a large range of fragilities.

The isobaric temperature dependence of the mean square displacement above T_g was found to correlate with the isobaric fragility when comparing systems at atmospheric pressure in agreement with earlier results in literature. However, no systematics were found regarding the value of the mean square displacement at T_g.

We have found that the pressure dependent Lindemann criterion holds for the liquids studied. This suggests that there is an intimate relation between the amplitudes of vibrations and the transition from glass to liquid, in agreement with the elastic model [Dyre, 2006]. Moreover, we find that the order of magnitude of the temperature dependence of $\langle u^2 \rangle$ above T_g agrees with the prediction of the elastic model. However, contributions from relaxational processes makes $\langle u^2 \rangle$ measured on the nanosecond timescale inadequate for precise quantitative test of the elastic model. The relaxational processes appear to have larger amplitude the more fragile the liquid is (see also section 8.3.3).

Résumé du chapitre 8

Le pic de bose est un excès des modes vibrationels par rapport au niveau de Debye, qui est observé dans tous les systèmes vitreux. L'origine des modes en excès n'est pas connue ce qui en fait une des questions centrales de la physique des verres. En particulier, la question de l'existence d'une relation entre les modes du pic de bose et la transition vitreuse est très intéressante.

Dans ce chapitre, on présente une étude du pic de bose faite par diffusion incohérente neutronique. L'étude est composée de deux parties. La première partie est consacrée à l'étude de la dépendance en pression du pic de bose du PIB. La deuxième partie porte sur la corrélation possible entre le pic de bose et la fragilité.

Dans les données obtenues sur le PIB, on observe que la fréquence du pic de bose augmente avec la pression. Ce décalage en fréquence est accompagné par une baisse de l'intensité dans les spectres à basse fréquence. Cependant, quand on compare l'évolution du pic de bose avec celle de la vitesse du son, on trouve que i) la fréquence du pic de bose est plus sensible à la pression que la vitesse du son, ii) l'intensité du pic de bose par rapport au niveau Debye augmente avec la pression, iii) la forme du pic de bose ne change pas avec la pression.

Le pic de bose a été étudié pour une grande série de liquides moléculaires avec des fragilités trés différentes. Sur la base du schéma developpé dans le chapitre trois, on discute l'effet respectif de la température et de la densité sur l'existence d'une corrélation entre l'inverse de l'intensité du pic de bose et la fragilité du liquide. On suggère que la fragilité à considérer dans le cadre d'une corrélation avec l'inverse de l'intensité du pic de bose est la fragilité isochore.

Chapter 8

Boson Peak

The low energy vibrations in crystalline solids are often quite well accounted for by the Debye model. In the Debye model the modes are assumed to be plane waves and the number of possible modes are counted in the Q-space. This leads to a density of vibrational states which is proportional to the square of the mode frequency $g_D(\omega) \propto \omega^2$. It is this dependence of the vibrational density of states which leads to the well known T^3 dependence of the heat capacity in solids at low temperatures. The Debye model is described in textbooks on solid states physics and thermodynamics e.g. [Kittel, 1996; Bairlein, 1999].

Disordered solids, on the other hand, have an excess in the vibrational density of states as compared to the ω^2 Debye behavior followed by crystals in the corresponding frequency range (approx 2 meV - 10 meV depending on system). The excess gives rise to a peak in the reduced density of vibrational states $g(\omega)/\omega^2$ (rDOS) and the peak is seen directly in incoherent inelastic neutron spectra, which essentially probes $g(\omega)/\omega^2$ as well as in Raman scattering spectra. The excess also gives rise to a peak in the reduced low temperature heat capacity $c_P(T)/T^3$.

The boson peak has been studied intensively experimentally as well as theoretically over the last decade, but its origin is still controversial. The proposed explanations for the boson peak fall in three categories. (i) Localized (harmonic) modes in soft potentials (SPM), the concept of soft localized soft modes being expressed differently in different models [Gurevich *et al.*, 2003, 2005; Klinger, 1999, 2001]. (ii) Quasilocalized sound like modes in structural regions of the nanometer size in the glass [Duval *et al.*, 1990; Schroeder *et al.*, 2004; Quitmann and Soltwisch, 1998], and (iii) Fluctuating elastic constants (FEC) giving rise to a peak in $g(\omega)/\omega^2$ [Maurer and Schirmacher, 2004]. The total density of vibrational states is in the two first cases described by Debye modes plus extra modes, which are ascribed to the disorder.

The FEC-model suggests a different picture, namely that the disorder distorts the Debye modes and a way which gives rise to a peak in the rDOS.

The inverse intensity of the boson peak is based on data compilations suggested to correlate with fragility (see section 8.3 for details). The origin of this correlation is (evidently) not understood, since neither the fragility nor the boson peak itself are understood. However, it is common for the models for the boson peak that its intensity is related to some notion of "amount of disorder" in the glass. The structure of the glass is the frozen-in structure of the liquid, and could in this sense carry a reminiscent signature of the dynamics in the liquid.

In this chapter we present a study of the boson peak measured by inelastic neutron scattering in a number of different systems. A section (8.2) is devoted to analyzing the pressure dependence of the boson peak, particularly in comparison to the pressure dependence of the other vibrational modes of the system, the aim being to shed light on the origin of the boson peak. This part of the study is based on experiments on a PIB-sample, which has a well resolved boson peak. A second section (8.3) is reserved for the discussion of the correlation between the boson peak intensity and fragility. We particularly discuss the role of density versus temperature for this type of correlation in light of the general ideas presented in chapter 3. We have for this purpose studied a set of samples which span a large range in isobaric as well as isochoric fragility.

8.1 Time of flight

8.1.1 Experimentals

The experiments were carried out at the time of flight spectrometer IN5 at the ILL. The energy of the scattered neutron is in time of flight measured via the time it takes the neutrons to arrive at the detector. The incoming beam is monochromatic and pulsed, the path length is known. The speed and the energy of the outgoing neutron can therefore readily be calculated. The pulsing and monochromation is in the case of IN5 done with a system of choppers. Monochromation can also be done with crystals (e.g. IN6) and the incoming beam can be intrinsically pulsed if it is generated by a spallation source.

The use of choppers gives the possibility of freely adjusting the wavelength of the incoming neutron and hereby the resolution in absolute values. The experiments reported in this chapter were all performed using incoming neutrons with a wave-

length of 5 Å yielding a resolution of FMHW=103 μeV. The resolution function, which is nearly Gaussian, was in all cases measured with the sample at 2 K.

The range in angle (2θ) goes from 14.5° to 132.5° with each detector covering approximately 1°. This corresponds to a elastic Q values of 0.4 Å^{-1} to 2.2 Å^{-1}, when the incoming neutron has λ=5 Å.

The PIB3580 sample (see appendix A for details) was studied in a pressure range from atmospheric pressure to 1.4 GPa and at temperatures ranging from 140 K to 430 K. The experiment was performed using a clamp pressure cell and *in situ* compression. The sample and the cell were kept in the beam during the entire experiment, which means that all the measurements on PIB3580 were obtained under the exact same conditions with regard to position in the beam and the amount of cell in the beam. The volume of the sample in the beam was also kept constant. However, the number of sample scattering centers depends on the density.

The compression of PIB3580 was performed at 430 K and the sample was subsequently cooled along the isobar. This procedure ensured that the compression was performed in the melt even when going to the highest pressure.

Cumene was studied at atmospheric pressure and at 1.2 GPa in a temperature range of 100 K to 300 K. The experiment at atmospheric pressure was performed using a standard aluminum cell while the pressure experiment was performed using the clamp cell with *in situ* pressurization. The pressure was applied at 300 K, which means that the liquid was well below P_g when compressed.

We moreover studied a set of liquids with very different isobaric and isochoric fragility: PB, sorbitol, m-toluidine, m-fluoroaniline and DBP (see appendix A for details on the samples). These experiments were performed at ambient pressure using aluminum cells in a temperature range from 100 K to T_g (in most cases $T_g \sim 200$ K).

The clamp and the aluminum cells used are exactly the same as those used in the back scattering experiments. The description of the cells is given in section 7.1.1. However the sample thickness used for the high pressure experiment was only 0.1 mm in this case. The transmission was ∼95% for the experiments in the aluminum cell and ∼88% for the high pressure experiments.

8.1.2 Corrections

The data underwent a standard correction procedure using the ILL program INX. INX converts the data from the measured intensity as a function of angle and time of flight to intensity as a function of angle and energy transfer, $I(2\theta, \omega)$ corrected for

the $\frac{Q_{out}}{Q_{in}}$ factor (see equation 4.3.17). INX is moreover used for correcting for the different detector efficiency by normalizing to the signal of a vanadium sample, it performs corrections for sample absorption, and subtracts a measured background signal.

Subtraction of the empty cell

The signal of the aluminum cell is negligible as compared to the signal of the hydrogenated sample. The procedure used for subtraction is therefore without significance for the final result. The pressure cell on the other hand, gives a significant signal (see also the discussion in 7.1.2). In figure 8.1 we illustrate the raw signal of sample plus pressure cell along with the signal of the pressure cell[1].

We are mostly interested in the energy region 1 meV - 10 meV. The cell signal in this region is a flat background with considerable lower intensity than the signal of the sample. The intensity of the cell signal becomes comparable in order of magnitude at energies somewhere around 15 meV. We therefore conclude that the result after subtraction of the cell is reliable up to $\sim$ 15 meV, while we exclude higher energies from the analysis. The elastic signal is also shown in figure 8.1. Here we see, consistent with the backscattering data, that the high pressure cell contributes with about half of the measured intensity.

8.1.3 Determining $S(\omega)$ and $g(\omega)$

The discussion of the time of flight data in this chapter is based on $S(\omega)$ obtained by normalizing to the elastic intensity and summing over all measured angles. In the following section we justify this procedure by showing that it gives less scattered data than interpolating to constant Q before summing, while the results are equivalent.

The data are interpolated from the measured $I(\theta, \omega)$ to the $I(Q, \omega)$ using the program IDA. We neglect coherent scattering which means that the measured intensity is proportional to the incoherent dynamical structure factor:

$$I(Q, \omega) = N \frac{\sigma_{inc}}{4\pi} S_{inc}(Q, \omega) \tag{8.1.1}$$

where N is the number of scatterers and σ_{inc} is the incoherent scattering cross section (see equation 4.3.17 and recall that the $\frac{Q_{out}}{Q_{in}}$ factor was corrected by INX).

[1]The presence of the sample gives a "shadow" and hence less scatter ($\sim$ 10%) from the cell, in the cell+sample situation as compared to the empty cell alone. The cell signal shown in figure 8.1 has been corrected to take this effect into account.

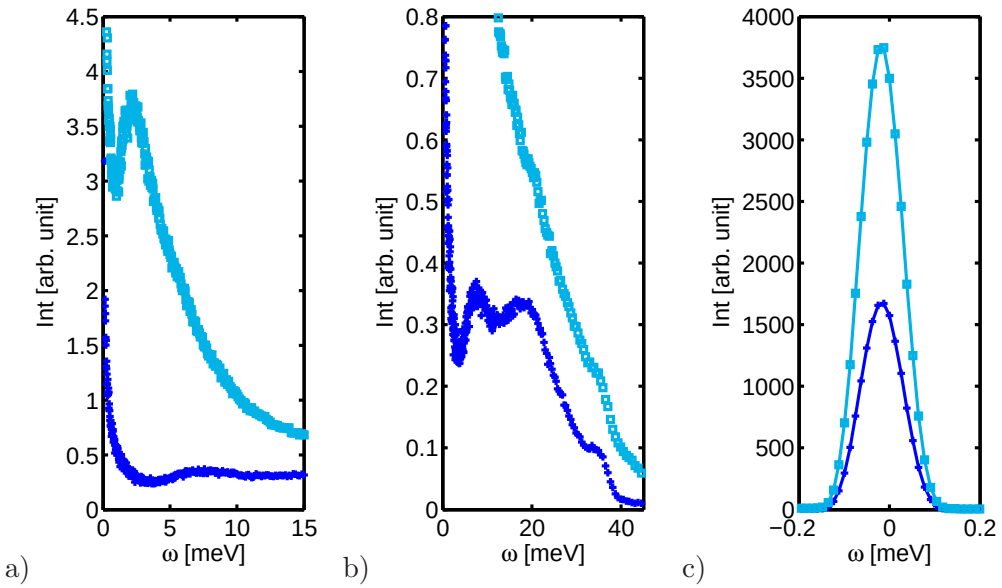

Figure 8.1: The signal of the high pressure cell (+), and the raw signal of the high pressure cell and PIB3580 (squares). Both curves are measured at T=140 K and P=0.1 MPa. The three sub-figures focus on three different regions of the energy axes. a) On this scale it is seen that the sample signal dominates over the cell signal. b) The inelastic signal of the cell becomes comparable to the signal of the sample at about 15 meV. The inelastic signal of the cell is due to phonons, and the intensity is found to grow in accordance with a bose factor as a function of temperature (not shown). c) The cell gives about half the measured elastic signal. Figure c can moreover be regarded as an illustration of the resolution function. Notice also that the intensity of the elastic signal is about 3 orders of magnitudes higher in intensity than the inelastic signal (The intensity unit is the same on all three sub-figures.).

We are mainly interested in studying the vibrational density of states obtained from the inelastic signal.

The theoretical expression for the inelastic one phonon single contribution to $S_{inc}(Q,\omega)$ is given by equation 4.3.35, which reads

$$S_{inel,inc}(Q,\omega) = \frac{1}{2M}\exp\left(-\frac{\langle u^2\rangle Q^2}{3}\right) Q^2 \frac{n(\omega)}{\omega} g(\omega). \tag{8.1.2}$$

where M is the mass of the molecule. Here the Q dependence and the energy dependence is totally disentangled. This means that the density of state (in arbitrary units) can be found from the energy dependence of the scattering function at any given constant Q. We primarily consider the data in the form $g(\omega)/\omega^2$. This quantity is obtained directly from equation 8.1.2 by correcting for the bose factor, that is dividing by $n(\omega)\omega$.

In the study of the pressure dependence of the boson peak in PIB3850, we compare the intensity of the boson peak at different pressures; this experiment is performed with a constant volume of the sample in the beam, however the number of scatterers is proportional to the pressure dependent number density. Moreover, the Debye Waller factor is also pressure dependent because $\langle u^2\rangle$ is pressure dependent. These effects are eliminated by normalizing to the elastic intensity, which is given by the number of scatterers and the Debye Waller factor:

$$I_{el,inc}(Q) = N\frac{\sigma_{inc}}{4\pi}\exp\left(-\frac{\langle u^2\rangle Q^2}{3}\right). \tag{8.1.3}$$

The resolution function measured at 2 K had a small wing up to about 2 meV, and has therefore been subtracted, when considering the inelastic signal of the low temperature data. The effect of this last correction is minor as soon as the temperature approaches T_g of the sample because the intensity of inelastic and quasi-elastic scattering increases.

In figure 8.2 we show the rDOS ($g(\omega)/\omega^2$) of PIB3580 obtained at a constant Q as well as the result obtained by summing over the angles. The data are in both cases corrected for the bose factor and normalized to the elastic intensity as described above. The data are finally adjusted by *one* pressure *in*dependent factor to make the data overlap. It is clearly seen that the results are in agreement, not only the shape and position of the boson peak, but also the pressure dependence of the intensity found by the two methods is the same.

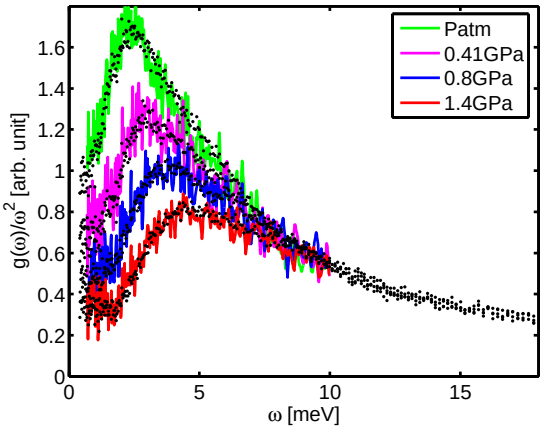

Figure 8.2: Spectra of PIB3580 at different pressures. The full lines give $g(\omega)/\omega^2$ obtained from $S(Q,\omega)$ measured at a fixed Q value (Q=1.7 Å^{-1}). The dots give $g(\omega)/\omega^2$ based on the $S(\omega)$ calculated by summing over all angles. (See the text for details). The results are in agreement, not only the shape and position of the boson peak, but also the pressure dependence of the intensity found by the two methods is the same.

The Q-dependence

From equation 8.1.2 it follows that only the Debye Waller factor and the Q^2-term are Q-depend. A Q independent quantity can therefore be found by dividing by these

$$\frac{S_{inel,inc}(Q,\omega)}{\exp\left(-\frac{\langle u^2\rangle Q^2}{3}\right)Q^2} = \frac{1}{2M}\frac{n(\omega)}{\omega}g(\omega). \tag{8.1.4}$$

In figure 8.3 we illustrate the above at 3 different Q values, with the Debye Waller factor taken from the measured elastic intensity. The three curves should overlap according to equation 8.1.4, but this is clearly not the case. However, the shape is the same and the curves can be brought to overlap by adjusting the Debye Waller factor (figure 8.4). Additionally we find that the pressure dependence of the intensity is the same at all Q-values. We therefore conclude that the measured frequency dependence shown in figure 8.2 gives a correct representation of the vibrational density of states.

Other techniques for extracting DOS from equation 8.1.2 exploit the Q dependence. Rewriting equation 8.1.2 to

$$\ln\left(\frac{S_{inc}(Q,\omega)\omega}{Q^2 n(\omega)}\right) = -\frac{\langle u^2\rangle Q^2}{3} + \ln(g(\omega)) \tag{8.1.5}$$

it is seen that the left hand side can be obtained directly from the raw data. Fitting

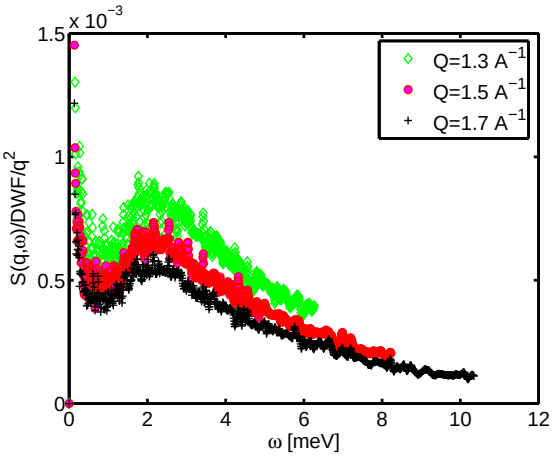

Figure 8.3: The $S(Q,\omega)$ divided by Q^2 and divided by the DWF found from the elastic intensity.

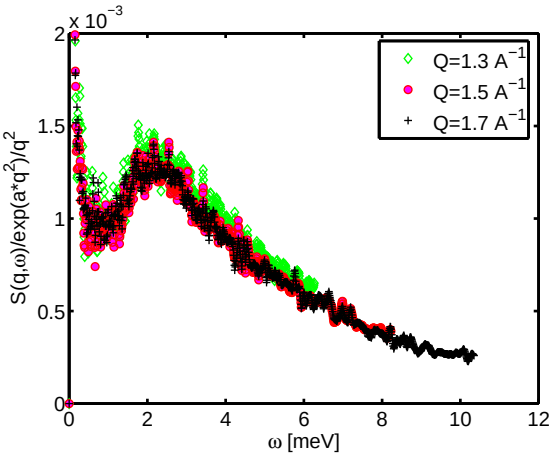

Figure 8.4: The $S(Q,\omega)$ divided by Q^2 and divided by a factor $\exp(-aQ^2)$ which is not taken from the elastic peak, but taken to make the inelastic part of spectra superimpose (as it is expected to). It is seen that the overlap is less convincing at lower Q and the discrepancy increases if Q is decreased further. It is not possible to adjust a Debye Waller factor of the form $\exp(-aQ^2)$, such that all data superimpose. However, the frequency dependence of the inelastic signal is independent of Q in the range $Q = 0.5$ A^{-1} to $Q = 2.1$ A^{-1}.

this as a linear function of Q^2, at fixed ω, will in the ideal case give $\ln(g(\omega))$ at the origin and $-\frac{\langle u^2 \rangle}{3}$ as slope. However, the Q^2-dependence is only found in the data at high Q, moreover, the $\langle u^2 \rangle$ found at different energies is not the same. The result of this procedure is therefore sensitive to the Q-range used. When only high Q's are used then it gives the same result as the constant Q or summing over angles, which we discussed in the previous section.

A last method is to extract the DWF and the Q-independent intensity factors, $\exp(-\langle u^2 \rangle Q^2)$, from the elastic intensity and determine $g(\omega)$ as the slope of the Q^2 dependence of the left hand side of the below:

$$\frac{S_{inc}(Q,\omega)\omega}{\exp(-\langle u^2 \rangle Q^2) n(\omega)} = Q^2 g(\omega). \tag{8.1.6}$$

It is not possible to obtain any reasonable result from this procedure. This is a natural consequence of the "incorrect" Q dependence in figure 8.3.

The deviation between the actual Q-dependence and the theoretical expected result could be related to an error in the subtraction of the high pressure cell signal. A relatively small error, which will not affect the measured inelastic signal will still effect the elastic signal and therefore the Debye Waller factor determined from the latter. However, we have similar problems with the data measured in aluminum cells. A more likely explanation is that the Q-dependence is distorted due to multiple scattering and multi-phonon scattering. It is also possible that the coherent contribution plays a role.

8.2 The origin of the excess modes

In this section we present and analyze the pressure dependence of the boson peak in PIB3850 at $T = 140$ K which is well below the glass transition temperature ($T_g \approx 195$ K) at atmospheric pressure. We also include the pressure dependence of Brillouin light scattering data from Begen *et al.* [2006 b]. This combination of data obtained by three different experimental techniques allows us to make a comparison of the pressure dependence of the sound modes and the boson peak position in an organic system, including sound modes in the boson peak energy region as well as both shear and longitudinal modes. The neutron data allow us to analyze the influence of pressure on the shape and intensity of the boson peak without the uncertainty from the unknown frequency dependence of the light to vibration coupling factor which influences the Raman spectra. Combining this data with literature data on the density of the sample we are moreover able to make the

comparison of the evolution in the boson peak intensity as compared to the intensity of the Debye level. The aim of this section is to better understand the origin of the boson peak. The question of whether there is a relation between the boson peak and the fragility is attacked in the following section (8.3).

8.2.1 Boson Peak as a function of pressure

In figure 8.5 we show the rDOS of PIB3580 measured at 4 different pressures ranging from atmospheric pressure to 1.4 GPa. A well resolved boson peak is seen at all pressures. The peak position increases as a function of pressure with a slope of $\sim$ 0.15 meV / 100 MPa (inset of fig. 8.5) in the whole range. The peak position shifts by a factor 2 from atmospheric pressure to 1.4 GPa.

The second striking effect of pressure is that it reduces the boson peak intensity. However, at high frequencies, from above roughly 8 meV there are no significant changes in the spectra.

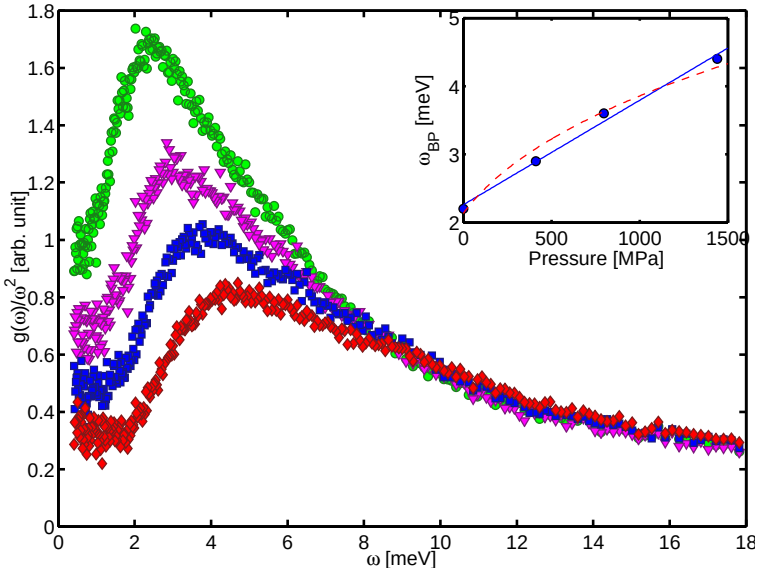

Figure 8.5: The rDOS ($g(\omega)/\omega^2$) of PIB at different pressures; atmospheric pressure (●), 4 MPa (▼) 8 MPa (■), and 14 MPa (♦). The inset shows the peak positions as a function of pressure. The full lines is the best straight line. The dashed line is the best fit to equation 19 of ref. Gurevich *et al.* [2005], P_0=204 MPa and $\omega_{BP} = 2.13$ meV.

The boson peak has mainly been studied at different temperatures and in glasses with different thermal history, while few studies report the effect of pressure on the boson peak. Moreover, the existing studies are mainly performed by Raman scattering [Andrikopoulos *et al.*, 2006; Schroeder *et al.*, 2004; Yamaguchi *et al.*, 1999; Sugai

and Onodera, 1996; Hemley *et al.*, 1986] in which the shape, position and intensity of the boson peak is altered by the light to vibration coupling factor. The latter by itself is pressure dependent [Begen *et al.*, 2006]. Relevant pressure studies of the boson peak by other techniques include low temperature heat capacity of polystyrene [Geilenkeuser *et al.*, 1999], and neutron scattering studies of polybutadiene [Frick and Alba-Simionesco, 2002]. The boson peak has also been studied in permanently densified SiO_2 by neutron spectroscopy [Inamura *et al.*, 2000, 2001] and in densified $Na_2FeSi_3O_3$ by nuclear inelastic scattering [Monaco *et al.*, 2006 b].

The shifts in the boson peak seen in figure 8.5 are by far the largest pressure induced shifts of the boson peak that we are aware of. However, the qualitative results reported in all the above cases are in agreement with our finding: the boson peak intensity decreases and the boson peak frequency increases, meaning that this behavior can be considered as general.

8.2.2 Boson peak position

Pressure increases the elastic constants of the material and this makes the frequency of all vibrational modes in the system increase as a function of pressure. It is therefore quite intuitively expected that also the boson peak shifts to higher pressure upon compression.

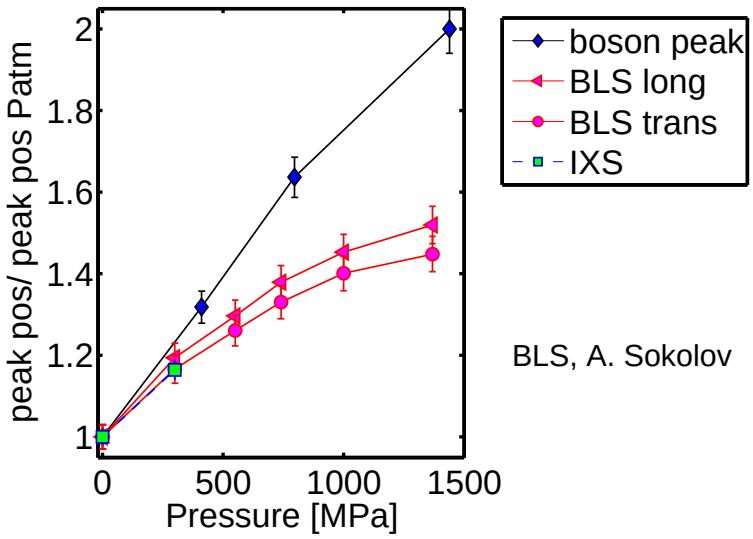

Figure 8.6: The relative shift in energy as a function of pressure. Diamonds: boson peak, triangles: BLS longitudinal modes, circles: BLS transverse modes, squares: IXS longitudinal modes.

In figure 8.6 we show the relative peak shift with pressure of transverse sound modes, longitudinal sound modes at low and high Qs and of the boson peak, as a function of pressure. All modes are shifted to higher frequency with increasing pressure. We have calculated the change in density with pressure using the equation of state of Sanchez and Cho [1995] in the melt and the expansion coefficient $\alpha_P = 10^{-4}K^{-1}$ at all pressures in the glass. Defining the Gruneisen parameter as $\frac{\mathrm{d}\log\omega_{peak}}{\mathrm{d}\log\rho}$ we find a value of 2.7 and 3.7 for the IXS mode at 2 nm^{-1} and the boson peak respectively. This clearly shows that the boson peak is more sensitive to pressure than any of the other modes. This result is consistent with the result of Schroeder *et al.* [2004] who find that changes of the boson peak frequency in Raman spectra under pressure were stronger than variations of the sound velocities. On the contrary it is found in a recent study by Monaco *et al.* [2006 b] of a permanently compressed inorganic glass that the shift in the boson peak corresponds to that of the sound speeds (more precisely they compare to the Debye-frequency, see below for the definition). In the study by Monaco *et al.* [2006 b] the density changes were quite small ($\sim 6\%$), while considerably larger variations ($\sim 20\%$) are achieved in our measurements. This could be part of the explanation of the different result as it is apparent from figure 8.6 that the differences increase with increasing pressure.

The sound modes measured by BLS are at much smaller frequencies than the boson peak, while the sound modes measured by IXS are at frequencies of the same order of magnitude as the boson peak frequency. It could therefore be argued that the boson peak should be compared to the latter. In line with this, it has been suggested, based on temperature dependences in silica glass, that the boson peak position is stronger coupled to the behavior of the high frequency IXS sound modes than the low frequency BLS sound modes [Masciovecchio *et al.*, 1999]. Our results on PIB do not support this view as we find that the longitudinal sound speed measured by BLS agrees with the sound speed found by IXS (figure 8.7). Moreover, the pressure dependence of the two is the same in the limited pressure range where both are studied. Based on this we assume that the IXS and the BLS modes have similar pressure dependences in the whole range, and conclude that the boson peak position has a more dramatic pressure dependence than the sound modes in the same energy range.

Note also in figure 8.7 that the position of the boson peak seen in the rDOS is in the regime where the dispersion of the longitudinal sound is linear.

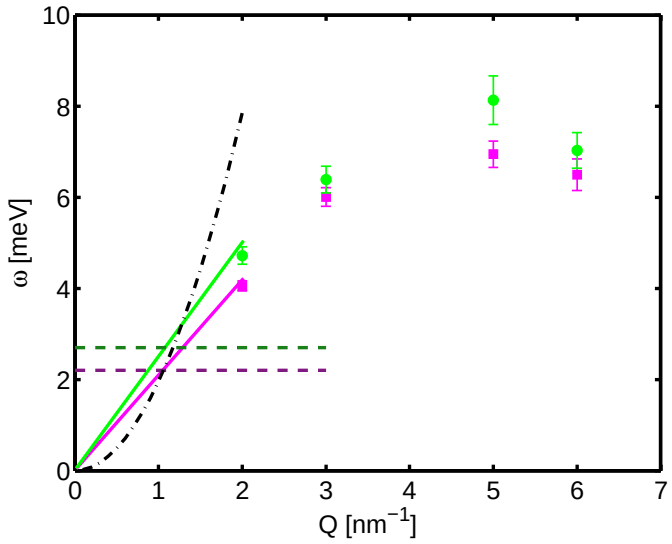

Figure 8.7: The dispersion of longitudinal sound modes measured by IXS. Squares are atmospheric pressure, circles 300 MPa. The full lines show the linear dispersion corresponding to the low Q sound speed measured by light scattering. The dashed lines indicates the position of the boson peak at the same pressures (higher energy higher pressure). The dashed-dotted line shows the estimated $\pi\Gamma$ (see text).

Ioffe-Regel limit

It is often suggested that the mean free path of the sound speed reaches the order of magnitude of the wavelength, the Ioffe-Regel limit, at the frequency of the boson peak position (e.g. references [Quitmann and Soltwisch, 1998; Schroeder *et al.*, 2004]). Such a general connection was most recently proposed by Ruffle *et al.* [2006] (and contested by Scopigno *et al.* [2006]), who define the Ioffe-Regel limit by $\omega_l = \pi\Gamma$ where ω_l is the frequency of the sound mode. In figure 8.5 we indicate the value of $\pi\Gamma$ based on the Γ-values estimated from on the IXS data. The sound attenuation was found to be pressure independent, which is why it is only indicated by one line (see section 6.2 for details).

The position of the boson peak at atmospheric pressure and at 300 MPa (interpolated from the data in figure 8.5) are indicated by horizontal lines in figure 8.7. This shows good agreement between the boson peak position and the Ioffe-Regel limit at both pressures.

Predictions/explanations by the models

The most detailed prediction regarding the peak position is given for the SPM model by Schober and coworkers in terms of the position of the peak in the rDOS. The prediction is that the peak position should follow a $(1 + P/P_0)^{(1/3)}$-dependence [Gurevich *et al.*, 2005]. The best fit to our data (inset of figure 8.5), is not convincing, as we find no significant deviation from linear pressure dependence in the studied pressure range. However, the change in elastic constants is not considered in the model and this obscures the comparison. Moreover, it is important to note that we compressed the sample in the melt and not in its glassy state. A different path of compression would lead to a different density change and the boson peak position would be different too [Chauty-Cailliaux, 2003]. Another complication when comparing to the SPM prediction, is that it does not take the shift in the sound speeds into account.

There are no explicit predictions regarding the pressure dependence of the boson peak for other models. Phonons localized in nanoscale domains (blobs) yield the relation $\omega_{BP} = av/L$ where v is the sound speed and L is the size of the blobs [Duval *et al.*, 1990; Schroeder *et al.*, 2004; Quitmann and Soltwisch, 1998]. We find that ω_{BP} increases more with pressure than the sound speed. In order for the above picture to be correct it is therefore required that the domain size decreases with pressure. There is no experimental evidence for the existence of blobs and it is therefore difficult to anticipate their dependence on pressure.

In the FEC model of Schirmacher and coworkers, in which the boson peak is due to the fluctuation of the elastic constants, it is predicted that the boson peak position shifts to higher energies if the sample gets more ordered in the sense that the amplitude of the fluctuations in the elastic constant is decreased [Maurer and Schirmacher, 2004]. This means that the shift in the boson peak, which we report should be due to a decrease in disorder when the liquid is compressed. It is easy to imagine that the compression and the resulting change in the packing of the molecules will lead to more structural order and therefore also less fluctuations of the elastic constants.

8.2.3 Boson peak intensity

The shift in energy should both for the SPM and the FEC model be accompanied with a decrease in boson peak intensity. The decrease of the boson peak is also seen in the raw data (figure 8.5). However, the Debye level also changes as a function of pressure. This means the that intensity of the rDOS intrinsically decreases at low energies. This effect is not considered in the models. Comparing data to models, it

therefore seems that the relevant evolution in intensity should be the relative intensity over the Debye density of states. We perform such a comparison in the following section. As an alternative approach we also consider the pressure dependence of the actual number of excess-states.

Comparison to the Debye density of states

In treating the data we have normalized to the number of scattering centers, the Debye Waller factor and the bose factor. Hence, the result shown in figure 8.5 is the reduced density of states defined by:

$$\mathrm{rDOS}(\omega) = A\frac{g(\omega)}{\omega^2}, \tag{8.2.1}$$

where A is a pressure independent arbitrary constant. The normalization to the number of scattering centers means that $g(\omega)$ is normalized, thus it satisfies

$$\int_0^\infty g(\omega)\,\mathrm{d}\omega = 1. \tag{8.2.2}$$

The corresponding situation for the Debye density of states is given by

$$\int_0^{\omega_D} \frac{3\omega^2}{\omega_D^3}\,\mathrm{d}\omega = 1. \tag{8.2.3}$$

where ω_D is the maximum cut-off frequency, which is also referred to as the Debye frequency. The Debye level in the reduced density of states is hence given by

$$\mathrm{rDOS}_D(\omega) = \frac{3}{\omega_D^3}. \tag{8.2.4}$$

The Debye frequency[2] is determined by the sound speeds and the number density

$$\omega_D = v_0(6\pi^2 n)^{1/3} \text{ where } \frac{1}{v_0^3} = \frac{1}{3}\left(\frac{1}{v_l^3} + \frac{2}{v_t^3}\right) \tag{8.2.5}$$

and n is the number density which is proportional to the density ρ. The average sound v_0 of PIB is strongly dominated by the transverse sound speed because it is about a factor 2 smaller than the longitudinal sound speed [Begen *et al.*, 2006,b],

[2]The expression here gives the Debye frequency in units of [Hz]. The corresponding Debye energy is as usual found by multiplying by $\hbar$; $E_D = \hbar\omega_D$

meaning that the Debye level essentially is given by

$$\mathrm{rDOS}_D(\omega) \propto \frac{1}{\rho v_t^3}. \tag{8.2.6}$$

In a Debye situation the hardening of the system (increase of elastic constants) pushes the Debye density of states. The Debye level gets lower and the cut-off frequency gets higher, while the total number of states of course stays constant. The intensity of rDOS will therefore naturally get lower, due to the decrease of the Debye level.

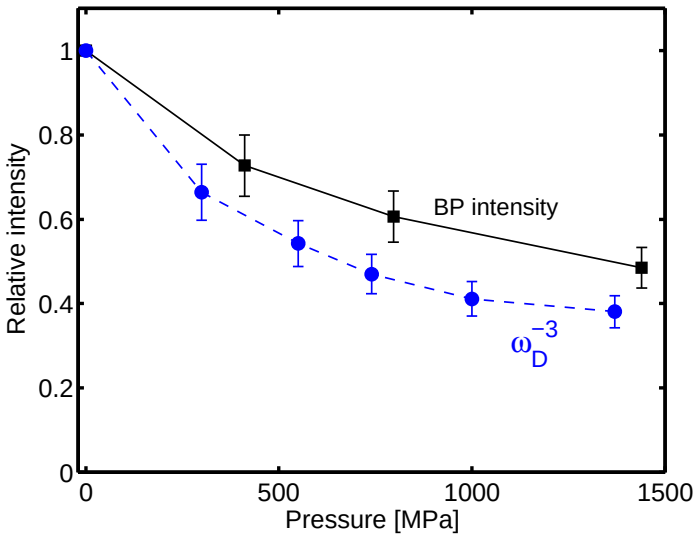

Figure 8.8: The Debye level (●) and the boson peak intensity (■) as a function of pressure.

In figure 8.8 we illustrate the decrease in the Debye level as a function of pressure. We compare this decrease to the decrease in the boson peak intensity. It is seen that the amplitude of the boson peak decreases less than the Debye level. Consequently we conclude that the boson peak intensity relative to the Debye level *increases* as a function of pressure. The analysis of the boson peak intensity relative to the Debye level was also performed in the study of densified glasses by Monaco *et al.* [2006 b] and in an earlier study by the same group on a hyper-quenched glass [Monaco *et al.*, 2006 a]. The finding in these studies was that boson peak intensity relative to the Debye level was unchanged. The difference between their conclusion and our finding could (as for the peak position discussed above) be due to the much larger change of density in the present study. Alternatively it is quite possible that the behavior is not universal but will depend on specific properties of the glass. Thirdly it is worth

mentioning that the studies by Monaco *et al.* were performed using nuclear inelastic scattering, which might not be sensitive to all the modes in the vibrational density of states [Chumakov *et al.*, 2004].

The excess in the density of states

It is possible to define the excess of modes with respect to the Debye modes by the total density of states minus the Debye density of states $g_{ex}(\omega) = g_(\omega) - g_D(\omega)$. If the boson peak is due to modes that superimpose to Debye modes, then these modes are described by $g_{ex}(\omega)$ and the number of excess modes is given by the integral of $g_{ex}(\omega)$.

The shift of the excess to a higher frequency gives a decrease in the boson peak seen in the rDOS. This is so because, as pointed out by Yannopoulos *et al.* [2006 a], the division by ω^2 leads to an intrinsic suppression of the peak intensity.

Assuming that the excess density of states does not change in intensity but just shifts to higher frequency then this effect will make the intensity of the boson peak seen in the *reduced excess* density of states $g_{ex}(\omega)/\omega^2$ inversely proportional to ω_{BP}^2. Note however, that this is true for the intensity of $g(\omega)/\omega^2$, because the Debye level gives an additional term. The total reduced density of states will be given by

$$g(\omega)/\omega^2 = g_D(\omega)/\omega^2 + g_{ex}(\omega)/\omega^2 = rDOS_D + g_{ex}(\omega)/\omega^2. \tag{8.2.7}$$

It follows that the $1/\omega^2$ dependence of the intensity only will be seen if the excess term $g_{ex}(\omega)/\omega^2$ dominates over the Debye term, even in the most simple situation where the Debye level itself is assumed to be pressure independent.

It is clear that to evaluate pressure dependence of the intensity the excess vibrational density of states it is necessary to determine the Debye level. Our neutron measurements do not give the vibrational density of states in absolute values, but only the relative evolution with pressure. We therefore use the ratio of the boson peak intensity over the Debye density of states at atmospheric pressure [Kanaya and Kaji, 2001] in order to get comparable scales of the two. Based on this we estimated excess densities of states at different pressures. The result is depicted in figure 8.9 b). The rather surprising result is that the number of excess states increases when pressure increases. It is difficult to anticipate the mechanism which could lead to such an increase in excess states. Our interpretation of the result is therefore that it is not physically correct to view the vibrational density of states as Debye modes plus excess modes.

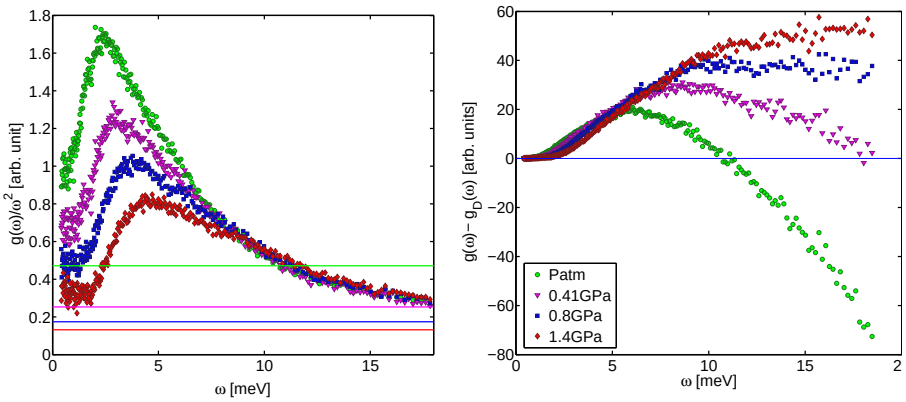

Figure 8.9: Left: the rDOS ($g(\omega)/\omega^2$) of PIB at different pressures. The Debye level is indicated with horizontal lines (see the text). Right: the excess density of states. Atmospheric pressure (●), 4 MPa (▼) 8 MPa (■), and 14 MPa (♦).

8.2.4 Shape of the boson peak

It has been found that the boson peak had a universal shape [Malinovsky *et al.*, 1990] when comparing the boson peak in various materials. In line with this, Chumakov *et al.* [2004] find a universal $\exp(-\omega/\omega_0)$ behavior at frequencies above the boson peak in $g(\omega)/\omega^2$. The $\exp(-\omega/\omega_0)$ behavior is also expected from the FEC model [Maurer and Schirmacher, 2004]. Based on the SPM model, Schober and coworkers predict that the universal behavior above the boson peak at ambient pressure should follow a ω^{-1} power law [Gurevich *et al.*, 2003].

The neutron data allow us to analyze the influence of pressure on the shape and intensity of the boson peak without the uncertainty from the unknown frequency dependence of the light to vibration coupling factor which influences the Raman spectra.

In figure 8.10 we show the boson peak at different pressures with the axis scaled by the boson peak position (ω_{BP}) and intensity respectively. The data overlap on a master curve roughly above $\omega_{BP}/2$. This is consistent with the picture of a universal shape of the boson peak not only on the high frequency part but also in the region of the peak itself. We find that the shape follows a $\exp(-\omega/\omega_0)$ behavior from ω_{BP} up to approximately $5\omega_{BP}$. This suggests that the mechanisms responsible for the boson peak are not altered as pressure is applied but rather pushed to higher frequencies due to an increase of the force constants in the material.

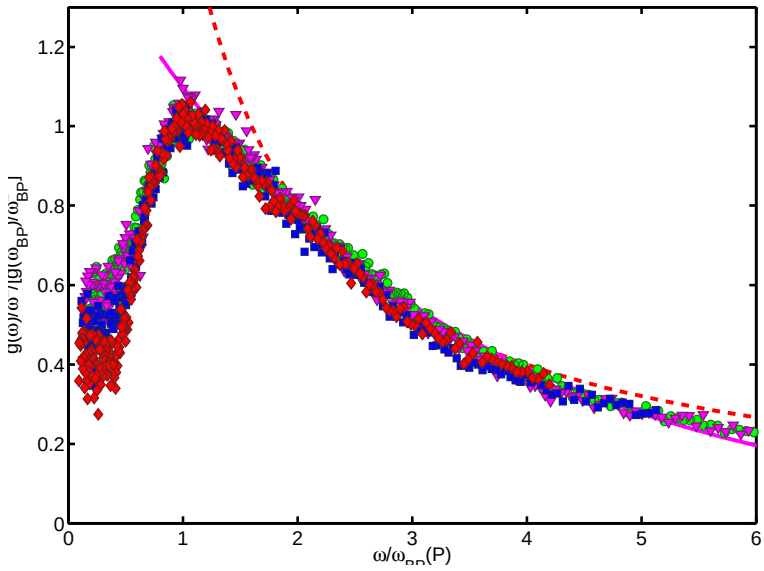

Figure 8.10: The boson peak at different pressures atmospheric pressure (●), 4 MPa (▼) 8 MPa (■), and 14 MPa (♦). The data scaled with the boson peak intensity and the boson peak position. The dashed line shows a $1/\omega$-behavior, the full line is $\exp(-\omega/\omega_0)$.

8.3 Boson Peak and fragility

In this section we will discuss the proposed correlation between the relative intensity of the boson peak and the fragility. The suggestion is that larger fragility should correlate to smaller relative intensity of the boson peak. This correlation is supported by data from several glass formers [Sokolov *et al.*, 1993, 1997; Rössler and Sokolov, 1996; Novikov *et al.*, 2005] though it has also been contested [Yannopoulos and Papatheodorou, 2000].

Two different measures are suggested for quantifying the relative intensity of the boson peak: (i) by normalizing the boson peak to the Debye density of states [Sokolov *et al.*, 1997] (see also section 2.7.3) or (ii) by normalizing the boson peak intensity at T_g to the intensity of quasi-elastic scattering at T_g [Sokolov *et al.*, 1993]. In the latter case a parameter, R, is defined as the quasi-elastic intensity divided by the boson peak intensity evaluated at T_g. Of these two measures R is by far the easiest to evaluate experimentally, because it does not require knowledge of $S(Q,\omega)$ in absolute values, nor does it require knowledge of the sound speeds of the system. Moreover, it has the advantage of being evaluated in the equilibrium liquid. For these reasons we will focus on the correlation with R in the main part of this chapter. It is suggested by Novikov *et al.* [2005] that the two measures of boson peak intensity essentially

are equivalent because the intensity of the quasi-elastic scattering appears to be universal at T_g. We shall question this proposition at the end of this chapter.

8.3.1 Comparing systems

We have studied a set of liquids which covers a large span in isochoric as well as isobaric fragility. In figure 8.11 we show the isobaric fragility as a function of the inverse relative boson peak intensity, R, while figure 8.12 depicts the isochoric fragility m_ρ as a function of R. We have in both figures included data from literature of samples where both R, m_ρ and m_P are available. Though the data is limited and somewhat scattered we find that both figures do show a correlation between fragility and R. The range in m_ρ is smaller (which is always the case because $m_\rho < m_P$), and this makes the correlation appear weaker. However, it is not evident from these figures if one correlation is more fundamental than the other.

Figure 8.13 show the relative contribution of density to the viscous slowing down, measured by m_P/m_ρ as a function of R. It is clear that there is no correlation between these two quantities. This suggests that R is insensitive to the relative effect of density on the relaxation time, meaning that the correlation to fragility is a signature of a correlation between R and the intrinsic effect of temperature on the alpha relaxation time.

8.3.2 Pressure dependence

For the samples PIB3580 and cumene we have measured $S_{inc}(\boldsymbol{Q}, \omega)$ at an elevated pressure on the T_g line. The raw data are depicted in figure 8.14 and 8.16. The cumene data were obtained using a different cell at atmospheric and elevated pressure respectively, and they are therefore not shown on the same scale. A shift of the boson peak position to higher energies is seen in both cases, similar to the result concerning the effect of pressure along an isotherm in the glass. For PIB where the intensity scales can be compared we moreover recognize the decrease in the boson peak intensity with increasing pressure.

Figures 8.15 and 8.17 show the same two sets of data, now with the axes scaled with boson peak intensity and position. It is striking, particularly for the well resolved boson peak of PIB, that the *entire* curve collapses with this scaling. The result is similar to what we saw when comparing spectra taken along a glassy isotherm (figure 8.10), but here it is even stronger because also the low frequency minimum in intensity falls on the "master curve". From the definition of R it follows directly

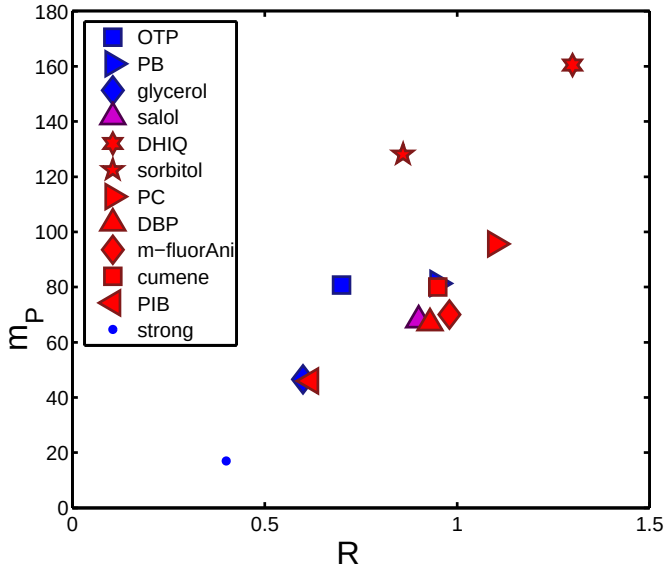

Figure 8.11: Isobaric fragility as a function of the inverse relative boson peak intensity, R. Red symbols are R values of this work. Blue symbols represent data from literature. See the appendix for values and references.

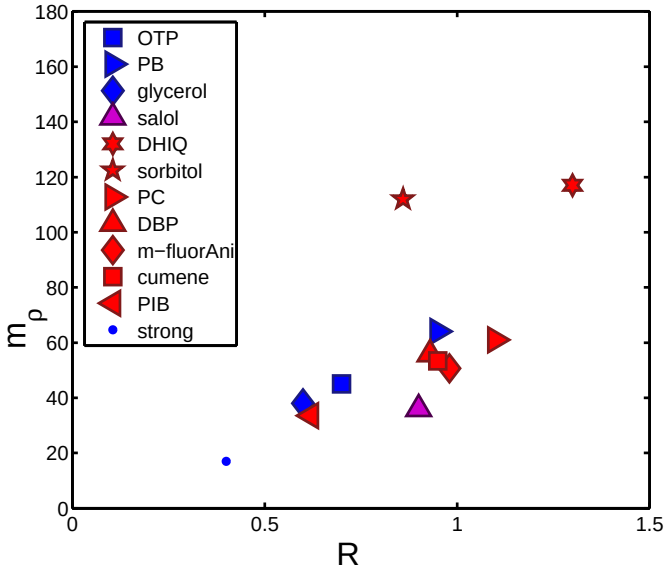

Figure 8.12: Isochoric fragility as a function of the inverse relative boson peak intensity, R. Red symbols are R values of this work. Blue symbols represent data from literature. See the appendix for values and references.

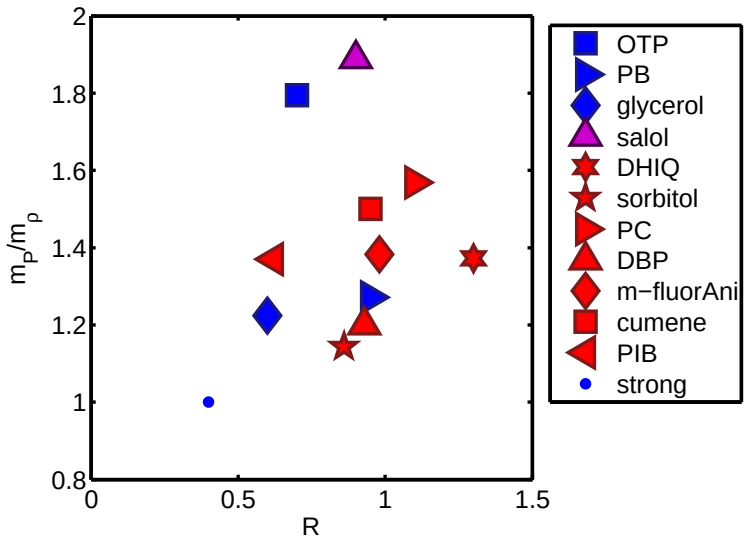

Figure 8.13: The relative contribution of density to the viscous slowing down, measured by m_P/m_ρ a function of the inverse relative boson peak intensity, R. Red symbols are R values of this work. Blue symbols represent data from literature. See the appendix for values and references.

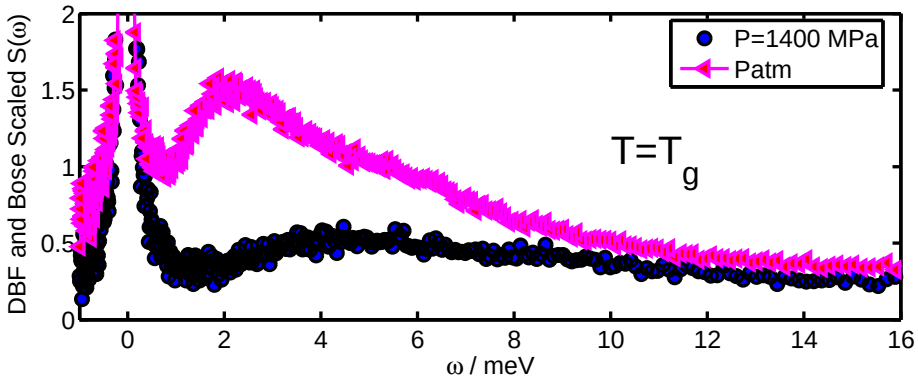

Figure 8.14: The boson peak of PIB3580 at atmospheric pressure and at 1.4 GPa at $T \approx T_g(P)$. The data are corrected for the temperature dependent bosefactor.

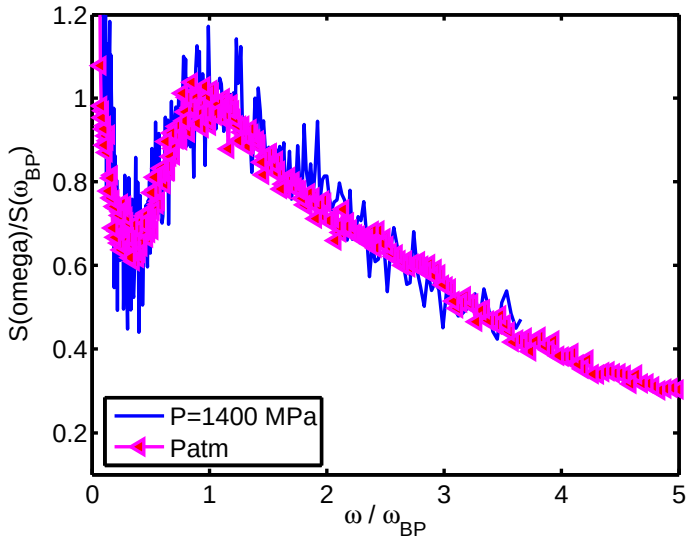

Figure 8.15: The boson peak of PIB3580 at atmospheric pressure and at 1.4 GPa at $T \approx T_g(P)$. The axis are scaled with the boson peak position and intensity. The data are corrected for the temperature dependent bosefactor.

from this scaling that R is independent of pressure. Two systems are not sufficient to state that this is a universal behavior of R. However if the finding is general, then it strongly supports the suggestion that the correlation between R and the isochoric fragility m_ρ, as the latter also stays constant as a function of pressure along the T_g-line (chapter 3).

8.3.3 The quasi-elastic intensity

The quantity R is a measure of the boson peak intensity *relative* to the minimum intensity at the low energy side of the peak. This latter is sometimes clearly influenced by quasi elastic scattering. It is therefore not *a priori* the boson peak intensity that determines R. In figures 8.18 and 8.19 we show the $S(\omega)$ of two liquids which both follow the correlations seen in figures 8.11 and 8.12 namely DBP and DHIQ. For both samples we show the data at $T = 100$ K and at $T = T_g = 180$ K, (all data at atmospheric pressure). The spectra deep in the glass at $T = 100$ K are quite similar for the two liquids, while this is not the case at T_g. For the less fragile DBP the main effect is an increase in intensity due to the temperature dependence of the bose factor. In the case of the very fragile DHIQ on the other hand, there is a quasi-elastic signal at T_g which totally swarms the boson peak. Hence, it is this quasi-elastic signal, rather than the nature of the boson peak which gives DHIQ its large value of R. This observation questions the proposed relation between R and

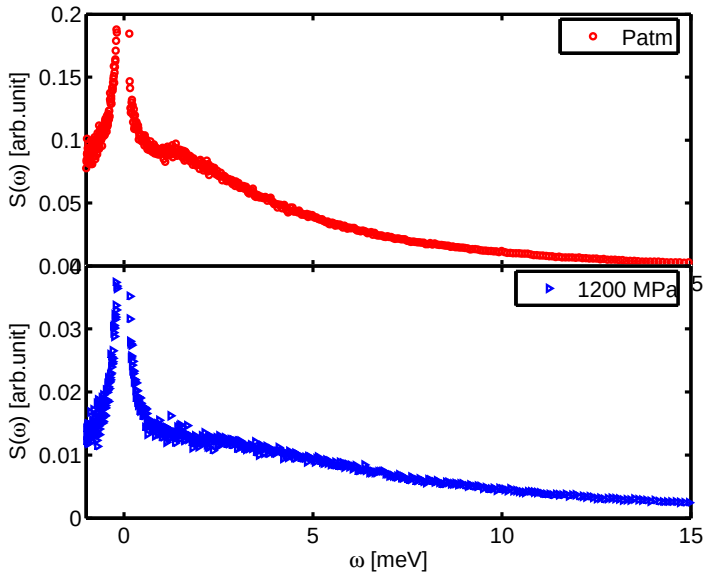

Figure 8.16: The boson peak of cumene at atmospheric pressure and at 1.2 GPa at $T \approx T_g(P)$. The data are corrected for the temperature dependent bosefactor.

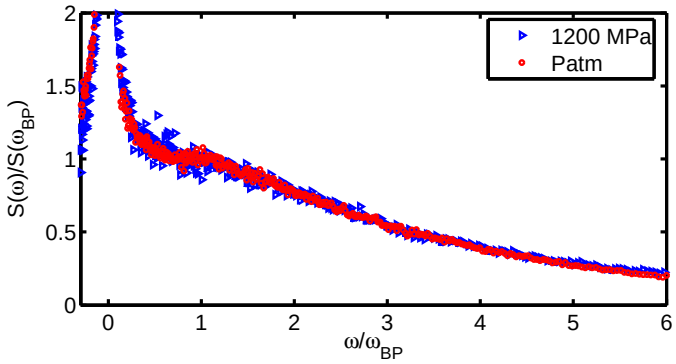

Figure 8.17: The boson peak of cumene at atmospheric pressure and at 1.2 GPa at $T \approx T_g(P)$. The axis are scaled with the boson peak position and intensity. The data are corrected for the temperature dependent bosefactor.

the boson peak intensity relative to the Debye level [Novikov *et al.*, 2005]. The pressure dependence of the two measures of boson peak intensity is also different. While R is independent of pressure we have seen in the previous section that the intensity of the boson peak intensity normalized to the Debye density of states *increases* as a function of pressure.

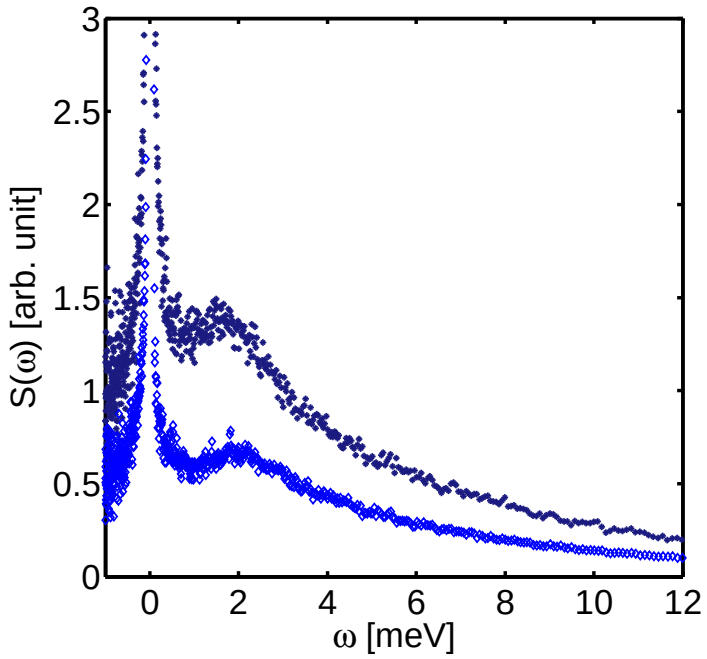

Figure 8.18: The $S(\omega)$ of DBP at T =100 K and $T = T_g$ = 180 K at atmospheric pressure. The increase in intensity is due to the increase in the bose factor.

It is interesting to note that the boson peak intensity over the Debye density of states increases with pressure, because the isobaric fragility is usually found to decrease with pressure. This means that there is a qualitative agreement in the pressure dependence of the boson peak intensity and its inverse correlation to the isobaric fragility. This all together suggests that the two correlations found between boson peak intensity and fragility i) by normalizing the boson peak to the Debye density of states [Sokolov *et al.*, 1997] or ii) by normalizing the boson peak intensity at T_g to the intensity of quasi-elastic scattering at T_g [Sokolov *et al.*, 1993], are fundamentally different. The first is a correlation between boson peak intensity and isobaric fragility, while the latter is a correlation between quasi-elastic scattering at T_g and isochoric fragility. The first is related to the vibrational properties of the system and to the density and temperature dependence of the relaxation time. The latter on the other hand, is related to the relaxations present at T_g and to the pure tem-

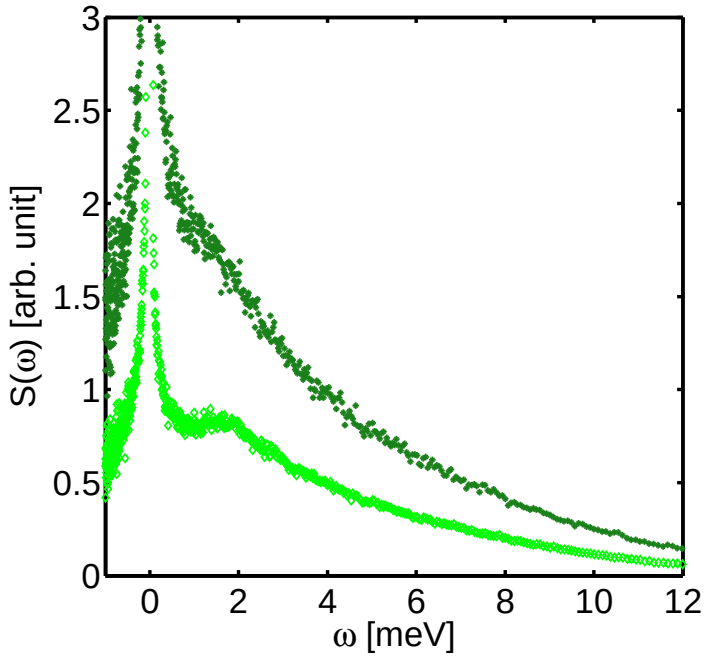

Figure 8.19: The $S(\omega)$ of DHIQ at T =100 K and $T = T_g = 180$ K at atmospheric pressure. At T_g there is quasi-elastic scattering which essentially makes the boson peak invisible.

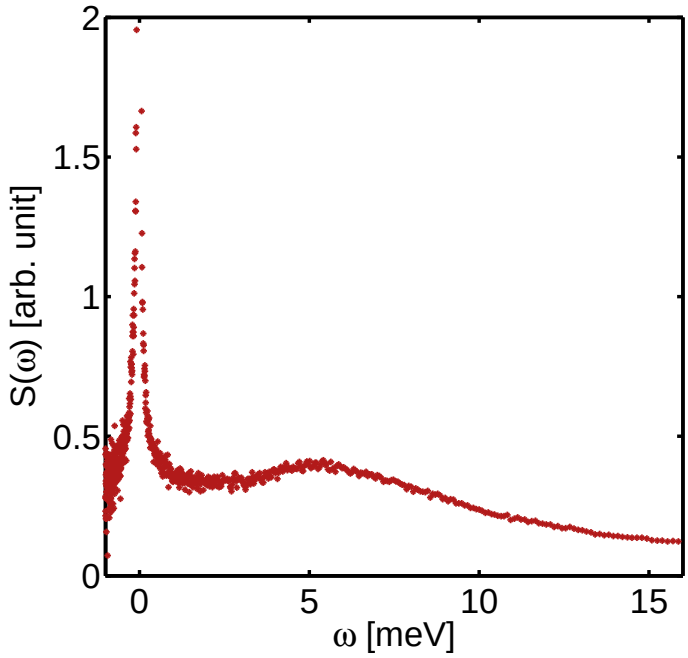

Figure 8.20: The $S(\omega)$ of sorbitol at $T = T_g = 273$ K atmospheric pressure. Sorbitol is a fragile liquid which has a well resolved boson peak in contradiction with the expectation based on the correlation between inverse boson peak intensity and fragility.

perature effect on the alpha relaxation. We stress that the interpretation above is a suggestion based on the very limited knowledge of the pressure dependence of the boson peak intensity. More studies would be needed to verify this interpretation.

It is clear that the correlation, if present at all, is a trend rather than a one to one correlation between fragility and R. The most prominent outlier in figure 8.11 and particularly in figure 8.12 is sorbitol. In figure 8.20 we show the $S(\omega)$ of sorbitol at T_g. The peak is remarkably different from the boson peak in the other systems we have studied. The boson peak energy is a factor 2 larger, and the shape is also distinctively different. Sorbitol is a hydrogen bonded system. This suggests that the boson peak is different in a hydrogen bonded system as compared to other molecular liquids.

8.4 Summary

This chapter has two main sections. The first section contains a study of the boson peak under pressure in glassy PIB (M_w=3580g/mol). We find i) that the boson peak energy increases faster with pressure than any of the other modes. ii) that intensity of $g(\omega)/g_D(\omega)$ increases with pressure. iii) the shape of the boson peak seen in the rDOS $g(\omega)/\omega^2$ is unaffected by pressure.

The decrease in the low frequency intensity seen directly in the rDOS (figure 8.5) has earlier been used to favor the interpretation that the shift in the boson peak is due to a suppression of specific modes rather than a shift of modes to higher frequencies [Gurevich *et al.*, 2005; Hizhnyakov *et al.*, 2000; Klinger, 1999, 2001; Inamura *et al.*, 2000, 2001]. Our results are in clear contradiction with this view, as we do not see a suppression of modes.

It has recently been suggested by Monaco *et al.* [2006 b] that the changes in boson peak due to pressure could be explained entirely by the pressure induced increase in the macroscopic force constants, and that they would disappear when normalizing to the Debye frequency and the amplitude of the Debye density of states. This is clearly not the case for the pressure dependence of the boson peak in PIB.

The second part of this chapter deals with proposed correlation between the fragility and the parameter R. This parameter is given by the intensity of the quasi-elastic scattering (plus the Debye level) relative to that of the boson peak evaluated at T_g. We test this correlation on a set of samples which span a large range in isobaric as well as isochoric fragility. In both cases we find a somewhat scattered correlation. We moreover find that the parameter R is constant along the glass transition isochrone

as is also the isochoric fragility. Based on this observation we suggest that the correlation to isochoric fragility is more fundamental. This indicates that the R could be related to the pure effect of temperature on the relaxation time rather than that of density.

We note that the pressure dependence of R and the pressure dependence of the inverse boson peak intensity in terms of $g_D(\omega)/g(\omega)$ are different. The first is independent of pressure while the latter decreases with pressure. We moreover note that it is seen directly from the raw data that the value of R is largely controlled by differences in the intensity of the quasi-elastic scattering. This leads us to speculate that the correlation with fragility (if present at all) is related to the amplitude of the quasi-elastic scattering rather than the amplitude of the boson peak.

Chapter 9

Summarizing discussion

When a liquid is cooled along an isobar the density increases and the temperature decreases. These two effects both contribute to the slowing down of the dynamics and the isobaric fragility is a combined measure of the two effects.

It has been found empirically over the last five years that the isochoric fragility, which gives a measure of the effect of temperature alone, is independent of density for a large group of different systems, while the isobaric fragility changes when evaluated at higher density. This change in isobaric fragility with pressure is therefore related to the change in the effect of density on the relaxation time.

The effect of density on the change of relaxation time upon cooling along an isobar is governed by two things. First the thermal expansivity α_P, or $\alpha_P T = \frac{\mathrm{d}\log\rho}{\mathrm{d}\log T}$, which measures how much density changes as a function of temperature, and secondly a term that measures how sensitive the relaxation time is to changes in density. The thermal expansivity decreases when pressure is increased. Thus the volume does not change very much as a function of temperature along high pressure isobars and a high pressure isobaric experiment is consequently closer to being isochoric. Or put in other words, the relative effect of density on the viscous slowing down is smaller at high pressure because density itself changes less as a function of temperature at high pressure. It is due to this effect that isobaric fragility most commonly decreases with increasing pressure. The change in fragility with increasing pressure is therefore due to a change in the thermodynamics rather than to a pressure induced change in the response to temperature changes. The pure effect of temperature as measured by the isochoric fragility is found to be independent of density, and in this sense to be intrinsic to the liquid. Based on these observation we conclude that a property which is related to the "pure" effect of temperature on the relaxation time, should correlate to the isochoric fragility (when comparing systems), and that it should

possess the same type of intrinsic character, that is be constant along an isochrone for a given system. Properties related to a combined effect of temperature and density are on the other hand expected to correlate with isobaric fragility and to have a pressure dependence that corresponds to its pressure dependence - that is most often decrease with increasing pressure.

The properties of a glass are essentially independent of temperature, because the structure is frozen in and nothing really changes as temperature is lowered; the moduli and the vibrational density of states stay unchanged when cooling below the glass transition temperature. This has the consequence that the temperature dependence of dynamics in the glass is dominated by the increasing thermal occupation of the vibrational modes. The decrease in temperature accordingly leads to a decrease in boson peak intensity as seen in the dynamical structure factor, a decrease in the mean square displacement, and an increase in the nonergodicity factor.

When a system is compressed it becomes harder and all the characteristic energies of the system increase. The sound speeds increase. The energy of the boson peak increases. The glass transition temperature increases. These effects are intuitively easy to anticipate. Nevertheless, they are more complicated than the temperature dependences, because they are due to real changes of the system rather than just changes in the occupation number. The amount of data so far is quite scarce, and it is difficult to know which behaviors are general and which are specific to the systems we have studied. However, it is clear that pressure allows to distinguish different types of behaviors, which appear similar when studied as a function of temperature. The pressure dependence of the dynamics therefore supplies valuable new information.

The mean square displacement, $\langle u^2 \rangle$, decreases when pressure is applied, even when compared to the square of the average distance between the molecules a^2 (which also decreases with increasing pressure). It thus found that $\langle u^2 \rangle / a^2$ decreases as a function of pressure along a given isotherm in the glass. The mean square displacement is an average property which averages over all Q's and it might be dominated by long wavelengths. Moreover $\langle u^2 \rangle$ is a property with no structural information - it always decreases when the mobility decreases, and this is why it always decreases when pressure is increased. However, the whole temperature dependence can be brought to collapse if the temperature is rescaled with the pressure dependent glass transition temperature. This suggests that there is an intimate relation between the energy barriers that control the freezing of the liquid and the moduli controlling $\langle u^2 \rangle$.

The inverse temperature dependence of the nonergodicity factor is also linear in

temperature in the harmonic approximation, but it differs by mean square displacement in two respects. There is no average over Q and it is a relative quantity which compares the amplitude of vibrations to the frozen in density fluctuations. The latter does not change much as a function of temperature in the glass. However, the frozen in fluctuations will also decrease as pressure is increased. This means that two competing effects govern the pressure dependence of the nonergodicity factor. In practice we find that the nonergodicity factor measured in the glass is essentially independent of pressure at a given temperature. Thus the data at different pressures essentially collapse (at least at low T) when comparing the temperature dependence on an absolute temperature scale. Scaling the temperature axis with the pressure dependent glass transition temperature therefore makes the curves separate and it has the consequence that the dimensionless parameter α increases when pressure increases. This increase of α is opposite the behavior expectation from the correlation between α and isobaric fragility. Also our data on different molecular weight polymers is in contradiction with the proposed correlation between α and fragility. As an alternative we suggest based on a combination of our data and literature data that the original finding is a consequence of a "hidden" correlation between the nonergodicity factor and the effect of density on the relaxation time. We find that $f(T_g)$ is smaller when the effect of density on the relaxation time is larger. This means that the vibrational part of the density fluctuations in the considered Q-range are larger when the effect of density on the relaxation time is larger. This suggests that the properties which govern these density fluctuations also couple to the density dependence of the relaxation time. More studies are needed to verify this interpretation - particularly studies of the pressure dependence of $f(T_g)$ are needed.

Following the work of Inamura *et al.* [2000, 2001] it has been thought that the boson peak intensity decreases when a sample is densificated. However, this work and several other results that have come out within the last year [Monaco *et al.*, 2006 a; Andrikopoulos *et al.*, 2006], clearly demonstrate that this is not the case. The boson peak intensity relative to the Debye density of states stays constant (or increases) as pressure is increased. The system becomes harder overall, but no specific modes appear to be suppressed. Also the shape of the boson peak stays constant as pressure is increased. In so far as the boson peak gives a signature of the type of disorder, this suggests that the type of disorder is not changed when the system is compressed.

Both the boson peak intensity and the quasi-elastic scattering measured directly in the dynamical structure factor at T_g decrease as a function of pressure. Moreover, both contributions change by the same ratio along the T_g-isochrone and the relative intensity of the boson peak as compared to the quasi-elastic intensity therefore stays

constant when evaluated at T_g. In addition we find that the ratio expressed by R tentatively correlates with fragility. The correlation is of similar quality when comparing R with the isochoric fragility or with the isobaric fragility. Based on the pressure independence of R (which we find in the two systems where it has been studied) we speculate that the correlation to the intrinsic isochoric fragility is the more fundamental. A direct comparison of the spectra from different systems at varying temperatures, suggests that R evaluated at T_g is more governed by the amount of quasi-elastic scattering than by the boson peak intensity. This indicates that more fragile systems might have more quasi-elastic scattering even at T_g, where the alpha relaxation most certainly does not enter the experimental window.

Chapter 10

Perspectives

In this work we have mainly used pressure experiments to test the robustness of empirically established "universalities". In addition we have tested the robustness of the elastic models for the viscous slowing down and discussed several different proposed models for the boson peak. These models are formulated as *explanations* of phenomenology observed at atmospheric pressure. High pressure experiments therefore gives a valuable possibility of testing their *predictive* power. This type of test is relevant for almost any type of model or theory claiming to explain a general phenomenon in glass-formers. Particularly for explaining the viscous slowing down, it is clear that the relevant governing parameter should be constant along isochrones in the system. This implies for example that the Adam-Gibbs model predicts $1/(TS_c(\rho,T))$=constant and the shoving model predicts $G_\infty(\rho,T)/T$=constant along an isochrone. Especially the latter of these prediction could easily be tested in practice.

Turning now to the phenomenology of glass-forming systems, we have established some trends that appear to be general. The system becomes harder when increasing pressure along the T_g-isochrone, and the characteristic energy (or energies) of the system increases. The activation energy is for example higher (but E_a/T is of course constant). The boson peak energy is higher at higher pressure and the mean square displacement has a lower amplitude. However, there are also a striking number of properties which are unaffected by pressure changes along the isochrone. (i) We find that the relative intensity of the boson peak is unaffected. (ii) The shape of the boson peak is not affected. (iii) The isochoric fragility is not affected. (iv) The shape of the alpha relaxation is not affected. (v) The mean square displacement normalised to the average molecular distance is not affected. Thus all these dynamical properties are intrinsic to a given system in the sense that they are unaffected by pressure - at least within a limited pressure range. From this we conclude that the mechanisms which govern the structural slowing down should have the same type of intrinsic character.

Bibliography

Adam, G. and Gibbs, J. H. [1965]. On temperature dependence of cooperative relaxation properties in glass-forming liquids, *J. Chem. Phys.* **43**: 139.

Alba-Simionesco, C., Cailliaux, A., Alegria, A. and Tarjus, G. [2004]. Scaling out the density dependence of the α relaxation in glass-forming polymers, *Europhys. Lett.* **68**: 58–64.

Alba-Simionesco, C., Fan, J. and Angell, C. A. [1999]. Thermodynamic aspects of the glass transition phenomenon. II. Molecular liquids with variable interactions, *J. Chem. Phys.* **110**: 5262–5272.

Alba-Simionesco, C., Fujimori, H., Morineau, D. and Frick, B. [1997]. A study of the glass transition of molecular liquids as a function of pressure and temperature, *Prog. Theor. Phys. Suppl.* **126**: 229–233.

Alba-Simionesco, C., Kivelson, D. and Tarjus, G. [2002]. Temperature, density, and pressure dependence of relaxation times in supercooled liquids, *J. Chem. Phys.* **116**: 5033–5038.

Alba-Simionesco, C. and Tarjus, G. [2006]. Temperature versus density effects in glassforming liquids and polymers: A scaling hypothesis and its consequences, *J. Non-Cryst. Solids* **352**: 4888–4894.

Alvarez, F., Alegria, A. and Colmenero, J. [1991]. Relationship between the time-domain kohlrausch-williams-watts and frequency-domain havriliak-negami relaxation functions, *Phys. Rev. B* **44**: 7306–7312.

Andrikopoulos, K. S., Christofilos, D., Kourouklis, G. A. and Yannopoulos, S. N. [2006]. Pressure dependence of the boson peak in glassy as_2s_3 studied by raman scattering, *J. Non-Cryst. Solids* **352**: 4594–4600.

Angell, C. A. [1991]. Relaxation in liquids, polymers and plastic crystals - strong fragile patterns and problems, *J. Non-Cryst. Solids* **131**: 13–31.

Angell, C. A. [1995]. Formation of glasses from liquids and biopolymers, *Science* **267**: 1924–1935.

Angell, C. A., Ngai, K. L., McKenna, G. B., McMillan, P. F. and Martin, S. W. [2000]. Relaxation in glassforming liquids and amorphous solids, *J. Appl. Phys.* **88**: 3113.

Bairlein, R. [1999]. *Thermal Physics*, Cambridge University Press.

Barlow, A. J., Lamb, J. and Matheson, A. J. [1966]. Viscous behaviour of supercooled liquids, *Proc. R. Soc. London A* **292**: 322.

Barlow, A. J., Lamb, J. and Taskopru, N. S. [1969]. Ultrasonic and viscoeleatic relaxation in bis(m-(mphenoxy phenocy)phenyl) ether, *J. Acoust. Soc. Amer.* **46**: 569.

Begen, B., Kisliuk, A., Novikov, V., Sokolov, A., Niss, K., Chauty-Cailliaux, A., Alba-Simionesco, C. and Frick, B. [2006]. Influence of pressure on fast dynamics in polyisobutylene, *J. Non-Cryst. Solids* **352**.

Begen, B., Kisliuk, A. and Sokolov, A. [2006 b]. Unpublished data. will appear in [Niss *et al.*, 2007 b].

Berthier, L., Biroli, G., Bouchaud, J. P., Cipelletti, L., Masri, D. E., L'hote, D., Ladieu, F. and Perino, M. [2005]. Direct experimental evidence of a growing length scale accompanying the glass transition, *Science* **310**: 1797–1800.

Birge, N. O. [1986]. Specific-heat spectroscopy of glycerol and propylene-glycol near the glass-transition, *Phys. Rev. B* **34**: 1631–1642.

Blochowicz, T., Gainaru, C., Medick, P., Tschirwitz, C. and Rossler, E. A. [2006]. The dynamic susceptibility in glass forming molecular liquids: The search for universal relaxation patterns ii, *J. Chem. Phys.* **124**: 134503.

Blochowicz, T., Tschirwitz, C., Benkhof, S. and Rössler., E. A. [2003]. Susceptibility functions for slow relaxation processes in supercooled liquids and the search for universal relaxation patterns, *J. Chem. Phys.* **118**: 7544–7555.

Böhmer, R., Ngai, K. L., Angell, C. A. and Plazek, D. J. [1993]. Nonexponential relaxations in strong and fragile glass formers, *J. Chem. Phys.* **99**: 4201–4209.

Boon, J. P. and Yip, S. [1980]. *Molecular Hydrodynamics*, McGraw-Hill Inc.

Bordat, P., Affouard, F., Descamps, M. and Ngai, K. L. [2004]. Does the interaction potential determine both the fragility of a liquid and the vibrational properties of its glassy state?, *Phys. Rev. Lett.* **93**: 105502.

Böttcher, C. J. F. [1973]. *Theory of electric polarization*, Vol. 1, 2 edn, Elsevier Scientific Publishing Company.

Bouchaud, J. P. and Biroli, G. [2004]. On the Adam-Gibbs-Kirkpatrick-Thirumalai-Wolynes scenario for the viscosity increase in glasses, *J. Chem. Phys.* **121**: 7347–7354.

Bouchaud, J. P. and Biroli, G. [2005]. Nonlinear susceptibility in glassy systems: A probe for cooperative dynamical length scales, *Phys. Rev. B* **72**: 064204.

Bridgman, P. W. [1932]. Volume-temperature-pressure relations for several non-volatile liquids, *Proc. Am. Acad. Arts Sci.* **67**: 1–27.

Bridgman, P. W. [1949]. Viscosities to 30,000 kg/cm^2, *Proc. of the Am. Chem. Soc.* **77**: 129.

Buchenau, U. and Wischnewski, A. [2004]. Fragility and compressibility at the glass transition, *Phys. Rev. B* **70**: 092201.

Buchenau, U. and Zorn, R. [1992]. A relation between fast and slow motions in glassy and liquid selenium, *Europhys. Lett.* **18**: 523–528.

Carpentier, L., Decressain, R. and Descamps, M. [2004]. Relaxation modes in glass forming meta-toluidine, *J. Chem. Phys.* **121**: 6470–6477.

Casalini, R., McGrath, K. J. and Roland, C. M. [2006]. Isobaric and isochoric properties of decahydroisoquinoline an extremly fragile glass former, *J. Non-Cryst. Solids* **352**: 4905–4909.

Casalini, R. and Ngai, K. L. [2001]. Structural dependence of fast relaxation in glass-forming substances and correlation with the stretch exponent of the slow structural alpha-relaxation, *J. Non-Cryst. Solids* **293**: 318–326.

Casalini, R., Paluch, M. and Roland, C. M. [2003]. Influence of molecular structure on the dynamics of supercooled van der Waals liquids, *Phys. Rev. E* **67**: 031505.

Casalini, R. and Roland, C. M. [2004]. Thermodynamical scaling of the glass transition dynamics, *Phys. Rev. E* **69**: 062501.

Casalini, R. and Roland, C. M. [2005 a]. Why liquids are fragile, *Phys. Rev. E* **72**: 031503.

Casalini, R. and Roland, C. M. [2005 b]. Scaling of the supercooled dynamics and its relation to the pressure dependences of the dynamic crossover and the fragility of glass formers, *Phys. Rev. B* **71**: 014210.

Casalini, R. and Roland, C. M. [2005 c]. Temperature and density effects on the local segmental and global chain dynamics of poly(oxybutylene), *Macromolecules* **38**: 1779–1788.

Chauty-Cailliaux, A. [2003]. *Thermodynamique, Structure, et Dynamique de Polymeres Amporphes sous Pression a l'appoche de la Transition Vitreuse*, PhD thesis, Universite Paris XI.

Christensen, T. E. [1994]. Description of a method of measuring the shear modulus of supercooled liquids and a comparison of their thermal and mechanical response functions, *Tekster fra IMFUFA* **279**.

Chumakov, A. I., Sergueev, I., burck, U. V., Schirmacher, W., Asthalter, T., Ruffer, R., Leupold, O. and Petry, W. [2004]. Collective nature of the boson peak and universal transboson dynamics of glasses, *Phys. Rev. Lett.* **92**: 245508.

Cohen, M. H. and Turnbull, D. [1959]. Molecular transport in liquids and glasses, *J. Chem. Phys.* **31**: 1164–1169.

Comez, L., Corezzi, S., Monaco, G., Verbeni, R. and Fioretto, D. [2005]. Ergodic to nonergodic transition in liquids with a local order: The case of m-toluidine, *Phys. Rev. Lett.* **94**: 155702.

Cook, R. L., Herbst, C. A. and King, H. E. [1993]. High-pressure viscosity of glass-forming liquids measured by the centrifugal force diamond anvil cell viscometer, *J. Phys. Chem.* **97**: 2355–2361.

Cook, R. L., King, H. E., Herbst, C. A. and Herschbach, D. R. [1994]. Pressure and temperature-dependent viscosity of 2 glass-forming liquids: Glycerol and dibutyl phthalate, *J. Chem. Phys.* **100**: 5178–5189.

Cutroni, M., Migliardo, P., Piccolo, P. A. and Alba-Simionesco, C. [1994]. The dynamic glass-transition of a fragile molecular liquid in the megahertz domain, *J. Phys-Condens. Mat.* **6**: 5283–5293.

Ding, Y. F., Novikov, V. N., Sokolov, A. P., Cailliaux, A., Dalle-ferrier, C., Alba-Simionesco, C. and Frick, B. [2004]. Influence of molecular weight on fast dynamics and fragility of polymers, *Macromolecules* **37**: 9264–9272.

Dixon, P. K. and Nagel, S. R. [1988]. Frequency-dependent specific-heat and thermal-conductivity at the glass-transition in ortho-terphenyl mixtures, *Phys. Rev. Lett.* **61**: 341–344.

Dixon, P. K., Wu, L., Nagel, S. R., Williams, B. D. and Carini, J. P. [1990]. Scaling in the relaxation of supercooled liquids, *Phys. Rev. Lett.* **65**: 1108–1111.

Dreyfus, C., Aouadi, A., Gapinski, J., Matos-lopes, M., Steffen, W., Patkowski, A. and Pick, R. M. [2003]. Temperature and pressure study of Brillouin transverse modes in the organic glass-forming liquid orthoterphenyl, *Physical Review E* **68**: 011204.

Dreyfus, C., grand, A. L., Gapinski, J., Steffen, W. and Patkowski, A. [2004]. Scaling the alpha-relaxation time of supercooled fragile organic liquids, *Eur. Phys. J. B* **42**: 309–319.

Duval, E., Boukenter, A. and Achibat, T. [1990]. Vibrational dynamics and the structure of glasses, *J. Phys-Condens. Mat.* **2**: 10227–10234.

Dyre, J. C. [2004]. Glasses - Heirs of liquid treasures, *Nature Materials* **3**: 749–750.

Dyre, J. C. [2006]. The glass transition and elastic models of glass-forming liquids, *Rev. Mod. Phys.* **78**: 953–972.

Dyre, J. C. and Olsen, N. B. [2004]. Landscape equivalent of the shoving model, *Phys. Rev. E* **69**: 042501.

Dyre, J. C., Olsen, N. B. and Christensen, T. [1996]. Local elastic expansion model for viscous-flow activation energies of glass-forming molecular liquids, *Phys. Rev. B* **53**: 2171.

Daz-Calleja, R., Riande, E. and Romn, J. S. [1993]. Interconversion between mechanical and dielectric relaxations for poly(cyclohexyl acrylate), *J. Polym Sci. Pol Phys.* **31**: 711.

Ediger, M. D. [2000]. Spatially heterogeneous dynamics in supercooled liquids, *Ann. Rev. Phys. Chem.* **51**: 99–128.

Ediger, M. D., Angell, C. A. and Nagel, S. R. [1996]. Supercooled liquids and glasses, *J. Phys. Chem.* **100**: 13200.

Egelstaff, P. A. [1994]. *An introduction to the Liquid State*, 2 edn, Oxford University Press.

Engberg, D., Wischnewski, A., Buchenau, U., Borjesson, L., Dianoux, A. J., Sokolov, A. P. and Torell, L. M. [1998]. Sound waves and other modes in the strong glass former b2o3, *Phys. Rev. B* **58**: 9087–9097.

Farago, B., Arbe, A., Colmenero, J., Faust, R., Buchenau, U. and Richter, D. [2002]. Intermediate length scale dynamics of polyisobutylene, *Phys. Rev. E* **65**: 051803.

Fatuzzo, E. and Mason, P. [1967]. A calculation of the complex dielectric constant of a polar liquid by the librating molecule method, *Proc. Phys. Soc. Lond.* **90**: 729.

Ferrer, M. L., Lawrence, C., Demirjian, B. G., Kivelson, D., Alba-Simionesco, C. and Tarjus, G. [1998]. Supercooled liquids and the glass transition: Temperature as the control variable, *J. Chem. Phys.* **109**: 8010–8015.

Fioretto, D., Buchenau, U., Comez, L., Sokolov, A., Masciovecchio, C., Mermet, A., Ruocco, G., Sette, F., Willner, L., Frick, B., Richter, D. and Verdini, L. [1999]. High-frequency dynamics of glass-forming polybutadiene, *Phys. Rev. E* **59**: 4470–4475.

Floudas, G., Mpoukouvalas, K. and Papadopoulos, P. [2006]. The role of temperature and density on the glass-transition dynamics of glass formers, *J. Chem. Phys.* **124**: 074905.

Frick, B. and Alba-Simionesco, C. [1999]. Comparison of the pressure and temperature dependence of the elastic incoherent scattering for the polymers polybutadiene and polyisobutylene, *Physica B* **266**: 13–19.

Frick, B. and Alba-Simionesco, C. [2002]. Pressure dependence of the Boson peak in poly(butadiene), *Appl. Phys. A* **74**: S549–S551 Part 1 Suppl. S DEC 2002.

Frick, B. and Alba-Simionesco, C. [2003]. Unpublished data.

Frick, B. and Richter, D. [1993]. Change of the vibrational dynamics near the glass-transition in polyisobutylene - inelastic neutron-scattering on a nonfragile polymer, *Phys. Rev. B* **47**: 14795–14804.

Fujimori, H., Oguni, M. and Alba-Simionesco, C. [1997]. Pressure effect as referred to the temperature effect on irreversible structural relaxations in liquid dibutylphthalate, *Prog. Theor. Phys. Suppl.* **SUPPLEMENT**: 235–238.

Gapinski, J., Paluch, M. and Patkowski, A. [2002]. Correlation between nonexponential relaxation and non-Arrhenius behavior under conditions of high compression, *Phys. Rev. E* **66**: 011501.

Geilenkeuser, R., Porschberg, T., Jackel, M. and Gladun, A. [1999]. Influence of high pressure on thermal properties of amorphous polystyrene, *Physica B* **263**: 276–279.

Goldstein, M. [1969]. Viscous liquids and glass transition - a potential energy barrier picture, *J. Chem. Phys.* **51**: 3728.

Gomez, D. and Alegria, A. [2001]. On the empirical functions describing the alpha-relaxation of glass-forming systems, *J. Non-Cryst. Solids* **287**: 246–251.

Granato, A. V. [2002]. The specific heat of simple liquids, *J. Non-Cryst. Solids* **307**: 376–386.

Gurevich, V. L., Parshin, D. A. and Schober, H. R. [2003]. Anharmonicity, vibrational instability, and the Boson peak in glasses, *Phys. Rev. B* **67**: 094203.

Gurevich, V. L., Parshin, D. A. and Schober, H. R. [2005]. Pressure dependence of the boson peak in glasses, *Phys. Rev. B* **71**: 014209.

Hansen, J.-P. and McDonald, I. [1986]. *Theory of Simple Liquids*, 2nd edn, Academic Press.

Hemley, R. J., Mao, H. K., Bell, P. M. and Mysen, B. O. [1986]. Raman-spectroscopy of sio_2 glass at high-pressure, *Phys. Rev. Lett.* **57**: 747–750.

Hensel-bielowka, S., Paluch, M. and Ngai, K. L. [2005]. Emergence of the genuine Johari-Goldstein secondary relaxation in m-fluoroaniline after suppression of hydrogen-bond-induced clusters by elevating temperature and pressure, *J. Chem. Phys.* **123**: 014502.

Hensel-Bielowka, S., Ziolo, J., Paluch, M. and Roland, C. M. [2002 b]. The effect of pressure on the structural and secondary relaxations in 1,1-bis(p-methoxyphenyl) cyclohexane, *J. Chem. Phys.* **117**: 2317–2323.

Hizhnyakov, V., Laisaar, A., Kikas, J., Kuznetsov, A., Palm, V. and Suisalu, A. [2000]. Transformation of soft localized modes in glasses under pressure, *Phys. Rev. B* **62**: 11296–11299.

Huang, D. H., Colucci, D. M. and Mckenna, G. B. [2002]. Dynamic fragility in polymers: A comparison in isobaric and isochoric conditions (vol 116, pg 3925, 2002), *J. Chem. Phys.* **117**: 7390–7390.

Huang, D. H. and McKenna, G. B. [2001]. New insights into the fragility dilemma in liquids, *J. Chem. Phys.* **114**: 5621–5630.

Inamura, Y., Arai, M., Nakamura, M., Otomo, T., Kitamura, N., Bennington, S. M., Hannon, A. C. and Buchenau, U. [2001]. Intermediate range structure and low-energy dynamics of densified vitreous silica, *J. Non-Cryst. Solids* **293**: 389–393.

Inamura, Y., Arai, M., Otomo, T., Kitamura, N. and Buchenau, U. [2000]. Density dependence of the boson peak of vitreous silica, *Physica B* **284**: 1157–1158.

Jakobsen, B., Niss, K. and Olsen, N. B. [2005]. Dielectric and shear mechanical alpha and beta relaxations in seven glass-forming liquids, *J. Chem. Phys.* **123**: 234511.

Johari, G. P. [2006]. On Poisson's ratio of glass and liquid vitrification characteristics, *Phil. Mag.* **86**: 1567–1579.

Kanaya, T. and Kaji, K. [2001]. Dynamics in the glassy state and near the glass transition of amorphous polymers as studied by neutron scattering, *Adv. Polym Sci.* **154**: 87–141.

Kilburn, D., Wawryszczuk, J., Dlubek, G., Pionteck, J., Hassler, R. and Alam, M. A. [2006]. Temperature and pressure dependence of the free volume in polyisobutylene from positron lifetime and pressure-volume-temperature experiments, *Macromolecular Chemistry And Physics* **207**: 721–734.

Kirkpatrick, T. R., Thirumalai, D. and Wolynes, P. G. [1989]. Scaling concepts for the dynamics of viscous-liquids near an ideal glassy state, *Phys. Rev. A* **40**: 1045–1054.

Kittel, C. [1996]. *Introduction to Solid State Physics*, 7 edn, Johf Wiley & Sons, Inc.

Kivelson, D. and Tarjus, G. [1998]. Superarrhenius character of supercooled glass-forming liquids, *J. Non-crys. Solids* **235**: 86.

Klinger, M. I. [1999]. Sound-wave-like modes or localized soft-mode vibrations in the boson peak of glasses: Differences in pressure effects, *Phys. Lett. A* **254**: 225–229.

Klinger, M. I. [2001]. Separation of soft-mode and acoustic dynamics in the boson peak of glasses: vast difference in high-pressure effects, *J. Non-Cryst. Solids* **293**: 345–347.

Laughlin, W. T. and Uhlmann, D. R. [1972]. Viscous flow in simple organic liquids, *J. Phys. Chem.* **76**: 2317.

Leonforte, F., Tanguy, A., Wittmer, J. and Barrat, J. [2006]. Inhomogeneous elastic response of silica glass, *Phys. Rev. Lett.* **97**: 05501.

Li, G., King, H. E., Oliver, W. F., Herbst, C. A. and Cummins, H. Z. [1995]. Pressure and temperature-dependence of glass-transition dynamics in a fragile glass former, *Phys. Rev. Lett.* **74**: 2280–2283.

Lindsey, C. P. and Patterson, G. D. [1980]. Detailed comparison of the williams-watts and cole-davidson functions, *J. Chem. Phys.* **73**: 3348–3357.

Ling, A. C. and Willard, J. E. [1968]. Viscosities of some organic glasses used as trapping matrices .2., *Journal Of Physical Chemistry* **72**: 3349.

Lovesey, S. W. [1984]. *Theory of Neutron Scattering from Condensed Matter*, Vol. 1, Oxford University Press.

Lunkenheimer, P. and Loidl, A. [2002]. Dielectric spectroscopy of glass-forming materials: alpha-relaxation and excess wing, *Chem. Phys.* **284**: 205–219.

Malinovsky, V. K., Novikov, V. N., Parshin, P. P., Sokolov, A. P. and Zemlyanov, M. G. [1990]. Universal form of the low-energy (2 to 10 mev) vibrational-spectrum of glasses, *Europhys. Lett.* **11**: 43–47.

Mandanici, A., Cutroni, M. and Richert, R. [2005]. Dynamics of glassy and liquid m-toluidine investigated by high-resolution dielectric spectroscopy, *J. Chem. Phys.* **122**: 084508.

Masciovecchio, C., Mazzacurati, V., Monaco, G., Ruocco, G., Scopigno, T., Sette, F., Benassi, P., Cunsolo, A., Fontana, A., Krisch, M., Mermet, A., Montagna, M., Rossi, F., Sampoli, M., Signorelli, G. and Verbeni, R. [1999]. Acoustic nature of the boson peak in vitreous silica, *Philos. Mag. B* **79**: 2013–2020.

Matic, A., Masciovecchio, C., Engberg, D., Monaco, G., Borjesson, L., Santucci, S. C. and Verbeni, R. [2004]. Crystal-like nature of acoustic excitations in glassy ethanol, *Phys. Rev. Lett.* **93**: 145502.

Maurer, E. and Schirmacher, W. [2004]. Local oscillators vs. elastic disorder: A comparison of two models for the boson peak, *J. Low Temp. Phys.* **137**: 453–470.

Mermet, A., Duval, E., Polian, A. and Krisch, M. [2002]. High-frequency dynamics of the glass former dibutylphthalate under pressure, *Phys. Rev. E* **66**: 031510.

Minassian, L. T., Bouzar, K. and Alba, C. [1988]. Thermodynamic properties of liquid toluene, *J. Phys. Chem.* **92**: 487–493.

Monaco, A., Chumakov, A. I., Monaco, G., Crichton, W. A., Meyer, A., Comez, L., Fioretto, D., Korecki, J. and Ruffer, R. [2006 b]. Effect of densification on the density of vibrational states of glasses, *Phys. Rev. Lett.* **97**: 135501.

Monaco, A., Chumakov, A. I., Yue, Y. Z., Monaco, G., Comez, L., Fioretto, D., Crichton, W. A. and Ruffer, R. [2006 a]. Density of vibrational states of a hyperquenched glass, *Phys. Rev. Lett.* **96**: 205502.

Ngai, K. L. [2000]. Dynamic and thermodynamic properties of glass-forming substances, *J. Non-Cryst. Solids* **275**: 7–51.

Ngai, K. L. [2004]. Why the fast relaxation in the picosecond to nanosecond time range can sense the glass transition, *Phil. Mag.* **84**: 1341–1353.

Ngai, K. L., Casalini, R., Capaccioli, S., Paluch, M. and Roland, C. M. [2005]. Do theories of the glass transition, in which the structural relaxation time does not define the dispersion of the structural relaxation, need revision?, *J. Phys. Chem. B* **109**: 17356–17360.

Ngai, K. L. and Rendell, R. W. [1990]. Comparison between frequency-dependent specific-heat and dielectric-relaxation of glycerol and propylene-glycol, *Phys. Rev. B* **41**: 754–756.

Ngai, K. L., Rendell, R. W. and Plazek, D. J. [1991]. Couplings between the cooperatively rearranging regions of the adam-gibbs theory of relaxations in glass-forming liquids, *J. Chem. Phys.* **94**: 3018–3029.

Nielsen, A., Cristensen, T., Olsen, N. B. and Dyre, J. C. [2006]. data. to be published.

Niss, K. and Alba-Simionesco, C. [2006]. Effects of density and temperature on correlations between fragility and glassy properties, *Phys. Rev. B* **74**: 024205.

Niss, K., Dalle-Ferrier, C., Tarjus, G. and Alba-Simionesco, C. [2007]. On the correlation between fragility and stretching in glassforming liquids, *J. Phys-Condens. Mat.* **19**: 076102.

Niss, K., Frick, B., Ollivier, J., Beraud, A., Sokolov, A., Begen, B., Novikov, V. and Alba-Simionesco, C. [2007 b]. Influence of pressure on the boson peak: Stronger than elastic medium transformation, Submitted *Phys. Rev. Lett.*

Niss, K. and Jakobsen, B. [2003]. Dielectric and shear mechanical relaxation in glass forming liquids, *Master Thesis, Texts from IMFUFA 424*, Department of Mathematics and Physics (IMFUFA), Roskilde University, P.O.Box 260, DK-4000 Roskilde, Denmark.

Niss, K., Jakobsen, B. and Olsen, N. B. [2005]. Dielectric and shear mechanical relaxations in glass-forming liquids: A test of the Gemant-DiMarzio-Bishop model, *J. Chem. Phys.* **123**: 234510.

Novikov, V. N., Ding, Y. and Sokolov, A. P. [2005]. Correlation of fragility of supercooled liquids with elastic properties of glasses, *Phys. Rev. E* **71**: 061501.

Novikov, V. N. and Sokolov, A. P. [2004]. Poisson's ratio and the fragility of glass-forming liquids, *Nature* **431**: 961–963.

Olsen, N. B. [2006]. Personal communication.

Olsen, N. B., Christensen, T. and Dyre, J. C. [2001]. Time-temperature superposition in viscous liquids, *Phys. Rev. Lett.* **86**: 1271.

Onsager, L. [1936]. Electric moments of molecules in liquids, *J. Am. Chem. Soc.* **58**: 1486.

Paluch, M., Casalini, R., Hensel-Bielowka, S. and Roland, C. M. [2002]. Effect of pressure on the alpha relaxation in glycerol and xylitol, *J. Chem. Phys.* **116**: 9839–9844.

Paluch, M., Ngai, K. L. and Hensel-Bielowka, S. [2001]. Pressure and temperature dependences of the relaxation dynamics of cresolphthalein-dimethylether: Evidence of contributions from thermodynamics and molecular interactions, *J. Chem. Phys.* **114**: 10872–10883.

Paluch, M., Pawlus, S., Hensel-bielowka, S., Kaminska, E., Prevosto, D., Capaccioli, S., Rolla, P. A. and Ngai, K. L. [2005]. Two secondary modes in decahydroisoquinoline: Which one is the true Johari Goldstein process?, *J. Chem. Phys.* **122**: 234506.

Paluch, M., Roland, C. M., Gapinski, J. and Patkowski, A. [2003 b]. Pressure and temperature dependence of structural relaxation in diglycidylether of bisphenol a, *J. Chem. Phys.* **118**: 3177–3186.

Paluch, M., Sekula, M., Pawlus, S., Rzoska, S. J., Ziolo, J. and Roland, C. M. [2003 a]. Test of the Einstein-Debye relation in supercooled dibutylphthalate at pressures up to 1.4 gpa, *Phys. Rev. Lett.* **90**: 175702.

Parisi, G., Ruocco, G. and Zamponi, F. [2004]. Fragility in p-spin models, *Phys. Rev. E* **69**: 061505.

Patkowski, A., Gapinski, J. and Meier, G. [2004]. Dynamics of supercooled van der Waals liquid under pressure. A dynamic light scattering study, *Coll. Polym. Sci.* **282**: 874–881.

Plazek, D. J. and Ngai, K. L. [1991]. Correlation of polymer segmental chain dynamics with temperature-dependent time-scale shifts, *Macromolecules* **24**: 1222–1224.

Qin, Q. and McKenna, G. B. [2006]. Correlation between dynamic fragility and glass transition temperature for different classes of glass forming liquids, *J. Non-Cryst. Solids* **352**: 2977–2985.

Quitmann, D. and Soltwisch, M. [1998]. Intermediate-range order and the liquid - glass transformation, *Phil. Mag. B* **77**: 287–296.

Reiser, A., Kasper, G. and Hunklinger, S. [2005]. Pressure-induced isothermal glass transition of small organic molecules, *Phys. Rev. B* **72**: 094204.

Richert, R. [2002]. Heterogeneous dynamics in liquids: fluctuations in space and time, *J. Phys-condens Mat.* **14**: R703–R738.

Richert, R., Duvvuri, K. and Duong, L. T. [2003]. Dynamics of glass-forming liquids. VII. Dielectric relaxation of supercooled *tris*-naphthylbenzene, squalane, and decahydroisoquinoline, *J. Chem. Phys.* **118**: 1828.

Roland, C. M. and Casalini, R. [2003a]. Temperature and volume effects on local segmental relaxation in poly(vinyl acetate), *Macromolecules* **36**: 1361–1367.

Roland, C. M. and Casalini, R. [2003b]. Temperature dependence of local segmental motion in polystyrene and its variation with molecular weight, *J. Chem. Phys.* **119**: 1838–1842.

Roland, C. M. and Casalini, R. [2004]. Comment on: "Disentangling density and temperature effects in the viscous slowing down of glass forming liquids" [J. Chem. Phys. 120, 6135 (2004)], *J. Chem. Phys.* **121**: 11503–11504.

Roland, C. M., Hensel-Bielowka, S., Paluch, M. and Casalini, R. [2005]. Supercooled dynamics of glass-forming liquids and polymers under hydrostatic pressure, *Rep. Prog. Phys.* **68**: 1405–1478.

Roland, C. M., Paluch, M., Pakula, T. and Casalini, R. [2004]. Volume and temperature as control parameters for the dielectric α relaxation of polymers and molecular glass formers, *Phil. Mag.* **84**: 1573–1581.

Rössler, E. and Sokolov, A. P. [1996]. The dynamics of strong and fragile glass formers, *Chemical Geology* **128**: 143–153.

Ruffle, B., Foret, M., Courtens, E., Vacher, R. and Monaco, G. [2003]. Observation of the onset of strong scattering on high frequency acoustic phonons in densified silica glass, *Phys. Rev. Lett.* **90**: 095502.

Ruffle, B., Guimbretiere, G., Courtens, E., Vacher, R. and Monaco, G. [2006]. Glass-specific behavior in the damping of acousticlike vibrations, *Phys. Rev. Lett.* **96**: 045502.

Ruocco, G., Sciortino, F., Zamponi, F., Michele, C. D. and Scopigno, T. [2004]. Landscapes and fragilities, *J. Chem. Phys.* **120**: 10666–10680.

Ruocco, G. and Sette, F. [2001]. High-frequency vibrational dynamics in glasses, *J. Phys-Condens. Mat.* **13**: 9141–9164.

Ruocco, G., Sette, F., leonardo, R. D., Monaco, G., Sampoli, M., Scopigno, T. and Viliani, G. [2000]. Relaxation processes in harmonic glasses?, *Phys. Rev. Lett.* **84**: 5788–5791.

Sanchez, I. C. and Cho, J. [1995]. A universal equation of state for polymer liquids, *Polymer* **36**: 2929–2939.

Schiener, B., Chamberlin, R. V., Diezemann, G. and Böhmer, R. [1997]. Nonresonant dielectric hole burning spectroscopy of supercooled liquids, *J. Chem. Phys.* **107**: 7746–7761.

Schiener, B., Loidl, A., Chamberlin, R. V. and Böhmer, R. [1996]. Dielectric study of supercooled triphenylphosphite and butyronitrile: Comparison with a mesoscopic model, *J. Mol. Liq.* **69**: 243–251.

Schroeder, J., Wu, W. M., Apkarian, J. L., Lee, M., Hwa, L. G. and Moynihan, C. T. [2004]. Raman scattering and Boson peaks in glasses: temperature and pressure effects, *J. Non-Cryst. Solids* **349**: 88–97.

Scopigno, T. [2007]. *et. al.* to be published.

Scopigno, T., Ruocco, G., Sette, F. and Monaco, G. [2003]. Is the fragility of a liquid embedded in the properties of its glass?, *Science* **302**: 849–852.

Scopigno, T., Suck, J. B., Angelini, R., Albergamo, F. and Ruocco, G. [2006]. High-frequency dynamics in metallic glasses, *Phys. Rev. Lett.* **96**: 135501.

Sekula, M., Pawlus, S., Hensel-bielowka, S., Ziolo, J., Paluch, M. and Roland, C. M. [2004]. Structural and secondary relaxations in supercooled di-n-butyl phthalate and diisobutyl phthalate at elevated pressure, *J. Phys. Chem. B* **108**: 4997–5003.

Sidebottom, D. L. and Sorensen, C. M. [1989]. Light-scattering study of the glass-transition in salol, *Phys. Rev. B* **40**: 461–466.

Sokolov, A. P., Calemczuk, R., Salce, B., Kisliuk, A., Quitmann, D. and Duval, E. [1997]. Low-temperature anomalies in strong and fragile glass formers, *Phys. Rev. Lett.* **78**: 2405–2408.

Sokolov, A. P., Rössler, E., Kisliuk, A. and Quitmann, D. [1993]. Dynamics of strong and fragile glass formers - differences and correlation with low-temperature properties, *Phys. Rev. Lett.* **71**: 2062–2065.

Squires [1978]. *Introduction to the theory of thermal neutron scattering*, Dover.

Srivastava, S. and Das, S. P. [2001]. Fragility and Boson peak formation in a supercooled liquid, *Phys. Lett. A* **286**: 76–79.

Starr, F. W., Sastry, S., Douglas, J. F. and Glotzer, S. C. [2002]. What do we learn from the local geometry of glass-forming liquids?, *Phys. Rev. Lett.* **89**: 125501.

Sugai, S. and Onodera, A. [1996]. Medium-range order in permanently densified SiO_2 and GeO_2 class, *Phys. Rev. Lett.* **77**: 4210–4213.

Tarjus, G., Kivelson, D., Mossa, S. and Alba-Simionesco, C. [2004 a]. Disentangling density and temperature effects in the viscous slowing down of glassforming liquids, *J. Chem. Phys.* **120**: 6135–6141.

Tarjus, G., Mossa, S. and Alba-simionesco, C. [2004 b]. Response to: "Comment on 'Disentangling density and temperature effects in the viscous slowing down of glassforming liquids' " [J. Chem. Phys. 121, 11503 (2004)], *J. Chem. Phys.* **121**: 11505–11506.

Tölle, A. [2001]. Neutron scattering studies of the model glass former ortho-terphenyl, *Rep. Prog. Phys.* **64**: 1473–1532.

Tölle, A., Schober, H., Wuttke, J., Randl, O. G. and Fujara, F. [1998]. Fast relaxation in a fragile liquid under pressure, *Phys. Rev. Lett.* **80**: 2374–2377.

Vogel, H. [1921]. Das temperatureabhägigkeitsgesestz der visocosität von flüssigkeiten, *Phys. Z.* **22**: 645–646.

Wang, L. M., Velikov, V. and Angell, C. A. [2002]. Direct determination of kinetic fragility indices of glassforming liquids by differential scanning calorimetry: Kinetic versus thermodynamic fragilities, *J. Chem. Phys.* **117**: 10184–10192.

Wilson, L. C., Wilson, H. L., Wilding, W. V. and Wilson, G. M. [1996]. Critical point measurements for fourteen compounds by a static method and a flow method, *J. Chem. Eng. Data* **41**: 1252–1254.

Würflinger, A. [n.d.]. data. private communication.

Yamaguchi, M., Nakayama, T. and Yagi, T. [1999]. Effects of high pressure on the Bose peak in a-GeS_2 studied by light scattering, *Physica B* **263**: 258–260.

Yannopoulos, S. N., Andrikopoulos, K. S. and Ruocco, G. [2006 a]. On the analysis of the vibrational boson peak and low-energy excitations in glasses, *J. Non-Cryst. Solids* **352**: 4541–4551.

Yannopoulos, S. N. and Johari, G. P. [2006]. Glass behaviour - Poisson's ratio and liquid's fragility, *Nature* **442**: E7–E8 AUG 3 2006.

Yannopoulos, S. N. and Papatheodorou, G. N. [2000]. Critical experimental facts pertaining to models and associated universalities for low-frequency Raman scattering in inorganic glass formers, *Phys. Rev. B* **62**: 3728–3734.

Appendix A

Details on the samples

This appendix gives an overview of the different properties of the liquids we have mainly studied. We give the details on the samples and where they have been acquired. The appendix moreover contains the references and/or calculations of the fragilities, scaling exponent, x, $T_g(P)$, and the equation of state, which are used throughout the thesis. The fragilites m_P and m_ρ as well as the exponent $x = \frac{\mathrm{d}\log e(\rho)}{\mathrm{d}\log\rho}$ are defined in chapter 3.

A.1 Cumene

Cumene is a popular name for isopropylbenzene (1-methyl ethylbenzene), which is a benzene ring with one side group consisting of a carbon atom with two methyl groups attached. The sum formula is C_9H_{12} and the density at ambient conditions is 0.864 g/mol.

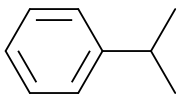

The sample used is from Sigma-Aldrich. The viscosity as a function of temperature is reported by Ling and Willard [1968] at temperatures from 130 K to 150 K and by Barlow *et al.* [1966] in the range 150 K to 303 K. Barlow *et al.* [1966] moreover report the density as a function of temperature at atmospheric pressure in the range 150 K to 320 K. The temperature dependence of the density is found to be linear in this range, and we assume that this dependence is continued down to 126 K, which is the lowest temperature of interest. The density as a function of pressure has been measured by Bridgman [1949] at room temperature from atmospheric pressure up

to 4 GPa. The viscosity as a function pressure at room temperature is reported by Li *et al.* [1995] who also measured light scattering spectra under pressure. We have combined the density and viscosity data in figure A.1. An extrapolation of the viscosity data at atmospheric pressure to $\eta = 10^{13}$ leads to a glass transition temperature $T_g = 126$ K and the fragility at atmospheric pressure is $m_P = 90 \pm 5$. The temperature dependent data and the pressure dependent data can be brought to collapse by using a scaling variable given by ρ^x/T with x=4.85. From this scaling we can estimate the glass transition density at room temperature exploiting the fact that the scaling variable is constant along the glass transition line $\rho_g^x/T_g = const$. We find $\rho_g = 1.19$ g/mL which corresponds to a glass transition pressure of P_g=2 MPa and $dT_g/dP = 0.086$ K.MPa^{-1}. The P_g value is 20% lower than the extrapolated value reported based on the same data by Li *et al.* [1995]. The method we use is of course also an extrapolation, however we believe that the use of the scaling yields a more reliable result.

We calculate the isobaric expansion coefficient from the density data at atmospheric pressure and obtain $\alpha_P T_g$x= 0.57 which gives us $m_\rho = m_P/1.57 = 57$.

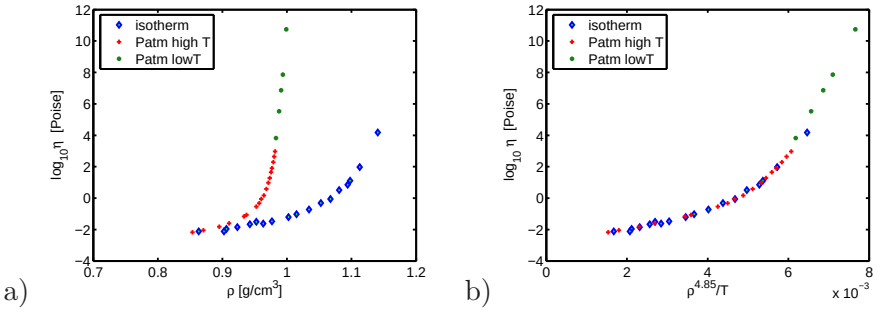

Figure A.1: a) The viscosity as a function of density at atmospheric pressure (varying temperature) and along the room temperature (293 K) isotherm. The high temperature data are from Barlow *et al.* [1966] the low temperature data are from Ling and Willard [1968]. The data on the isotherm are from Li *et al.* [1995]. The density data are from Barlow *et al.* [1966] and Bridgman [1949]. b) The same viscosity data as in figure a) now plotted against the scaling variable ρ^x/T with x=4.85.

In order to estimate the pressure dependence of the isobaric fragility we need the density as a function of pressure and temperature over the whole relevant range. We have estimated equation of state from the available data in the following way. The pressure and temperature dependence of α_P is calculated at temperatures higher than 240 K using the formula in Minassian *et al.* [1988] for toluene rescaled to cumene by using its critical temperature and density ($T_c = 631.1$ K $P_c = 321$ kPa [Wilson *et al.*, 1996]). The expansion coefficient calculated in this way agrees with

the value found from the density measure at atmospheric pressure. The density is calculated at $T > 240$ K from the density at room temperature and the expansion coefficient. This gives essentially linear temperature dependence at all pressures and this temperature dependence is finally extrapolated to low temperature. As a consistency check we verify that $\rho_g^x/T_g = const$ holds on the T_g line at all pressures.

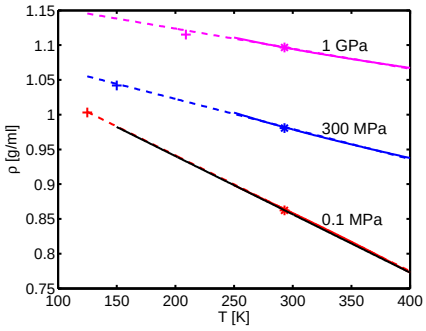

Figure A.2: Illustration of the determination of the density of cumene as a function of pressure and temperature. Stars are measured densities from Bridgman [1949]. Black fill line is the density from Barlow *et al.* [1966]. Colored full lines are calculated from the estimated pressure dependent expansion coefficient (see the text for details). Crosses are densities found on the T_g-line by assuming that the density scaling holds yielding $\rho^x/T =$ constant.

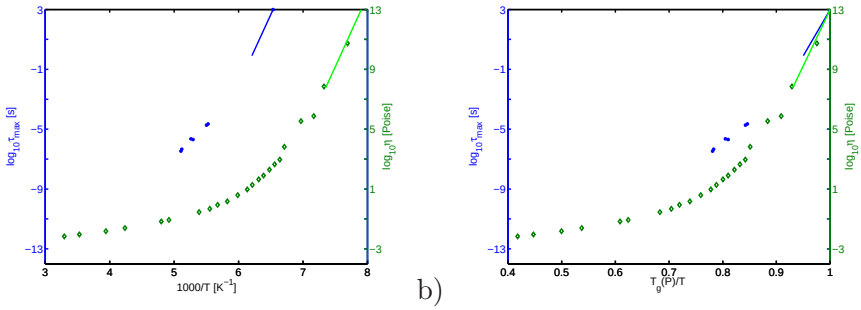

Figure A.3: The relaxation time (●) at 300 MPa and viscosity (♦) at atmospheric pressure of cumene as a function of temperature under isobaric conditions. The full lines illustrate the position of $T_g(P)$ and $m_P(P)$. Figure a shows the data on an absolute temperature scale (1000/T) and figure b) shows the data versus T_g/T.

Based on the density data we can calculate $x\alpha_P T_g$ at all pressures. Assuming that the scaling shown in figure A.1 holds we calculate the pressure dependent isobaric fragility using $m_P = m_\rho(1 + x\alpha_P T_g)$. We find that the isobaric fragility decreases with pressure and that it is 20% lower at 300 MPa giving a fragility of $m_P(P = 300MPa) = 72$.

The relatively low $T_g = 127$ K of cumene makes it difficult to measure with our di-

electric setup in Orsay (see section 5.1.1) because the alpha relaxation does not enter the experimental window of frequencies at lower than 1 MHz within the pressure and temperature range accessible. By using liquid nitrogen we did however obtain a few spectra at 300 MPa in the temperature range 180 K - 195 K. The results are consistent with the analysis above which is illustrated in figure A.1.

A.2 PIB

Polyisobutylene (PIB) is a polymer, with a unit consisting of a backbone of carbons with two methyl groups on every second carbon $(\text{-}CH_2\text{-}C(CH3)_2\text{-})_n$

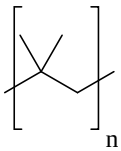

PIB does as other polymers have molecular weight dependent thermodynamic and dynamics properties. In this work we consider 4 different samples PIB680, PIB1190, PIB3580 and PIB500k. PIB680 (Mw=680 g/mol, Mw/Mn=1.06) PIB3580 (Mw=3580 g/mol, Mw/Mn=1.23) are from Polymer Standard service, PIB500k (Mw=500.000 g/mol, Mw/Mn=2.5) is from Sigma Aldrich while the sample PIB1190 (Mw=1190 g/mol, Mw/Mn=1.08) is supplied by Alexei Sokolov. The polydispersity is higher for PIB500k because it is more difficult to separate and characterize high molecular weight polymers. We believe that this is of minor importance, because the molecular weight dependence of different properties saturates at high molecular weight, meaning that a precise characterization is less important.

The density at ambient conditions increases weakly as a function of molecular weight. The high molecular weight PIB has a density of 0.92 g/mL at room temperature and atmospheric pressure.

The T_g increases with about 10% from the lowest to the highest molecular weight, with the Mw-dependence saturating close to 10000 g/mol where it reaches a value of $T_g \approx 205$ K [Ding *et al.*, 2004; Chauty-Cailliaux, 2003].

PIB has a low dipole moment which makes it inadequate to study it by dielectric spectroscopy.

The fragility of high molecular weight PIB is reported by Plazek and Ngai [1991] to be $m = 46$ based on shear mechanical creep data.

The temperature dependent relaxation time of the low molecular weight sample PIB680 has been measured by shear mechanical spectroscopy by Niels Boye Olsen at Roskilde University. The technique covers the frequency range from 1 mHz up to more than 10 kHz [Christensen, 1994]. Based on this data we find that $T_g = 195K$ and m=80. We use only the data at low temperatures in this determination as a secondary relaxation strongly influences the peak position at higher temperatures (figure A.4). The result shows that the low molecular weight sample has a higher

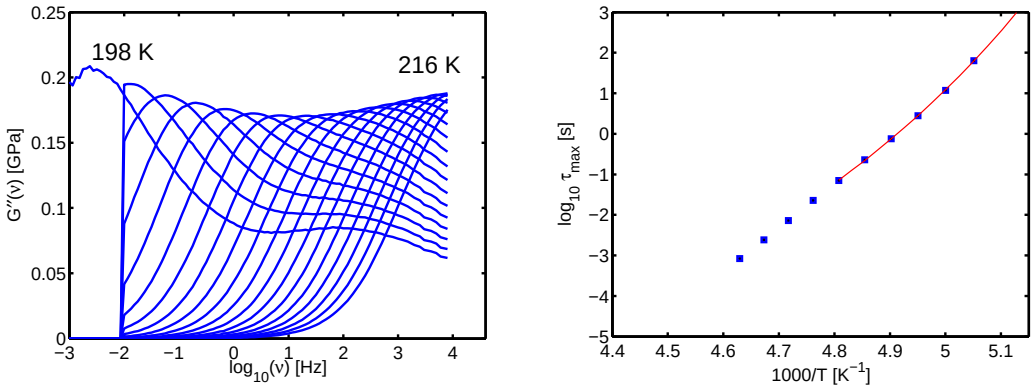

Figure A.4: The temperature dependence of the frequency dependent shear modulus of PIB680. The left figure shows the imaginary part of the modulus as a function of frequency at different temperatures. The right figure shows the alpha relaxation time determined as $\tau_\alpha = 1/\omega_{max}$ as a function of $1000/T$. The red line shows the fit used to determine T_g and fragility.

fragility than the high molecular weight sample. This is in agreement with the conclusion by Ding *et al.* [2004] where the fragility of PIB680 and PIB500k is estimated based on calorimetric data.

We use the equations of state given for high molecular weight PIB by Sanchez and Cho [1995] and Kilburn *et al.* [2006]. The sample we mainly study under pressure is PIB3580. This molecular weight has dynamical properties very close to the high molecular weight limit and we assume that the same is true for the thermodynamics.

The pressure dependence of T_g is also dependent on molecular weight, being weakest for the lowest molecular weights [Chauty-Cailliaux, 2003]. PIB3580 has $T_g \approx 195$ K and $dT_g/dP \approx 0.1$ K/MPa determined by isothermal calorimetry [Chauty-Cailliaux, 2003]. Using the equation of state and this T_g-line we find that $\alpha_P/|\alpha_\tau| = 0.2 \pm 0.05$, meaning that $m_P/m_\rho = 1.2 \pm 0.05$. Assuming that the scaling holds with a simple power law for $e(\rho)$ gives $x \approx 2$. However, $(T_g\alpha_\tau)^{-1}$ appears to increase with pressure which indicates a more complicated form for $e(\rho)$ or alternatively that the scaling does not hold. $\alpha_P/|\alpha_\tau|$ is weakly increasing with pressure, which indicates

an increase of m_P with pressure. The situation is hence similar to that of DBP.

A.3 DHIQ

Decahydro-isoquinoline (DHIQ) consists of a cyclohexane with another saturated ring of three carbons and a nitrogen attached:

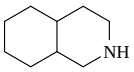

The sum formula is $C_9H_{17}N$ and the density at room conditions is 0.936 g /mL. The sample used in the experiments are used as acquired from Sigma-Aldrich. DHIQ reacts with oxygen and we therefore handled the sample in a glow box with a nitrogen atmosphere.

DHIQ is one of the most fragile molecular glass formers known. This was first reported by Wang *et al.* [2002] who determined $m_P = 128$ based on differential scanning calorimetry. The corresponding heat capacity jump is reported to be $\delta c_P = 0.84$ $\mathrm{Jg^{-1}K^{-1}}$.

More direct determinations of the fragility determined by dielectric spectroscopy are reported by Richert *et al.* [2003] who finds $m_P = 158$ based on a VTF fit. In an earlier work we found that the fragility was $m_P = 154$ based on dielectric spectroscopy while shear mechanical data lead to a fragility of $m_P = 143$ [Niss and Jakobsen, 2003] (the data are also reported in [Jakobsen *et al.*, 2005; Niss *et al.*, 2005]). The glass transition temperature defined by $1/(2\pi\nu_m ax) = 100$ s is at atmospheric pressure $T_g = 179.5$ K.

Dielectric spectra taken at 500 MPa are reported by Paluch *et al.* [2005], and T_g is found to shift 50 degrees. The density as a function of pressure was determined in the temperature range of 300 K - 375 K and a pressure range up to 200 MPa by Casalini *et al.* [2006]. The dynamical data are combined with extrapolations of the obtained equation of state. This is used to determine $m_\rho/m_P = 0.71 \pm 0.02$ and $\gamma = 3.55$ [Casalini *et al.*, 2006].

Finally it is worth noticing that all these determinations of fragility are based on the position of the maximum. DHIQ does however have an extremely pronounced secondary beta relaxation[1]. This secondary relaxation alters the shape of the loss

[1]The pressure experiment actually reveals that at least two different secondary relaxations can be detected [Paluch *et al.*, 2005].

peak differently at different temperatures and it consequently has an effect on the determined temperature dependence of the peak position.

A.4 DBP

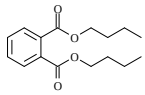

Dibutyl-phthalate (DBP) is a benzene ring with two identical side groups. The sum formula is $C_{16}H_{22}O_4$ and the density at ambient conditions is $\rho = 1.0459$ g/mL. The sample used for the experiments is from Sigma-Aldrich and it has been used as acquired.

The dynamical quantities are determined in this work and we also discuss the agreement with literature data. We find $m_P = 67$, $m_\rho = 56$ and $T_g = 176$ and $dT_g/dP = 0.1$ K.MPa^{-1} in the low pressure limit. We moreover find that the exponent, $x = d\log e(\rho)/d\log\rho$ is dependent on density (see section 5.2.1).

The determination of m_ρ and x requires knowledge of the density dependence of the relaxation times. To do this, we need the pressure and temperature dependence of the density. However, this data is only available at high temperatures [Bridgman, 1932]. In the following we give a detailed description of how we have extrapolated these data to lower temperatures and higher pressures and we carefully verify that the extrapolations do not lead large errors on the results reported in section 5.2.1.

The expansion coefficient, α_P, is calculated at two temperatures from the data of Bridgman [1932], this gives a weakly decreasing α_P with decreasing temperature. We assume that the temperature dependence of α_P is linear in the whole temperature range and integrate $\alpha_P\rho\,\mathrm{d}T$ to obtain ρ on the atmospheric pressure isobar. The pressure dependence of the densities reported by Bridgman [1932] are well described by the Tait equation fits given by Cook *et al.* [1993], these fits give temperature dependent Tait parameters c and b (which are directly related to the compressibility and its first order pressure derivative). We have linearly extrapolated the temperature dependence of these parameters and used the corresponding temperature dependent Tait equation to calculate the pressure dependence along each isotherm. The extrapolation of the derivatives rather than direct extrapolation of the densities gives is expected to give a smaller error on the obtained density. We have moreover checked that this procedure gives physically reasonable pressure and temperature dependencies of the expansivity and the compressibility [Minassian *et al.*, 1988].

The pressure and temperature dependences of the density are of course a crucial input to the scaling shown in section 5.2.1. In order to evaluate the effect of the extrapolations we have performed, we focus on the scaling for the high-pressure room-temperature data of Paluch and the data at atmospheric pressure, because the extrapolation of the density is smallest in these cases. The discrepancies seen in figure 5.6 could be accounted for, if the density at high pressure and room temperature were higher than what we have estimated or if the density at low-temperature were lower than what we have estimated. The high-density dynamical data are taken at room temperature. The experimental density data are also taken at room temperature and they are only extrapolated above 1.2 GPa. If the actual density is higher than what we have estimated, then it means that the compressibility is larger than what we have taken. However, the compressibility at 1.2 GPa is already in the high-pressure domain where it is very low and almost pressure independent (it is slightly decreasing with increasing pressure). The most conservative estimate we could make is to keep the compressibility constant for pressures above the last experimental point at 1.2 GPa. Such an approach changes the ratio $\rho^{2.5}/T$ by less than one percent, and, therefore, can not account for the discrepancy seen in figure 5.6. An alternative explanation would be that the actual low temperature density is lower than we have estimated, meaning that we have overestimated the expansion coefficient α_P. This latter has been calculated at two different high temperatures based on the data in reference Bridgman [1932]. This leads to a slight decrease in expansion coefficient with decreasing temperature. If the expansion coefficient is to be smaller than the estimate from this temperature dependence, then it would mean that the temperature dependence of the expansion coefficient should increase as temperature decreases. This is the opposite of the normal behavior in liquids, where α_P at atmospheric pressure tends to a constant at low temperatures [Minassian *et al.*, 1988]. It is actually most common to assume that the α_P of molecular liquids is constant below room temperature (e.g.[Reiser *et al.*, 2005]). This type of assumption would enhance the discrepancy in figure 5.6. We therefore conclude that the absence of collapse of the high-pressure data in Fig. 5.6 using a simple power law form for $e(\rho)$ cannot be explained by errors made in the estimation of the PVT data.

A.5 m-Toluidine

m-toluidine is a benzene ring with a methyl group and a amino side group. The sum formula is C_7H_9N and the density of the sample at ambient pressure and room

temperature is 0.999 g/cm^3. 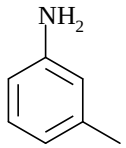

The sample used is from Sigma-Aldrich and it was twice distilled before usage.

The glass transition temperature at atmospheric pressure is $T_g = 187$ K (for $\tau_\alpha = 100$ s) and the isobaric fragility based on dielectric spectra is reported to be $m_P = 82 \pm 3$ [Mandanici *et al.*, 2005; Alba-Simionesco *et al.*, 1999]. (There has been some controversy about the dielectric relaxation in m-toluidine, see reference [Mandanici *et al.*, 2005] and references therein.)

Pressure dependence of the alpha relaxation is reported in section 5.2.2 of this work. We find $x = 2.3$ and a ratio of $m_P/m_\rho = 1.2$. The slope of the glass transition line is $dT_g/dP = 0.085$ K.MPa^{-1}.

Density data are available along four isotherms in the 278.4 K $-$ 305.4 K range for pressures up to 300 MPa [Würflinger, n.d.]. Tait fits and thermal expansivity in this range were extrapolated by using the scheme described above for DBP in order to determine density both as a function of temperature down to T_g, and as a function of pressure on the 216.4 K isotherm.

A.6 Other samples

In addition to the samples presented above, which have all been used in at least two of the different studies in chapter 5 to 8 there are also a few samples which have only been studied by time of flight at ambient pressure (chapter 8).

These samples where all acquired from Sigma-Aldrich.

Salol, T_g =220 K, it is crystalline at ambient conditions so it was melted prior to use. The sample did not recrystallize, which is easily verified from the absence of Bragg peaks in measured neutron scattering data. 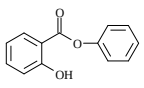

Sorbitol T_g =273 K is crystalline at ambient conditions it was melted prior to use. The sample did not recrystallize, which is easily verified from the absence of Bragg

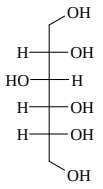

peaks in measured neutron scattering data.

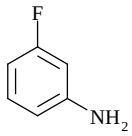

3-fluoroaniline T_g =173 K, density at ambient conditions 1.156 g/cm^3

Propylene carbonate (PC) T_g =156 K, density at ambient conditions 1.189g/cm^3

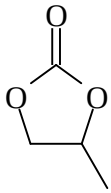

The fragilities and related properties along with relevant references are listed in the following appendix.

Appendix B

Data compilations

B.1 Data compilation

ortho-terphenyl

$m_P = 76, 81, 82, 84, 86$ [Paluch *et al.*, 2001], [Dixon and Nagel, 1988], [Alba-Simionesco *et al.*, 2004], [Huang and McKenna, 2001], [Dreyfus *et al.*, 2004]

$m_\rho = 45$ [Alba-Simionesco *et al.*, 2004]

$R = 0.7$ [Sokolov *et al.*, 1993]

$\beta = 0.52, 0.57$ [Tölle, 2001], [Dixon and Nagel, 1988]

$\left.\frac{\partial \log\langle u^2\rangle}{\partial \log T}\right|_P = 3.5$ * [Tölle, 2001]

$x = 4$ [Tölle *et al.*, 1998],[Dreyfus *et al.*, 2003],[Alba-Simionesco *et al.*, 2004]

$\alpha = 0.58,\ f_Q(T_g) = 0.63$ [Scopigno *et al.*, 2003]

Dibutylphtalate

$m_P = 75$ (this work)

$m_\rho = 63$ (this work)

$x = 1.5$ (this work)

$R = 0.93$ (this work)

$\beta = 0.57$ (this work)

$\left.\frac{\partial \log\langle u^2\rangle}{\partial \log T}\right|_P = 5$ (this work)

$\alpha = 0.16,\ f_Q(T_g) = 0.86$ [Scopigno *et al.*, 2003],[Mermet *et al.*, 2002]

Propylen carbonate

$m_P = 90, 93, 104$ [Paluch *et al.*, 2001], [Richert *et al.*, 2003], [Qin and McKenna, 2006]

$m_\rho = 57, 65^*$ [Casalini and Roland, 2005 b], [Reiser *et al.*, 2005]

$R = 1.1$ (this work)

$\beta = 0.73$ [Paluch *et al.*, 2001]

BMPC = 1,1'-bis(p-methoxyphenyl)cyclohexane

$m_P = 70, 90$ [Casalini and Roland, 2005 c], [Patkowski *et al.*, 2004]

$m_\rho = 26$ [Casalini and Roland, 2005 c]

$\beta = 0.6$ [Hensel-Bielowka *et al.*, 2002 b]

BMMPC = 1,1'-di(4-methoxy-5-methylphenyl)cyclohexane

$m_P = 58, 59$ [Casalini and Roland, 2005 b], [Gapinski *et al.*, 2002]

$m_\rho = 25$ [Casalini and Roland, 2005 b]

$\beta = 0.55$ [Casalini *et al.*, 2003]

DEP A = diglycidylether of bisphenol A

$m_P = 95$ [Roland *et al.*, 2004]

$m_\rho = 57$ [Roland *et al.*, 2004]

$\beta = 0.38$ [Paluch *et al.*, 2003 b]

KDE = cresolphtalein-dimethyl-ether

$m_P = 64, 68, 73$ [Casalini and Roland, 2005 b], [Roland and Casalini, 2003b], [Paluch *et al.*, 2001]

$m_\rho = 34$ [Casalini and Roland, 2005 b]

$\beta = 0.75$ [Paluch *et al.*, 2001]

DHIQ = Decahydroisoquinoline

$m_P = 158, 163$ [Richert *et al.*, 2003], [Casalini *et al.*, 2006]

$m_\rho = 117$ [Casalini *et al.*, 2006]

$R = 1.3$ (this work)

$\beta = 0.36$ [Richert *et al.*, 2003]

$\left.\frac{\partial \log\langle u^2\rangle}{\partial \log T}\right|_P = 5$ (this work)

Cumene

$m_P = 90^*$ [Barlow *et al.*, 1966]

$m_\rho = 57^*$ [Barlow *et al.*, 1966; Bridgman, 1949]

$x = 4.85^8$ [Barlow *et al.*, 1966; Bridgman, 1949]

$R = 0.95$ (this work)

$\beta = 0.66$ (this work)

$\left.\frac{\partial \log\langle u^2\rangle}{\partial \log T}\right|_P = 4.1$ (this work)

$\alpha = 0.44,\ f_Q(T_g) = 0.6$ (this work)

Salol

$m_P = 63, 68, 73$ [Laughlin and Uhlmann, 1972], [Roland *et al.*, 2005],[Paluch *et al.*, 2001]

$m_\rho = 36$ [Roland *et al.*, 2005]

$R = 0.85, 0.95$ [Sokolov *et al.*, 1993], (this work)

$\beta = 0.53, 0.6$ [Böhmer *et al.*, 1993], [Sidebottom and Sorensen, 1989]

$\alpha = 0.64$ [Scopigno *et al.*, 2003]

$x = 5.2$ [Roland *et al.*, 2005]

Glycerol

$m_P = 40, 53, 54$ [Alba-Simionesco *et al.*, 2004], [Birge, 1986], Paluch *et al.* [2002]

$m_\rho = 38$ [Alba-Simionesco *et al.*, 2004]

x =1.8,1.4 [Alba-Simionesco *et al.*, 2004][Dreyfus *et al.*, 2004][Reiser *et al.*, 2005]

$R = 0.6$ (this work)

$\beta = 0.65, 0.7, 0.75$ [Birge, 1986], [Ngai and Rendell, 1990], [Dixon *et al.*, 1990]

$\left.\frac{\partial \log\langle u^2\rangle}{\partial \log T}\right|_P = 3.2$ (this work)

$\alpha = 0.32,\ f_Q(T_g) = 0.76$ [Scopigno *et al.*, 2003]

Sorbitol

$m_P = 128$ [Casalini and Roland, 2004]

$m_\rho = 112$ [Casalini and Roland, 2004]

$R = 0.86$ (this work)

$\beta = 0.5$ [Ngai *et al.*, 1991]

***meta*-fluoroaniline**

$m_P = 70$ [Roland *et al.*, 2005]

$m_\rho = 51^*$ [Reiser *et al.*, 2005]

$R = 0.98$ (this work)

$\beta = 0.35, 0.64$ [Cutroni *et al.*, 1994], [Hensel-bielowka *et al.*, 2005]

***meta*-toluidine**

$m_P = 79, 84$ [Alba-Simionesco *et al.*, 1999], [Mandanici *et al.*, 2005]

$m_\rho = 68$ (this work)

$x = 2.3$ (this work)

$\beta = 0.57$ (this work)

$\left.\frac{\partial \log\langle u^2\rangle}{\partial \log T}\right|_P = 4.7$ (this work)

$\alpha = 0.57,\ f_Q(T_g) = 0.68$ [Scopigno *et al.*, 2003],[Comez *et al.*, 2005]

Triphenylphosphite

$m_P = 160$ [Schiener *et al.*, 1996]

$\left.\frac{\partial \log\langle u^2\rangle}{\partial \log T}\right|_P = 3.4$ [Frick and Alba-Simionesco, 2003]

B_2O_3

$m_P = 32$ [Böhmer *et al.*, 1993]

$\left.\frac{\partial \log\langle u^2\rangle}{\partial \log T}\right|_P = 2.5^*$ [Engberg *et al.*, 1998]

Polyisobutylene

$m_P = 46$ [Plazek and Ngai, 1991]

$m_\rho = 34^*$ [Chauty-Cailliaux, 2003]

$x = 2.6^*$ [Chauty-Cailliaux, 2003]

$R = 0.62$ [Ding *et al.*, 2004]

$\beta = 0.55$ [Plazek and Ngai, 1991]

$\left.\frac{\partial \log\langle u^2\rangle}{\partial \log T}\right|_P = 3.1\ ^*$ [Frick and Richter, 1993]

$\alpha = 0.55,\ f_Q(T_g) = 0.65$ (this work)

Polyvinylchloride

$m_P = 160, 191$ [Huang *et al.*, 2002], [Plazek and Ngai, 1991]

$m_\rho = 140$ [Huang *et al.*, 2002]

$\beta = 0.25$ [Plazek and Ngai, 1991]

Polyvinylacetate

$m_P = 78, 95, 130$ [Roland *et al.*, 2005], [Alba-Simionesco *et al.*, 2004], [Huang *et al.*, 2002]

$m_\rho = 52, 61, 130$ [Roland *et al.*, 2005], [Alba-Simionesco *et al.*, 2004], [Huang *et al.*, 2002]

$x = 1.4, 2.6$ [Alba-Simionesco *et al.*, 2004],[Roland and Casalini, 2003a]

$\beta = 0.43$ [Plazek and Ngai, 1991]

$f_Q(T_g) = 0.73$ [Buchenau and Wischnewski, 2004]

Polystyrene

$m_P = 77, 133$ [Huang *et al.*, 2002], [Plazek and Ngai, 1991]

$m_\rho = 55$ [Huang *et al.*, 2002]

$\beta = 0.35$ [Plazek and Ngai, 1991]

Polymethylmethacrylate

$m_P = 102, 102, 122$ [Huang *et al.*, 2002], [Plazek and Ngai, 1991], [Roland *et al.*, 2004]

$m_\rho = 80, 94$ [Huang *et al.*, 2002], [Roland *et al.*, 2004]

$\beta = 0.41$ [Plazek and Ngai, 1991]

1,4 Polybutadiene

$m_P = 60, 77, 107$ [Scopigno *et al.*, 2003],[Alba-Simionesco *et al.*, 2004],[Huang and McKenna, 2001]

$m_\rho = 64$ [Alba-Simionesco *et al.*, 2004]

$x = 1.8$ [Alba-Simionesco *et al.*, 2004]

$\alpha = 0.4,\ f_Q(T_g) = 0.71$ [Scopigno *et al.*, 2003],[Fioretto *et al.*, 1999]

The * indicates that the value is not given in the corresponding reference but is calculated from the data therein.

The molecular weight of polymers are not always given in the references. However, for PIB and PS data are for this high molecular samples.

Appendix C

Dielectric setup

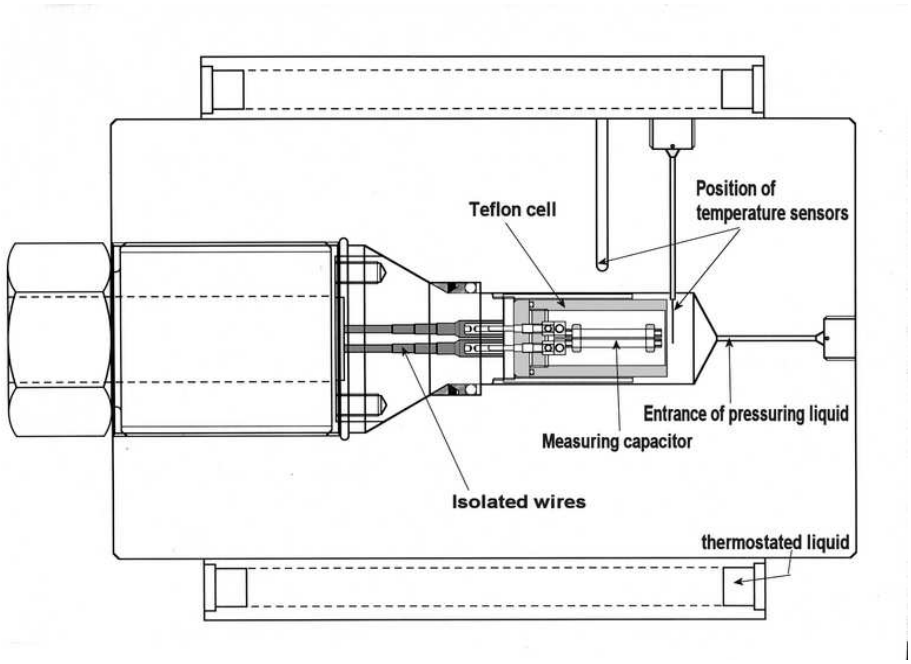

Figure C.1: The experimental setup for dielectric spectroscopy under pressure at Orsay. The Teflon parts shown in grey to distinguish from the metal. The length of the autoclave is $\sim$ 30 cm, the Teflon cell is 5 cm.

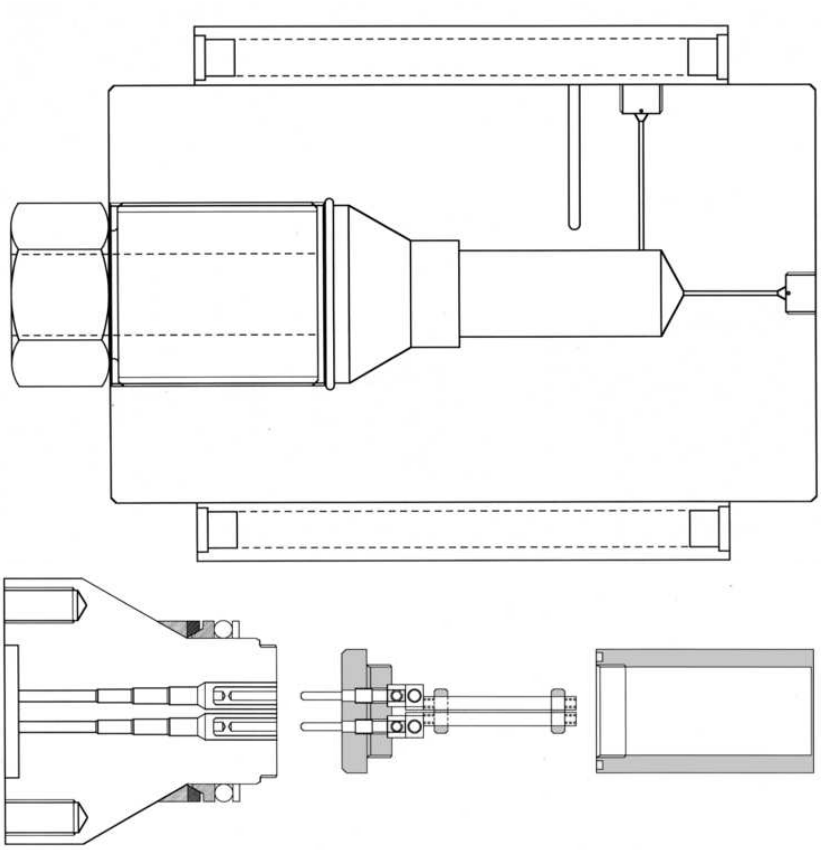

Figure C.2: The experimental setup shown in figure C.1. The upper part of the figure shows the autoclave. The lower part of the figure shows the Teflon cell, the measuring capacitor and the closing piece.

Abstract

The degree of departure from Arrhenius temperature dependence of the relaxation time in the viscous liquid, the fragility, has in the course of the last decade been shown to (or suggested to) correlate with a large number of properties in the liquid and the corresponding glass. Here we develop a set of criteria for scrutinizing these types of correlations by introducing pressure as a control variable in addition to temperature. These criteria are used in the analysis of an extensive new set of data. We particularly study the width of the alpha relaxation by dielectric spectroscopy, the relative intensity of the boson peak and the mean square displacement by neutron scattering and the nonergodicity factor by inelastic X-ray scattering.

In the study of the width of the alpha relaxation as well as the relative intensity of the boson peak we find that they do not relate to the effect of density on the relaxation time, and that a physically meaningful correlation in these cases should be a correlation to *isochoric* fragility rather than to the conventional isobaric fragility. The mean square displacement is found to relate to a balanced combination of temperature and density, while we suggest that the nonergodicity factor evaluated at T_g is correlated with the relative effect of density on the viscous slowing down.

Résumé

Il a été montré durant la dernière décennie que la fragilité, qui traduit le caractère plus ou moins non-Arrhénien d'un liquide, peut être correlée à de nombreuses propriétés de ce liquide et de son verre. Dans ce travail, des critères de test de ces corrélations utilisant la pression comme nouveau paramètre extérieur ont été mis au point. Ils ont été appliqués à l'étude d'un nouveau jeu de données obtenu pendant ce travail. On a particulièrement étudié la largeur du pic de relaxation alpha par spectroscopie diélectrique, l'intensité relative du pic de bose et le déplacement carré moyen par diffusion de neutron, ainsi que le facteur de non-ergodicité par diffusion inélastique des rayons X.

La largeur du pic de relaxation alpha et l'intensité relative du pic du bose ne semblent pas liés a l'effet de la densité sur le temps de relaxation. Pour ces grandeurs, la bonne corrélation à considérer serait alors celle avec la fragilité *isochore* et non la fragilité isobare usuelle. Le déplacement carré moyen est pour sa part, lié aux effets de température et de densité. Par ailleurs, le facteur de non-ergodicité pris à T_g est, lui, correlé à l'effet de la densité sur la ralentissement visqueux.